LOW-TEMPERATURE PROTONATION STUDIES OF TRANSITION METAL ALKYL COMPLEXES AND THE SYNTHESIS AND CHARACTERIZATION OF EARLY TRANSITION METAL PCP PINCER COMPLEXES AND TWO-COORDINATE ALKYLAMIDO COMPLEXES

BY

BRIAN B. TRINH

DISSERTATION

Submitted in partial fulfillment of the requirements
for the degree of Doctor of Philosophy in Chemistry
in the Graduate College of the
University of Illinois at Urbana-Champaign, 2020

Urbana, Illinois

Doctoral Committee:

Professor Gregory S. Girolami, Chair
Professor Martin D. Burke
Associate Professor Alison R. Fout
Professor Thomas B. Rauchfuss

ABSTRACT

We recently reported NMR studies of an osmium alkane complex, $[Cp^*Os(DFMPM)(CH_4)]^+$, where Cp* is pentamethylcyclopentadienyl and DFMPM is bis(bis(trifluoromethyl)phosphino)methane. As part of an effort to continue these studies, the procedures to synthesize the DFMPM ligand and the Cp*Os(DFMPM)Br intermediate have been improved. A laboratory-scale procedure was developed to synthesize diethylzinc in which the α-CH_2 positions are isotopically labeled with carbon-13 and/or deuterium; these reagents were then employed to synthesize isotopically labeled analogs of Cp*Os(DFMPM)Et.

Protonation of Cp*Os(DFMPM)Et with HOTf in $CDCl_2F$ at -130 °C affords the alkane complex $[Cp^*Os(DFMPM)(CH_3CH_3)][OTf]$. The dissociation of the ethane ligand follows first-order kinetics characterized by activation parameters of $\Delta H^{\ddagger} = 14.4 \pm 4.2$ kcal/mol and $\Delta S^{\ddagger} = 7 \pm 20$ cal mol^{-1} K^{-1}. These values are within error for those of the methane analog, $\Delta H^{\ddagger} = 14.9 \pm 1.5$ kcal/mol and $\Delta S^{\ddagger} = 12.3 \pm 8.8$ cal mol^{-1} K^{-1}. IPR studies of the ethane complex indicate that the ethane coordinates to $[Cp^*Os(DFMPM)]^+$ through a single hydrogen atom in either an η^2- or κ^1-fashion, depending on whether or not the carbon atom is significantly involved in the bonding interaction. The IPR studies afford chemical shifts of $\delta_T = 1.99 \pm 0.17$ and $\delta_B = -10.99 \pm 0.32$ for the terminal and bridging hydrogen atoms of the α-methyl group of the ethane ligand, respectively. δ_T for the ethane complex is significantly deshielded compared to the methane analog ($\delta_T = 0.39 \pm 0.05$) and δ_B for the ethane complex is significantly shielded compared to the methane analog ($\delta_B = -8.92 \pm 0.17$). These data support the hypothesis that the chemical shifts of the alkane ligand are significantly affected by diamagnetic anisotropy. The upfield chemical shift of the α-carbon in the ^{13}C NMR spectra of the ethane and methane complexes can be explained in the same way, and are not necessarily indicative of a bonding interaction with osmium.

Improvements were made to the procedures for the synthesis of (^{R}PCP)M(CH_3), where ^{R}PCP is a 2,6-bis(dialkylphosphinomethyl)phenyl pincer ligand and M is a group 10 transition metal. Complexes where R is isopropyl were prepared with nickel, palladium, and platinum. Additionally, complexes where R is *t*-butyl or adamantyl were prepared for nickel. Protonation of these complexes with HOTf in $CDCl_2F$ did not afford observable alkane complexes. In the cases of nickel and palladium, free alkane was generated even at -130 °C; the bonding interaction between the metal and the alkane is evidently very weak. In the case of platinum, protonation was slow until the reaction was warmed to -60 °C, at which point free alkane was generated; no alkyl/hydride or alkane coordination complexes could be observed. More electron-rich metal centers may be required to prepare alkane complexes of group 10 transition metals that can be studied by NMR spectroscopy.

Procedures for the synthesis of(^{tBu}PCP)$TiCl_2$ and (^{tBu}PCP)$CrCl_2$(THF), where (^{tBu}PCP) is 2,6-bis(di-*tert*-butylphosphinomethyl)phenyl, were developed. The titanium compound reacts with $LiBH_4$ to afford (^{tBu}PCP)Ti(BH_4)$_2$. (^{tBu}PCP)$CrCl_2$(THF) can be desolvated to afford (^{tBu}PCP)$CrCl_2$ by application of heat under vacuum. (^{tBu}PCP)$CrCl_2$ undergoes reduction and decomposition when treated with $LiBH_4$ but affords the chromium(II) product (^{tBu}PCP)CrCl when reduced by KC_8. All compounds were characterized crystallographically.

A multi-gram-scale synthetic procedure was developed for Mn(TMP)$_2$, where TMP is 2,2,6,6-tetramethylpiperidide). Mn(TMP)$_2$ is a potential precursor compound for the chemical vapor deposition of manganese nitride films. The compound was crystallographically characterized. The solid state structure of Mn(TMP)$_2$ is isomorphous to that of its iron analog Fe(TMP)$_2$.

ACKNOWLEDGMENTS

The journey to obtaining a Ph.D. is a long and arduous road that no one completes alone. The list of people who have supported me so that I can get this far is too long for me to put on paper. Thank you for all of your love and support. Having said that, it would behoove me to make a few special mentions.

First, I would like to mention my committee members: Professor Girolami, Professor Burke, Associate Professor Fout, and Professor Rauchfuss. I was able to collect the data presented in this dissertation thanks to your continued support and guidance. How you managed to assist me while simultaneously guiding all of the other students who have you on their committees is a testament to your inclusion in the ranks of the world's best. You are amazing.

To the former Girolami group members, thank you for all of your work. Your accumulated knowledge and wisdom was the foundation upon which I, and future Girolami members, could build upon. You also provided me with invaluable examples for mentorship. I will carry your lessons with me as I go on to teach others.

To the current Girolami group members, you are a bundle of curiosity. Thank you for making CLSL more than a workplace. I look forward to seeing what you accomplish both in and out of the labs.

To the administrative assistants of the Department of Chemistry, you are magicians. You break through interpersonal barriers for breakfast. Your positivity is a beacon of hope for those of us slogging through the challenges associated with research. I don't know how the department would function without you.

To my family and friends, you mean the world to me. Thank you for giving me stability and encouragement. You stood by my side when I needed you most and celebrated my accomplishments with me.

Xiling, you are my best friend and love. You picked me up during my darkest times. You call me out when I'm being stubborn and help me tackle my problems head on. Your influence has made me a better person. I'm excited to see how we develop through a lifetime of adventure together. I love you.

TABLE OF CONTENTS

CHAPTER 1

ISOTOPIC PERTUBATION OF RESONANCE AND THE PREPARATION OF ISOTOPICALLY LABELED DIALKYLZINC REAGENTS

Introduction

Isotopic labeling is a powerful tool for understanding chemical reactions. Isotopic labeling experiments can identify which bonds are made or broken during a chemical reaction, elucidate which bonds are involved in the rate-limiting step of a reaction, and give information about chemical structure. Particularly relevant to the last of these applications is isotopic perturbation of resonance (IPR). IPR can be used to determine the nature of agostic interactions with metal centers.[1] Our group has previously used IPR to determine which of the following coordination modes describes the structure of methane coordinated to a transition metal center:

Figure 1.1: The four coordination modes of methane to a single metal center.

If the coordinated methane is frozen in place, the coordination mode of the bound methane can be determined simply from the relative ^{1}H NMR integrals of the resonances due to the hydrogen atoms in the terminal C-H positions versus the C-H positions that bridge to the metal in the ^{1}H NMR spectrum. However, if the terminal and bridging C-H positions are in rapid exchange on the NMR timescale, the resonance for the terminal and bridging C-H positions will coalesce into a single resonance positioned at the weighted average chemical shift. Because experimentally

only one resonance is seen, determination of the coordination mode by integration is not possible, and instead the coordination mode must be determined by other means.

The observed chemical shift of the bound methane in the ^{1}H NMR spectrum is a *weighted* average of the chemical shifts of the terminal (δ_T) and bridging (δ_B) C-H positions. Because C-D bonds have a lower zero-point energy than analogous C-H bonds, and the zero point energy difference is larger if the C-H stretching frequency is larger, deuterium atoms in a bound methane complex will prefer to reside in sites characterized by higher-frequency C-H stretching modes, i.e., in terminal positions as opposed to bridging positions. As a result, replacing increasing numbers of hydrogen atoms in the bound methane with deuterium will change the weight-averaged ^{1}H NMR chemical shift of the remaining hydrogen atoms on the bound methane towards δ_B. How much the chemical shift changes with deuterium incorporation depends on (1) the difference between δ_T and δ_B, (2) the energy difference between having hydrogen or deuterium in the bridging site(s) (ΔE_{BI}), (3) the temperature, and (4) the coordination mode of the methane. The following equations describe the relationship between these values, where *R* is the ideal gas constant (see Appendix A for a derivation of these equations).[2]

$\boldsymbol{\eta^2/\kappa^1}$**:**

$$\boldsymbol{\delta_{M-CH_4} = \frac{3\delta_T+\delta_B}{4}} \quad \textbf{(1.1)}$$

$$\boldsymbol{\delta_{M-CH_3D} = \frac{\left(2+e^{-\frac{\Delta E_{BI}}{RT}}\right)\delta_T+\delta_B}{3+e^{-\frac{\Delta E_{BI}}{RT}}}} \quad \textbf{(1.2)}$$

$$\boldsymbol{\delta_{M-CH_2D_2} = \frac{\left(1+2e^{-\frac{\Delta E_{BI}}{RT}}\right)\delta_T+\delta_B}{2+2e^{-\frac{\Delta E_{BI}}{RT}}}} \quad \textbf{(1.3)}$$

$$\boldsymbol{\delta_{M-CHD_3} = \frac{\left(3+e^{-\frac{\Delta E_{BI}}{RT}}\right)\delta_T+\delta_B}{1+3e^{-\frac{\Delta E_{BI}}{RT}}}} \quad \textbf{(1.4)}$$

κ^2:

$$\delta_{M-CH_4} = \frac{\delta_T + \delta_B}{2} \quad (1.5)$$

$$\delta_{M-CH_3D} = \frac{\left(1+2e^{-\frac{\Delta E_{BI}}{RT}}\right)\delta_T + \left(2+e^{-\frac{\Delta E_{BI}}{RT}}\right)\delta_B}{3+3e^{-\frac{\Delta E_{BI}}{RT}}} \quad (1.6)$$

$$\delta_{M-CH_2D_2} = \frac{\left(2e^{-\frac{\Delta E_{BI}}{RT}}+e^{-\frac{2\Delta E_{BI}}{RT}}\right)\delta_T + \left(1+2e^{-\frac{\Delta E_{BI}}{RT}}\right)\delta_B}{1+4e^{-\frac{\Delta E_{BI}}{RT}}+e^{-\frac{2\Delta E_{BI}}{RT}}} \quad (1.7)$$

$$\delta_{M-CHD_3} = \frac{\left(e^{-\frac{\Delta E_{BI}}{RT}}\right)\delta_T + \delta_B}{1+e^{-\frac{\Delta E_{BI}}{RT}}} \quad (1.8)$$

κ^3:

$$\delta_{M-CH_4} = \frac{\delta_T + 3\delta_B}{4} \quad (1.9)$$

$$\delta_{M-CH_3D} = \frac{\left(e^{-\frac{\Delta E_{BI}}{RT}}\right)\delta_T + \left(1+2e^{-\frac{\Delta E_{BI}}{RT}}\right)\delta_B}{1+3e^{-\frac{\Delta E_{BI}}{RT}}} \quad (1.10)$$

$$\delta_{M-CH_2D_2} = \frac{\left(e^{-\frac{\Delta E_{BI}}{RT}}\right)\delta_T + \left(2+e^{-\frac{\Delta E_{BI}}{RT}}\right)\delta_B}{2+2e^{-\frac{\Delta E_{BI}}{RT}}} \quad (1.11)$$

$$\delta_{M-CHD_3} = \frac{\left(e^{-\frac{\Delta E_{BI}}{RT}}\right)\delta_T + 3\delta_B}{3+e^{-\frac{\Delta E_{BI}}{RT}}} \quad (1.12)$$

Using these equations, we can calculate the expected ^{1}H NMR spectra of the different coordination modes with the assumption that δ_T is downfield of δ_B (Figure 1.2). The exact chemical shifts of the resonances are not important for assigning the coordination mode, rather it is how the difference in chemical shifts change with successive deuteration that is important. For the η^2/κ^1 coordination mode, the change in chemical shift increases with increasing deuteration. For the κ^2 case, the change in chemical shift is constant. Finally, for the κ^3 coordination mode, the change in chemical shift decreases with increasing deuteration.

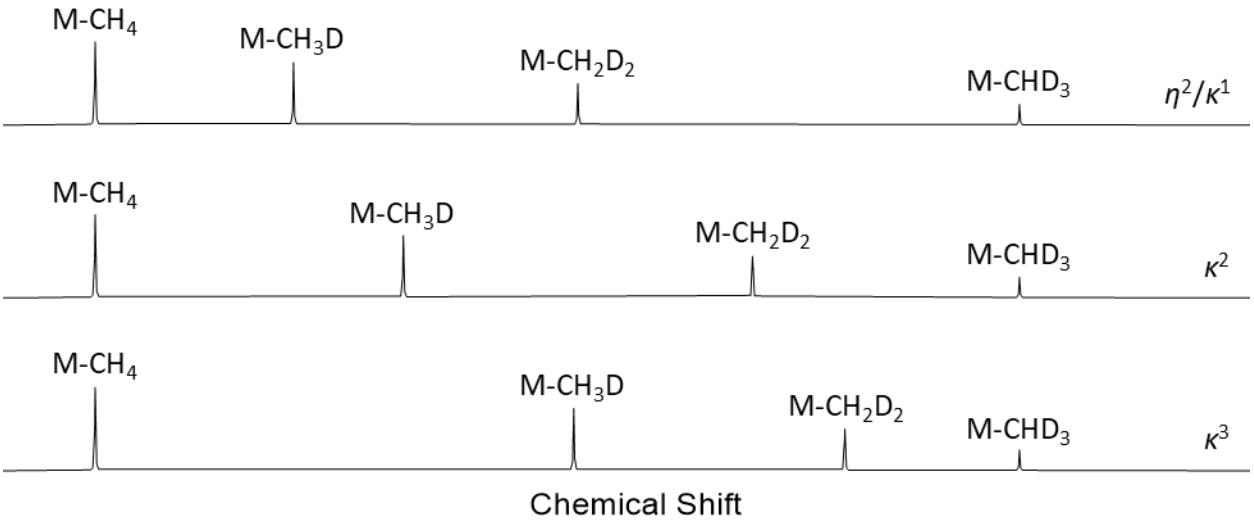

Figure 1.2: The calculated ^{1}H NMR patterns for M-$CH_{4-n}D_n$, where n is 0-3, for the η^2/κ^1, κ^2, and κ^3 coordination modes.[2] The spectra have been scaled so that the chemical shift difference between the M-CH_4 and M-CHD_3 isotopologs is constant.

Once the coordination mode has been established, the proper set of equations can be solved to determine δ_T, δ_B, and ΔE_{BI}. Because IPR determines only the number of hydrogen atoms that bridge to the metal center, it cannot distinguish between η^2 and κ^1 coordination modes, which differ in whether the carbon atom is significantly involved in bonding to the metal center. These equations and calculated spectra apply only to methane that is bound to a single metal center. For larger alkanes, in which the carbon atoms bear fewer than four hydrogen atoms, the equations and patterns will be different. However, the theory remains the same and equations for the bound CH_3R or CH_2R_2 groups (where $R \neq H$) can be generated using the same logic. IPR can also be used to deconvolute the ^{13}C coupling constants of the terminal and bridging hydrogen atoms, simply by replacing the chemical shift terms in the appropriate equations with their corresponding coupling constant terms.

Sempsrott characterized the methane coordination mode in the organoosmium complex $[Cp^*Os(DFMPM)]^+$, where Cp* is η^5-1,2,3,4,5-pentamethylcyclopentadienyl and DFMPM is bis[bis(trifluoromethyl)phosphino]methane, in $CDCl_2F$ by NMR spectroscopy.[2] IPR experiments led to the conclusion that the methane ligand is bound in the η^2/κ^1 coordination mode, and that $\delta_T = 0.39 \pm 0.05$, $\delta_B = -8.92 \pm 0.17$, $\Delta E_{BI} = 0.264 \pm 0.005$ kcal/mol, $J_T = 141 \pm 4$ Hz, and $J_B = 83 \pm 11$ Hz. Sempsrott also measured the rate of methane dissociation from the complex at several temperatures to determine that $\Delta H^‡ = 14.9 \pm 1.5$ kcal/mol and $\Delta S^‡ = 12.3 \pm 8.8$ cal mol^{-1} K^{-1} for this process.

It was our desire to expand this study to include higher alkanes, beginning with ethane. In order to carry out the requisite IPR experiments, it is necessary to prepare alkane ligands that contain varying amounts of deuterium (and ^{13}C if one is interested in studying the $^1J_{CH}$ coupling constants) in the α-position of the ligand of interest. This requirement imposes challenges of its own.

Sempsrott generated $[Cp^*Os(DFMPM)(CH_4)]^+$ by protonation of $Cp^*Os(DFMPM)(CH_3)$, which was generated from $Cp^*Os(DFMPM)Br$ and $Zn(CH_3)_2$.[2] For his IPR experiments, appropriately labeled methyl iodide was commercially available, from which the isotopically labeled dimethylzinc reagents were prepared. To conduct analogous experiments on the corresponding ethane analog of the methane coordination complex, it will be necessary to synthesize two isotopologs of Cp*Os(DFMPM)Et, one in which the α-carbon of the ethyl ligand is ^{13}C-labeled and the other in which the α-carbon is both ^{13}C-labeled and which also bears one or two deuterium atoms; isotopic labeling of the β-carbon of the ethyl ligand is irrelevant for IPR. Ethyl halides labeled at the 1-position with ^{13}C are commercially available. However, ethyl halides

with 1-^{13}C-1-D or 1-^{13}C-1,1-D_2-labeling are not. Here we describe laboratory-scale syntheses of these isotopically labeled ethyl halides.

Results and Discussion

$$Zn(CH_2CH_3)_2 \Longrightarrow CH_3CH_2X \Longrightarrow CH_3CH_2OH \Longrightarrow CH_3COOH$$

Scheme 1.1: Retrosynthesis of diethylzinc from acetic acid.

There are well-established syntheses of ethyl halides from ethanol.[3-6] However, these procedures use large quantities (> 100 g) of fairly pure ethanol (> 80%). Because we wish to prepare isotopically labeled materials, we want a procedure that is amenable to much smaller reaction scales (ca. 1 g) and that limits the need for isolation of intermediates (and the losses associated with such procedures). Reduction of $CH_3{}^{13}COOH$ with $LiAlD_4$ should afford $CH_3{}^{13}CD_2OH$ but isolation of the labeled ethanol from the reaction solvent and H_2O (introduced by aqueous quenching of the $LiAlD_4$) at this scale is nontrivial. The introduction of H_2O can be avoided if the reaction mixture is quenched with a solution of HCl in Et_2O. However, too much ethanol is lost if the Et_2O is subsequently removed by distillation. Therefore, it was necessary to find a procedure to convert ethanol into an ethyl halide that is tolerant of Et_2O. This requirement excluded the use of HX or PX_3 reagents, which react with Et_2O to afford natural abundance ethyl halides. We considered several routes to convert ethanol to ethyl halides on ~1 g scale.

Alcohols can be transformed into alkyl halides by the Mitsunobu reagent.[7] In this preparation, diethyl diazodicarboxylate (DEAD) is added to an ethereal solution of PPh_3 at 0 °C. Addition of a lithium halide salt, followed by the alcohol, yields the alkyl halide. Manna et al. studied this reaction with relatively high-boiling alcohols and alkyl halides, and isolated the

products by extraction and subsequent distillation; this method would not work well if the solvent and the alkyl halide product have similar boiling points. In order to adapt this procedure for our purposes, tetraglyme could be used as the reaction solvent, allowing the ethyl halide to be separated from the solvent, and the other components of the reaction mixture, by vacuum transfer. Et_2O present from the preparation of the ethanol would be carried over, but its presence would not interfere with the subsequent conversion to the dialkylzinc reagent.

The Appel reaction converts alcohols into alkyl halides using PPh_3 and a halide source such as CX_4 or X_2.[8] We foresaw several issues with the Appel reaction. Dichloromethane and chloroform, which are commonly used solvents for these reactions, would co-distill with the ethyl halide product and would interfere with the synthesis of the dialkylzinc reagent. In addition, using X_2 reagents results in the formation of HX, which will react with the Et_2O to form unlabeled ethyl halide. A few studies have employed alternative sources of halide.[9-11] However, solvents other than low-boiling chlorocarbons were either not explored or resulted in low yields.

Alkyl halides may also be prepared from alcohols by means of multi-step processes. In one such preparation, the alcohol is first converted to the tosylate by action of TsCl.[12] Pyridine is added to remove HCl that is generated from the reaction. This reaction is time sensitive because the products can react further to produce alkyl chlorides and alkylpyridinium tosylates.[12-13] Once isolated, the tosylate can be converted into the halide by the Finkelstein reaction (treatment with an alkali metal halide).

We chose this last route to synthesize ethyl iodide. To circumvent the issues of overreaction, and to simplify the separation procedure, we replaced the volatile base, pyridine, with NaH. The reaction is tolerant of the Et_2O carried over from the synthesis of the ethanol. NaCl and excess NaH are removed by filtration, and the Et_2O can be removed by evaporation with

limited loss of ethyl tosylate, which was purified by column chromatography. The ethyl tosylate was dissolved in HMPA, a nonvolatile solvent, and addition of NaI afforded ethyl iodide, which was isolated by vacuum transfer. The overall yield, starting from acetic acid, is about 15%, which is sufficient for our needs.

Conversion of alkyl iodides to dialkylzinc reagents can be performed in several ways. Excellent yields are obtained when ethyl iodide is treated with a mixture of zinc and lithium powder.[14] The more traditional zinc-copper couple can afford good yields but suffers from reproducibility issues that arise from inconsistencies in the preparation of the zinc-copper couple.[15-16] Conversion of alkyl iodides to Grignard reagents by action of magnesium metal, followed by transmetallation with anhydrous $ZnCl_2$, affords smaller yields of the dialkylzinc, but does so reliably.[17-18]

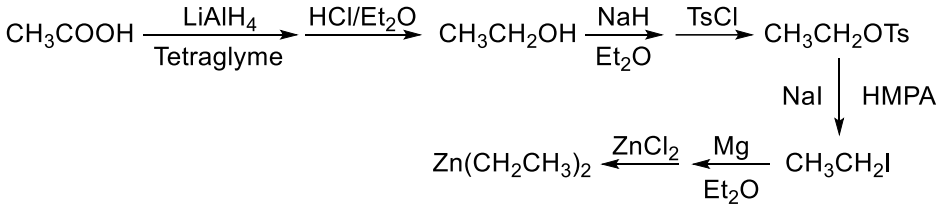

Scheme 1.2: Small-scale synthetic route to $ZnEt_2$ from acetic acid. Site-specific isotopic labeling is achievable with this route using the appropriately labeled acetic acid and $LiAlH_4$.

Conclusion

A synthetic route for preparing diethylzinc that is isotopically labeled at the α-carbon was developed that works well on small (~1 g) scales. The use of nonvolatile solvents such as tetraglyme and HMPA aided in the separation of some of the volatile intermediates. Quenching the $LiAlH_4$ with HCl in Et_2O avoided the introduction of H_2O. Converting the ethanol to sodium

ethoxide followed by addition of tosyl chloride circumvented the issues of overreaction that occur when pyridine is used is used as the base.

Experimental Details

Unless otherwise stated, all operations were conducted under argon using standard Schlenk line and glovebox techniques. Liquid reagents were dried over sodium-benzophenone ketyl (Et_2O), sodium (tetraglyme), CaH_2 (HMPA, 1,2-dibromoethane), or acetic anhydride (acetic acid) and distilled before use. Ethyl acetate and hexanes (Fisher Scientific Company, L.L.C.); 2 M HCl in Et_2O and $ZnCl_2$ (Sigma-Aldrich, Inc.); $LiAlH_4$ (Strem Chemicals, Inc.); magnesium turnings (Alfa Aesar); NaH, 60 wt% dispersion in mineral oil, and TsCl (Oakwood Products, Inc.); NaI (JT Baker Chemicals); and CH_3CD_2Br, $CH_3{}^{13}CH_2I$, and C_6D_6 (Cambridge Isotopes Laboratories, Inc.) were purchased from commercial sources and used as received.

Unless otherwise stated, NMR spectra were acquired on Varian (400 MHz, 500 MHz, and 600 MHz) and Bruker (500 MHz) spectrometers at room temperature. ^1H and ^{13}C NMR spectra are reported in δ units (positive chemical shifts to higher frequency) relative to TMS as determined from residual solvent signals.[19] NMR spectra were processed with the MestReNova NMR software package.

Ethyl Tosylate, EtOTs. $LiAlH_4$ (2.738 g, 72.2 mmol) was suspended in tetraglyme (50 mL) and cooled to 0 °C. A solution of acetic acid (1.00 mL, 17.5 mmol) in tetraglyme (50 mL) was added dropwise. The mixture was allowed to warm to room temperature and quenched with HCl (100 mL of a 2 M solution in Et_2O, 200 mmol). The mixture was freeze-pump-thawed for three cycles and then vacuum transferred into a Schlenk flask. NaH, (7.01 g of 60 wt% dispersion in mineral oil) was washed with pentane (3 × 50 mL) and suspended in Et_2O (20 mL). The NaH

slurry was cooled to 0 °C and the solution of ethanol in Et_2O that had been vacuum transferred in the previous step was added dropwise. The mixture was warmed to room temperature and to it was added a solution of TsCl (3.585 g, 18.8 mmol) in Et_2O (30 mL). The mixture was filtered and the filtrate was taken to dryness by rotary evaporation. The white solid residue was dissolved in minimal ethyl acetate and loaded into a silica gel column. The column was washed with hexanes until elution of unreacted TsCl was completed, as monitored by UV light. Then the column was washed with ethyl acetate until the product finished eluting, as monitored by UV light. The fractions containing the product were combined and dried by rotary evaporation. Residual ethyl acetate was removed under vacuum overnight with gentle heating (30 °C) to afford the product as a pale yellow oil. Yield: 1.04 g (30%).

Ethyl Iodide, EtI. To a solution of EtOTs (2.658 g, 13.3 mmol) in HMPA (25 mL) was added NaI (2.030 g, 13.5 mmol). The mixture was allowed to stir overnight and the product was vacuum transferred out of the mixture with the source flask at room temperature and the receiving flask cooled to -196 °C. Yield: 1.101 g (53%).

Diethylzinc, $ZnEt_2$. Magnesium turnings (4.598 g, 189 mmol) were suspended in Et_2O (50 mL) and activated with 1,2-dibromoethane (0.100 mL, 1.16 mmol). EtI (1.00 mL, 12.4 mmol) was added and the mixture was brought to reflux overnight. The mixture was cooled to room temperature and filtered onto anhydrous $ZnCl_2$ (1.210 g, 8.88 mmol). The mixture was stirred overnight at room temperature and filtered. The filtrate was concentrated by distilling off Et_2O with a 60 °C oil bath and then was vacuum transferred with the source flask heated to 100 °C and the receiving flask cooled to -196 °C to afford the product as a 19 wt% solution in Et_2O. Yield: 2.55 g of solution (66 %). ^{1}H NMR (C_6D_6): δ 1.18 (t, $^3J_{HH}$ = 8 Hz, 6 H, CH_3), 0.18 (q, $^3J_{HH}$ = 8 Hz, 4 H, CH_2).

Di(ethyl-1,1-d$_2$)zinc, Zn(CD$_2$CH$_3$)$_2$. This compound was synthesized analogously to $ZnEt_2$ using CH_3CD_2Br instead of EtI. ^{1}H NMR (C_6D_6): δ 1.14 (m, CH_3).

Di(ethyl-1-^{13}C)zinc, Zn(^{13}CH$_2$CH$_3$)$_2$. This compound was synthesized analogously to $ZnEt_2$ using $CH_3{}^{13}CH_2I$ instead of EtI. ^{1}H NMR (C_6D_6): δ 1.18 (m, 6 H, CH_3), 0.16 (dq, $^1J_{CH}$ = 121 Hz, $^3J_{HH}$ = 8 Hz, 4 H, CH_2). ^{13}C{^{1}H} NMR (C_6D_6): δ 6.56 (CH_2), there was insufficient signal-to-noise to observe the terminal methyl resonance, which is reported to appear at δ 10.4.[20]

References

1. Calvert, R. B.; Shapley, J. R., Decacarbonyl(methyl)hydrotriosmium: NMR evidence for a carbon··hydrogen··osmium interaction. *J. Am. Chem. Soc.* **1978,** *100*, 7726-7.
2. Sempsrott, P. J. Low-temperature protonation studies of an electron-poor osmium methyl complex, and molecular precursors for the construction of graphene nanostructues with atomically precise edge structures. Ph.D. Dissertation, University of Illinois at Urbana-Champaign, 2018.
3. Hunt, B. E. A., Preparation of ethyl iodide. *J. Chem. Soc., Trans.* **1920,** *117*, 1592-4.
4. Kamm, O.; Marvel, C. S.; Goshorn, R. H.; Boyd, T.; Degering, E. F., Alkyl and alkylene bromides. *Org. Synth.* **1921,** *I*, 1-13.
5. Weston, F. E., The preparation of ethyl bromide. *J. Chem. Soc., Trans.* **1915,** *107*, 1489-90.
6. Holt, A., Preparation of ethyl bromide. *J. Chem. Soc., Trans.* **1916,** *109*, 1-2.
7. Manna, S.; Falck, J. R.; Mioskowski, C., A convenient preparation of alkyl halides and cyanides from alcohols by modification of the Mitsunobu procedure. *Synth. Commun.* **1985,** *15*, 663-8.

8. Appel, R., Tertiary phosphane/tetrachloromethane, a versatile reagent for chlorination, dehydration, and P-N linkage. *Angew. Chem.* **1975,** *87*, 863-74.

9. Chen, J.; Lin, J.-H.; Xiao, J.-C., Halogenation through deoxygenation of alcohols and aldehydes. *Org. Lett.* **2018,** *20*, 3061-3064.

10. Pouliot, M.-F.; Mahé, O.; Hamel, J.-D.; Desroches, J.; Paquin, J.-F., Halogenation of primary alcohols using a tetraethylammonium halide/$[Et_2NSF_2]BF_4$ Combination. *Org. Lett.* **2012,** *14*, 5428-5431.

11. Jordan, A.; Denton, R. M.; Sneddon, H. F., Development of a more sustainable Appel reaction. *ACS Sustainable Chem. Eng.* **2020,** *8*, 2300-2309.

12. Wiseman, P. A.; Betras, S.; Lindley, B., Conversion of a primary alcohol to an alkyl halide via a tosylate intermediate. *J. Chem. Educ.* **1974,** *51*, 348-9.

13. Edgell, W. F.; Parts, L., Synthesis of alkyl and substituted alkyl fluorides from *p*-toluenesulfonic acid esters. The preparation of *p*-toluenesulfonic acid esters of lower alcohols. *J. Am. Chem. Soc.* **1955,** *77*, 4899-902.

14. Smit, C. J.; Van Der Koppel, N. C. Process for the preparation of di-alkyl compounds of Group 2B metals. GB2268489A, 1994.

15. Krug, R. C.; Tang, P. J. C., The preparation of dialkyl zinc compounds. *J. Am. Chem. Soc.* **1954,** *76*, 2262-3.

16. Hota, N. K.; Willis, C. J., An improved preparation of dialkylzinc compounds. *J. Organomet. Chem.* **1967,** *9*, 169-70.

17. Schrock, R. R.; Fellmann, J. D., Multiple metal-carbon bonds. 8. Preparation, characterization, and mechanism of formation of the tantalum and niobium neopentylidene complexes, $M(CH_2CMe_3)_3(CHCMe_3)$. *J. Am. Chem. Soc.* **1978,** *100*, 3359-70.

18. Thiele, K. H.; Wilcke, S.; Ehrhardt, M., Über dicylcoalkyl-verbindungen des zinks. *J. Organometal. Chem.* **1968,** *14*, 13-19.

19. Fulmer, G. R.; Miller, A. J. M.; Sherden, N. H.; Gottlieb, H. E.; Nudelman, A.; Stoltz, B. M.; Bercaw, J. E.; Goldberg, K. I., NMR chemical shifts of trace impurities: common laboratory solvents, organics, and gases in deuterated solvents relevant to the organometallic chemist. *Organometallics* **2010,** *29*, 2176-2179.

20. Müller, H.; Rösch, L.; Erb, W.; Zeisberg, R., ^{13}C-NMR-Spektroskopische untersuchungen an elementorganischen verbindungen. *J. Organomet. Chem.* **1977,** *140*, C17-C20.

CHAPTER 2

SYNTHESIS AND CHARACTERIZATION OF AN OSMIUM ETHANE COMPLEX

Introduction

The selective functionalization of C-H bonds of saturated hydrocarbons has the potential to be one of the most valuable classes of chemical transformations.[1] There are several approaches to accomplishing C-H functionalization: radical and electrophilic reagents can abstract $H^{\bullet}$ or H^{-}, respectively, and transition metals can insert into C-H bonds through oxidative addition reactions.[2] Of these approaches, C-H activation by oxidative addition at transition metals usually is more selective and is more likely to be tunable, because radicals are not involved, and the nature of the metal and its ancillary ligands greatly affect the process.

One mechanism for the activation of C-H bonds by transition metal complexes proceeds through short-lived σ-complexes, in which an intact C-H bond coordinates to the transition metal.[3-10] The study of these complexes has given insight into the inner workings of transition metal C-H activation. By utilizing UV/vis spectroscopy, time-resolved infrared spectroscopy, and photoacoustic calorimetry, the energies for binding of alkanes to many transition metal centers have been measured.[11-14] NMR studies of these systems mostly suggest that the alkanes coordinate to the transition metals through a single C-H bond.[15-16] The preference for the alkane to coordinate to the metal through terminal CH_3 or through internal CH_2 groups varies, and depends on the nature of the metal and ancillary ligands.[15, 17-20]

There have been a few successful approaches to preparing transition metal alkane complexes that can be observed directly. A notable approach involves the ejection of a labile ligand by photolysis of the complexes in frozen alkane matrices, in alkane solutions, or in the gas phase.[8, 11-12, 15, 17, 19, 21-30] These approaches provided the first direct evidence for the existence of

transition metal alkane complexes; today more transition metal alkane complexes have been prepared in this fashion than by any other. In a different approach, Macgregor and Weller hydrogenated single crystals of transition metal diene complexes to afford alkane complexes, and were able to characterize the products crystallographically.[31-35] There are a small number of other crystallographic studies of metal alkane coordination complexes: two cobalt alkane complexes grown from solution[36] exhibit much less positional disorder of the alkane than Reed's Fe^{II} heptane complex[37] and Meyer's U^{III} cycloalkane complexes.[38]

Two groups have directly observed transition metal alkane complexes prepared by protonation of transition metal alkyl complexes at low temperature.[39-41] Protonation of (PONOP)RhCH_3 by $HBAr^F_4 \cdot 2Et_2O$, where PONOP is 2,6-($^tBu_2PO)_2C_5H_3N$ and BAr^F_4 is B[3,5-$(CF_3)_2C_6H_3]_4$, in $CDCl_2F$ at -110 °C affords [(PONOP)Rh(CH_4)][BAr^F_4].[39] A single resonance in the ^1H NMR spectrum for the bound methane indicated that the coordinated (i.e., metal-bridging) C-H bonds were in fast exchange with the non-coordinated (terminal) C-H bonds of the methane ligand. The methane ligand dissociates from the $[(PONOP)Rh]^+$ fragment at -87 °C with a $\Delta G^‡$ of 14.5 ± 0.4 kcal/mol. DFT calculations suggest that the methane coordinates to $[(PONOP)Rh]^+$ through a single C-H bond.

The same group showed that protonation of the corresponding rhodium ethyl complex with $HBAr^F_4 \cdot 2Et_2O$ at -150 °C in a mixture of $CDCl_2F$ and CD_2Cl_2 affords the ethane complex [(PONOP)Rh(CH_3CH_3)][BAr^F_4].[40] This compound is less stable than its methane analog and requires handling at lower temperatures. The ethane coordinates to $[(PONOP)Rh]^+$ in an end-on fashion, as evidenced by the presence of two ethane resonances in the ^1H NMR spectrum. The ethane ligand dissociates at -132 °C with a $\Delta G^‡$ of 10.9 ± 0.2 kcal/mol, and the α- and β-CH_3 groups of the bound ethane exchange with one another with a $\Delta G^‡$ of 7.2 ± 0.1 kcal/mol at -132

°C. As for its methane analog, DFT calculations suggest that the ethane coordinates through a single C-H bond. The decreased thermal stability of the ethane complex compared to the methane complex was explained by steric hindrance imposed by the ^{t}Bu groups of the PONOP ligand.

The other low-temperature protonation study was done by our group. Protonation of Cp*Os(DFMPM)(CH_3), where DFMPM is $(CF_3)_2PCH_2P(CF_3)_2$, with the acids $HN(SO_2CF_3)_2$ or HOTf, in $CDCl_2F$ at -130 °C affords the methane coordination complex [Cp*Os(DFMPM)$(CH_4)^+$].[41] The coordinated methane dissociates at -100 °C with a $\Delta G^{\ddagger}$ of 12.8 ± 0.1 kcal/mol. Sempsrott used isotopic perturbation of resonance (IPR)[42] to determine that the coordinated methane binds to [Cp*Os(DFMPM)]$^+$ through a single C-H bond. Having successfully studied an osmium methane complex, we sought to synthesize and characterize osmium complexes of higher alkanes.

Results and Discussion

Sempsrott reported the preparation of Cp*Os(DFMPM)Br, the starting material for making his osmium-methyl and methane coordination complexes, on a 100 mg scale.[41] Here we describe our successful efforts to scale up the synthesis. In addition, we describe some refinements of his route to synthesize the diphosphine ligand, DFMPM, which improve the reproducibility and the safety of the procedure. This ligand synthesis involves three main steps: the preparation of the chlorodiphosphine $Cl_2PCH_2PCl_2$, conversion of the latter to the phenoxydiphosphine $(PhO)_2PCH_2P(OPh)_2$, and finally trifluoromethylation to afford DFMPM.

Synthesis of $Cl_2PCH_2PCl_2$. The first step in the synthesis of DFMPM is to prepare $Cl_2PCH_2PCl_2$ from Al powder, CH_2Cl_2, and PCl_3, using iodine and CH_2Br_2 to initiate the reaction and $POCl_3$ to aid in isolation of the product.[41, 43-44] After being activated with I_2 and CH_2Br_2, the

Al powder is heated to reflux in CH_2Cl_2. This reaction is very exothermic and problems related to over-heating and pressurization of the apparatus can arise depending on the quality and mesh size of the Al powder used. We recommend carrying out this reaction on a 2-mole scale of Al (half of the scale Sempsrott used), and using Al particle sizes no smaller than 325 mesh. Under these conditions, the reaction is exothermic enough to heat the mixture to reflux, without external heating, for over a day, but avoids the violent reaction excursions seen if smaller particle sizes or larger reaction scales are used.

Once the aluminum-methylene reagent ("$Cl_2AlCH_2AlCl_2$") has been prepared as a slurry in CH_2Cl_2, the reagent is added to PCl_3 through a 3/8" ID Teflon cannula in as small aliquots as possible. This reaction is particularly exothermic and the boiling point of CH_2Cl_2 is relatively low. It is imperative that the slurry of the methylene aluminum reagent be added slowly so as to prevent a runaway exotherm and flash-boiling of the CH_2Cl_2 solvent. However, if one takes too long to complete the transfer (> 6 h), the yield of the isolated product drops significantly, presumably due to slow diffusion of air into the receiving flask. The transfer can be completed safely within 1.5-2 h if the reaction is performed on the scale of 2 moles of Al.

After the $POCl_3$ has been added to precipitate the $AlCl_3$ byproduct, the unwanted solids are separated from the solution by filtration. Depending on the particle sizes of the solids, this filtration step can be difficult. We find that separating the majority of the solids by decanting the solution, and then conducting the filtration with the decantate, helps with the subsequent filtration. The filtrate is then evaporated under vacuum to remove the solvent and other volatile components, and the resulting oil is purified by distillation at reduced pressure (300 mTorr, 56 °C) to afford the chlorodiphosphine product.

Synthesis of $(PhO)_2PCH_2P(OPh)_2$. We find that the next intermediate in the preparation of DFMPM, the phenoxydiphosphine $(PhO)_2PCH_2P(OPh)_2$, is best synthesized by treating $Cl_2PCH_2PCl_2$ with NaOPh.[41, 45] This method is more convenient, especially in the workup steps, than an alternative procedure that installs the phenoxy groups by treatment with PhOH and pyridine.[44] We made four improvements in this method to prepare $(PhO)_2PCH_2P(OPh)_2$.

First, Sempsrott synthesized NaOPh in situ from NaH and PhOH in Et_2O.[41] This method works provided that an excess of NaH is employed, so as to avoid contamination of the product with phenol. We find that a better method to make anhydrous NaOPh, which depends less on the purity of the starting materials, is from NaOH and PhOH following a literature protocol.[46] Second, an excess of NaOPh must be added to $Cl_2PCH_2PCl_2$ to ensure complete substitution; separation of $(PhO)_2PCH_2P(OPh)_2$ from the partially substituted species is difficult. Third, NaOPh is very flocculent, so that large glassware must be used to enable scale-up; for example, a reaction using 15 mL of $Cl_2PCH_2PCl_2$ must be performed in a 1-L flask. Fourth, if this phenoxylation step is carried out in diethyl ether, some sticky white solids form that can interfere with the filtration step during workup. By suspending the NaOPh in pentane, instead of Et_2O, we find that subsequent addition of $Cl_2PCH_2PCl_2$ affords a solution containing $(PhO)_2PCH_2P(OPh)_2$ that can be easily separated from NaCl and excess NaOPh by filtration. After the pentane is removed from the filtrate under vacuum and the resulting oil is dissolved in Et_2O, a white solid precipitates from solution that adsorbs onto the sides of the flask; the solution is then easily decanted to remove the unwanted solid byproduct. The solvent is subsequently removed from the decantate to afford the phenoxydiphosphine.

Synthesis of $(CF_3)_2PCH_2P(CF_3)_2$, DFMPM. The procedure to synthesize DFMPM from $(PhO)_2PCH_2P(OPh)_2$ is largely unchanged from Sempsrott's route.[41] However, we would like to

emphasize some important points. Sempsrott added excess CF_3SiMe_3 dropwise to an Et_2O slurry of CsF and $(PhO)_2CH_2P(OPh)_2$ at 0 °C and then let the mixture warm to room temperature overnight. We discovered that about 1.5 h after such a mixture reaches room temperature, an exothermic reaction occurs that can result in the production of a large amount of gas, either from boil-off of the Et_2O or from decomposition of CF_3SiMe_3. It appears that the process that is responsible for the induction period does not proceed at an appreciable rate at 0 °C. The magnitude of the exotherm seems to depend on how much excess CF_3SiMe_3 is added, i.e., beyond 4 equivalents per equivalent of $(PhO)_2PCH_2P(OPh)_2$. Using a room temperature bath to help draw heat away from the reaction flask, and adding an initial charge of no more than 4.5 molar equivalents of CF_3SiMe_3 to $(PhO)_2PCH_2P(OPh)_2$, helps limit the amount of gases produced. This stage of the reaction should be conducted behind a blast shield with the hood sash as low as possible in the event that the glassware ruptures due to overpressurization. Proper PPE, including a face shield, is strongly recommended.

The reaction should be monitored by $^{31}P\{^1H\}$ NMR spectroscopy, and additional CF_3SiMe_3 can be added if the trifluoromethylation of $(PhO)_2PCH_2P(OPh)_2$ is still incomplete. At this stage of the synthesis, CF_3SiMe_3 reacts violently with the reaction mixture and therefore the silane must be added slowly. At the end of the reaction, a solution of HCl in diethyl ether is added to protonate the $[(CF_3)_2PCHP(CF_3)_2^-]$ anion that is the direct product of the trifluoromethylation reaction. The excess Et_2O is removed by distillation at atmospheric pressure through a 15-cm Vigreux column. It is best to conduct this distillation slowly because otherwise some DFMPM co-distills with the Et_2O. It is unnecessary to remove all of the Et_2O; the synthesis of $(PhO)_2PCH_2P(OPh)_2$ from $[Cp^*OsBr_2]_2$, DFMPM, and Zn works well with a solution of the

phosphine in this solvent. If HCl remains in the solution, however, some Cp*Os(DFMPM)Cl will be formed as a side product.

Synthesis of Cp*Os(DFMPM)Br. Sempsrott devised a convenient synthetic protocol for Cp*Os(DFMPM)Br on a 100-mg scale by treatment of Cp*Os(DFMPM)Br with excess zinc and excess DFMPM in refluxing ethanol.[41] As he noted, however, attempts to carry out this reaction on larger reaction scales have led to a dramatic lowering of the yield. Because one of our goals is to study the protonation of a family of Os alkyl complexes, the ability to scale up the production of Cp*Os(DFMPM)Br is very desirable.

Sempsrott noted that an excess of zinc powder was required (2 molar equivalents of zinc per osmium) to afford reasonable yields of the desired product. We find that the reaction tolerates large excesses of zinc; increasing the amount of zinc to 5 molar equivalents per osmium increases the reliability of the procedure with no adverse effect on the yield. In early efforts to improve the synthesis, we found that the reaction does not require 5 equivalents of DFMPM per osmium; 1.1 equivalents is sufficient. In addition, the reaction need not be conducted in refluxing ethanol; the reaction proceeds readily at room temperature in Et_2O, with the additional benefit that this solvent is easier to remove under vacuum.

Although the above changes to the synthesis of Cp*Os(DFMPM)Br were beneficial, the yields obtained on larger scales were still very low. We then explored decoupling the zinc reduction step from the coordination of DFMPM to osmium. Stirring $[Cp^*OsBr_2]_2$ with zinc powder results in the generation of intractable reduced osmium species; subsequent addition of DFMPM gives Cp*Os(DFMPM)Br in very low yields. However, mixing $[Cp^*OsBr_2]_2$ with DFMPM in Et_2O at room temperature affords nearly quantitative yields of a mixture of Cp*Os(DFMPM)Br_2 and Cp*Os(DFMPM)Br_3. The reaction of $[Cp^*OsBr_2]_2$ with Lewis bases to

afford osmium(III) compounds of stoichiometry $Cp^*Os(L)Br_2$ has been described previously, where L is an organo-amine, -phosphine, -arsine, or -sulfide.[47] The Os^{IV} compound, $Cp^*Os(DFMPM)Br_3$, which is a minor component (~10%) of the mixture, is probably generated from adventitious air oxidation; $[Cp^*OsBr_2]_2$ is known to react with O_2 to give osmium(IV) species. Separation of the osmium(III) and osmium(IV) products is unnecessary because zinc is able to reduce both compounds to $Cp^*Os(DFMPM)Br$. With this improvement, we were able to obtain as much as 1.8 g of $Cp^*Os(DFMPM)Br$ (in 66% yield from $[Cp^*OsBr_2]_2$) in a single run.

From this study, we conclude that initial efforts to scale up the original preparation of $Cp^*Os(DFMPM)Br$ failed because it was not understood that the reaction between $[Cp^*OsBr_2]_2$ and zinc powder rapidly gives intractable species that do not react with DFMPM to give the desired product. On larger scales, the longer times involved caused more of the $[Cp^*OsBr_2]_2$ starting material to undergo this unproductive side reaction.

Characterization of $Cp^*Os(\kappa^1\text{-DFMPM})Br_3$ and $Cp^*Os(\kappa^1\text{-DFMPM})Br_2$. As mentioned previously, mixing $[Cp^*OsBr_2]_2$ with DFMPM in Et_2O affords a mixture of $Cp^*Os(\kappa^1\text{-DFMPM})Br_3$ and $Cp^*Os(\kappa^1\text{-DFMPM})Br_2$. $Cp^*Os(\kappa^1\text{-DFMPM})Br_3$ precipitates out of solution as it is formed and can be isolated from the mixture by filtration as a reddish brown powder. This diamagnetic compound is sparingly soluble in C_6D_6. The ^{19}F NMR spectrum contains two doublets (Figure 2.1) for the unidentate phosphine, one doublet for the two CF_3 groups that are proximal to the Os center and a second doublet for the two CF_3 groups that are distal. The ^1H NMR spectrum shows resonances at δ 3.73 and 1.17 that correspond to the hydrogen atoms on the DFMPM and Cp* ligands, respectively. The resonance at δ 3.73 is a doublet of doublets due to coupling with the chemically inequivalent P atoms. The two H atoms on the κ^1-DFMPM ligand are chemically equivalent; in contrast, when the ligand coordinates to Cp*OsX in a κ^2 fashion, the

H atoms become diastereotopic with one H being proximal, and the other distal, to the Cp* ligand.[41]

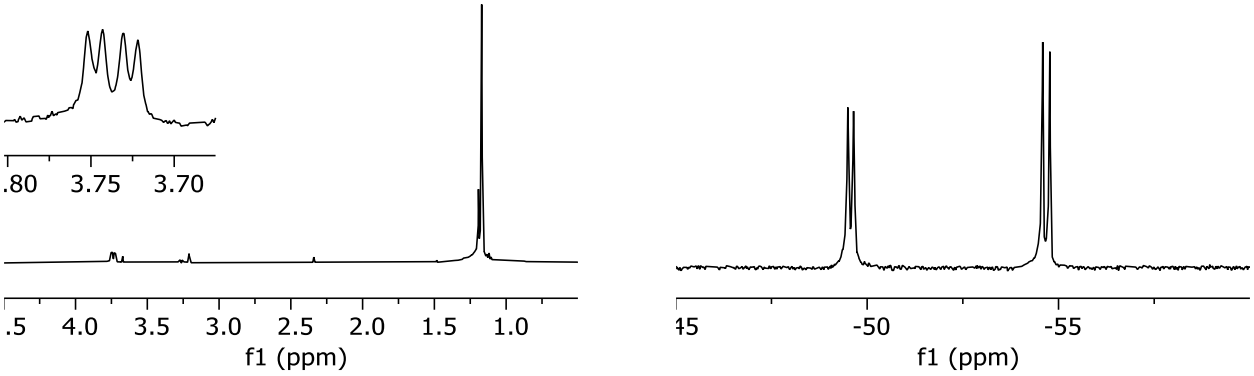

Figure 2.1: NMR spectra of Cp*Os(κ^1-DFMPM)Br_3 in C_6D_6. Left: ^{1}H NMR spectrum. The inset shows the peak structure of the H atoms of the κ^1-DFMPM ligand. Right: ^{19}F NMR spectrum.

The major component of the reaction, Cp*Os(κ^1-DFMPM)Br_2, is Et_2O soluble and can be isolated as a red solid by taking the filtrate from the reaction mixture to dryness under vacuum. This Os^{III} (d^5) compound is paramagnetic, as is evident by the broad and shifted resonances in the ^{1}H and ^{19}F NMR spectra (Figure 2.2). The ^{19}F NMR spectrum contains two resonances that are shifted 16 ppm downfield compared to the chemical shifts of the Os^{IV} compound. Owing to the line broadening caused by the paramagnetism, the coupling patterns of the resonances are not resolved.

Single crystals of Cp*Os(κ^1-DFMPM)Br_3 and Cp*Os(κ^1-DFMPM)Br_2 can be grown by cooling saturated CH_2Cl_2 or Et_2O solutions, respectively. The compounds crystallize in the $P2_1/n$ and $P2_12_12_1$ space groups, respectively, as red prisms. Crystallographic data are given in Tables 2.1 and 2.2. The solid-state structures of the two compounds (Figures 2.14 and 2.15) are similar; the major differences between the two being the different number of Br^- ligands and the different conformation adopted by the diphosphine.

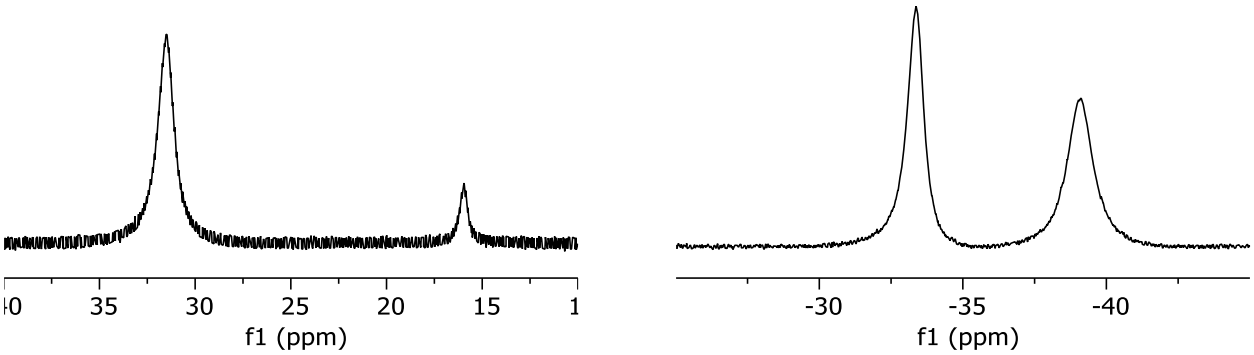

Figure 2.2: NMR spectra of Cp*Os(κ^1-DFMPM)Br_2 in C_6D_6. Left: ^{1}H NMR spectrum. Right: ^{19}F NMR spectrum.

The average Os-Br distance of 2.5381(1) Å in the osmium(IV) compound Cp*Os(κ^1-DFMPM)Br_3 is longer than the average Os-Br distance of 2.4990(2) Å in the osmium(III) compound Cp*Os(κ^1-DFMPM)Br_2; similarly, the Os-P distance of 2.3098(6) Å in the osmium(IV) compound is longer than the average Os-P distance of 2.2511(6) Å in the osmium(III) compound. Higher oxidation states usually exhibit shorter metal-ligand distances, so these differences must be due to the higher coordination number of the osmium(IV) compound.

Preparation of Cp*Os(DFMPM)Et. Sempsrott reported some preliminary studies of the synthesis of Cp*Os(DFMPM)Et by the reaction of Cp*Os(DFMPM)Br with $ZnEt_2$.[41] Whether the reaction was performed in refluxing toluene or at 50 °C, significant amounts of what appear to be β-hydrogen elimination products, Cp*Os(DFMPM)H and Cp*Os(κ^1-DFMPM)(CH_2=CH_2)H, are formed, and of these species from the desired product was non-trivial.

In light of this complication, we investigated alternative methods to alkylate Cp*Os(DFMPM)Br. We hypothesized that performing the alkylation at lower temperatures could reduce the amount of hydride that was formed. Treatment of Cp*Os(DFMPM)Br with ethyllithium or ethylmagnesium reagents at -78 °C affords a new compound, which is not the

desired Os-Et compound but instead is a lithium or magnesium salt of the $Cp^*Os[(CF_3)_2PCHP(CF_3)_2]Br^-$ anion, **1** (Scheme 2.1), which is the result of deprotonation of the methylene backbone of the DFMPM ligand (Figure 2.3). Addition of MeOH to **1** does not result in protonation and regeneration of Cp*Os(DFMPM)Br, but instead yields a new compound, in which one of the C-P bonds of the DFMPM ligand undergoes methanolytic cleavage (Figure 2.4). The identity of this compound, $Cp^*Os[P(CF_3)_2Me][P(CF_3)_2OMe]Br$, **2**, was confirmed crystallographically (Figures 2.16 and 2.17).

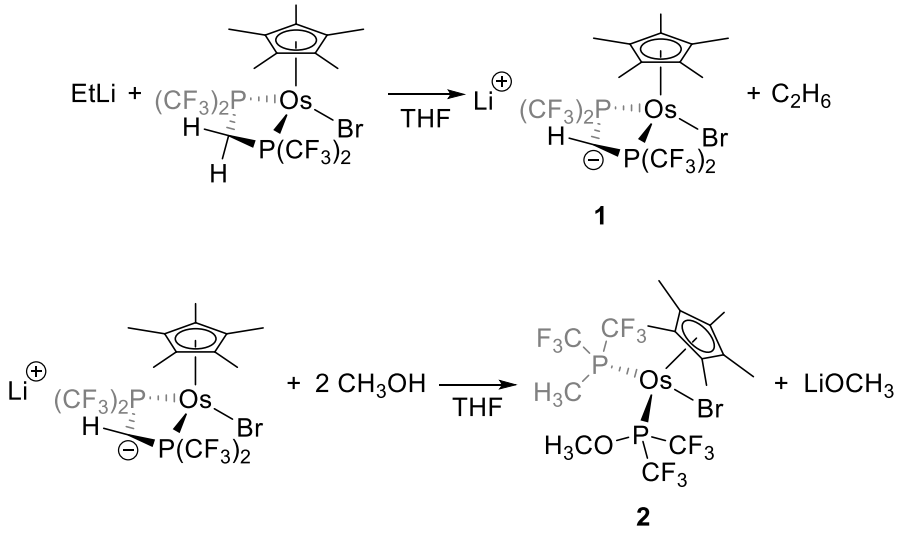

Scheme 2.1: Deprotonation of Cp*Os(DFMPM)Br by EtLi. Subsequent addition of MeOH results in cleavage of the C-P bond in the DFMPM ligand.

Amines such as *N*,*N*,*N*′,*N*′-tetramethylethylenediamine, TMEDA, are known to increase the reactivity of alkylzinc reagents.[48] Although Cp*Os(DFMPM)Br reacts with $ZnEt_2$ at lower temperatures in the presence of TMEDA, the major product of the reaction is actually the hydride Cp*Os(DFMPM)H (Figure 2.5). We have noted that TMEDA is able to promote the production of Cp*Os(DFMPM)H in other reactions (see below).

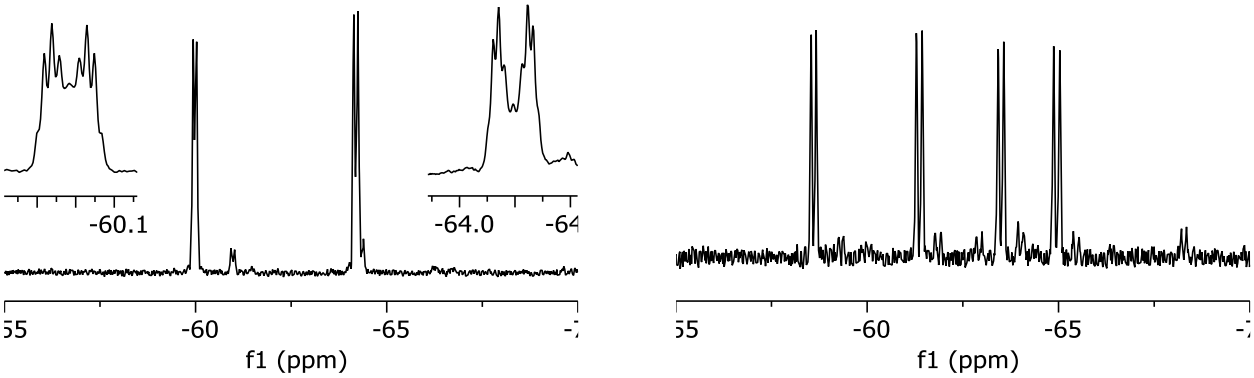

Figure 2.3: ^{19}F NMR spectra of the products from the reaction of Cp*Os(DFMPM)Br with EtLi in THF. The spectrum on the left is before addition of MeOH. The insets show the additional peak structure for the two resonances corresponding to **1** in solution. The two minor resonances correspond to the Cl analog of **1** (an impurity which arises from the HCl used to make DFMPM, see above). The spectrum on the right is after addition of MeOH. There are two minor impurities: the doublets at δ -59.32, -61.86, -62.93, and -65.47 correspond to the Cl analog of **2**, whereas the doublets at δ -64.02 and -68.28 correspond to Cp*Os(DFMPM)H.

Because we did not achieve the desired results with Cp*Os(DFMPM)Br, we turned our attention to alkylating the triflate analog, Cp*Os(DFMPM)(OTf). The synthesis of Cp*Os(DFMPM)(OTf) from Cp*Os(DFMPM)(CH_3) and HOTf in pentane was previously reported by Sempsrott.[41] A slight modification was made to the synthesis to increase the yield of the product: decreasing the amount of pentane used in the reaction results in the precipitation of more product as it is formed. The compound can then be isolated by filtration. It is important to ensure that the HOTf is the limiting reagent, because separation of Cp*Os(DFMPM)(OTf) from HOTf is troublesome. Any unreacted Cp*Os(DFMPM)(CH_3) can be recovered from the filtrate.

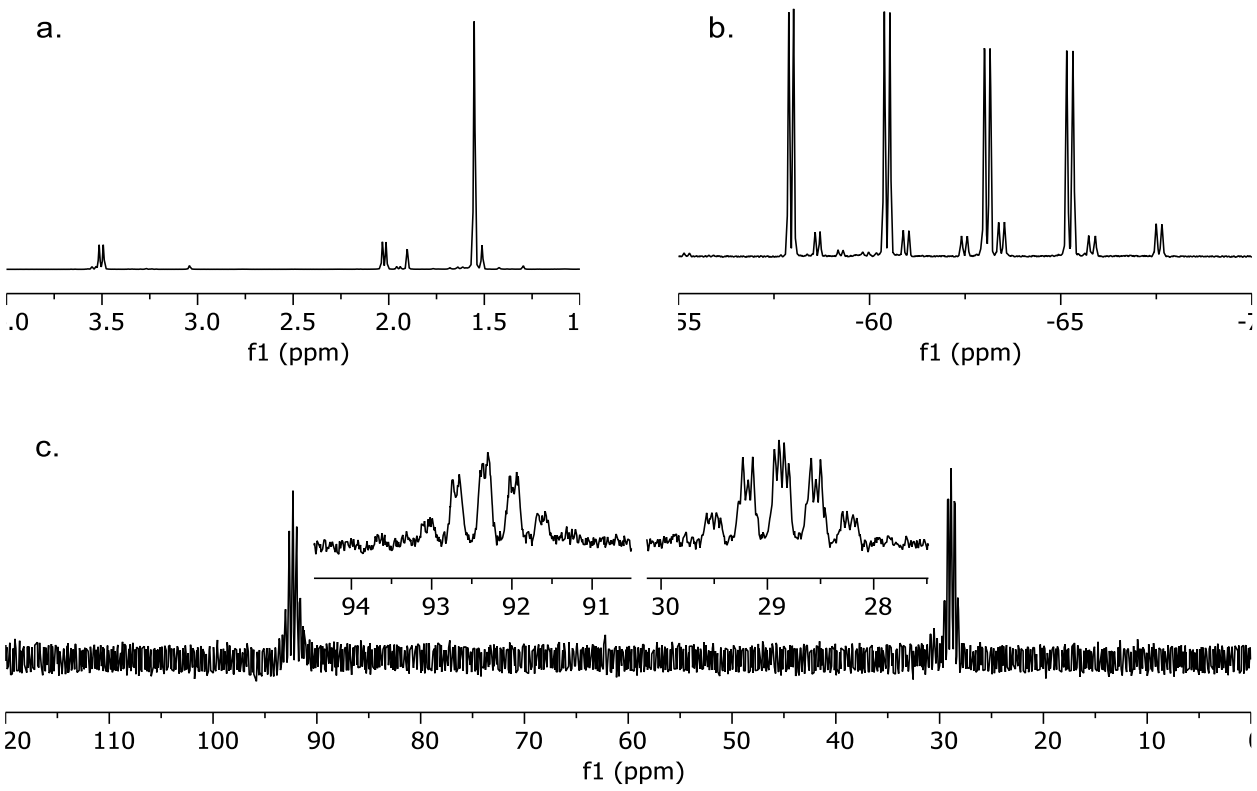

Figure 2.4: NMR spectra of **2** in C_6D_6. a. ^1H NMR spectrum. The minor resonances at δ 1.51 and 1.90 correspond to the Cp* resonance of the chloride analog of **2** and the Cp* resonance of Cp*Os(DFMPM)H, respectively. b. ^{19}F NMR spectrum. The downfield resonances correspond to the CF_3 groups bound to the methylphosphine and the upfield resonances correspond to the CF_3 groups bound to the methoxyphosphine. The impurities correspond to the chloride analog of **2** and Cp*Os(DFMPM)H. c. $^{31}P\{^1H\}$ NMR spectrum. Both resonances are a quartet of quartet of doublets. The resonance at δ 92.3 is due to the methoxyphosphine and the resonance at δ 28.8 is due to the methylphosphine.

Attempts to alkylate Cp*Os(DFMPM)(OTf) with ethyllithium, ethylmagnesium chloride, and diethylzinc did not proceed cleanly. In addition, the major product of these reactions was Cp*Os(DFMPM)H, even when the reactions were conducted at -78 °C. As seen for the reaction of Cp*Os(DFMPM)Br, addition of TMEDA to the $ZnEt_2$ reaction *increased* the amount of Cp*Os(DFMPM)H produced. One possible explanation of this behavior is that the soluble zinc triflates interact with one of the phosphine arms of the DFMPM ligand to free a coordination site on the osmium complex, and thus promote β-hydride elimination.

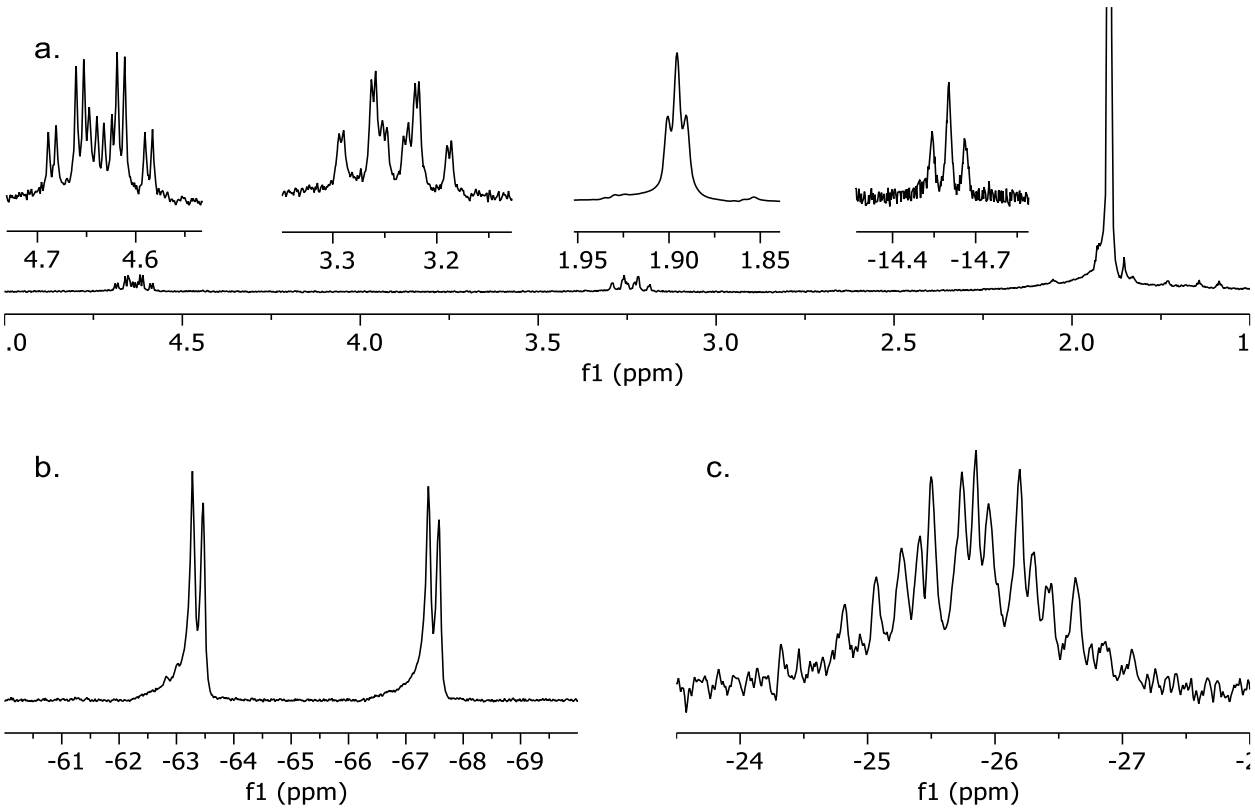

Figure 2.5: NMR spectra of Cp*Os(DFMPM)H in C_6D_6. a. ^1H NMR spectrum. The two resonances at δ 4.63 and 3.24 correspond to the diastereotopic CH_2 atoms of the DFMPM ligand. Both hydrogen atoms couple to each other, to the phosphine atoms, and to the Os-H ligand. An inset shows the Os-H resonance at δ -14.6. b. ^{19}F NMR spectrum. c. $^{31}P\{^1H\}$ NMR spectrum.

To date, the best route found for synthesizing Cp*Os(DFMPM)Et is treatment of Cp*Os(DFMPM)Br with $ZnEt_2$ in hot toluene. This reaction produces Cp*Os(DFMPM)Et as the principal product, along with smaller amounts of the byproducts Cp*Os(DFMPM)($H_2C=CH_2$)H and Cp*Os(DFMPM)H. The temperature of the reaction affects the product distribution: performing the reaction at 80 °C for 16 h allows for complete consumption of Cp*Os(DFMPM)Br and the generation of the highest yields of Cp*Os(DFMPM)Et with minimal β-hydride elimination (Figure 2.6). At both higher and lower temperatures, larger amounts of the hydride are formed.

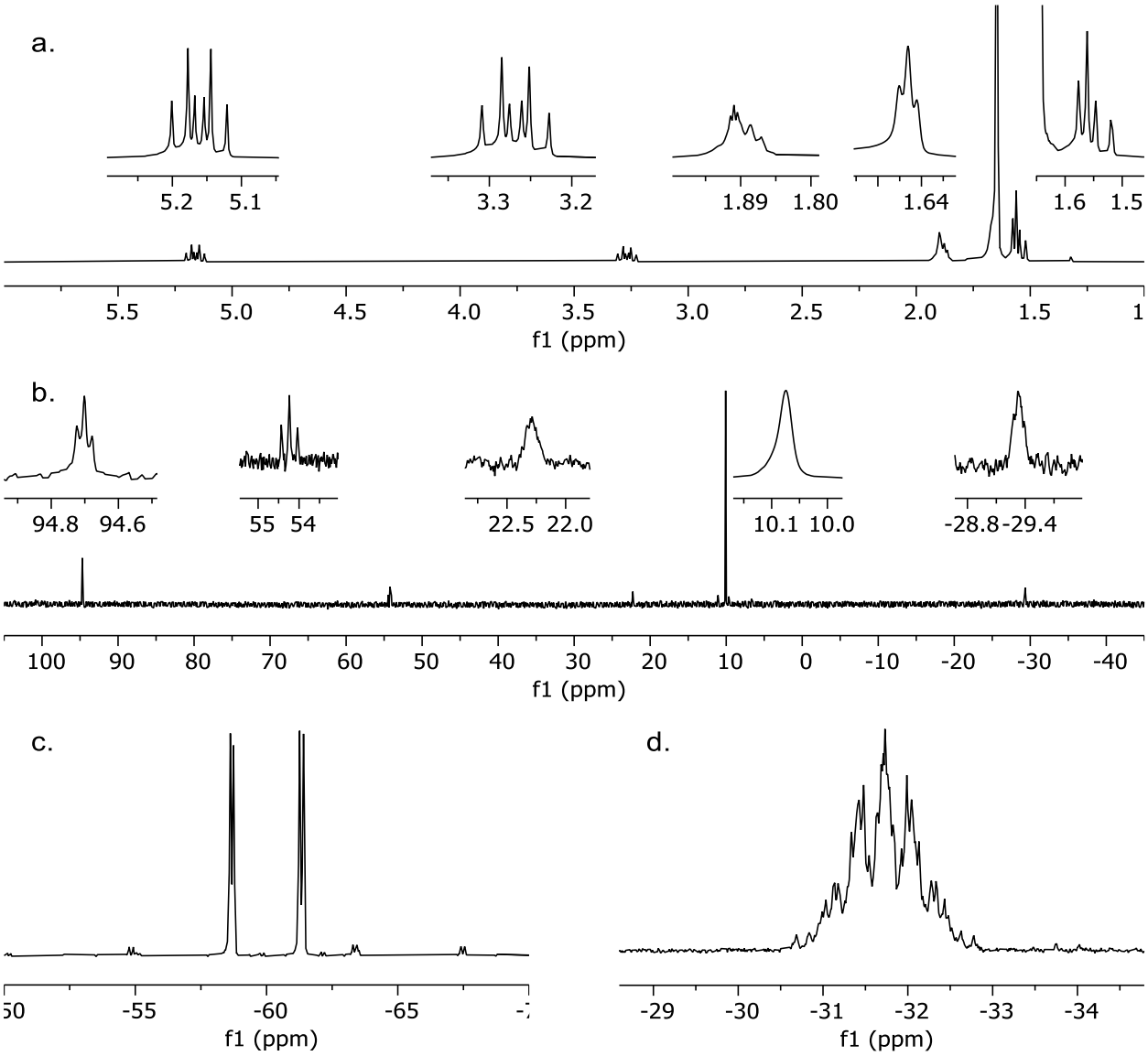

Figure 2.6: NMR spectra of Cp*Os(DFMPM)Et in C_6D_6. a. ^1H NMR spectrum. The resonances at δ 1.88 and 1.56 correspond to the α- and β-hydrogens of the ethyl ligand, respectively. The resonances at δ 1.90 and 1.52 correspond to the Cp* resonances of Cp*Os(DFMPM)H and Cp*Os(DFMPM)(H_2C=CH_2)H impurities, respectively. b. $^{13}C\{^1H\}$ NMR spectrum. The resonances at δ -29.33 and 22.29 correspond to the α- and β-carbons of the ethyl ligand, respectively. c. ^{19}F NMR spectrum. The resonances at δ -63.36 and -67.5 correspond to Cp*Os(DFMPM)H and those at δ -54.84, -62.14, and -63.36 correspond to Cp*Os(DFMPM)(H_2C=CH_2)H. d. $^{31}P\{^1H\}$ NMR spectrum.

Single crystals of Cp*Os(DFMPM)Et were grown by cooling a saturated pentane solution to -20 °C. The compound crystallizes in the $P\bar{1}$ space group as yellow prisms. Crystallographic

data are given in Table 2.2. The molecular structure of Cp*Os(DFMPM)Et (Figure 2.18) is nearly identical with that of the methyl analog Cp*Os(DFMPM)Me.[41] Selected distances and angles are listed in Table 2.6.

Protonation Studies of Cp*Os(DFMPM)Et. As shown by Sempsrott for the methane analog,[41] we were interested in protonating the osmium ethyl compound Cp*Os(DFMPM)Et in order to prepare the osmium-ethane complex $[Cp^*Os(DFMPM)(CH_3CH_3)]^+$. Although our current procedure produces Cp*Os(DFMPM)Et mixed with small amounts (~10%) of the reaction byproducts Cp*Os(DFMPM)H and Cp*Os(DFMPM)($H_2C=CH_2$)H, the mixture is more than suitable for our protonation studies.

Interestingly, the acid Sempsrott employed in his protonation study, $HN(SO_2CF_3)_2$, does not react with Cp*Os(DFMPM)Et below -20 °C, at least on timescales of several hours. At -20 °C and above, protonation does take place, but the resulting protonated product immediately loses ethane and cannot be studied by NMR spectroscopy. Because the osmium center in Cp*Os(DFMPM)Et should be more basic (electron rich) than Cp*Os(DFMPM)Me, the lack of reactivity between Cp*Os(DFMPM)Et and $HN(SO_2CF_3)_2$ cannot be an electronic effect: it must be a steric effect arising from the greater steric bulk of ethyl vs. methyl.

In order to overcome the steric barrier toward protonation, we explored two strategies: employing a stronger acid, and employing a less sterically bulky acid. Perfluoroalkyl sulfonic acids are less sterically demanding than $HN(SO_2CF_3)_2$ and ought to be sufficiently acidic to protonate Cp*Os(DFMPM)Et. Somewhat to our surprise, perfluorooctane sulfonic acid, $HOSO_2C_8F_{17}$, the most readily available solid perfluoroalkyl sulfonic acid, is essentially insoluble in $CDCl_2F$ at -130 °C, and efforts to carry out the protonation of Cp*Os(DFMPM)Et led to no reaction.

We then turned to the simplest perfluoroalkyl sulfonic acid, triflic acid (HOTf); we chose this liquid acid even though in previous work we preferred solid acids because they are easier to measure out by mass. The following procedure proved effective for liquid acids. The osmium complex is first loaded into the NMR tube by itself, and a minimal amount of the $CDCl_2F$ solvent is vacuum transferred onto the solid. Because acid is not present, the mixture can be warmed to the boiling point of the solvent to ensure dissolution of the osmium complex. Once the solid is dissolved, the solution is frozen at -196 °C and additional $CDCl_2F$ solvent is condensed on top of the solution. The second portion of solvent is then thawed, and then the acid is added to the NMR tube with a microliter syringe while keeping the portion of the sample containing the osmium complex frozen. This procedure allows the liquid acid to dissolve into the solvent without premature reaction with the osmium complex.

However, administering the acid presents several challenges. Because $CDCl_2F$ is a gas at room temperature (b.p. 9 °C), it is difficult to dispense solutions of the acid in this solvent with a microliter syringe. Therefore, the acid is best added neat. Addition of too much HOTf (> 20 μL) to $CDCl_2F$, however, raises the freezing point of the solution above -130 °C, and this effect interferes with the intended NMR experiment. Furthermore, HOTf is a very corrosive acid and reacts with the rubber of septa. If one is not careful, impurities from the reaction of the rubber septa and HOTf can be introduced into the NMR sample.

We find that Cp*Os(DFMPM)Et reacts with HOTf in $CDCl_2F$ at -130 °C to afford [Cp*Os(DFMPM)(CH_3CH_3)][OTf]. The ethane ligand is bound to the osmium atom through a single CH_3 group as evidenced by the presence of two distinct quartets in the ^{1}H NMR spectrum at δ -2.35 and 1.20 (Figure 2.7). These resonances are assigned to the proximal and distal (or α and β) methyl group of the coordinated ethane ligand; the three-bond J_{HH} coupling constant is 6

Hz. Thus, binding of ethane to osmium causes a "desymmetrization" of the ethane molecule which is evident in the NMR spectrum.

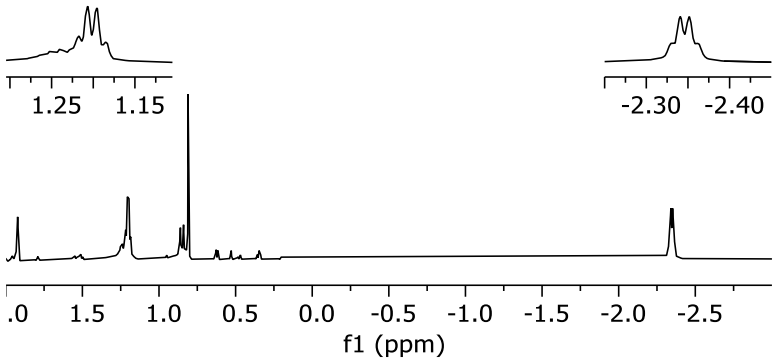

Figure 2.7: ^{1}H NMR spectrum of [Cp*Os(DFMPM)(CH_3CH_3)][OTf] in $CDCl_2F$ at -100 °C. The resonances at δ -2.35 and 1.20 correspond to the α- and β-CH_3 groups of the bound ethane.

As seen for the corresponding methane complex, it is not possible from this spectrum to determine the number of hydrogen atoms that bridge between the proximal methyl group and the osmium center: the terminal and bridging hydrogen atoms on the proximal methyl group are in rapid exchange, so that the chemical shift of δ -2.35 is a population-weighted average of the chemical shifts for the terminal and bridging hydrogen atoms in the static structure. Unlike with Brookhart's [(PONOP)Rh(CH_3CH_3)]$^+$ complex,[40] no line broadening is observed with increasing temperature; in other words, there is no evidence of exchange between the α- and β-CH_3 groups in our system.

Dissociation of the bound ethane complex is very slow at -105 °C and does not occur to a measurable extent even after 1 hour. But at higher temperatures the dissociation to form free ethane follows first-order kinetics with half-lives of 109 and 33 min at -100 and -95 °C, respectively. An Eyring plot of the dissociation rate yields activation parameters of $\Delta H^{\ddagger}$ = 14.4 ± 4.2 kcal/mol and

$\Delta S^{\ddagger}$ = 7 ± 20 cal mol^{-1} K^{-1}, which correspond to a Gibbs free energy of activation of $\Delta G^{\ddagger}$ = 13.1 ± 0.2 kcal/mol at -100 °C (Figure 2.8).

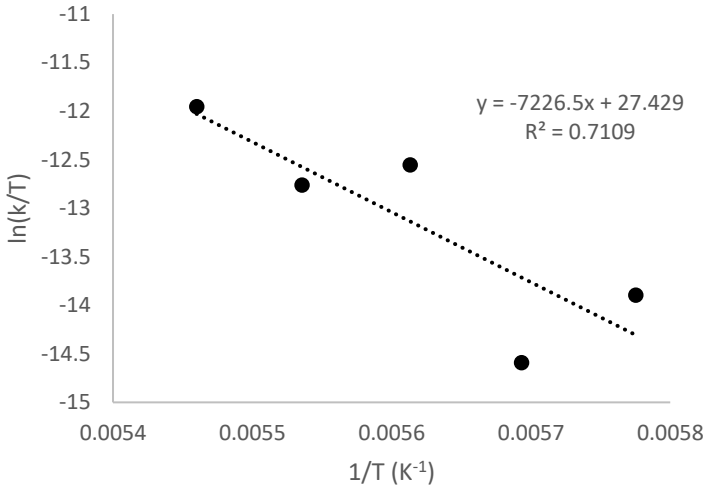

Figure 2.8: Eyring plot of the dissociation of ethane from [Cp*Os(DFMPM)(CH_3CH_3)][OTf].

From these data, we conclude that the ethane complex is more thermally stable than its methane analog, which has half-lives of 44 and 12 min at -100 and -95 °C, respectively.[41] This same trend was seen in Bergman and Moore's Cp*Rh(CO)$_2$ system[49] but the opposite trend was observed in Brookhart's (PONOP)Rh system, in which the ethane complex is less stable than the methane complex.[40]

Isotopic Labeling of Cp*Os(DFMPM)Et. As with the methane analog studied by Sempsrott,[41] we are interested in determining how the ethane binds (i.e., how many hydrogen atoms bridge between carbon and osmium). In addition, we would like to determine, for the static structure, the chemical shifts of the terminal (δ_T) and bridging (δ_B) hydrogens attached to the α-carbon atom, and the coupling constants between the α-carbon and its terminal (J_T) and bridging (J_B) hydrogens. This information, which will provide significant insights into how much the

structure of the ethane molecule is perturbed when it is bound to a metal center, can be obtained through isotopic perturbation of resonance (IPR) experiments.

In order to carry out such IPR experiments, we need to prepare a mixture of isotopologs in which the ethane ligand carries different numbers of deuterium atoms. The best way to prepare such a mixture is to add a mixture of H^+ and D^+ to the Os-$^{13}CH_2CH_3$ and Os-$^{13}CD_2CH_3$ isotopologs of the ethyl complex, as shown in Scheme 2.2. Although the ethane-1,1,1-d_3 complex will be ^1H NMR silent, the ^1H NMR chemical shifts of the other three isotopologs and their ^{13}C coupling constants will offer six observables allowing for calculation of the chemical shifts and coupling constants mentioned above.

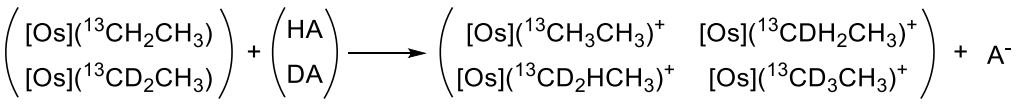

Scheme 2.2: The reaction between two isotopologs of the ethyl complex and a mixture of protio- and deutero-acid affords a mixture of four isotopologs of the ethane complex. [Os] refers to the Cp*Os(DFMPM) fragment.

In initial experiments, we carried out the reaction between Cp*Os(DFMPM)Br and Zn($^{13}CH_2CH_3$)$_2$, with the intention of preparing Cp*Os(DFMPM)($^{13}CH_2$-CH_3). The ^1H and $^{13}C\{^1H\}$ NMR spectra of the resulting product (Figure 2.9) showed that it consisted of an approximately 50:50 mixture of the desired compound Cp*Os(DFMPM)($^{13}CH_2$-CH_3) along with the isotopolog Cp*Os(DFMPM)(CH_2-$^{13}CH_3$) in which the ^{13}C label has scrambled to the β-site of the ethyl group. Evidently, reversible β-hydride elimination occurs under the alkylation conditions, presumably via the intermediate Cp*Os(κ^1-DFMPM)(H_2C=CH_2)H. This result was unexpected, because we employed alkylation conditions that we found minimized the amount of Cp*Os(DFMPM)H that is formed. This result shows that the ethylene ligand in Cp*Os(κ^1-

DFMPM)($H_2C=CH_2$)H does not readily dissociate from the osmium center, even after prolonged heating at 80 °C. In addition, it appears that there is an equilibrium between the ethylene hydride complex and the ethyl complex, which greatly favors the latter. From this finding, we conclude that the high yield of Cp*Os(DFMPM)H from the reaction of the osmium triflate complex with $ZnEt_2$ at room temperature does not occur by dissociation of ethylene from Cp*Os(κ^1-DFMPM)-($H_2C=CH_2$)H.

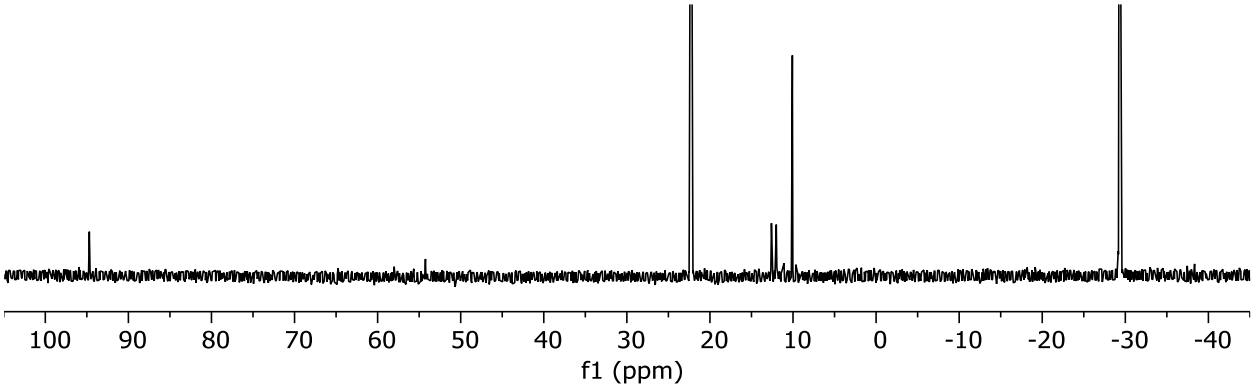

Figure 2.9: $^{13}C\{^1H\}$ NMR spectrum of Cp*Os(DFMPM)(Et-$^{13}C_1$) in C_6D_6. The carbon-13 label has scrambled between both the α- and β-carbons of the ethyl ligand, which appear at δ -29.33 and 22.29, respectively; the Cp* resonances appear at δ 94.70 and 10.07. The doublet at δ 12.66 corresponds to the β-hydride elimination product, Cp*Os(κ^1-DFMPM)($H_2{}^{13}C=CH_2$)H. The ethylene carbon is coupled to the bound phosphorus atom of the κ^1-DFMPM ligand.

Reversible β-hydride elimination presents an obstacle for preparing site-specific deuterated isotopologs of the Os-ethyl complex, and the presence of a mixture of isotopologs will complicate the IPR experiments. Owing to scrambling of the isotopic labels between the α- and β-sites, adding a mixture of H^+ and D^+ to a mixture of d_0- and d_2-Os-ethyl complexes, both carrying a single ^{13}C label, would create as many as 16 isotopologs. The resulting signal overlap and low signal-to-noise for any one isotopolog would make it difficult to extract the desired chemical shift and coupling constant information.

In view of these findings, we chose to break the IPR experiment into two parts. In one experiment, a mixture of Cp*Os(DFMPM)Et and Cp*Os(DFMPM)(Et-d_2) was made to react with a mixture of HOTf and DOTf in $CDCl_2F$. The chemical shifts of the α-methyl group of the bound ethane ligand as a function of the extent of deuteration were used to calculate δ_T, δ_B, and ΔE_{BI}. This latter term is the difference in energy between the species with a bridging hydrogen versus a bridging deuterium (ΔE_{BI}); it reflects the different zero-point energies of H vs. D. In a second experiment, Cp*Os(DFMPM)(Et-$^{13}C_1$) was treated with a mixture of HOTf and DOTf. If we make the assumption that ΔE_{BI} does not change with carbon-13 labeling (which seems reasonable), this experiment allows for the calculation of the remaining variables of interest, J_T and J_B.

IPR Studies of Cp*Os(DFMPM)Et. Our earlier studies of $[Cp^*Os(DFMPM)(CH_4)]^+$ showed that the bound methane ligand coordinates to the osmium center in a η^2/κ^1 manner.[41] In order to determine how ethane in $[Cp^*Os(DFMPM)(CH_3CH_3)]^+$ coordinates to osmium, we make use of the following equations that relate the "frozen" NMR parameters δ_T and δ_B to the observed chemical shifts of the isotopologs in the ^1H NMR spectrum; the observed chemical shifts are expected to be averages owing to rapid exchange between the bridging and terminal sites (see Appendix A for the derivation of these equations):

η^2/κ^1:

$$\delta_{Os-CH_3CH_3} = \frac{2\delta_T+\delta_B}{3} \quad \textbf{(2.1)}$$

$$\delta_{Os-CH_2DCH_3} = \frac{\left(1+e^{-\frac{\Delta E_{BI}}{RT}}\right)\delta_T+\delta_B}{2+e^{-\frac{\Delta E_{BI}}{RT}}} \quad \textbf{(2.2)}$$

$$\delta_{Os-CHD_2CH_3} = \frac{\left(2e^{-\frac{\Delta E_{BI}}{RT}}\right)\delta_T+\delta_B}{1+2e^{-\frac{\Delta E_{BI}}{RT}}} \quad \textbf{(2.3)}$$

κ^2:

$$\delta_{Os-CH_3CH_3} = \frac{\delta_T + 2\delta_B}{3} \quad \textbf{(2.4)}$$

$$\delta_{Os-CH_2DCH_3} = \frac{e^{-\frac{\Delta E_{BI}}{RT}}\delta_T + \left(1 + e^{-\frac{\Delta E_{BI}}{RT}}\right)\delta_B}{1 + 2e^{-\frac{\Delta E_{BI}}{RT}}} \quad \textbf{(2.5)}$$

$$\delta_{Os-CHD_2CH_3} = \frac{\left(e^{-\frac{2\Delta E_{BI}}{RT}}\right)\delta_T + 2\left(e^{-\frac{\Delta E_{BI}}{RT}}\right)\delta_B}{e^{-\frac{2\Delta E_{BI}}{RT}} + 2e^{-\frac{\Delta E_{BI}}{RT}}} \quad \textbf{(2.6)}$$

κ^3:

$$\delta_{Os-CH_3CH_3} = \delta_B \quad \textbf{(2.7)}$$

$$\delta_{Os-CH_2DCH_3} = \delta_B \quad \textbf{(2.8)}$$

$$\delta_{Os-CHD_2CH_3} = \delta_B \quad \textbf{(2.9)}$$

The equations above are the key to establishing the ethane binding mode: they describe the dependence of the chemical shift of the α (i.e., proximal) methyl group of the bound ethane ligand as a function of the extent of deuteration. Specifically, there are different patterns for the chemical shift differences $\Delta\delta_{01}$ and $\Delta\delta_{12}$, where $\Delta\delta_{01}$ is the chemical shift difference between the α-d_0 and α-d_1 isotopologs, etc. ($\Delta\delta_{23}$ is not observable because the α-d_3 isotopolog is silent in the ^{1}H NMR spectrum; we could determine this parameter from the ^{2}H NMR spectrum, but we do not need to know it to carry out the IPR analysis). For the η^2/κ^1 binding mode, Equations 2.1-2.3 show that the Δδ values *increase* with increasing deuteration. For the κ^2 binding mode, equations 2.4-2.6 indicate that the Δδ values *decrease* with increasing deuteration. Finally, for the κ^3 binding mode, Equations 2.7-2.9 show that the Δδ values are all zero (Figure 2.10).

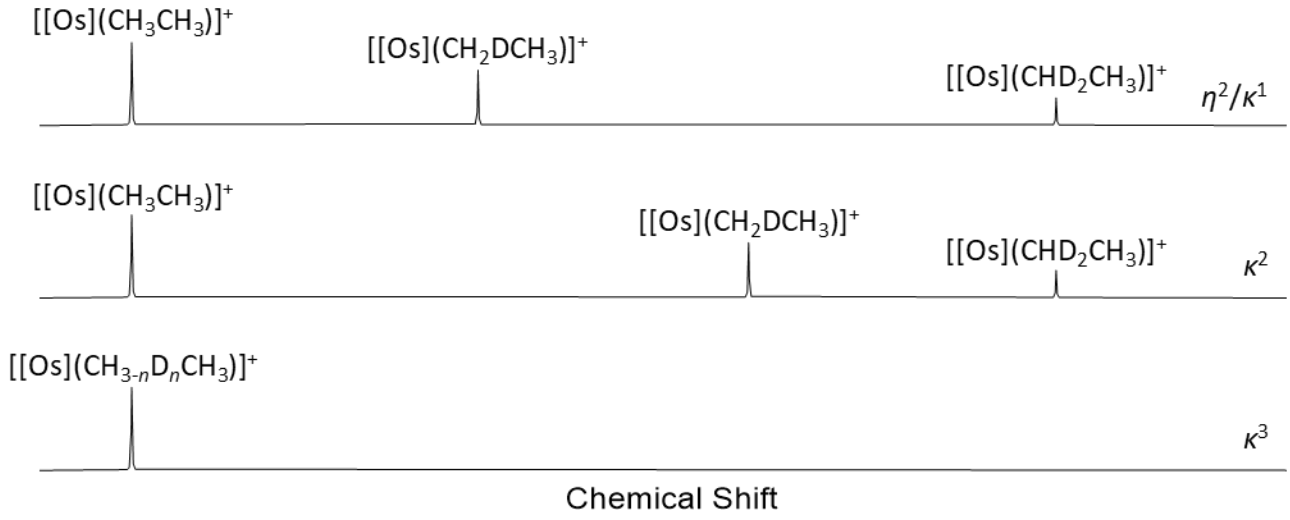

Figure 2.10: Calculated ^{1}H NMR patterns for the α-methyl resonances of [Cp*Os(DFMPM)-($CH_{3-n}D_nCH_3$)]$^+$, where *n* is 0-2, for the η^2/κ^1, κ^2, and κ^3 coordination modes. The only assumption is that δ_T is downfield of δ_B.

A 1:2 mixture of Cp*Os(DFMPM)Et and Cp*Os(DFMPM)(Et-d_2) was treated with a 1:3 mixture of HOTf and DOTf in $CDCl_2F$ at -130 °C. A larger amount of the deuterated osmium compound was employed to compensate for the fact that it consisted of several isotopologs, owing to the scrambling that occurs during its synthesis. An excess of the deuterated acid was used, in order to compensate for different rates of protonation vs. deuteration (i.e., a kinetic isotope effect). Because an excess of the acids was used, pre-deuteration of the NMR tube was unnecessary to prevent loss of the deuterium label through exchange with H^+ ions on the surface of the glass.

The reaction afforded a mixture of eight isotopologs, [Cp*Os(DFMPM)($CH_3CH_{3-n}D_n$)]-[OTf] where *n* is 0 or 2, [Cp*Os(DFMPM)($CH_2DCH_{3-n}D_n$)][OTf] where *n* is 0, 1 or 2, [Cp*Os(DFMPM)($CHD_2CH_{3-n}D_n$)][OTf] where *n* is 0 or 1, and [Cp*Os(DFMPM)($CD_3CH_{3-n}D_n$)]-[OTf], where *n* is 0; the lattermost of these isotopologs is silent in the ^{1}H NMR spectrum. The experimental result is as follows: the Δδ values for the α-methyl group of the bound ethane increase

with increasing deuteration (Figure 2.11). This result proves that the coordination of the ethane to the osmium involves only one bridging hydrogen atom. This is the same binding mode as that seen for the methane analog.

^{1}H NMR spectra of the mixture were collected at -130, -120, -110, -100, and -90 °C. The relatively large linewidths of the resonances of the α-CH_3 groups can be ascribed to unresolved coupling to the β-methyl protons, and also to the presence of multiple deuterated isotopologs. We solved Equations 2.1-2.3 for δ_T, δ_B, and ΔE_{BI} at each temperature; the results suggest that these parameters show no clear temperature-dependence (and there should be very little over this temperature range). Therefore, we averaged the values, yielding $\delta_T = 1.99 \pm 0.17$, $\delta_B = -10.99 \pm 0.32$, and $\Delta E_{BI} = 0.322 \pm 0.012$ kcal/mol. According to these values, the terminal hydrogens of the ethane complex are significantly deshielded compared to the terminal hydrogens of the methane analog ($\delta_T = 0.39 \pm 0.05$), and the bridging hydrogen of the ethane complex is significantly shielded compared to the bridging hydrogen of the methane analog ($\delta_B = -8.92 \pm 0.17$).[41]

In order to calculate J_T and J_B, Cp*Os(DFMPM)(Et-$^{13}C_1$) was treated with a 1:3 mixture of HOTf and DOTf in $CDCl_2F$ at -130 °C to generate a mixture of four isotopologs: Cp*Os(DFMPM)($^{13}CH_3$-CH_3)$^+$, Cp*Os(DFMPM)($^{13}CH_2D$-CH_3)$^+$, Cp*Os(DFMPM)(CH_3-$^{13}CH_3$)$^+$, and Cp*Os(DFMPM)(CH_2D-$^{13}CH_3$)$^+$. ^{1}H NMR spectra were acquired at -130, -120, -110, -100, and -90 °C. Because the carbon-13 label was scrambled, the ^{1}H NMR resonance for the α-methyl group of the undeuterated ethane ligand consists of two overlapping components: a broad doublet due the isotopolog in which the ^{13}C label is in the α site, and a broad singlet due to the isotopolog in which the ^{13}C label is in the β site. Because the ^{13}C label is equally partitioned between the α

and β sites, the ^{1}H NMR line shape in both the undeuterated and singly-deuterated regions appears (deceptively) to be a 1:2:1 triplet (Figure 2.12).

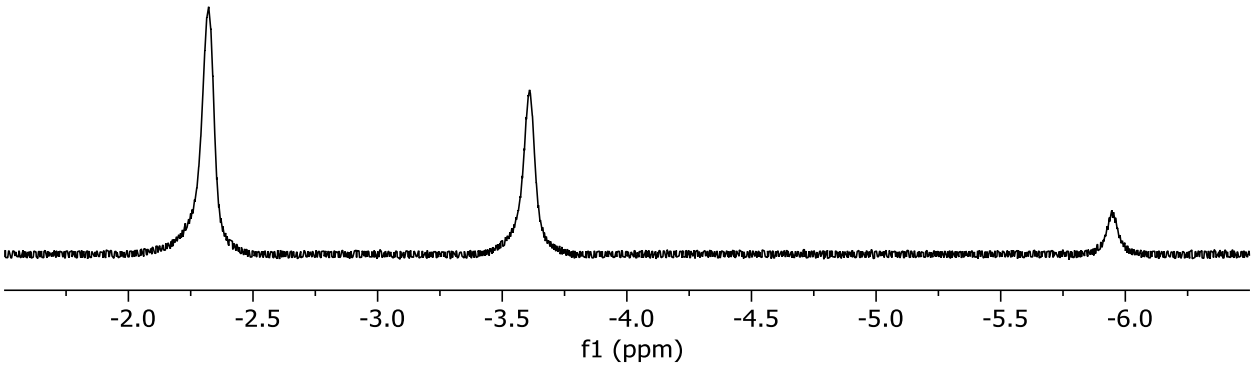

Figure 2.11: The α-methyl region of the ^{1}H NMR spectrum of the reaction between a mixture of Cp*Os(DFMPM)Et and Cp*Os(DFMPM)(Et-d_2) and a mixture of HOTf and DOTf in $CDCl_2F$ at -130 °C. The increase in Δδ with an increase in deuteration is diagnostic of a η^2/κ^1 binding mode. In this spectrum, the $^{3}J_{HH}$ coupling between the α and β sites is obscured owing to unresolved coupling to deuterium and the presence of multiple deuterated isotopologs.

The overlapping resonances were deconvoluted by simulating the experimental spectra with the spin simulation package in MestReNova. From the resulting average value of J as a function of the extent of deuteration, Equations 2.1-2.3 can be adapted to calculate J_T and J_B by substituting in the coupling constants for the chemical shifts. If we make the reasonable assumption that ΔE_{BI} does not change significantly with carbon-13 labeling, the equations can be solved to yield J_T = 144 ± 3 Hz and J_B = 74 ± 4 Hz. These values are equal within error to those of J_T (144 ± 4 Hz) and J_B (83 ± 11 Hz) that Sempsrott calculated for [Cp*Os(DFMPM)(CH_4)]-[$N(SO_2CF_3)_2$].[41]

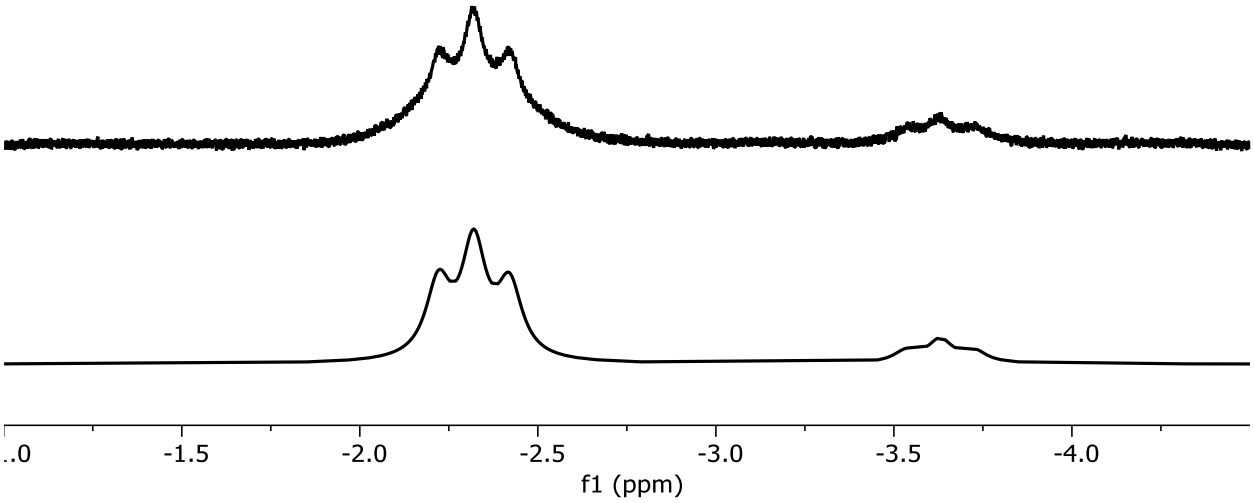

Figure 2.12: Experimental (top) and simulated (bottom) ^{1}H NMR spectra in the α-methyl region of the reaction between Cp*Os(DFMPM)(Et-$^{13}C_1$) and a mixture of HOTf and DOTf at -130 °C. There are two sets of overlapping resonances due to scrambling of the carbon-13 label during the synthesis of Cp*Os(DFMPM)(Et-$^{13}C_1$). In this spectrum, the $^{3}J_{HH}$ coupling between the α and β sites, as well as the $^{2}J_{CH}$ coupling constant when the ^{13}C label is in the β site, are smaller than the linewidth.

General Observations on the Coordination of Alkanes to [Cp*Os(DFMPM)]$^{+}$. DFT studies of the coordination of methane to [Cp*Os(L_2)]$^{+}$, where L_2 is a diphosphine ligand, indicate that the κ^1 coordination mode is lower in energy than the η^2 coordination mode.[50-51] In contrast, in most other reports of transition metal alkane complexes, the alkane is thought to be bound in an η^2 fashion, in which both a hydrogen atoms and the proximal carbon atom are involved in bonding to the metal center.[15, 31-34, 39-40, 52-53] Interestingly, protonation of Brookhart's rhodium methyl and ethyl complexes results in an upfield ^{13}C NMR shift for the proximal carbon atoms.[39-40] Ball claimed that such upfield shifts of the proximal carbon atom in the ^{13}C NMR spectrum are indicative of direct interaction between carbon and the transition metal.[15] However, the rhodium(I) alkane complexes reported by Macgregor and Weller have close Rh-C distances (2.38-2.52 Å) but no ^{13}C NMR resonances upfield of δ 0,[32, 34, 52] suggesting that ^{13}C NMR chemical shifts may not

be the best method of determining whether or not there is direct interaction between a transition metal and a carbon atom. Sempsrott explained the strong shielding in the ^{13}C NMR spectrum of $[Cp^*Os(DFMPM)(CH_4)]^+$ (δ -45.1) in terms of a diamagnetic anisotropy effect; the weak interaction between the CH_4 and the osmium atom lowers the energy of some of the d-orbitals and creates low-lying paramagnetic excited states that can mix with the ground state.[41]

We find that the hydrogen and carbon atoms of the β-CH_3 group of the ethyl ligand of Cp*Os(DFMPM)Et shift upfield in the ^1H and ^{13}C NMR spectra when the compound is protonated to $[Cp^*Os(DFMPM)(CH_3CH_3)]^+$ (Figure 2.13). For comparison, protonation of Cp*Os(DFMPM)Me has little effect on the ^{13}C NMR resonance of the carbon atom.[41]

As mentioned above, the bridging hydrogen of the ethane compound is significantly shielded compared to the bridging hydrogen of the methane analog, whereas the terminal hydrogen atoms of the α-CH_3 groups are significantly deshielded compared to the terminal hydrogens in the methane analog.[41] The different shielding behavior of the methane and ethane complexes requires some explanation. Let us assume that the diamagnetic anisotropy generated by the weakly-bound alkane ligand is characterized by a cone whose axis is aligned with the metal-alkane bond. Nuclei that lie inside the cone are shielded, whereas nuclei that lie outside of the cone are deshielded. In the methane complex, rotation about the C-H_B bond is rapid, and this motion means that all three terminal hydrogen atoms spend some time within the shielding region. For the ethane complex, the presence of the β-Me group means that there will be a preferred rotameric conformation with respect to the C-H_B bond axis. It is possible that, in the preferred conformation, the terminal hydrogens in the ethane complex spend most or all of their time outside the shielding region of the diamagnetic anisotropy, causing them to be deshielded.

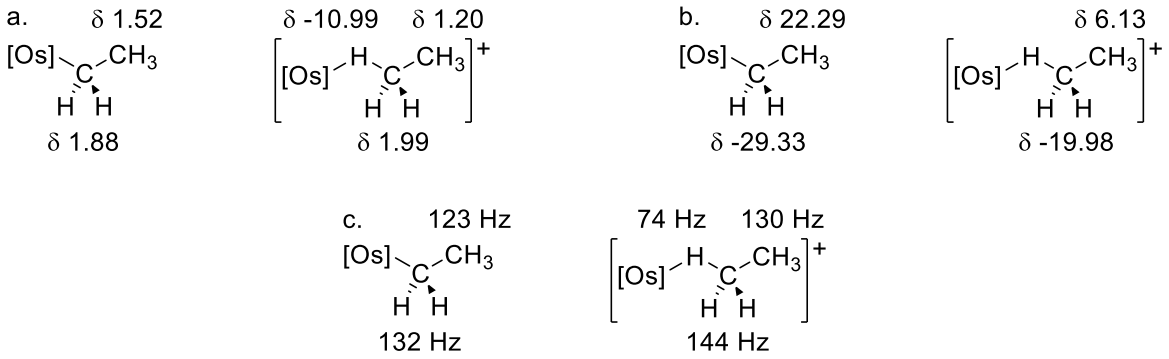

Figure 2.13: NMR data for the ethyl and ethane complexes of $[Cp^*Os(DFMPM)]^+$. a. ^1H NMR chemicals shifts. b. ^{13}C NMR chemical shifts. c. $^1J_{CH}$ coupling constants.

Preliminary Investigation of Cp*Os(DFMPM)Np. We attempted to prepare the neopentyl complex Cp*Os(DFMPM)Np, where Np = CH_2CMe_3. The reaction between Cp*Os(DFMPM)Br and $ZnNp_2$ is slow, and conversion of the bromo compound to products takes more than 10 days at 80 °C, even with 30 molar equivalents of $ZnNp_2$. The reaction products were not separable by sublimation. TMEDA catalyzes the consumption of Cp*Os(DFMPM)Br but, as seen for the ethyl analog, a significant amount of Cp*Os(DFMPM)H is formed. Reactions between Cp*Os(DFMPM)(OTf) and either $ZnNp_2$ or NpLi produced intractable mixtures.

One compound that is a product in all of these reactions (as judged by its characteristic ^{19}F NMR shifts) is the hydride Cp*Os(DFMPM)H. Because the neopentyl ligand does not contain any β-hydrogens and, therefore, cannot undergo β-hydrogen elimination, this hydride ligand must be generated by some other mechanism, such as activation of the solvent. It is possible that the similar formation of Cp*Os(DFMPM)H in the reaction of Cp*Os(DFMPM)(OTf) with $ZnEt_2$ at room temperature, which we concluded cannot occur by loss of ethylene from Cp*Os(DFMPM)($H_2C=CH_2$)(H), occurs in this same way.

Conclusions

Several of the synthetic procedures previously devised to prepare the phosphine and osmium complexes in this project were modified to increase their reproducibility and their safety. The scale of the reaction to produce $Cl_2PCH_2PCl_2$ was reduced by a factor of 2, which aids in keeping the exothermic reactions under control. Anhydrous NaOPh is more safely and reliably obtained through deprotonation of PhOH by NaOH than by NaH. The use of pentane instead of diethyl ether as the reaction solvent for synthesizing $(PhO)_2PCH_2P(OPh)_2$ simplifies the isolation of the product. The reaction to synthesize $(CF_3)_2PCH_2P(CF_3)_2$ was made safer by slowing the rate of addition of the trifluoromethylating agent CF_3SiMe_3. Finally, in the synthesis of Cp*Os(DFMPM)Br, a large increase in yield was obtained by reversing the order of addition of the zinc and phosphine; the reaction between $[Cp^*OsBr_2]_2$ and DFMPM should be allowed to produce Cp*Os(DFMPM)Br_2 before addition of zinc.

Alkylation of these osmium complexes are best performed by treating Cp*Os(DFMPM)Br with alkylzinc reagents in toluene at 80 °C for 16 h. The use of alkyllithium or alkylmagnesium reagents results in deprotonation of the DFMPM ligand rather than alkylation of the osmium. The use of a more labile leaving group (i.e., OTf^- instead of Br^-) and/or the addition of a catalyst (TMEDA) leads to detrimental side reactions and results in the formation of significant amounts of Cp*Os(DFMPM)H.

Protonation of Cp*Os(DFMPM)Et by HOTf at -130 °C affords the ethane coordination complex [Cp*Os(DFMPM)(CH_3CH_3)][OTf]. The ethane ligand is desymmetrized by the bind, so that the proximal and distal methyl groups are chemically inequivalent; furthermore, we see no evidence of exchange between these two environments. IPR experiments show that ethane is bound to the osmium center by means of one bridging hydrogen atom; the interaction leads to a

significant weakening of the C-H bond, so that the $^1J_{CH}$ coupling constant is reduced from ca. 120 Hz in free ethane to 74 ± 4 Hz. Concomitantly, $^1J_{CH}$ coupling constants for the two terminal hydrogen atoms on the proximal methyl group increase from 120 Hz to 144 ± 4 Hz.

The coordination of the ethane to $[Cp^*Os(DFMPM)]^+$ is marginally stronger than that of methane. The ethane complex has a higher onset temperature for dissociation than the methane complex; there was no measurable dissociation of the ethane complex at -105 °C over the course of 1 h. An Eyring plot of the dissociation of the ethane complex suggests that the increased stability of the ethane complex compared to the methane complex is due to a lower entropy of activation but the error in the data is too large to be conclusive. The coordination behavior of alkanes with $[Cp^*Os(DFMPM)]^+$ and with $[(PONOP)Rh]^+$ are different, so that with the current data one cannot make generalizations about how alkanes coordinate to different metal centers. Both methane and ethane coordinate to $[Cp^*Os(DFMPM)]^+$ through one bridging hydrogen atom; this coordination mode differs from the η^2 coordination proposed to be present in alkane complexes of $[(PONOP)Rh]^+$.[39-40]

Experimental Details

Unless otherwise stated, all operations were conducted under argon using standard Schlenk line and glovebox techniques. Solvents were dried over CaH_2 (CH_2Cl_2), sodium-benzophenone ketyl (Et_2O, pentane, and THF), or Mg (MeOH) and distilled before use. Al powder (325 mesh) and iodine were purchased from Alfa Aesar; dibromomethane, 2 M HCl in Et_2O, Mg turnings, PCl_3, $POCl_3$, and $ZnEt_2$ (14.5 wt% in toluene) from Sigma-Aldrich; CF_3SiMe_3, and CsF, from Oakwood Chemicals; and HOTf was purchased from SynQuest Laboratories. These reagents were used without further purification. $[Cp^*OsBr_2]_2$,[54] $Cp^*Os(DFMPM)(CH_3)$,[41] $CDCl_2F$,[55] and

DOTf[56] were prepared according to literature procedures. $Zn(CD_2CH_3)_2$ and $Zn(^{13}CH_2CH_3)$ were prepared as described in Chapter 1.

Elemental analyses were performed by the School of Chemical Sciences Microanalysis Laboratory at the University of Illinois at Urbana-Champaign. Unless otherwise stated, NMR spectra were acquired on Varian (400 MHz, 500 MHz, and 600 MHz) and Bruker (500 MHz) spectrometers at room temperature. ^{1}H and ^{13}C NMR spectra are reported in δ units (positive chemical shifts to higher frequency) relative to TMS as determined from residual solvent signals.[57] ^{19}F and ^{31}P NMR spectra are reported in δ units relative to external samples of $CFCl_3$ in $CHCl_3$ and H_3PO_4 in H_2O, respectively. NMR spectra were processed with the MestReNova NMR software package. X-ray crystallographic data were collected by the George L. Clark X-Ray Facility and 3M Materials Laboratory.

Bis(dichlorophosphino)methane, $Cl_2PCH_2PCl_2$. This compound was synthesized by a modified literature procedure.[41, 43-44] To a 2-L three-necked round-bottomed flask equipped with a mechanical stirrer was added Al powder (62.5 g, 2.32 mol), CH_2Cl_2 (500 mL, 7.83 mol), CH_2Br_2 (45.0 mL, 0.641 mol), and a few crystals of I_2. The mixture was heated to reflux for 4 days to afford a dark slurry. To a 3-L three-necked round-bottomed flask equipped with a mechanical stirrer was added PCl_3 (250 mL, 2.86 mol). The Al/CH_2Cl_2 reaction mixture was cannula transferred into the PCl_3 using a Teflon cannula (ID: 3/8") over 1.5 h while vigorously stirring both flasks. CAUTION: The reaction is extremely exothermic. The Al/CH_2Cl_2 mixture should be added to the PCl_3 in as small portions as possible and paused if effervescence is observed. The reaction mixture was heated to reflux overnight. The mixture was cooled to room temperature and $POCl_3$ (250 mL, 2.67 mol) was added. The mixture was heated to reflux for 4 h. The flask was sealed and cooled to -20 °C overnight, affording a yellow solution over grey solids. The solution

was decanted and the remaining solids were removed by filtration. The filtrate was taken to dryness under vacuum and the product was purified from the resulting oil by distillation (300 mTorr, 56 °C). Yield: 55.33 g (22%). ^{1}H NMR (C_6D_6): δ 2.47 (t, $^{2}J_{PH}$ = 17 Hz). ^{31}P{^{1}H} NMR (C_6D_6): δ 176.02 (s).

Bis(diphenoxyphosphino)methane, $(PhO)_2PCH_2P(OPh)_2$. This compound was synthesized by a modified literature procedure.[41, 45-46] To a 1-L three-necked round-bottomed flask was added a solution of NaOH (23.307 g, 583 mmol) in MeOH (400 mL). To this solution was added a solution of PhOH (59.194 g, 629 mmol) in toluene (300 mL). The methanol was removed by distillation until the temperature of the distillate was 110 °C, adding additional toluene as necessary. The mixture was allowed to cool to room temperature and the supernatant was removed by filter cannula. The flocculent white powder was washed with pentane (3 × 50 mL). The powder was suspended in pentane (500 mL) and $Cl_2PCH_2PCl_2$ (15.0 mL, 110 mmol) was added dropwise. The mixture was filtered and the solids washed with pentane (3 × 50 mL). The pentane was removed by distillation, affording a cloudy viscous oil. The oil was dissolved in Et_2O (100 mL) and decanted into a fresh flask. The Et_2O was removed under vacuum at 50 °C to afford a colorless oil. Yield: 34.89 g (71%). ^{1}H NMR (C_6D_6): δ 7.10 (d, $^{3}J_{HH}$ = 8 Hz, 8 H, ortho-H), 6.96 (t, $^{3}J_{HH}$ = 8 Hz, 8 H, meta-H), 6.79 (4 H, t, $^{3}J_{HH}$ = 7 Hz, para-H), 2.75 (t, $^{2}J_{PH}$ = 17 Hz, 2 H, PCH_2P). ^{31}P{^{1}H} NMR (C_6D_6): δ 177.43 (s).

Bis[bis(trifluoromethyl)phosphino]methane, $(CF_3)_2PCH_2P(CF_3)_2$, DFMPM. This compound was synthesized by a modified literature procedure.[41] CsF (16.812 g, 111 mmol) was finely ground with a mortar and pestle and then dried overnight under vacuum at 125 °C. The powder was suspended in Et_2O (25 mL) and $(PhO)_2PCH_2P(OPh)_2$ (35.0 mL of a 0.96 M solution in Et_2O, 33.6 mmol) was added. The mixture was placed in a room temperature water bath and

CF_3SiMe_3 (22.0 mL, 149 mmol) was added dropwise. CAUTION: No more than 4.5 equivalents of CF_3SiMe_3 should be added to $(PhO)_2PCH_2P(OPh)_2$ initially; if more than this amount is added, the mixture can react violently and overpressurize the reaction vessel. The addition of CF_3SiMe_3 should be paused if effervescence is observed at any time. The use of a blast shield is strongly recommended for the addition. The mixture was allowed to stir overnight, eventually affording a cloudy amber mixture. The reaction was monitored by $^{31}P\{^1H\}$ NMR spectroscopy and additional CF_3SiMe_3 should be added if the substitution is incomplete. The mixture was filtered and the solids were washed with Et_2O (50 mL). The filtrate and washings were combined and cooled to 0 °C. A solution of HCl (20 mL of a 2 M solution in Et_2O, 40 mmol) was added dropwise. A white powder precipitated from solution and the solution color turned yellow. The mixture was allowed to stir overnight and then was filtered. The solids were washed with Et_2O (50 mL). The filtrate and washing were combined, and the volatile material was transferred under vacuum to a separate flask. From this distillate, the majority of the Et_2O was removed by distillation at atmospheric pressure using a 15-cm Vigreux column in an oil bath at 55 °C. The non-distilled residue was collected to afford the product as a 8 mL of a 1.6 M solution of $(CF_3)_2PCH_2P(CF_3)_2$ in Et_2O. Yield: 6.40 g (54%). ^1H NMR (C_6D_6): δ 2.20 (t, $^2J_{PH}$ = 3 Hz), ^{19}F NMR (C_6D_6): -55.49 (m). $^{31}P\{^1H\}$ NMR: δ -6.33 (m).

(η^5-Pentamethylcyclopentadienyl)(κ^1-bis[bis(trifluoromethyl)phosphino]methane)-tribromoosmium(IV), Cp*Os(DFMPM)Br$_3$. To a suspension of $[Cp^*OsBr_2]_2$ (0.999 g, 1.03 mmol) in Et_2O (30 mL) was added DFMPM (0.600 mL, 1.11 mmol). The mixture was allowed to stir overnight, affording a cloudy red mixture. The mixture was filtered and the resulting solid was dried under vacuum to afford the product as a reddish brown powder. X-ray quality crystals can be grown by cooling a saturated CH_2Cl_2 solution. Yield: 0.185 g (10%). ^1H NMR (C_6D_6): δ

3.73 (dd, J_{PH} = 11 Hz, $^2J_{PH}$ = 4 Hz, 2 H, PCH_2P), 1.17 (d, $^4J_{PH}$ = 1 Hz, 15 H, Cp*). ^{19}F NMR (C_6D_6): δ -49.57 (d, $^2J_{PF}$ = 56 Hz, 6 F), -54.68 (d, $^2J_{PF}$ = 70 Hz, 6 F).

(η^5-Pentamethylcyclopentadienyl)(κ^1-bis[bis(trifluoromethyl)phosphino]methane)-dibromoosmium(III), Cp*Os(DFMPM)Br$_2$. This product was isolated as a red solid by taking the Et_2O filtrate from the above reaction to dryness under vacuum. X-ray quality crystals can be grown by cooling a saturated Et_2O solution. Yield: 1.336 g (78%). ^1H NMR (C_6D_6): δ 31.47 (br, 15 H, Cp*, fwhm = 500 Hz), 15.94 (br, 2 H, PCH_2P, fwhm = 250 Hz). ^{19}F NMR (C_6D_6): δ -33.38 (br, 6 F, fwhm = 250 Hz), -39.07 (br, 6 F, fwhm = 400 Hz).

(η^5-Pentamethylcyclopentadienyl)(κ^2-bis[bis(trifluoromethyl)phosphino]methane)-bromoosmium(II), Cp*Os(DFMPM)Br. To $[Cp^*OsBr_2]_2$ (1.748 g, 1.80 mmol) was added Et_2O (100 mL) and DFMPM (2.20 mL of a 1.85 M solution in Et_2O, 4.07 mmol). The mixture was stirred overnight, affording a cloudy red mixture. Zn powder (2.411 g, 36.9 mmol) was added. The solution became bright orange after several minutes. The mixture was filtered and the solids were washed with Et_2O (3 × 20 mL). The Et_2O was removed under vacuum and the product was extracted with pentane (3 × 30 mL). The pentane was removed under vacuum and the product was purified by sublimation (10^{-2} Torr, 100 °C). Yield: 1.813 g (66%). ^1H NMR (C_6D_6): δ 5.34 (dt, $^2J_{HH}$ = 17 Hz, $^2J_{PH}$ = 11 Hz, 1 H, PCH_2P), 3.44 (dt, $^2J_{HH}$ = 17 Hz, $^2J_{PH}$ = 12 Hz, 1 H, PCH_2P), 1.63 (t, $^4J_{PH}$ = 2 Hz, 15 H, Cp*). ^{19}F NMR (C_6D_6): δ -55.18 (d, $^2J_{PF}$ = 62 Hz, 6 F), -59.89 (d, $^2J_{PF}$ = 71 Hz, 6 F). $^{31}P\{^1H\}$ NMR (C_6D_6): δ -25.99 (m).

(η^5-Pentamethylcyclopentadienyl)(κ^2-bis[bis(trifluoromethyl)phosphino]methane)-ethylosmium(II), Cp*Os(DFMPM)Et. To a solution of Cp*Os(DFMPM)Br (0.105 g, 0.138 mmol) in toluene (20 mL) was added $ZnEt_2$ (0.300 mL of a 14.5 wt% solution in toluene, 0.305 mmol). The solution was heated to 80 °C overnight to afford a light yellow solution, and then was

taken to dryness under vacuum. The residue was extracted with pentane (3 × 10 mL), and the pentane extracts were filtered, combined, and taken to dryness under vacuum. The product was purified by sublimation (10^{-2} Torr, 100 °C). Yield: 0.071 g (72%). Dec: 164 °C. Anal. Calc. for $C_{17}H_{22}F_{12}OsP_2$: C, 28.9; H, 3.14; N, 0.00. Found: C, 28.24; H, 3.26; N, 0.19. ^{1}H NMR (C_6D_6): δ 5.15 (dt, $^2J_{HH}$ = 17 Hz, $^2J_{PH}$ = 12 Hz, 1 H, PCH_2P), 3.26 (dt, $^2J_{HH}$ = 17 Hz, $^2J_{PH}$ = 12 Hz, 1 H, PCH_2P), 1.88 (m, 2 H, $OsCH_2CH_3$), 1.64 (t, $^4J_{PH}$ = 2 Hz, 15 H, Cp*), 1.56 (t, $^3J_{HH}$ = 7 Hz, 3 H, $OsCH_2CH_3$). ^{13}C{^{1}H} NMR (C_6D_6): δ 94.70 (t, $^2J_{PC}$ = 3 Hz, C_5Me_5), 54.23 (t, $^1J_{PC}$ = 25 Hz, PCH_2P), 22.29 ($OsCH_2CH_3$), 10.07 (s, C_5Me_5), -29.33 ($OsCH_2CH_3$). ^{19}F NMR (C_6D_6): δ -58.69 (d, $^2J_{PF}$ = 57 Hz, 6 F), -61.34 (d, $^2J_{PF}$ = 70 Hz, 6 F). ^{31}P{^{1}H} NMR (C_6D_6): δ -31.62 (m). IR (cm^{-1}): 2364 (w), 2295 (w), 2234 (w), 1261 (w), 1180 (vs), 1145 (vs), 1108 (m), 1083 (m), 1031 (m), 988 (w), 884 (w), 769 (s), , 704 (s), 649 (m), 598 (s), 558 (s), 519 (m), 489 (s), 450 (s).

Synthesis of [Cp*Os(DFMPM)(ethane)][OTf]. A detailed description of the apparatus and procedure is given in Appendix B. In a glovebox, an oven-dried 5-mm NMR tube topped with a 14/20 female ground glass joint was charged with Cp*Os(DFMPM)Et (10 mg, 0.014 μmol). While still in the glovebox, the tube was fitted with a spinner, a gas inlet adapter, and a vacuum transfer apparatus, using Krytox™ grease on all ground glass joints. The stopcocks were closed and the apparatus was brought out of the glovebox and attached to a Schlenk line through the vacuum transfer apparatus and the gas inlet adapter. The inert gas used in the Schlenk line was N_2, not argon, because the latter condenses too easily in liquid nitrogen. The $CDCl_2F$ source flask was attached to the other end of the vacuum transfer apparatus. The apparatus was evacuated and the NMR tube was cooled with liquid N_2. The stopcocks to the Schlenk line were closed so that the apparatus was under static vacuum. The stopcock for the $CDCl_2F$ source flask was opened briefly to condense a minimal amount of $CDCl_2F$ in the NMR tube. The NMR tube was allowed

to warm and the Cp*Os(DFMPM)Et was dissolved in the $CDCl_2F$. The solution was frozen with liquid N_2 and additional $CDCl_2F$ was vacuum transferred onto the frozen Cp*Os(DFMPM)Et solution. The second portion of $CDCl_2F$ was allowed to thaw while taking care to keep the Cp*Os(DFMPM)Et solution frozen. The NMR tube was back-filled with N_2 and the vacuum transfer apparatus was removed. TfOH (5 μL, 0.06 μmol) was added to the thawed $CDCl_2F$ using a glass microsyringe. The TfOH solution was frozen and the NMR tube was flame sealed under dynamic vacuum. The sample was kept in liquid nitrogen until it was inserted into the NMR probe, which was pre-cooled to -130 °C. The contents of the NMR tube were allowed to thaw inside the probe and mix at -130 °C for 30 min before spectra were collected.

(κ^2-Bis[bis(trifluoromethyl)phosphino]methane)(ethane)(η^5-pentamethylcyclopenta-dienyl)osmium(II) triflate, [Cp*Os(DFMPM)(CH_3CH_3)][OTf]. ^{1}H NMR ($CDCl_2F$, -100 °C): δ 6.02 (dt, $^2J_{HH}$ = 18 Hz, $^2J_{PH}$ = 11 Hz, 1 H, PCH_2P), 4.12 (dt, $^2J_{HH}$ = 18 Hz, $^2J_{PH}$ = 11 Hz, 1 H, PCH_2P), 2.05 (s, 15 H, Cp*), 1.20 (q, $^3J_{HH}$ = 6 Hz, 3 H, Os-CH_3CH_3), -2.34 (q, $^3J_{HH}$ = 6 Hz, 3 H, Os-CH_3CH_3).

(η^5-Pentamethylcyclopentadienyl)(κ^2-bis(bis(trifluoromethyl)phosphino)methane)-(ethyl-d_2)osmium(II), Cp*Os(DFMPM)(Et-d_2). This mixture of isotopologs was prepared analogously to Cp*Os(DFMPM)Et from Cp*Os(DFMPM)Br (0.223 g, 0.295 mmol) and $Zn(CD_2CH_3)_2$ (0.400 mL of a 1.2 M solution in Et_2O, 0.48 mmol). Yield: 0.170 g (82%). ^{1}H NMR (C_6D_6): δ 5.15 (dt, $^2J_{HH}$ = 17 Hz, $^2J_{PH}$ = 12 Hz, 1 H, PCH_2P), 3.25 (dt, $^2J_{HH}$ = 17 Hz, $^2J_{PH}$ = 12 Hz, 1 H, PCH_2P), 1.88 (m, $OsCH_2CH_3$), 1.65 (t, $^4J_{PC}$ = 2 Hz, 15 H, Cp*), 1.56 (m, $OsCH_2CH_3$). ^{19}F NMR (C_6D_6): δ -58.69 (m, 6 F), -61.36 (d, $^2J_{PF}$ = 70 Hz, 6 F). ^{31}P{^{1}H} NMR (C_6D_6): δ -31.52 (m).

(η^5-Pentamethylcyclopentadienyl)(κ^2-bis[bis(trifluoromethyl)phosphino]methane)-(ethyl-$^{13}C_1$)osmium(II), Cp*Os(DFMPM)(Et-$^{13}C_1$). This mixture of isotopologs was prepared analogously to Cp*Os(DFMPM)Et using Cp*Os(DFMPM)Br (0.109 g, 0.144 mmol) and a solution of Zn($^{13}CH_2CH_3$)$_2$ (0.490 g, 0.535 mmol) in Et_2O. Yield: 0.083 g (82%). ^{1}H NMR (C_6D_6): δ 5.16 (dt, $^2J_{HH}$ = 17 Hz, $^2J_{PH}$ = 12 Hz, 1 H, PCH_2P), 3.27 (dt, $^2J_{HH}$ = 17 Hz, $^2J_{PH}$ = 12 Hz, 1 H, PCH_2P), 1.88 (dq, $^1J_{CH}$ = 132 Hz, $^3J_{HH}$ = 8 Hz, Os$^{13}C\mathit{H}_2CH_3$, 1.88 (m, Os$C\mathit{H}_2{}^{13}CH_3$), 1.65 (t, $^4J_{PC}$ = 2 Hz, 15 H, C_5Me_5), 1.56 (dt, $^1J_{CH}$ = 123 Hz, $^3J_{HH}$ = 8 Hz, Os$CH_2{}^{13}C\mathit{H}_3$, 1.56 (td, $^3J_{HH}$ = 8 Hz, $^2J_{CH}$ = 5 Hz, Os$^{13}CH_2C\mathit{H}_3$). ^{13}C{^{1}H} NMR (C_6D_6): δ 94.70 (t, $^2J_{PC}$ = 3 Hz, C_5Me_5), 54.24 (s, PCH_2P), 22.29 (t, $^3J_{PC}$ = 7 Hz, Os$CH_2\mathit{C}H_3$), 10.07 (s, $C_5\mathit{Me}_5$), -29.33 (t, $^2J_{PC}$ = 7 Hz, Os$\mathit{C}H_2CH_3$). ^{19}F NMR (C_6D_6): δ -58.69 (d, $^2J_{PF}$ = 58 Hz, 6 F), -61.34 (d, $^2J_{PF}$ = 66 Hz, 6 F). ^{31}P{^{1}H} NMR (C_6D_6): δ -31.75 (m).

Synthesis of Isotopically Labeled [Cp*Os(DFMPM)(ethane)][OTf]. The procedure described above to prepare natural abundance [Cp*Os(DFMPM)(ethane)][OTf] was followed. To make a mixture of [Cp*Os(DFMPM)(ethane-d$_n$)][OTf], where *n* is 0-3, a mixture of Cp*Os(DFMPM)Et (7 mg, 10 μmol) and Cp*Os(DFMPM)(Et-d_2) (14 mg, 20 μmol) was protonated with a solution of HOTf in DOTf (1:3, 10 μL). To make a mixture of [Cp*Os(DFMPM)(ethane-$^{13}C_1$-d$_n$)][OTf], where *n* is 0-1, Cp*Os(DFMPM)(Et-$^{13}C_1$) (10 mg, 14 μmol) was protonated with a solution of HOTf in DOTf (1:3, 5 μL).

(κ^2-Bis[bis(trifluoromethyl)phosphino]methane)(ethane-d$_n$)(η^5-pentamethylcyclopenta-dienyl)osmium(II) triflate, [Cp*Os(DFMPM)(ethane-d$_n$)][OTf]. ^{1}H NMR ($CDCl_2F$, -100 °C): δ 6.02 (dt, $^2J_{HH}$ = 17 Hz, $^2J_{PH}$ = 11 Hz, 1 H, PCH_2P), 4.12 (dt, $^2J_{HH}$ = 18 Hz, $^2J_{PH}$ = 12 Hz, 1 H, PCH_2P), 2.05 (s, 15 H, Cp*), 1.20 (m, Os-$CH_3C\mathit{H}_3$), -2.34 (m, Os-$C\mathit{H}_3CH_3$), -3.42 (m, Os-$C\mathit{H}_2DCH_3$), -5.14 (m, Os-$C\mathit{H}D_2CH_3$).

(κ^2-Bis[bis(trifluoromethyl)phosphino]methane)(ethane-$^{13}C_1$-d$_n$)(η^5-pentamethyl-cyclopentadienyl)osmium(II) triflate, [Cp*Os(DFMPM)(ethane-$^{13}C_1$-d$_n$)][OTf]. ^{1}H NMR ($CDCl_2F$, -130 °C): δ 6.02 (m, PCH_2P), 4.12 (m, PCH_2P), 2.05 (s, Cp*), 1.20 (m, Os-$^{13}CH_3CH_3$), 1.20 (m, Os-$CH_3{}^{13}CH_3$) -2.32 (d, $^1J_{CH}$ = 120 Hz, Os-$^{13}CH_3CH_3$), -2.32 (s, Os-$CH_3{}^{13}CH_3$), -3.63 (d, $^1J_{CH}$ = 115 Hz, Os-$^{13}CH_2DCH_3$), -3.63 (s, Os-$CH_2D{}^{13}CH_3$). ^{13}C NMR ($CDCl_2F$, -130 °C): δ 6.13 (q, $^1J_{CH}$ = 130 Hz, Os-$CH_3{}^{13}CH_3$), -19.98 (q, $^1J_{CH}$ = 120 Hz, Os-$^{13}CH_3CH_3$). The signal-to-noise ratio was not sufficient to identify the chemical shifts of the unlabeled ligands or of the ethane-$^{13}C_1$-d$_1$ isotopomers.

(η^5-Pentamethylcyclopentadienyl)(κ^2-bis[bis(trifluoromethyl)phosphino]methane)-(trifluoromethanesulfonato)osmium(II), Cp*Os(DFMPM)(OTf). To TfOH (0.22 g, 1.5 mmol, obtained by taking 14.5 mL of a 0.1 M solution in CH_2Cl_2 to dryness in vacuum at room temperature) was treated with a solution of Cp*Os(DFMPM)(CH_3) (0.979 g, 1.41 mmol) in pentane (30 mL). An orange powder gradually precipitated from the solution. The solid was collected by filtration and dried under vacuum. Yield: 0.717 g (60%). Unreacted Cp*Os(DFMPM)(CH_3) (32%) was recovered from the filtrate by drying under vacuum. ^{1}H NMR (C_6D_6): δ 5.55 (dt, $^2J_{HH}$ = 17 Hz, $^2J_{PH}$ = 11 Hz, 1 H, PCH_2P), 3.69 (dt, $^2J_{HH}$ = 17 Hz, $^2J_{PH}$ = 13 Hz, 1 H, PCH_2P), 1.46 (s, 15 H, Cp*). ^{19}F NMR (C_6D_6): δ -56.43 (d, $^2J_{PF}$ = 76 Hz, 6 F, DFMPM), -58.99 (d, $^2J_{PF}$ = 72 Hz, 6 F, DFMPM), -77.21 (s, 3 F, OTf). ^{31}P{^{1}H} NMR (C_6D_6): δ -17.97 (m).

(η^5-Pentamethylcyclopentadienyl)[bis(trifluoromethyl)methylphosphine][bis(trifluoromethyl)methoxyphosphine]bromoosmium(II). To a solution of Cp*Os(DFMPM)Br (0.104 g, 0.137 mmol) in THF (20 mL) at -78 °C and was added dropwise EtLi (0.260 mL of a 0.57 M solution in cyclohexane/benzene, 0.148 mmol). The solution was allowed to warm to room temperature and MeOH (1 mL) was added. The solution was taken to dryness under vacuum and

the product was extracted with pentane (3 × 10 mL). The extract was filtered, concentrated, and cooled to -20 °C to afford yellow crystals. Yield: 0.100 g (93%). ^{1}H NMR (C_6D_6): δ 3.50 (d, $^{3}J_{PH}$ = 11 Hz, 3 H, OMe), 2.02 (d, $^{2}J_{PH}$ = 9 Hz, 3 H, PMe), 1.55 (s, 15 H, Cp*). ^{19}F NMR (C_6D_6): δ -58.60 (d, $^{2}J_{PF}$ = 60 Hz, 3 F), -61.36 (d, $^{2}J_{PF}$ = 68 Hz, 3 F), -63.50 ($^{2}J_{PF}$ = 70 Hz, 3 F), -64.95 ($^{2}J_{PF}$ = 76 Hz, 3 F). ^{31}P{^{1}H} (C_6D_6): δ 92.3 (qqd, $^{2}J_{PF}$ = 76 Hz, $^{2}J_{PF}$ = 70 Hz, $^{2}J_{PP}$ = 15 Hz, 1 P, $P(CF_3)_2OMe$), 28.9 (qqd, $^{2}J_{PF}$ = 68 Hz, $^{2}J_{PF}$ = 60 Hz, $^{2}J_{PP}$ = 15 Hz, 1 P, $P(CF_3)_2Me$).

(η^5-Pentamethylcyclopentadienyl)(κ^2-bis[bis(trifluoromethyl)phosphino]methane)-hydridoosmium(II), Cp*Os(DFMPM)H. To a solution of Cp*Os(DFMPM)Br (0.211 g, 0.279 mmol) in toluene (20 mL) was added $ZnEt_2$ (0.550 mL of a 14.5 wt% solution in toluene, 0.560 mmol) and TMEDA (0.090 mL, 0.600 mmol). After 16 h, the solution color was pale yellow. The solution was taken to dryness under vacuum, and the residue was extracted with pentane (3 × 10 mL). The extracts were filtered, combined, and taken to dryness under vacuum. The product was obtained by sublimation (10^{-2} Torr, 55 °C). Yield of crude product: 0.179 g (67%). The product can be purified by recrystallization from a saturated pentane solution. ^{1}H NMR (C_6D_6): δ 4.64 (dtd, $^{2}J_{HH}$ = 17 Hz, $^{2}J_{PH}$ = 11 Hz, $^{4}J_{HH}$ = 3 Hz, 1 H, PCH_2P), 3.24 (dtd, $^{2}J_{HH}$ = 17 Hz, $^{2}J_{PH}$ = 12 Hz, $^{4}J_{HH}$ = 2 Hz, 1 H, PCH_2P), 1.90 (t, $^{4}J_{PH}$ = 2 Hz, 15 H, Cp*), -14.60 (t, $^{2}J_{PH}$ = 24 Hz, $^{4}J_{HH}$ = 3 Hz, $^{4}J_{HH}$ = 2 Hz, 1 H,Os-H). ^{19}F NMR (C_6D_6): δ -63.37 (d, $^{2}J_{PF}$ = 35 Hz, 6 F), -67.48 (d, $^{2}J_{PF}$ = 35 Hz, 6 F). ^{31}P NMR (C_6D_6): δ -25.85 (m).

NMR Data Analysis. NMR data were analyzed as described by Sempsrott.[41] Secondary isotope effects from deuteration of the α-carbon of the bound ethane were estimated to be upfield shifts of δ 0.018 and 0.036 for single or double deuteration based on the ^{1}H{^{2}D} NMR chemical shifts of CH_2DCD_3 and CHD_2CD_3 compared to CH_3CD_3.[58] Our deuteration experiments generate a mixture of isotopologs with varying levels of deuteration of the β-carbon. The secondary isotope

effect on the chemical shift of the CH_3 groups in CH_3CD_3 and CH_3CH_3[58] was taken as an upper bound for the secondary isotope effects due to deuteration of the β-carbon of our ethane coordination complex. Because these effects could not be resolved in our spectra, the secondary isotope effects from deuteration of the β-carbon were incorporated as 0.02 ppm contribution to the uncertainty of the exchange-averaged ^{1}H NMR chemical shifts of the α-carbon. The secondary isotope effect on $^1J_{CH}$ due to deuterium substitution of ethane is -0.2(3) Hz.[59] This value much smaller than the uncertainty of the coupling constants from our spectra (estimated to be 1 Hz). Therefore, the coupling constants deduced for the ethane coordination complex were not adjusted for secondary isotope effects.

General Crystallographic Details.[60] The following details were common to all of the crystal structure determinations; for details about individual compounds, see the SI. Crystals mounted on Nylon fibers with Paratone® oil were transferred onto the diffractometer and kept at -173 °C in a cold nitrogen gas stream. Intensity data were collected on a Bruker D8 Venture kappa diffractometer equipped with a Photon 100 CMOS detector. An Iμs microfocus source provided the Mo Kα radiation (λ = 0.71073 Å) that was monochromated with multilayer mirrors. Standard peak search and indexing procedures gave rough cell dimensions. The collection, cell refinement and integration of intensity data were carried out with the APEX3 software (Bruker). The measured intensities were reduced to structure factor amplitudes and their estimated standard deviations by correction for background, scan speed, and Lorentz and polarization effects. No corrections for crystal decay were necessary. Systematically absent reflections were deleted and symmetry equivalent reflections were averaged to yield the set of unique data.

The initial model was obtained by Patterson methods for Cp*Os(DFMPM)Et and Cp*Os(DFMPM)Br_2, and by direct methods for the other compounds (SHELXS).[61] The

remaining non-hydrogen atoms were located from difference maps obtained from full-matrix least-squares refinements (SHELXL).[61] In the final cycle of least squares, independent anisotropic displacement factors were refined for the non-hydrogen atoms, with isotropic restraints applied to the minor site carbon, oxygen, and fluorine atoms. Hydrogen atoms were placed in idealized positions; the methyl groups were allowed to rotate about the C-X axis to find the best least-squares positions. The displacement parameters for methylene hydrogens were set equal to 1.2 times U_{eq} for the attached carbon; those for methyl hydrogens were set to 1.5 times U_{eq}. Successful convergence was indicated by the maximum shift/error of 0.001 for the last cycle. No correction for decay was necessary, but absorption corrections were conducted by face-indexed or multi-scan methods (SADABS).[62] Data collection and final refinement parameters are given in Tables 2.1 and 2.2. A final analysis of variance between observed and calculated structure factors showed no apparent errors. Solutions were checked with PLATON for missed crystallographic symmetry.

Cp*Os(DFMPM)Br$_2$. Single crystals of Cp*Os(DFMPM)Br$_2$ were grown by cooling a saturated Et$_2$O solution. The systematic absences for $h00$ ($h \neq 2n$), $0k0$ ($k \neq 2n$), and $00l$ ($l \neq 2n$) were uniquely consistent with the space group $P2_12_12_1$. A multi-scan absorption correction was applied, the minimum and maximum transmission factors being 0.50 and 0.75. Five reflections (004, 012, 020, 112, and -112) were obscured by the beamstop and were deleted. The quantity minimized by the least-squares program was $\Sigma w(F_o^2 - F_c^2)^2$, where $w = \{[\sigma(F_o^2)]^2 + (0.0055P)^2 + 5.1509P\}^{-1}$ and $P = (F_o^2 + 2F_c^2)/3$. An isotropic extinction parameter was refined to a final value of $x = 1.22(3) \times 10^{-6}$ where F_c is multiplied by the factor $k[1 + F_c^2 x\lambda^3/\sin 2\theta]^{-1/4}$ with k being the overall scale factor. Analysis of the diffraction intensities that the correct absolute structure had been chosen (Flack parameter = 0). The largest peak in the final Fourier difference map (1.10 eÅ^{-3}) was located 0.77 Å from Os1.

Cp*Os(DFMPM)Br$_3$. Single crystals of Cp*Os(DFMPM)Br$_3$ were grown by cooling a saturated CH_2Cl_2 solution. Systematic absences for $0k0$ ($k \neq 2n$) and $h0l$ ($h + l \neq 2n$) were uniquely consistent with the space group $P2_1/n$. A face-indexed absorption correction was applied, the minimum and maximum transmission factors being 0.026 and 0.321. The -111 reflection was obscured by the beamstop and was deleted. The quantity minimized by the least-squares program was $\Sigma w(F_o^2 - F_c^2)^2$, where $w = \{[\sigma(F_o^2)]^2 + (0.0144P)^2 + 3.4598P\}^{-1}$ and $P = (F_o^2 + 2F_c^2)/3$. An isotropic extinction parameter was refined to a final value of $x = 2.41(7) \times 10^{-6}$ where F_c is multiplied by the factor $k[1 + F_c^2 x\lambda^3/\sin 2\theta]^{-1/4}$ with k being the overall scale factor. The largest peak in the final Fourier difference map (0.82 eÅ^{-3}) was located 0.99 Å from Os1.

Cp*Os[P(CF$_3$)$_2$Me][P(CF$_3$)$_2$Me]Br. Single crystals of Cp*Os[P(CF$_3$)$_2$Me][P(CF$_3$)$_2$Me]-Br were grown by cooling a saturated pentane solution. The orthorhombic symmetry and systematic absences suggested the space group $P2_12_12_1$, which was confirmed by the success of the subsequent refinement. A multi-scan absorption correction was applied, the minimum and maximum transmission factors being 0.3296 and 0.7461. Three reflections (002, 020, 012, and 101) were obscured by the beamstop, and four others (013, 201, 021, and 004) were later found to be statistical outliers; these reflections were deleted. The two phosphorus ligands were disordered with one another as entire units; as a result, the P-Me and P-OMe groups, and also the carbon and fluorine atoms of all four CF_3 groups, were disordered over two sites (only the phosphorus locations were unaffected by the disorder). The occupancies of the two sites were constrained to add to 1; the site occupancy factor for the major occupancy CF_3, P-Me, P-OMe groups refined to 0.686(6). All P-C distances were restrained to 1.870(1) Å, and all C-F distances were restrained to 1.350(1) Å; in addition, all F···F distances within each disordered CF_3 component, all disordered P-O distances, and all disordered O-C distances were restrained to be equal within 0.01 Å. The

quantity minimized by the least-squares program was $\Sigma w(F_o^2 - F_c^2)^2$, where $w = \{[\sigma(F_o^2)]^2 + (0.021P)^2 + 5.5P\}^{-1}$ and $P = (F_o^2 + 2F_c^2)/3$. An isotropic extinction parameter was refined to a final value of $x = 2.9(2) \times 10^{-6}$ where F_c is multiplied by the factor $k[1 + F_c^2 x\lambda^3/\sin 2\theta]^{-1/4}$ with k being the overall scale factor. Analysis of the diffraction intensities suggested slight inversion twinning; therefore, the intensities were calculated from the equation $I = xI_a + (1-x)I_b$, where x is a scale factor that relates the volumes of the inversion-related twin components. The volume of the major twin individual refined to a value of 0.97(1). The largest peak in the final Fourier difference map (1.36 eÅ^{-3}) was located 0.67 Å from Os1.

Cp*Os(DFMPM)Et. Single crystals of Cp*Os(DFMPM)Et were grown by cooling a saturated pentane solution. The triclinic lattice and the average values of the normalized structure factors suggested the space group $P\bar{1}$, which was confirmed by the success of the subsequent refinement. A multi-scan absorption correction was applied, the minimum and maximum transmission factors being 0.33 and 0.75. Electron density near the ethyl ligand showed that the molecule had co-crystallized with a very small amount of Cp*Os(DFMPM)Br; a disorder model was constructed in which the site occupancies of the atoms of the ethyl group and the site occupancy of the bromide were constrained to add to 1; the Br site occupancy factor refined to 0.024. The quantity minimized by the least-squares program was $\Sigma w(F_o^2 - F_c^2)^2$, where $w = \{[\sigma(F_o^2)]^2 + (0.0076P)^2 + 1.0014P\}^{-1}$ and $P = (F_o^2 + 2F_c^2)/3$. In the final cycle of least squares, Br1 was refined isotropically. An isotropic extinction parameter was refined to a final value of $x = 3.77(14) \times 10^{-6}$ where F_c is multiplied by the factor $k[1 + F_c^2 x\lambda^3/\sin 2\theta]^{-1/4}$ with k being the overall scale factor. The largest peak in the final Fourier difference map (1.00 eÅ^{-3}) was located 0.75 Å from Os1.

Table 2.1: Crystallographic data for $Cp^*Os[P(CF_3)_2Me][P(CF_3)_2OMe]Br$ and $Cp^*Os(DFMPM)Br_2$

Formula	$C_{16}H_{21}BrF_{12}OOsP_2$	$C_{15}H_{17}Br_2F_{12}OsP_2$
Formula weight	789.38	837.24
T (K)	100(2)	100(2)
λ (Å)	0.71073	0.71073
Crystal system	Orthorhombic	Orthorhombic
Space group	$P2_12_12_1$	$P2_12_12_1$
a (Å)	10.1817(3)	11.3842(3)
b (Å)	12.8644(3)	15.4016(4)
c (Å)	18.1281(4)	26.8887(7)
V (Å^3)	2374.45(10)	4714.5(2)
Z, ρ_{calc} (g/cm^3)	4, 2.208	8, 2.359
μ (mm^{-1})	7.289	9.03
F(000)	1496	3128
Crystal size (mm)	0.150×0.175×0.446	0.181×0.247×0.267
θ range (°)	2.55 – 30.54	2.01 – 28.34
R(int)	0.0468	0.0454
Absorption correction	Multi-scan	Multi-scan
Max., min. transmission factors	0.75, 0.33	0.75, 0.50
Data/restraints/parameters	7244/426/481	11739/0/588
GOF on F^2	1.067	1.040
R_1 [$I > 2\sigma(I)$]	0.0243	0.0131
wR_2 (all data)	0.0545	0.0284
max., min. $\Delta\rho_{elect}$ (eÅ^{-3})	1.36, -0.94	1.10, -0.54

Table 2.2: Crystallographic data for Cp*Os(DFMPM)Br_3 and Cp*Os(DFMPM)Et

Formula	$C_{15}H_{17}Br_3F_{12}OsP_2$	$C_{17}H_{22}F_{12}OsP_2$
Formula weight	917.15	706.48
T (K), λ (Å)	100(2), 0.71073	100(2), 0.71073
Crystal system	Monoclinic	Triclinic
Space group	$P2_1/n$	$P\bar{1}$
a (Å)	8.4045(3)	8.6309(3)
b (Å)	12.9380(4)	9.3024(3)
c (Å)	22.6552(7)	14.6449(5)
α (°)	90	96.285(1)
β (°)	97.297(1)	95.534(1)
γ (°)	90	105.416(1)
V (Å^3)	2443.52(14)	1116.98(7)
Z, ρ_{calc} (g/cm^3)	4, 2.493	2, 2.101
μ (mm^{-1}), F(000)	10.349, 1704	5.953, 676.0
Crystal size (mm)	0.188×0.489×0.540	0.108×0.260×0.708
θ range (°)	2.40 – 30.60	2.29 – 30.57
R(int)	0.0606	0.0456
Absorption correction	Face-indexed	Multi-scan
Max., min. transmission factors	0.32, 0.03	0.75, 0.33
Data/restraints/parameters	7470/0/304	6839/0/301
GOF on F^2	1.090	1.025
R_1 [$I > 2\sigma(I)$], wR_2 (all data)	0.0200, 0.0456	0.0185, 0.0359
max., min. $\Delta\rho_{elect}$ (eÅ^{-3})	0.82, -1.35	1.00, -0.86

Table 2.3: Selected distances and angles for a representative molecule of Cp*Os(κ^1-DFMPM)Br_2

Distances (Å)			
Os1-C1	2.2348(32)	Os1-P1	2.2519(8)
Os1-C2	2.2063(33)	P1-C11	1.9091(37)
Os1-C3	2.2491(32)	P1-C12	1.8959(37)
Os1-C4	2.2617(32)	P1-C13	1.8450(32)
Os1-C5	2.2435(33)	P2-C13	1.8524(34)
Os1-Cg	1.8786(13)	P2-C14	1.8864(38)
Os1-Br1	2.4968(3)	P2-C15	1.8913(37)
Os1-Br2	2.4904(3)		
Angles (°)			
Cg-Os1-Br1	121.0(1)	Os1-P1-C13	122.28(11)
Cg-Os1-Br2	118.2(1)	C11-P1-C12	96.01(18)
Cg-Os1-P1	135.1(1)	C11-P1-C13	102.11(16)
Br1-Os1-Br2	101.40(1)	C12-P1-C13	94.66(16)
Br1-Os1-P1	84.66(2)	P1-C13-P2	118.33(18)
Br2-Os1-P1	87.32(2)	C13-P2-C14	99.13(16)
Os1-P1-C11	118.39(13)	C13-P2-C15	95.09(15)
Os1-P1-C12	118.03(12)	C14-P2-C15	95.15(17)

Cg refers to the centroid of the Cp* ligand. The uncertainties of angles involving Cg were estimated to be 0.1°.

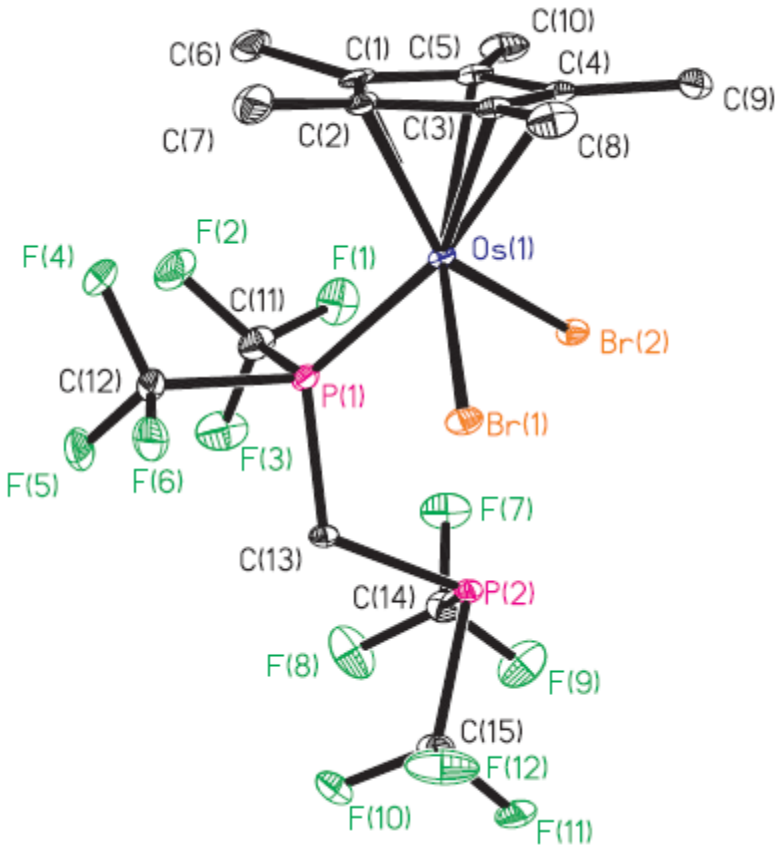

Figure 2.14: Molecular structure of Cp*Os(DFMPM)Br_2. Ellipsoids are drawn at the 35% probability level; hydrogen atoms are omitted for clarity.

Table 2.4: Selected distances and angles for Cp*Os(κ^1-DFMPM)Br_3

Distances (Å)			
Os1-C1	2.3016(21)	Os1-Br3	2.5372(2)
Os1-C2	2.3333(22)	Os1-P1	2.3098(6)
Os1-C3	2.3197(22)	P1-C11	1.9200(28)
Os1-C4	2.2462(22)	P1-C12	1.9073(26)
Os1-C5	2.2350(21)	P1-C13	1.8445(24)
Os1-Cg	1.9347(10)	P2-C13	1.8470(25)
Os1-Br1	2.5369(2)	P2-C14	1.8849(30)
Os1-Br2	2.5401(3)	P2-C15	1.8942(28)
Angles (°)			
Cg-Os1-Br1	108.7	Os1-P1-C11	119.37(8)
Cg-Os1-Br2	119.6	Os1-P1-C12	118.11(9)
Cg-Os1-Br3	107.6	Os1-P1-C13	122.52(8)
Cg-Os1-P1	135.8	C11-P1-C12	97.34(13)
Br1-Os1-Br2	79.27(1)	C11-P1-C13	100.02(12)
Br1-Os1-Br3	143.52(1)	C12-P1-C13	93.92(11)
Br1-Os1-P1	79.27(2)	P1-C13-P2	114.88(12)
Br2-Os1-Br3	80.04(1)	C13-P2-C14	99.10(13)
Br2-Os1-P1	104.58(2)	C13-P2-C15	96.97(11)
Br3-Os1-P1	77.32(2)	C14-P2-C15	95.74(14)

Cg refers to the centroid of the Cp* ligand. The uncertainties of angles involving Cg were estimated to be 0.1°.

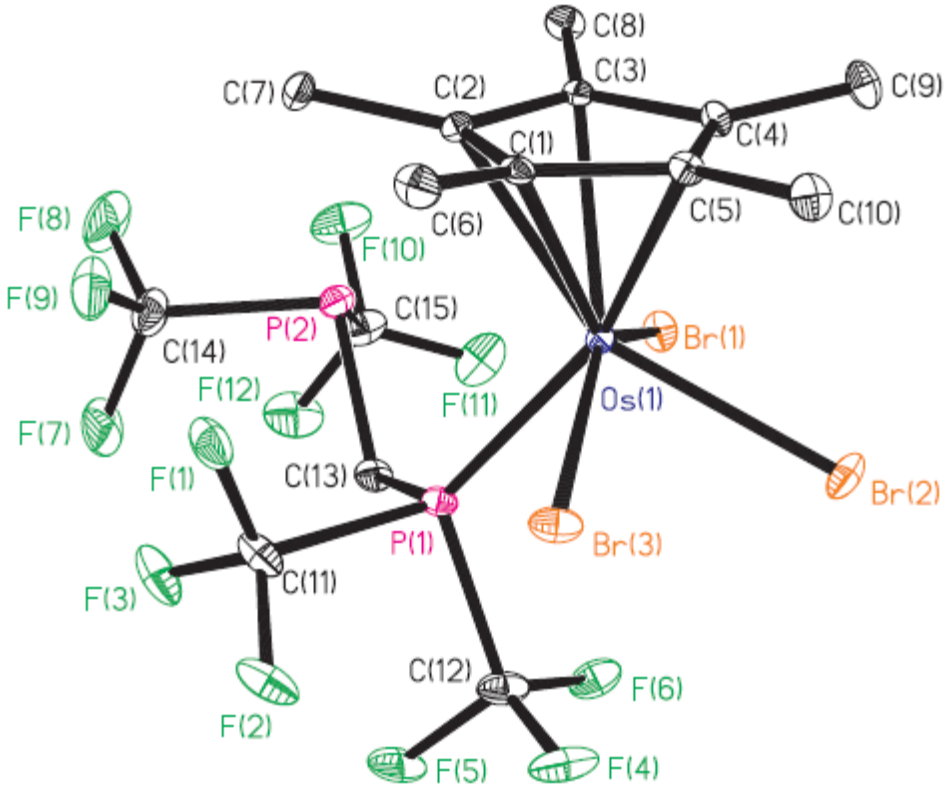

Figure 2.15: Molecular structure of Cp*Os(DFMPM)Br_3. Ellipsoids are drawn at the 35% probability level; hydrogen atoms are omitted for clarity.

Table 2.5: Selected distances and angles for Cp*Os[P(CF_3)$_2$Me][P(CF_3)$_2$Me]Br

Distances (Å)			
Os1-C1	2.3022(49)	Os1-P2	2.2275(15)
Os1-C2	2.2574(52)	P1-O1A	1.6058(79)
Os1-C3	2.2465(51)	P1-C11A	1.8698(14)
Os1-C4	2.2924(53)	P1-C12A	1.8717(14)
Os1-C5	2.2395(45)	O1A-C13A	1.3999(139)
Os1-Cg	1.9137(23)	P2-C14A	1.8682(14)
Os1-Br1	2.5445(6)	P2-C15A	1.8711(14)
Os1-P1	2.2225(14)	P2-C16A	1.8702(14)
Angles (°)			
Cg-Os1-Br1	117.4(1)	C11A-P1-C12A	93.06(28)
Cg-Os1-P1	129.0(1)	C11A-P1-O1A	95.44(34)
Cg-Os1-P2	128.3(1)	C12A-P1-O1A	94.84(38)
Br1-Os1-P1	89.03(4)	Os1-P2-C14A	122.49(25)
Br1-Os1-P2	88.02(5)	Os1-P2-C15A	115.97(25)
P1-Os1-P2	92.69(6)	Os1-P2-C16A	119.73(41)
Os1-P1-C11A	120.17(17)	C14A-P2-C15A	81.73(43)
Os1-P1-C12A	117.55(24)	C14A-P2-C16A	98.07(54)
Os1-P1-O1A	127.91(33)	C15A-P2-C16A	95.65(55)

Distances and angles are listed only for the major component of the disorder model. Cg refers to the centroid of the Cp* ligand. The uncertainties of angles involving Cg were estimated to be 0.1°.

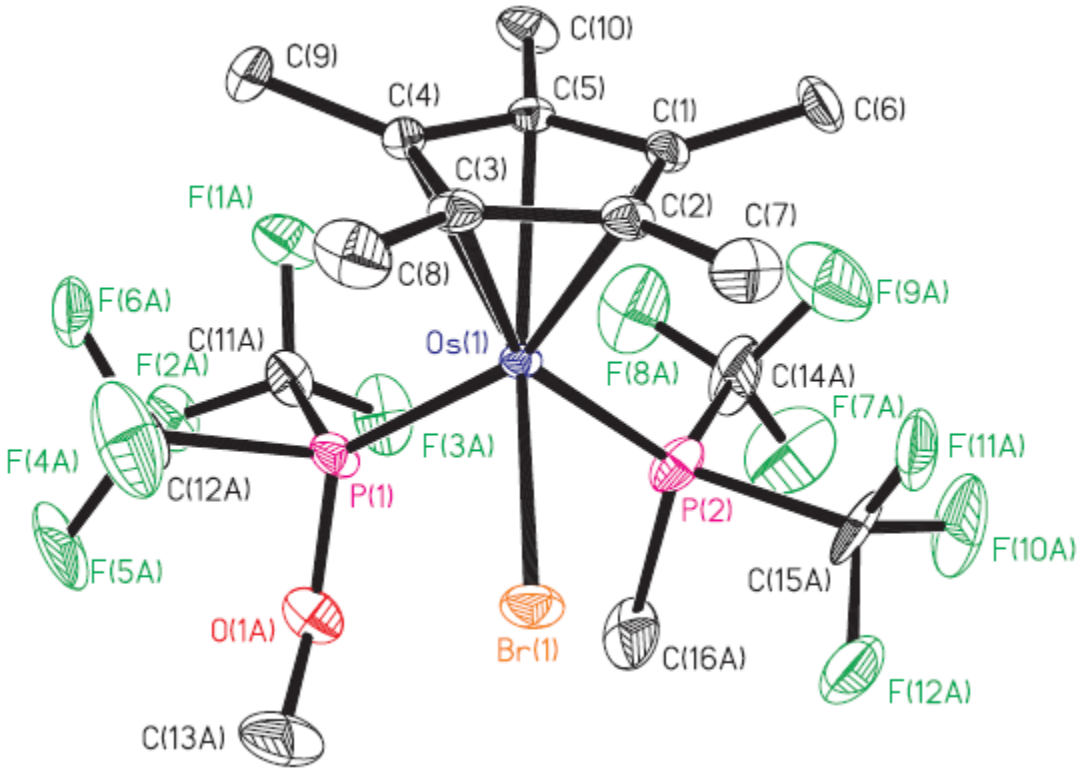

Figure 2.16: Molecular structure of the major component of Cp*Os[P(CF_3)$_2$(CH_3)][P(CF_3)$_2$(OCH_3)]Br. Ellipsoids are drawn at the 35% probability level.; hydrogen atoms are omitted for clarity.

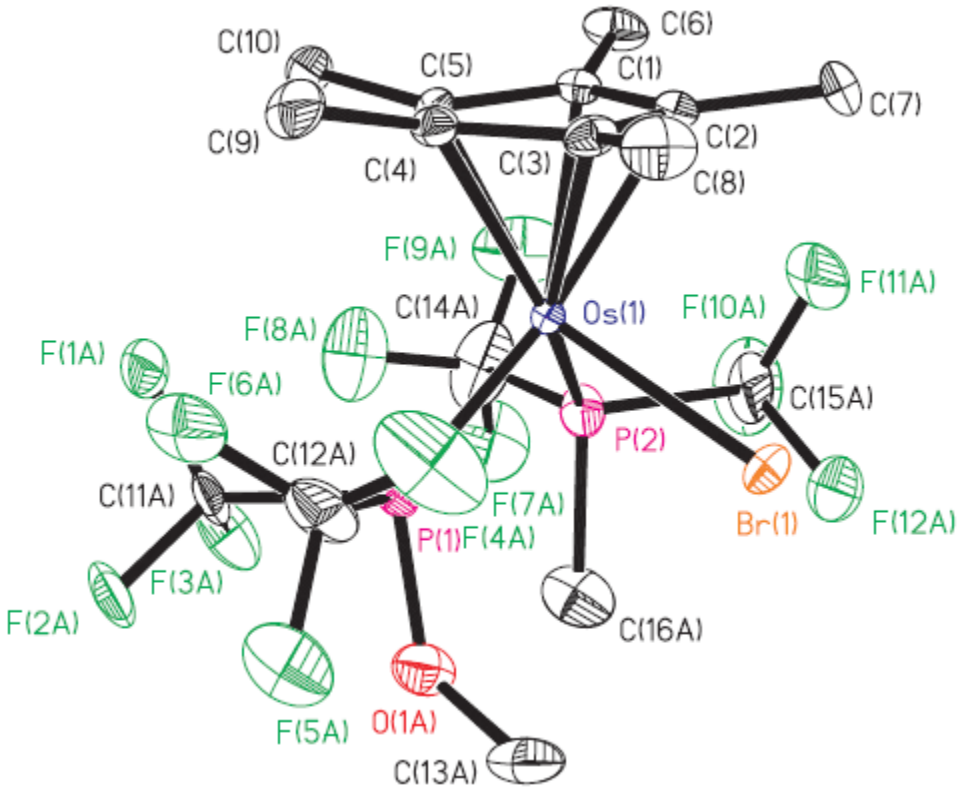

Figure 2.17: An alternative view of Cp*Os[P(CF$_3$)$_2$(CH$_3$)][P(CF$_3$)$_2$(OCH$_3$)]Br.

Table 2.6: Selected distances and angles for Cp*Os(DFMPM)Et

Distances (Å)			
Os1-C1	2.2350(20)	Os1-P2	2.2068(5)
Os1-C2	2.2515(19)	C16-C17	1.5350(34)
Os1-C3	2.3049(20)	P1-C11	1.8946(23)
Os1-C4	2.2677(19)	P1-C12	1.8975(22)
Os1-C5	2.2509(19)	P1-C13	1.8523(20)
Os1-Cg	1.9051(9)	P2-C13	1.8503(20)
Os1-C16	2.1973(23)	P2-C14	1.8869(22)
Os1-P1	2.2040(5)	P2-C15	1.9082(22)
Angles (°)			
Cg-Os1-C16	117.1(1)	C11-P1-C13	101.77(10)
Cg-Os1-P1	138.9(1)	C12-P1-C13	103.95(10)
Cg-Os1-P2	136.9(1)	P1-C13-P2	86.36(9)
C16-Os1-P1	89.89(6)	Os1-P2-C13	100.99(6)
C16-Os1-P2	86.42(7)	Os1-P2-C14	124.04(7)
P1-Os1-P2	70.12(2)	Os1-P2-C15	125.35(7)
Os1-P1-C11	123.87(7)	C13-P2-C14	102.35(10)
Os1-P1-C12	127.37(7)	C13-P2-C15	105.40(10)
Os1-P1-C13	101.03(6)	C14-P2-C15	95.71(10)
C11-P1-C12	95.10(10)		

Distances and angles are listed only for the major component of the disorder model. Cg refers to the centroid of the Cp* ligand. The uncertainties of the angles involving Cg were estimated to be 0.1°.

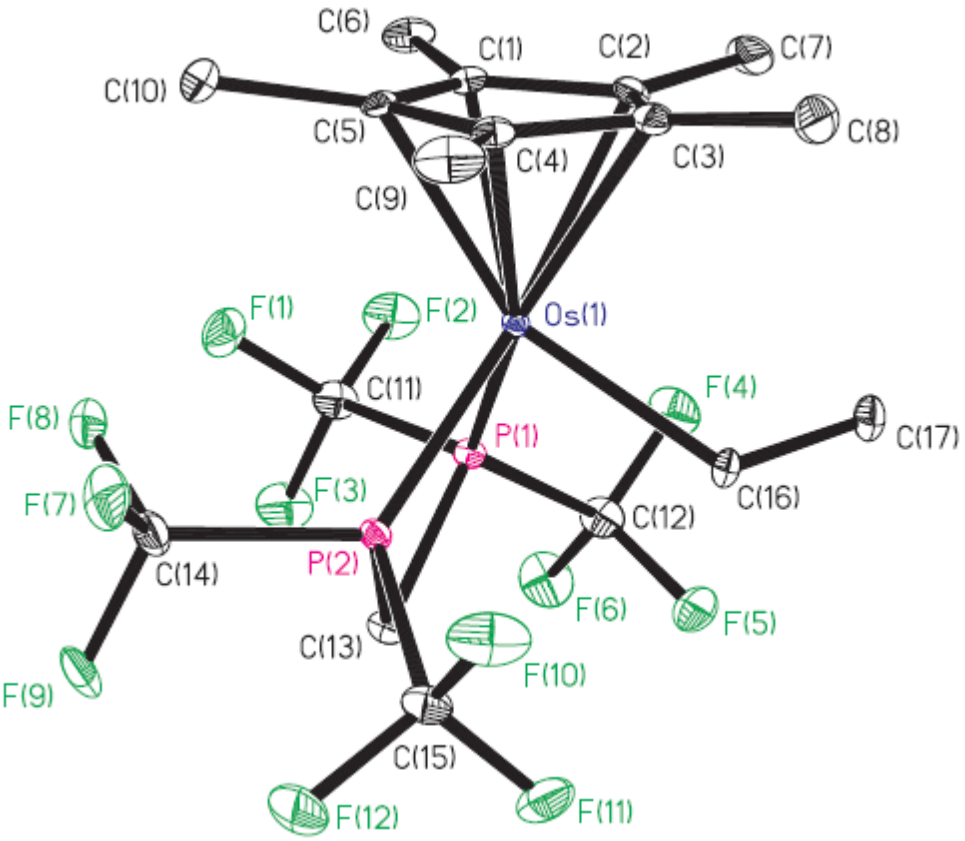

Figure 2.18: Molecular structure of Cp*Os(DFMPM)Et. Ellipsoids are drawn at the 35% probability level; hydrogen atoms are omitted for clarity.

References

1. Goldman, A. S.; Goldberg, K. I., Organometallic C-H bond activation: an introduction. *ACS Symp. Ser.* **2004,** *885*, 1-43.
2. Crabtree, R. H., Organometallic alkane CH activation. *J. Organomet. Chem.* **2004,** *689*, 4083-4091.
3. Buchanan, J. M.; Stryker, J. M.; Bergman, R. G., A structural, kinetic, and thermodynamic study of the reversible thermal C-H activation/reductive elimination of alkanes at iridium. *J. Am. Chem. Soc.* **1986,** *108*, 1537-50.
4. Jones, W. D.; Feher, F. J., Isotope effects in arene carbon-hydrogen bond activation by [(C_5Me_5)Rh(PMe_3)]. *J. Am. Chem. Soc.* **1986,** *108*, 4814-19.
5. Periana, R. A.; Bergman, R. G., Isomerization of the hydridoalkylrhodium complexes formed on oxidative addition of rhodium to alkane carbon-hydrogen bonds. Evidence for the intermediacy of η^2-alkane complexes. *J. Am. Chem. Soc.* **1986,** *108*, 7332-46.
6. Bullock, R. M.; Headford, C. E. L.; Hennessy, K. M.; Kegley, S. E.; Norton, J. R., Intramolecular hydrogen exchange among the coordinated methane fragments of $Cp_2W(H)CH_3$. Evidence for the formation of a σ complex of methane prior to elimination. *J. Am. Chem. Soc.* **1989,** *111*, 3897-908.
7. Gould, G. L.; Heinekey, D. M., Reductive elimination of methane from a cationic rhenium methyl hydride. Evidence for an intermediate methane complex. *J. Am. Chem. Soc.* **1989,** *111*, 5502-4.
8. Geftakis, S.; Ball, G. E., Direct observation of a transition metal alkane complex, $CpRe(CO)_2$(cyclopentane), using NMR spectroscopy. *J. Am. Chem. Soc.* **1998,** *120*, 9953-9954.

9. Parkin, G.; Bercaw, J. E., Elimination processes for alkyl, hydride, and hydroxy derivatives of permethyltungstenocene. *Organometallics* **1989,** *8*, 1172-9.

10. Ball, G. E.; Brookes, C. M.; Cowan, A. J.; Darwish, T. A.; George, M. W.; Kawanami, H. J.; Portius, P.; Rourke, J., A delicate balance of complexation vs. activation of alkanes interacting with [Re(Cp)(CO)(PF_3)] studied with NMR and time-resolved IR spectroscopy. *Proc. Natl. Acad. Sci. U. S. A.* **2007,** *104*, 6927-6932.

11. Ishikawa, Y.; Brown, C. E.; Hackett, P. A.; Rayner, D. M., Interaction of alkanes with unsaturated metal centers: the complex $W(CO)_5C_2H_6$ in the gas phase. *Chem. Phys. Lett.* **1988,** *150*, 506-10.

12. Morse, J. M., Jr.; Parker, G. H.; Burkey, T. J., Enthalpy of CO dissociation from $M(CO)_6$ (M = Cr, Mo, W) in alkane solvent: determination of intermolecular agostic bond strengths. *Organometallics* **1989,** *8*, 2471-4.

13. Brown, C. E.; Ishikawa, Y.; Hackett, P. A.; Rayner, D. M., Interaction of alkanes with unsaturated metal centers. 2. Complexes of alkanes and fluoroalkanes with $W(CO)_5$ in the gas phase. *J. Am. Chem. Soc.* **1990,** *112*, 2530-6.

14. Leu, G.-L.; Burkey, T. J., Alkane coordination by molybdenum and chromium pentacarbonyls: an examination of the energetics of intermolecular agostic bonding. *J. Coord. Chem.* **1995,** *34*, 87-97.

15. Lawes, D. J.; Geftakis, S.; Ball, G. E., Insight into binding of alkanes to transition metals from NMR spectroscopy of isomeric pentane and isotopically labeled alkane complexes. *J. Am. Chem. Soc.* **2005,** *127*, 4134-4135.

16. Lawes, D. J.; Darwish, T. A.; Clark, T.; Harper, J. B.; Ball, G. E., A rhenium-cyclohexane complex with preferential binding of axial C-H bonds: a probe into the relative ability of

C-H, C-D, and C-C bonds as hyperconjugative electron donors? *Angew. Chem., Int. Ed.* **2006,** *45*, 4486-4490.

17. Calladine, J. A.; Torres, O.; Anstey, M.; Ball, G. E.; Bergman, R. G.; Curley, J.; Duckett, S. B.; George, M. W.; Gilson, A. I.; Lawes, D. J.; Perutz, R. N.; Sun, X.-Z.; Vollhardt, K. P. C., Photoinduced N_2 loss as a route to long-lived organometallic alkane complexes: a time-resolved IR and NMR study. *Chem. Sci.* **2010,** *1*, 622-630.

18. Young, R. D.; Lawes, D. J.; Hill, A. F.; Ball, G. E., Observation of a tungsten alkane σ-complex showing selective binding of methyl groups using FTIR and NMR spectroscopies. *J. Am. Chem. Soc.* **2012,** *134*, 8294-8297.

19. Torres, O.; Calladine, J. A.; Duckett, S. B.; George, M. W.; Perutz, R. N., Detection of σ-alkane complexes of manganese by NMR and IR spectroscopy in solution: (η^5-C_5H_5)$Mn(CO)_2$(ethane) and (η^5-C_5H_5)$Mn(CO)_2$(isopentane). *Chem. Sci.* **2015,** *6*, 418-424.

20. Yau, H. M.; McKay, A. I.; Hesse, H.; Xu, R.; He, M.; Holt, C. E.; Ball, G. E., Observation of cationic transition metal-alkane complexes with moderate stability in hydrofluorocarbon solution. *J. Am. Chem. Soc.* **2016,** *138*, 281-288.

21. Perutz, R. N.; Turner, J. J., Photochemistry of the Group VI hexacarbonyls in low-temperature matrices. II. Infrared spectra and structures of ^{13}CO-enriched hexacarbonyls and pentacarbonyls of chromium, molybdenum, and tungsten. *Inorg. Chem.* **1975,** *14*, 262-70.

22. Perutz, R. N.; Turner, J. J., Photochemistry of the Group 6 hexacarbonyls in low-temperature matrixes. III. Interaction of the pentacarbonyls with noble gases and other matrices. *J. Am. Chem. Soc.* **1975,** *97*, 4791-800.

23. Breckenridge, W. H.; Sinai, N., Pulsed laser photolysis of chromium hexacarbonyl in the gas phase. *J. Phys. Chem.* **1981,** *85*, 3557-60.

24. Kelly, J. M.; Long, C.; Bonneau, R., Laser flash photolysis of $M(CO)_6$ (M = Cr, Mo, or W) in perfluoromethylcyclohexane. The generation of highly reactive coordinatively unsaturated species. *J. Phys. Chem.* **1983,** *87*, 3344-9.

25. Church, S. P.; Grevels, F. W.; Hermann, H.; Schaffner, K., Structures and kinetics of $Cr(CO)_5$ and $Cr(CO)_5 \cdot H_2O$ in cyclohexane solution. Flash photolysis study of $Cr(CO)_6$ with infrared and visible detection. *Inorg. Chem.* **1985,** *24*, 418-22.

26. Brookhart, M.; Chandler, W.; Kessler, R. J.; Liu, Y.; Pienta, N. J.; Santini, C. C.; Hall, C.; Perutz, R. N.; Timney, J. A., Matrix isolation and transient absorption studies of [bis[bis(pentafluoroethyl)phosphino]ethane]tetracarbonylchromium: intermolecular alkane complexes and intramolecular F-coordination. *J. Am. Chem. Soc.* **1992,** *114*, 3802-15.

27. Hall, C.; Perutz, R. N., Transition metal alkane complexes. *Chem. Rev. (Washington, D. C.)* **1996,** *96*, 3125-3146.

28. Sun, X.-Z.; Grills, D. C.; Nikiforov, S. M.; Poliakoff, M.; George, M. W., Remarkable stability of $(\eta^5\text{-}C_5H_5)Re(CO)_2L$ (L = *n*-heptane, Xe, and Kr): a time-resolved infrared spectroscopic study of $(\eta^5\text{-}C_5H_5)Re(CO)_3$ in conventional and supercritical fluid solution. *J. Am. Chem. Soc.* **1997,** *119*, 7521-7525.

29. Calladine, J. A.; Duckett, S. B.; George, M. W.; Matthews, S. L.; Perutz, R. N.; Torres, O.; Vuong, K. Q., Manganese alkane complexes: an IR and NMR spectroscopic investigation. *J. Am. Chem. Soc.* **2011,** *133*, 2303-2310.

30. Bartlett, S. A.; Besley, N. A.; Dent, A. J.; Diaz-Moreno, S.; Evans, J.; Hamilton, M. L.; Hanson-Heine, M. W. D.; Horvath, R.; Manici, V.; Sun, X.-Z.; Towrie, M.; Wu, L.; Zhang, X.; George, M. W., Monitoring the formation and reactivity of organometallic alkane and fluoroalkane complexes with silanes and Xe using time-resolved X-ray absorption fine structure spectroscopy. *J. Am. Chem. Soc.* **2019,** *141*, 11471-11480.

31. Pike, S. D.; Thompson, A. L.; Algarra, A. G.; Apperley, D. C.; MacGregor, S. A.; Weller, A. S., Synthesis and characterization of a rhodium(I) σ-alkane complex in the solid state. *Science (Washington, DC, U. S.)* **2012,** *337*, 1648-1651.

32. Pike, S. D.; Chadwick, F. M.; Rees, N. H.; Scott, M. P.; Weller, A. S.; Krämer, T.; Macgregor, S. A., Solid-state synthesis and characterization of σ-alkane complexes, $[Rh(L_2)(\eta^2,\eta^2\text{-}C_7H_{12})][BAr^{F4}]$ (L_2 = bidentate chelating phosphine). *J. Am. Chem. Soc.* **2015,** *137*, 820-833.

33. Chadwick, F. M.; Rees, N. H.; Weller, A. S.; Kraemer, T.; Iannuzzi, M.; MacGregor, S. A., A rhodium-pentane sigma-alkane complex: characterization in the solid state by experimental and computational techniques. *Angew. Chem., Int. Ed.* **2016,** *55*, 3677-3681.

34. Martínez-Martínez, A. J.; Tegner, B. E.; McKay, A. I.; Bukvic, A. J.; Rees, N. H.; Tizzard, G. J.; Coles, S. J.; Warren, M. R.; Macgregor, S. A.; Weller, A. S., Modulation of σ-alkane interactions in $[Rh(L_2)(alkane)]^+$ solid-state molecular organometallic (SMOM) systems by variation of the chelating phosphine and alkane: access to η^2,η^2-σ-alkane Rh(I), η^1-σ-alkane Rh(III) complexes, and alkane encapsulation. *J. Am. Chem. Soc.* **2018,** *140*, 14967-14979.

35. Boyd, T. M.; Tegner, B. E.; Tizzard, G. J.; Martinez-Martinez, A. J.; Neale, S. E.; Hayward, M. A.; Coles, S. J.; Macgregor, S. A.; Weller, A. S., A structurally characterized cobalt(I) σ-alkane complex. *Angew. Chem., Int. Ed.* **2020,** *59*, 6177-6181.

36. Millard, M. D. Isolation of four-coordinate iridium(I) monohydrides and the X-ray crystal structure of a cobalt tris-isocyanide alkane sigma-complex. Ph.D. Dissertation, University of California, San Diego, 2013.

37. Evans, D. R.; Drovetskaya, T.; Bau, R.; Reed, C. A.; Boyd, P. D. W., Heptane coordination to an iron(II) porphyrin. *J. Am. Chem. Soc.* **1997,** *119*, 3633-3634.

38. Castro-Rodriguez, I.; Nakai, H.; Gantzel, P.; Zakharov, L. N.; Rheingold, A. L.; Meyer, K., Evidence for alkane coordination to an electron-rich uranium center. *J. Am. Chem. Soc.* **2003,** *125*, 15734-15735.

39. Bernskoetter, W. H.; Schauer, C. K.; Goldberg, K. I.; Brookhart, M., Characterization of a rhodium(I) σ-methane complex in solution. *Science (Washington, DC, U. S.)* **2009,** *326*, 553-556.

40. Walter, M. D.; White, P. S.; Schauer, C. K.; Brookhart, M., Stability and dynamic processes in 16VE iridium(III) ethyl hydride and rhodium(I) σ-ethane complexes: experimental and computational studies. *J. Am. Chem. Soc.* **2013,** *135*, 15933-15947.

41. Sempsrott, P. J. Low-temperature protonation studies of an electron-poor osmium methyl complex, and molecular precursors for the construction of graphene nanostructues with atomically precise edge structures. Ph.D. Dissertation, University of Illinois at Urbana-Champaign, 2018.

42. Calvert, R. B.; Shapley, J. R., $HOs_3(CO)_{10}CH_3$: NMR evidence for a carbon··hydrogen··osmium interaction. *J. Am. Chem. Soc.* **1978,** *100*, 7726-7.

43. Novikova, Z. S.; Prishchenko, A. A.; Lutsenko, I. F., Synthesis of tetrachloromethylenediphosphine and its derivatives. *Zh. Obshch. Khim.* **1977,** *47*, 775-81.

44. Manojlović-Muir, L.; Jobe, I. R.; Maya, B. J.; Puddephatt, R. J., Platinum(II) complexes with ligands $(RO)_2PCH_2P(OR)_2$ (R = Me, Et, Ph, or C_6H_4Me-4); crystal structure of *cis*,*cis*-$[Pt_2Me_4\{\mu\text{-}(EtO)_2PCH_2P(OEt)_2\}_2]$. *J. Chem. Soc., Dalton Trans.* **1987**, 2117-24.

45. Karsch, H. H., Alkylsubstituierte diphosphinomethane: gemischte Cl/*t*-Bu- and Me/CH_2SiMe_3- derivate. *Z. Naturforsch., B: Anorg. Chem., Org. Chem.* **1983,** *38B*, 1027-30.

46. Mills, L. E. Method of preparing anhydrous alkali metal phenoxides. US1955080, 1934.

47. Gross, C. L.; Girolami, G. S., Synthesis and characterization of osmium(IV) polyhydride complexes of stoichiometry $(C_5Me_5)OsH_3(L)$. Crystal structures of $(C_5Me_5)OsH_3(AsPh_3)$ and $(C_5Me_5)OsH_3(PPh_3)$. *Organometallics* **2006,** *25*, 4792-4798.

48. Inoue, S.; Imanaka, Y., Reactions of organozinc coordination compounds. II. Reactivity with secondary amines. *J. Organometal. Chem.* **1972,** *35*, 1-7.

49. McNamara, B. K.; Yeston, J. S.; Bergman, R. G.; Moore, C. B., The effect of alkane structure on rates of photoinduced C-H bond activation by $Cp^*Rh(CO)_2$ in liquid rare gas media: an infrared flash kinetics study. *J. Am. Chem. Soc.* **1999,** *121*, 6437-6443.

50. Martin, R. L., Hydrogen exchange between hydride and methyl ligands in $[Cp^*Os(dmpm)(CH_3)H^+]$. *J. Am. Chem. Soc.* **1999,** *121*, 9459-9460.

51. Flener-Lovitt, C.; Woon, D. E.; Dunning, T. H.; Girolami, G. S., A DFT and ab initio benchmarking study of metal-alkane interactions and the activation of carbon-hydrogen bonds. *J. Phys. Chem. A* **2010,** *114*, 1843-1851.

52. McKay, A. I.; Krämer, T.; Rees, N. H.; Thompson, A. L.; Christensen, K. E.; Macgregor, S. A.; Weller, A. S., Formation of a σ-alkane complex and a molecular rearrangement in the solid-state: [Rh($Cyp_2PCH_2CH_2PCyp_2$)(η^2:η^2-C_7H_{12})][BAr^{F4}]. *Organometallics* **2017,** *36*, 22-25.

53. McKay, A. I.; Martinez-Martinez, A. J.; Griffiths, H. J.; Rees, N. H.; Waters, J. B.; Weller, A. S.; Krämer, T.; MacGregor, S. A., Controlling structure and reactivity in cationic solid-state molecular organometallic systems using anion templating. *Organometallics* **2018,** *37*, 3524-3532.

54. Gross, C. L.; Brumaghim, J. L.; Jefferis, J. M.; Dickinson, P. W.; Girolami, G. S.; Gribble, C. W.; Tilley, T. D., Mono(η^5-pentamethylcyclopentadienyl) complexes of osmium. *Inorg. Synth.* **2014,** *36*, 72-77.

55. Siegel, J. S.; Anet, F. A. L., Dichlorofluoromethane-*d*: a versatile solvent for VT-NMR experiments. *J. Org. Chem.* **1988,** *53*, 2629-30.

56. Smith, R. J.; Pagni, R. M., Reaction of di-*tert*-butylnitroxide with methyl trifluoromethanesulfonate. Unexpected formation of *N*-*tert*-butylhydroxylamine radical cation in trifluoromethanesulfonic acid. *J. Org. Chem.* **1981,** *46*, 4307-9.

57. Fulmer, G. R.; Miller, A. J. M.; Sherden, N. H.; Gottlieb, H. E.; Nudelman, A.; Stoltz, B. M.; Bercaw, J. E.; Goldberg, K. I., NMR chemical shifts of trace impurities: common laboratory solvents, organics, and gases in deuterated solvents relevant to the organometallic chemist. *Organometallics* **2010,** *29*, 2176-2179.

58. Loaiza, A.; Borchardt, D.; Zaera, F., A NMR method for the analysis of mixtures of alkanes with different deuterium substitutions. *Spectrochim. Acta, Part A* **1997,** *53A*, 2481-2493.

59. Berger, S.; Van Etten, R. L.; Risley, J. M.; Sergeyev, N. M., *Isotope effects in NMR spectroscopy*. Springer-Verlag: 1990; Vol. 22, p 171.

60. Brumaghim, J. L.; Priepot, J. G.; Girolami, G. S., Synthesis of hydride and alkyl compounds containing the Cp*Os(NO) fragment. Crystal structure of $[Cp^*Os(\mu\text{-}NO)]_2$. *Organometallics* **1999,** *18*, 2139-2144.

61. Sheldrick, G. M., Crystal structure refinement with SHELXL. *Acta Crystallogr., Sect. C: Struct. Chem.* **2015,** *71*, 3-8.

62. Krause, L.; Herbst-Irmer, R.; Sheldrick, G. M.; Stalke, D., Comparison of silver and molybdenum microfocus X-ray sources for single-crystal structure determination. *J. Appl. Crystallogr.* **2015,** *48*, 3-10.

CHAPTER 3

LOW-TEMPERATURE PROTONATION STUDIES OF METHYL COMPLEXES OF GROUP 10 TRANSITION METALS

Introduction

The study of alkane σ-complexes is motivated, in large part, by the desire to understand the mechanism of alkane C-H bond activation processes, and thus aid in the development of efficient and selective C-H activation catalysts. One such C-H activation process of great interest is the partial oxidation of methane to methanol. Methane is an abundant natural resource which is currently being underutilized due to the cost of its capture, transport, and storage. A cost-efficient process to convert methane into a methanol would enable the use of this natural resource in our liquid-fuel infrastructure as well as increase the utility of methane as a chemical feedstock.[1] Heterogeneous catalysts suffer from over-oxidation of methane; the C-H bonds of methanol are weaker than those of methane. Recent work with copper zeolites addresses the issue of selectivity by employing low conversion rates or stepwise procedures.[2]

Homogeneous catalysts offer the potential to effect selective transformations, but there currently are no economical processes for the conversion of methane to methanol. The first system that demonstrated the capability of selective partial methane oxidation was reported by Shilov.[3-4] His system uses $PtCl_4^{2-}$ as the catalyst but employs stoichiometric $PtCl_6^{2-}$ as the oxidant; the process suffers from low turnover numbers due to decomposition of the catalyst into metallic platinum.[5] Periana et al. developed a method to convert methane into a methyl ester by employing a platinum bipyrimidine catalyst dissolved in fuming sulfuric acid.[6] Unfortunately, difficulties associated with the subsequent hydrolysis of methylbisulfate to methanol and separation of the latter render this system impractical. Strassner and coworkers used a similar approach with a

palladium catalyst bearing an N-heterocyclic carbene (NHC).[7] Strassner's palladium NHC catalysts are stable in carboxylic acids, from which methanol can be separated more easily than from fuming sulfuric acid. However, these catalytic systems suffer from low turnover numbers (TON < 30).[8]

σ-Alkane complexes are proposed to be intermediates in alkane C-H activation processes that do not rely on one-electron (radical) chemistry.[9] For Shilov's catalyst and related systems, the coordination of the alkane to the metal center and formation of the σ-alkane complex is the rate limiting step and also determines the selectivity of the subsequent transformation.[10] Understanding how alkanes coordinate to group 10 metal centers can allow for the rational design of superior catalysts. As mentioned in Chapter 2, σ-alkane complexes with group 6,[11-12] 7,[13] 8,[14-15] and 9[16-25] transition metals as well as uranium[26] have been reported. Here we describe our efforts to extend these studies to include the group 10 transition metals nickel, palladium, and platinum.

Results and Discussion

Synthesis of the Pincer Ligands. In order to investigate the synthesis of group 10 alkane complexes, we chose PCP pincers with a 2,6-bis[(dialkylphosphino)methyl]phenyl architecture as the ancillary ligand: $(^{R}PCP)^{-}$ where R is iso-propyl (^{i}Pr), tert-butyl (^{t}Bu), or adamantyl (Ad). These ligands were selected for several reasons. A tridentate pincer will occupy three coordination sites on the metal center; for square-planar Ni^{II}, Pd^{II}, and Pt^{II} metal centers, only one coordination site will remain for the bound alkyl or alkane group, thus simplifying the protonolysis study (Figure 3.1). In addition, previous studies of the methyl complexes $(^{R}PCP)M(CH_3)$ indicate that acids react selectively with the methyl group and not the PCP ligand.[27-28] The variety of substituents on the PCP ligand enables us to explore metal centers with varying degrees of electron richness. More

strongly donating ligands will help strengthen the M-CH_4 interaction, but if they are too donating then the methyl/hydride structure, M^{IV}-(CH_3)(H), will be more stable than the M^{II}-CH_4 tautomer.[29] The ligand should be strongly donating enough so that the methane dissociation barrier is large, but not so donating that oxidative cleavage of the C-H bond is thermodynamically favored.

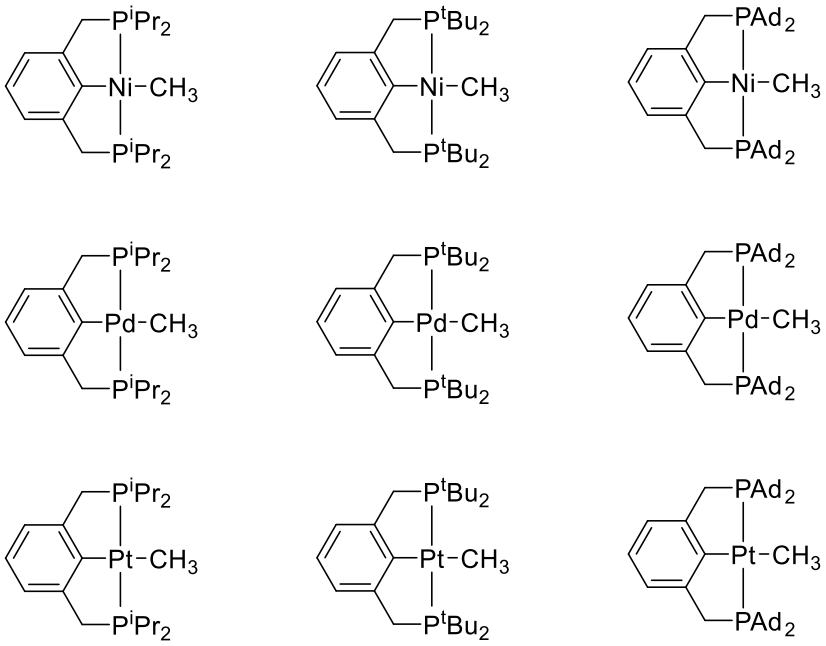

Figure 3.1: Our target complexes for this study.

We found that the reported preparations of proligands H(^{iPr}PCP), (^{iPr}PCP)Br, and (^{tBu}PCP)Br could be improved. Montag et al. synthesized H(^{iPr}PCP) by heating a solution of ^{i}Pr$_2$PH and α,α′-dibromo-*m*-xylene in MeOH to reflux for 2 days.[30] Et_3N was added to neutralize the resulting phosphonium salt. Then, the mixture was taken to dryness under vacuum and the product was extracted with Et_2O. We found that both Et_3NHBr and H(^{iPr}PCP) are soluble in Et_2O and thus are difficult to separate; extraction with pentane instead of Et_2O makes the separation of the phosphine product much easier owing to the low solubility of the alkylammonium salt in this solvent. By treatment of 2-bromo-1,3-bis(bromomethyl)benzene with the appropriate secondary

phosphine, the 2-brominated proligands (^{iPr}PCP)Br and (^{tBu}PCP)Br can also be prepared by means of this modified procedure.

Several additional modifications were required for the preparation of (^{Ad}PCP)Br. Goerlich and Schmutzler reported that the starting material Ad_2PH can be made by the reaction of Ad_2POCl with $LiAlH_4$, followed by quenching with 1 M HCl (aq).[31] We found that quenching the reaction with the Fieser workup (every 1 g of $LiAlH_4$ is quenched by addition of 1 mL of H_2O, 1 mL of 6 M NaOH (aq), and 4 mL of H_2O) gave significantly improved yields. We also found that the subsequent reaction of Ad_2PH with 2-bromo-1,3-bis(bromomethyl)benzene does not work well; we believe that the reason is related to the low solubility of Ad_2PH in MeOH. The reaction proceeds with good yield, however, in refluxing toluene in the presence of excess Et_3N. The Et_3NHBr precipitate is removed by filtering the reaction mixture while the solvent is boiling. Owing to the low solubility of (^{Ad}PCP)Br in toluene, cooling the filtrate to room temperature results in crystallization of the product. The crystals are collected by filtration and washed with pentane and acetone to afford (^{Ad}PCP)Br as a white solid. Our attempts to prepare H(^{Ad}PCP) from Ad_2PH and α,α′-dibromo-*m*-xylene were unsuccessful.

Synthesis of the Nickel, Palladium, and Platinum Methyl Complexes (^{R}PCP) (CH_3). Cámpora et al. reported that the nickel(II) bromo complex (^{iPr}PCP)NiBr can be prepared from (^{iPr}PCP)Br and $Ni(COD)_2$.[32] The reagents were mixed in THF, the solution was taken to dryness under vacuum, and the product was extracted with Et_2O. We find that the reaction works just as well when Et_2O is used as the reaction solvent, which is easier to remove than THF. The tert-butyl analog (^{tBu}PCP)NiBr can be prepared by this same procedure. However, the preparation of the adamantyl analog (^{Ad}PCP)NiBr should be performed in THF owing to the insolubility of (^{Ad}PCP)Br in Et_2O. Filtering the mixture and taking the filtrate to dryness yields (^{Ad}PCP)NiBr.

We have obtained a crystal structure of the bromo complex (^{Ad}PCP)NiBr (Figure 3.2). The complex crystallizes from CH_2Cl_2 in the *C*2/*c* space group with one molecule of CH_2Cl_2 in the asymmetric unit. The (^{Ad}PCP)NiBr molecule, which lies on a crystallographic two-fold rotational axis that passes through the Ni-C(ipso) and Ni-Br bonds, contains a square-planar Ni^{II} center. The aryl ring is rotated 11.44(5)° with respect to the square plane. The Ni-Br, Ni-C, and Ni-P bond distances of 2.3876(4) Å, 1.9323(25) Å, and 2.2086(4) Å, respectively, as well as the Br-Ni-C, Br-Ni-P, C-Ni-P, and P-Ni-P bond angles of 180°, 95.32(1)°, 84.68(1)°, and 169.36(3)°, respectively, are nearly identical to those for the ^{t}Bu analog (^{tBu}PCP)NiBr.[33]

The preparation of the nickel methyl complex (^{iPr}PCP)Ni(CH_3) by reaction of (^{iPr}PCP)NiBr with MeLi in Et_2O was reported by Martínez-Prieto et al.[28] (^{Ad}PCP)NiBr can be methylated by the same procedure if the solvent is changed to toluene. However, this procedure does not work with (^{tBu}PCP)NiBr. Instead, methylation of (^{tBu}PCP)NiBr is best performed with MeMgBr in benzene at 45 °C as reported by Schmeier et al.[34] The need to increase the temperature for methylating (^{tBu}PCP)NiBr may be attributed to an increase in the reaction barrier owing to the steric bulk of the ^{t}Bu substituents of the (^{tBu}PCP)$^-$ ligand, which is the most sterically bulky of the three pincer ligands we have studied.

The preparations of the palladium complexes (^{iPr}PCP)PdCl and (^{iPr}PCP)Pd(CH_3) reported by Frech et al.[35] and Martínez-Prieto et al.,[28] respectively, were used without modification.

Clark and Manzer reported a preparation for (COD)Pt(CH_3)Cl.[36] (COD)PtI_2 was treated with slightly over 2 equiv of MeLi in Et_2O at 0 °C. Subsequent workup afforded (COD)Pt(CH_3)$_2$, which was converted into (COD)Pt(CH_3)Cl by action of acetyl chloride. In our hands, treatment of (COD)PtI_2 with MeLi affords a significant amount of black precipitate, presumably Pt^0, and low yields of the desired dimethyl compound (COD)Pt(CH_3)$_2$. Methylation with MeMgBr avoids this

issue. However, subsequent quenching of the reaction with saturated NH_4Cl (aq) at 0 °C gives a mixture of (COD)Pt(CH_3)$_2$ and (COD)Pt(CH_3)I. We hypothesized that interaction of NH_3 with the Pt center might be responsible for producing a mixture of products. Quenching the reaction instead with saturated NEt_2H_2Cl (aq) at room temperature gives (COD)Pt(CH_3)I. Just as (^{iPr}PCP)PtCl can be synthesized from (COD)Pt(CH_3)Cl,[27] we found that (^{iPr}PCP)PtI can be synthesized in an analogous manner from (COD)Pt(CH_3)I.

Poverenov et al. reported that treatment of (^{iPr}PCP)PtCl with MeLi in toluene affords (^{iPr}PCP)Pt(CH_3).[27] In our hands, treatment of (^{iPr}PCP)PtCl with MeLi or MeMgBr in toluene did not work well, but changing the reaction solvent to benzene resulted in the generation of (^{iPr}PCP)Pt(CH_3) in good yield.

Protonation Studies. We began with some preliminary experiments to study the low-temperature protonation of (^{R}PCP)M(CH_3) complexes. Protonation of (^{iPr}PCP)Ni(CH_3) and (^{iPr}PCP)Pt(CH_3) with $HN(SO_2CF_3)_2$ is slow: resonances that would be indicative of the formation of $[M^{IV}\text{-}(CH_3)(H)]^+$ or $[M^{II}\text{-}CH_4]^+$ species were not observed in the ^{1}H NMR spectra. Instead, resonances due to (^{iPr}PCP)M(CH_3) persisted until the temperature was raised above -20 °C. These results indicated that protonation of these organometallic complexes with $HN(SO_2CF_3)_2$ is characterized by a large barrier, which is probably related to the steric bulk of the acid.

Protonation of (^{tBu}PCP)Ni(CH_3) with the sterically less demanding acid HOTf in $CDCl_2F$ proceeds at -130 °C. However, the resulting protonation product is unstable towards dissociation of methane. Mr. Nicolas Capra and I also investigated the protonation of the palladium and platinum complexes (^{iPr}PCP)Pd(CH_3) and (^{iPr}PCP)Pt(CH_3); these metals are expected to form stronger metal-alkane bonds. Treatment of the palladium complex (^{iPr}PCP)Pd(CH_3) with the carbon acid $H_2C(SO_2CF_3)_2$ at -130 °C resulted in complete protonation and release of CH_4 before

NMR spectra could be acquired. In contrast, the platinum analog (^{iPr}PCP)Pt(CH_3) reacts with $H_2C(SO_2CF_3)_2$ and HOTf slowly below -60 °C. The methyl resonance for (^{iPr}PCP)Pt(CH_3) diminishes as the resonance for free methane grows in. However, no resonances upfield of δ 0, which would be diagnostic for the presence of a methane coordination complex or a methyl hydride complex, were observed.

Conclusions

Several adjustments were made to literature procedures to afford a series of group 10 PCP pincer complexes of nickel, palladium, and platinum. Protonation of (^{tBu}PCP)Ni(CH_3) and (^{iPr}PCP)Pd(CH_3) results in the loss of methane, even at -130 °C, without observation of any alkane or alkyl/hydride intermediates. Protonation of (^{iPr}PCP)Pt(CH_3) even with HOTf is slow until the temperature is raised to -60 °C, and under these conditions the protonation also results in the immediate loss of methane.

The results suggest that, in order to stabilize methane coordination complexes of square-planer Ni^{II}, Pd^{II}, or Pt^{II}, more electron-rich metal centers will be required. Adding electron donating substituents to the para-position of the PCP ligand should increase the electron density on the metal; alternatively, the phosphine substituents of the pincer ligand could be replaced with NHC or amine substituents.

Experimental Details

Unless otherwise stated, all operations were conducted under argon using standard Schlenk line and glovebox techniques. Solvents were dried over sodium-benzophenone ketyl (Et_2O, pentane, THF, and benzene), CaH_2 (DCM), $CaCl_2$ (acetone), magnesium (MeOH), or sodium

(toluene) and distilled before use. MeLi in Et_2O and MeMgBr in Et_2O were purchased from Sigma-Aldrich and titrated by a literature procedure.[37] NBS was recrystallized from H_2O and dried in a vacuum desiccator. The compounds $^{i}Pr_2PH$ and $^{t}Bu_2PH$,[38] $Ni(COD)_2$,[39] (^{iPr}PCP)NiBr and (^{tBu}PCP)NiBr,[32] (^{iPr}PCP)$NiCH_3$,[28] (^{tBu}PCP)$NiCH_3$,[34] (^{iPr}PCP)$PdCH_3$,[28] (COD)PtI_2[36], and $CDCl_2F$[40] were prepared according to literature procedures.

Elemental analyses were performed by the School of Chemical Sciences Microanalysis Laboratory at the University of Illinois at Urbana-Champaign. Unless otherwise stated, NMR spectra were acquired on Varian (400 MHz, 500 MHz, and 600 MHz) and Bruker (500 MHz) spectrometers at room temperature. ^{1}H and ^{13}C NMR spectra are reported in δ units (positive chemical shifts to higher frequency) relative to TMS as determined from residual solvent signals.[41] ^{31}P NMR spectra are reported in δ units relative to an external sample of 85% H_3PO_4 in H_2O, respectively. NMR spectra were processed with the MestReNova NMR software package. X-ray crystallographic data were collected by the George L. Clark X-Ray Facility and 3M Materials Laboratory.

2-Bromo-1,3-bis(bromomethyl)benzene. This compound was synthesized in air. To a mixture of NBS (35.615 g, 200 mmol), 75% benzoyl peroxide (2.02 g, 6.25 mmol), and 2-bromo-*m*-xylene (13.0 mL, 97.6 mmol) was added $CHCl_3$ (250 mL). The mixture heated to reflux overnight. The mixture was taken to dryness by rotary evaporation and the residue was suspended in hexanes (200 mL). The mixture was heated to boiling and vacuum-filtered while still hot. The product, which crystallized as the filtrate cooled, was collected and dried in a vacuum desiccator. Yield: 18.86 g (56%). ^{1}H NMR (C_6D_6): δ 6.68 (AB_2, J_{AB} = 7.7 Hz, 2 H, Ar-H), 6.59 (AB_2, J_{AB} = 7.7 Hz, 1 H, Ar-H), 4.06 (s, 4 H, CH_2).

1,3-Bis(diisopropylphosphinomethyl)benzene, H(^{iPr}PCP). To a solution of α,α′-dibromo-*m*-xylene (8.68 g, 32.9 mmol) in MeOH (60 mL) was added a solution of $^{i}Pr_2PH$ (8.37 g, 70.8 mmol) in MeOH (30 mL). The solution was heated to reflux for 2 days. Et_3N (30 mL) was added, causing precipitation of a white solid. The mixture was taken to dryness under vacuum and the product was extracted with pentane (3 × 20 mL). The combined pentane extracts were filtered, combined, and taken to dryness under vacuum to afford the product as a cloudy oil. Yield: 7.07 g (63%). ^{1}H NMR (C_6D_6): δ 7.44 (s, 1 H, Ar-H), 7.19-7.12 (m, 3 H, Ar-H), 2.69 (s, 4 H, CH_2), 1.61 (sept of d, $^{3}J_{HH}$ = 7 Hz, $^{2}J_{PH}$ = 2 Hz, 4 H, C*H*Me$_2$), 1.02 (d, $^{3}J_{HH}$ = 7 Hz, 12 H, CH*Me*$_2$), 0.99 (dd, $^{3}J_{HH}$ = 7 Hz, $^{3}J_{PH}$ = 1 Hz, 12 H, CH*Me*$_2$). $^{31}P\{^{1}H\}$ NMR (C_6D_6): δ 10.50. The NMR data are consistent with literature values.[42]

2-Bromo-1,3-bis(diisopropylphosphinomethyl)benzene, (^{iPr}PCP)Br. This compound was synthesized as described for H(^{iPr}PCP) from $^{i}Pr_2PH$ and 2-bromo-1,3-bis(bromomethyl)-benzene. The product was isolated as a low-melting solid. Yield: 2.93 g (71%). M.p: 18 °C. Anal. Calc. for $C_{20}H_{35}BrP_2$: C, 57.6; H, 8.45; Br, 19.2. Found: C, 57.0; H, 8.04; Br, 18.8. ^{1}H NMR (C_6D_6): δ 7.26 (d, $^{3}J_{HH}$ = 8 Hz, 2 H, Ar-H), 6.94 (t, $^{3}J_{HH}$ = 8 Hz, 1 H, Ar-H), 2.97 (d, $^{2}J_{PH}$ = 2 Hz, 4 H, CH_2), 1.67 (sd, $^{3}J_{HH}$ = 7 Hz, $^{2}J_{PH}$ = 1 Hz, 4 H, C*H*Me$_2$), 1.03 (dd, $^{3}J_{HH}$ = 7 Hz, $^{3}J_{PH}$ = 4 Hz, 12 H, CH*Me*$_2$), 1.01 (dd, $^{3}J_{HH}$ = 7 Hz ,$^{3}J_{PH}$ = 5 Hz, 12 H, CH*Me*$_2$). $^{31}P\{^{1}H\}$ NMR (C_6D_6): δ 10.11 (s). The ^{1}H NMR data are consistent with literature values but the $^{31}P\{^{1}H\}$ NMR resonance is shifted downfield by δ 3.46 compared to the literature value.[42]

2-Bromo-1,3-bis(di-tert-butylphosphinomethyl)benzene, (^{tBu}PCP)Br. This compound was synthesized as described for H(^{iPr}PCP) from $^{t}Bu_2PH$ and 2-bromo-1,3-bis(bromomethyl)-benzene. The product was isolated as a white solid. Yield: 4.79 g (95%). ^{1}H NMR (C_6D_6): δ 7.69

(dd, $^3J_{HH}$ = 8 Hz, $^4J_{PH}$ = 3 Hz, 2 H, Ar-H), 7.04 (t, $^3J_{HH}$ = 8 Hz, 1 H, Ar-H), 3.11 (d, $^2J_{PH}$ = 3 Hz, 4 H, CH_2), 1.11 (d, $^3J_{PH}$ = 11 Hz, 24 H, CMe_3). $^{31}P\{^1H\}$ NMR (C_6D_6): δ 34.35 (s).

Di-1-adamantylphosphine, Ad_2PH. To a mixture of adamantane (20.073 g, 147 mmol) and $AlCl_3$ (21.003 g, 158 mmol) was added PCl_3 (65.0 mL, 745 mmol). The mixture was heated to reflux, affording a cloudy orange mixture. The majority of excess PCl_3 was removed by distillation, yielding a thick orange sludge. The sludge was diluted with $CHCl_3$ (150 mL) and deionized water (100 mL) was slowly added to the orange mixture. Effervescence and warming were observed. The mixture was vacuum-filtered open to air. The organic layer was separated from the aqueous layer and the aqueous layer was washed with $CHCl_3$ (3x30 mL). The organic portions were combined, dried over $MgSO_4$, and filtered to afford a pale yellow solution. The solution was dried by rotary evaporation until a viscous pale yellow oil remained. The oil was dried under dynamic vacuum with heating to 60 °C, affording a white powder. The powder was dissolved in THF (500 mL) and added dropwise to a cold (0 °C) slurry of $LiAlH_4$ (3.523 g, 92.8 mmol) in THF (50 mL). The mixture was allowed to warm to room temperature after the addition was complete and the mixture was stirred overnight. Excess $LiAlH_4$ was quenched with H_2O (3.5 mL), followed by a 6 M NaOH (aq) solution (3.5 mL), and finally H_2O (14 mL). The mixture was filtered and the solids washed with THF (50 mL). The filtrate and washing were combined and dried under vacuum, affording a white powder. Yield: 20.15 g (90%). ^1H NMR (C_6D_6): δ 2.92 (d, $^1J_{PH}$ = 202 Hz, 1 H, P-H), 2.03-1.62 (m, 60 H, $C_{10}H_{15}$). $^{31}P\{^1H\}$ NMR (C_6D_6): 18.71 (s). The NMR data differed somewhat from those given in the literature but a different solvent was used.[31]

2-Bromo-1,3-bis(di-1-adamantylphosphinomethyl)benzene, (^{Ad}PCP)Br. To a mixture of Ad_2PH (2.514 g, 8.31 mmol) and 2-bromo-1,3-bis(bromomethyl)benzene (1.409 g, 4.11 mmol) was added toluene (25 mL) and Et_3N (7.50 mL, 53.8 mmol). The mixture was heated to reflux for

2 days. The mixture was filtered hot and the filtrate was allowed to cool to room temperature. A white solid crystallized out of solution. The solid was collected by filtration, washed with pentane (3 × 10 mL) and acetone (70 mL), and dried under vacuum. Yield: 1.980 g (61%). Anal. Calc. for $C_{48}H_{67}BrP_2$: C, 73.4; H, 8.59; Br, 10.2. Found: C, 73.0; H, 8.72; Br, 10.6. ^{1}H NMR (C_6D_6): δ 7.88 (dd, $^3J_{HH}$ = 8 Hz, $^4J_{PH}$ = 3 Hz, 2 H, Ar-H), 3.19 ($^2J_{PH}$ = 3 Hz, 4 H, CH_2), 2.04-1.60 (m, 60 H, $C_{10}H_{15}$); the last Ar-H resonance is obscured underneath the residual solvent peak. ^{31}P{^{1}H} NMR (C_6D_6): δ 31.37 (s).

[2,6-Bis(di-*tert*-butylphosphinomethyl)phenyl]bromonickel(II), (^{tBu}PCP)NiBr. To a mixture of $Ni(COD)_2$ (0.976 g, 3.55 mmol) and (^{tBu}PCP)Br (1.731 g, 3.66 mmol) was added Et_2O (200 mL). The mixture was stirred for 16 h and taken to dryness under vacuum to afford a dark yellow solid. Yield: 1.512 g (80%). ^{1}H NMR (C_6D_6): δ 7.02 (t, $^3J_{HH}$ = 7 Hz, 1 H, Ar-H), 6.85 (d, $^3J_{HH}$ = 7 Hz, 2 H, Ar-H), 2.93 (A part of an $A_2A'_2XX'$ spin system, $^2J_{PH}$ = 5 Hz, $^2J_{PP'}$ = 5 Hz, $^4J_{PH}$ = 2.4 Hz, 4 H, CH_2), 1.41 (A part of an $A_{18}A'_{18}XX'$ spin system, $^3J_{PH}$ = 9 Hz, $^2J_{PP'}$ = 5 Hz, $^5J_{PH}$ = 4 Hz, 36 H, CMe_3). ^{31}P{^{1}H} NMR (C_6D_6): δ 67.33 (s). The NMR data are consistent with literature values.[33]

[2,6-Bis(di-1-adamantylphosphinomethyl)phenyl]bromonickel(II), (^{Ad}PCP)NiBr. To a mixture of $Ni(COD)_2$ (0.179 g, 0.651 mmol) and (^{Ad}PCP)Br (0.503 g, 0.640 mmol) was added THF (20 mL). The mixture was stirred for 16 h and taken to dryness under vacuum to afford a dark yellow solid. Yield: 0.411 g (76%). Anal. Calc. for $C_{48}H_{67}BrNiP_2$: C, 68.3; H, 8.00; Br, 9.46; Ni, 6.95. Found: C, 67.1; H, 7.90; Br, 8.84; Ni, 6.2. ^{1}H NMR (C_6D_6): δ 7.09 (t, $^3J_{HH}$ = 8 Hz, 1 H, Ar-H), 6.99 (d, $^3J_{HH}$ = 8 Hz, 2 H, Ar-H), 3.03 (m, 4 H, CH_2), 2.63-1.53 (m, 60 H, $C_{10}H_{15}$). ^{31}P{^{1}H} NMR (C_6D_6): δ 57.41 (s).

[2,6-Bis(di-1-adamantylphosphinomethyl)phenyl](methyl)nickel(II), (^{Ad}PCP)NiCH$_3$. To a solution of (^{Ad}PCP)NiBr (0.117 g, 0.139 mmol) in toluene (20 mL) at -78 °C was added MeLi (0.080 mL of a 1.7 M solution in Et_2O, 0.14 mmol) dropwise. The solution was stirred at room temperature for 16 h, then cooled to -78 °C and treated with MeOH (2 mL) dropwise. The mixture was warmed to room temperature and filtered. The filtrate was taken to dryness under vacuum, affording the product as a yellow solid. Yield: 0.069 g (62%). ^{1}H NMR: δ 7.26-6.99 (m, 3 H, Ar-H), 3.30 ("t", $^2J_{PH}$ = 3 Hz, $^4J_{PH}$ = 3 Hz, 4 H, CH_2), 2.37-1.57 (m, 60 H, $C_{10}H_{15}$). ^{31}P{^{1}H} NMR (C_6D_6): δ 63.83 (s).

(1,5-Cyclooctadiene)(methyl)iodoplatinum(II), (COD)PtMeI. To a suspension of (COD)PtI_2 (2.974 g, 5.34 mmol) in benzene (30 mL) was added MeMgBr (3.60 mL of a 3.0 M solution in Et_2O, 10.8 mmol) dropwise, affording a colorless solution. Immediately afterwards, excess MeMgBr was quenched by adding a saturated aq. Et_2NH_2Cl (ca. 2 mL). The mixture immediately darkened, effervescence was observed, and a brown precipitate formed. Deionized water (ca. 10 mL) was added to dissolve the solids. The aqueous and benzene layers were separated and the aqueous layer was washed with benzene (3 × 10 mL). The benzene portions were combined, dried over anhydrous Na_2SO_4, and filtered. The filtrate was taken to dryness by rotary evaporation affording a dirty yellow residue, which was dried further in a vacuum desiccator. Yield: 2.182 g (92%). ^{1}H NMR ($CDCl_3$): δ 5.54 (m, 2 H, $^2J_{PtH}$ = 45 Hz, CH), 4.66 (m, $^2J_{PtH}$ = 74 Hz, 2 H, CH), 2.57-1.89 (m, 8 H, CH_2), 1.11 (s, $^2J_{PtH}$ = 72 Hz, 3 H, Pt-Me).

[2,6-Bis(diisopropylphosphinomethyl)phenyl]iodoplatinum(II), (^{iPr}PCP)PtI. To a solution of (COD)PtMeI (0.337 g, 0.756 mmol) in toluene (30 mL) was added H(^{iPr}PCP) (0.265 mL, 0.750 mmol). Effervescence was observed. The solution was stirred, heated to reflux overnight, and then taken to dryness under vacuum. The product was extracted from the residue

with pentane (3 × 20 mL). The extracts were filtered and combined. The solution was concentrated to saturation at reflux and then cooled to -20 °C to crystallize the product. The pale yellow crystals were collected by filtration and dried under vacuum. Yield: 0.126 g (26%). ^{1}H NMR (C_6D_6): δ 7.05 (d, $^{3}J_{HH}$ = Hz, 2 H, Ar-H), 2.75 (m, 4 H, CH_2), 2.34 (m, 4 H, C*H*Me$_2$), 1.35 (m, 12 H, CH*Me*$_2$), 0.82 (m, 12 H, CH*Me*$_2$). ^{31}P{^{1}H} NMR (C_6D_6): δ 57.74 (s, $^{1}J_{PtP}$ = 2789 Hz).

[2,6-Bis(diisopropylphosphinomethyl)phenyl](methyl)platinum(II), (^{iPr}PCP)PtCH$_3$. To a solution of (^{iPr}PCP)PtCl (0.243 g, 0.428 mmol) in benzene (5 mL) was added dropwise MeLi (0.600 mL of a 1.6 M solution in Et_2O, 0.960 mmol). The solution, which became deeper yellow and cloudy, was stirred overnight and then taken to dryness under vacuum. The product was extracted with Et_2O (3 × 10 mL). The extracts were filtered and combined. The solution was concentrated to saturation and then cooled to -20 °C to crystallize the product. The yellow crystals were collected by filtration and dried under vacuum. Yield: 0.109 g (46%). ^{1}H NMR (C_6D_6): δ 7.28 (m, 3 H, Ar-H), 3.05 (A part of an $A_2A'_2XX'$ spin system with additional Pt coupling, $^{2}J_{PP'}$ = ca. 100 Hz, $^{3}J_{PtH}$ = 18 Hz, $^{2}J_{PH}$ = 8.2 Hz, 4 H, CH_2), 2.06 (C part of an $A_6A'_6B_6B'_6CC'XX'$ spin system, $^{2}J_{PP'}$ = ca. 100 Hz, $^{3}J_{HH}$ = 7 Hz, $^{2}J_{PH}$ + $^{2}J_{P'H}$ = 5 Hz, 4 H, C*H*Me$_2$), 1.17 (A part of an $A_6A'_6B_6B'_6CC'XX'$ spin system, $^{2}J_{PP'}$ = ca. 100 Hz, $^{3}J_{PH}$ + $^{3}J_{P'H}$ = 14 Hz, $^{3}J_{HH}$ = 7 Hz, 12 H, CH*Me*$_2$) 0.92 (“s”, $^{2}J_{PtH}$ = 10 Hz, 3 H, Pt-Me), 0.88 (B part of an $A_6A'_6B_6B'_6CC'XX'$ spin system, $^{2}J_{PP'}$ = ca. 100 Hz, $^{3}J_{PH}$ + $^{3}J_{P'H}$ = 14 Hz, $^{3}J_{HH}$ = 7 Hz, 12 H, CH*Me*$_2$). ^{31}P{^{1}H} NMR (C_6D_6): δ 57.17 (s, $^{1}J_{PtP}$ = 2903 Hz). For reasons that are unclear, the ^{1}H NMR chemical shifts deviate by as much as 0.5 ppm from the values reported in the literature, although the ^{31}P NMR chemical shift and Pt coupling constant agree exactly.[27]

Crystallographic Details.[43] Single crystals of (^{Ad}PCP)NiBr were grown by cooling a saturated CH_2Cl_2 solution. A crystal mounted on a Nylon fiber with Paratone® oil was transferred

onto the diffractometer and kept at -173 °C in a cold nitrogen gas stream. Intensity data were collected on a Bruker D8 Venture kappa diffractometer equipped with a Photon 100 CMOS detector. An Iμs microfocus source provided the Mo Kα radiation (λ = 0.71073 Å) that was monochromated with multilayer mirrors. Standard peak search and indexing procedures gave rough cell dimensions, and least squares refinement using 50977 reflections yielded the cell dimensions given in Table 3.1.

Data were collected with an area detector by using the measurement parameters listed in Table 3.1. The systematic absences *hkl* ($h + k \neq 2n$) and *h*0*l* ($l \neq 2n$) were consistent with the space groups *Cc* and *C*2/*c*. The average values of the normalized structure factors suggested the space group *C*2/*c*, and this choice was confirmed by successful refinement of the proposed model. The measured intensities were reduced to structure factor amplitudes and their estimated standard deviations by correction for background, scan speed, and Lorentz and polarization effects. No corrections for crystal decay were necessary, but a face-indexed absorption correction (SADABS)[44] was applied, the minimum and maximum transmission factors being 0.61 and 0.69. Systematically absent reflections were deleted and symmetry equivalent reflections were averaged to yield the set of unique data. All 5932 unique data were used in the least squares refinement.

The structure was solved using Patterson methods (SHELXS).[45] Correct positions for Br1, Ni1, and P1 atoms were deduced from a Patterson map. Subsequent least-squares refinement and difference Fourier calculations (SHELXL)[45] revealed the positions of the remaining non-hydrogen atoms. The quantity minimized by the least-squares program was $\Sigma w(F_o^2 - F_c^2)^2$, where $w = \{[\sigma(F_o^2)]^2 + (0.0352P)^2 + 17.0021P\}^{-1}$ and $P = (F_o^2 + 2F_c^2)/3$. The analytical approximations to the scattering factors were used, and all structure factors were corrected for both real and imaginary components of anomalous dispersion. In the final cycle of least squares, independent anisotropic

displacement factors were refined for the non-hydrogen atoms. Hydrogen atoms were placed in idealized positions; the methyl groups were allowed to rotate about the C-C axis to find the best least-squares positions. The displacement parameters for methylene and methine hydrogens were set equal to 1.2 times U_{eq} for the attached carbon; those for methyl hydrogens were set to 1.5 times U_{eq}. An isotropic extinction parameter was refined to a final value of $x = 2.90(12) \times 10^{-6}$ where F_c is multiplied by the factor $k[1 + F_c^2 x\lambda^3/\sin 2\theta]^{-1/4}$ with k being the overall scale factor. Successful convergence was indicated by the maximum shift/error of 0.001 for the last cycle. Final refinement parameters are given in Table 3.1. The largest peak in the final Fourier difference map (1.10 eÅ^3) was located 0.77 Å from Cl1. A final analysis of variance between observed and calculated structure factors showed no apparent errors. Solutions were checked with PLATON for missed crystallographic symmetry.

Table 3.1: Crystallographic data for (^{Ad}PCP)NiBr

Formula	$C_{50}H_{71}BrCl_4NiP_2$
Formula weight	1014.42
T (K)	100(2)
λ (Å)	0.71073
Crystal system	Monoclinic
Space group	$C2/c$
a (Å)	11.8364(5)
b (Å)	17.0215(7)
c (Å)	24.0747(12)
β (°)	100.168(1)
V (Å^3)	4774.2(4)
Z, ρ_{calc} (g/cm^3)	4, 1.411
μ (mm^{-1})	1.57
F(000)	2128
Crystal size (mm)	0.316×0.365×0.394
θ range (°)	2.393 – 30.511
R(int)	0.0349
Absorption correction	Face-indexed
Max., min. transmission factors	0.69, 0.61
Data/restraints/parameters	5932/0/265
GOF on F^2	1.049
R_1 [$I > 2\sigma(I)$]	0.0340
wR_2 (all data)	0.0846
max., min. $\Delta\rho_{elect}$ (eÅ^{-3})	1.10, -1.08

Table 3.2: Selected distances and angles for (^{Ad}PCP)NiBr

Distances (Å)			
Ni1-Br1	2.3876(4)	P1-C16	1.9806(19)
Ni1-P1	2.2086(4)	C1-C2	1.4428(21)
Ni1-C1	1.9323(25)	C2-C3	1.3968(25)
P1-C5	1.8480(19)	C2-C5	1.5427(25)
P1-C6	1.8032(17)	C3-C4	1.4169(24)
Angles (°)			
Br1-Ni1-P1	95.32(1)	C6-P1-C16	116.10(8)
Br1-Ni1-C1	180.00	Ni1-C1-C2	121.23(11)
P1-Ni1-C1	84.68(1)	C2-C1-C2A	117.55(22)
P1-Ni1-P1A	169.36(3)	C1-C2-C3	120.94(18)
Ni1-P1-C5	105.06(6)	C1-C2-C5	119.80(16)
Ni1-P1-C6	103.78(6)	C2-C3-C4	120.20(18)
Ni1-P1-C16	124.15(5)	C3-C4-C3A	120.06(24)
C5-P1-C6	105.88(8)	C2-C5-P1	103.93(12)
C5-P1-C16	99.96(8)		

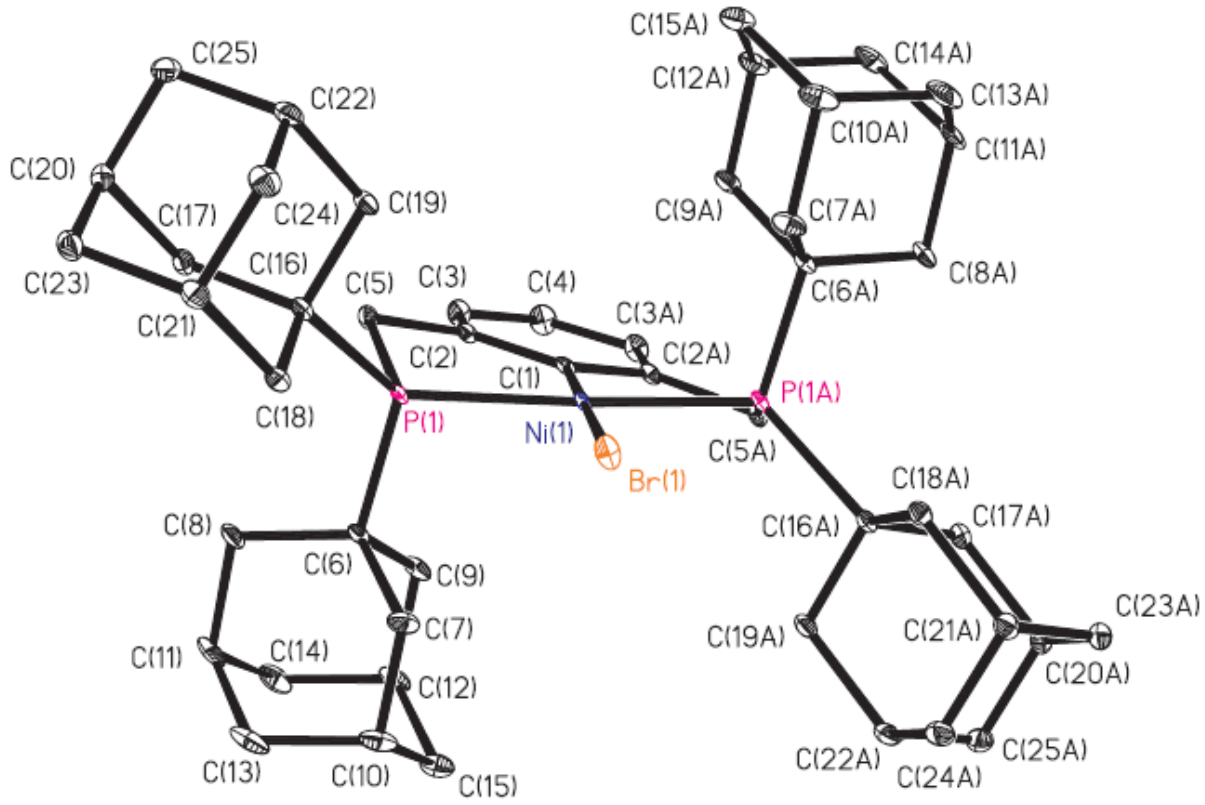

Figure 3.2: Molecular structure of (^{Ad}PCP)NiBr. Ellipsoids are drawn at the 35% probability level; hydrogen atoms and solvent molecules are omitted for clarity.

References

1. Lersch, M.; Tilset, M., Mechanistic aspects of C-H activation by Pt complexes. *Chem. Rev. (Washington, DC, U. S.)* **2005,** *105*, 2471-2526.
2. Park, M. B.; Park, E. D.; Ahn, W.-S., Recent progress in direct conversion of methane to methanol over copper-exchanged zeolites. *Front. Chem. (Lausanne, Switz.)* **2019,** *7*, 514.
3. Gol'dshleger, N. F.; Tyabin, M. B.; Shilov, A. E.; Shteinman, A. A., Activation of saturated hydrocarbons. Deuterium-hydrogen exchange in solutions of transition metal complexes. *Zh. Fiz. Khim.* **1969,** *43*, 2174-5.
4. Gol'dshleger, N. F.; Es'kova, V. V.; Shilov, A. E.; Shteinman, A. A., Reactions of alkanes in solutions of platinum chloride complexes. *Zh. Fiz. Khim.* **1972,** *46*, 1353-4.
5. Heyduk, A. F.; Zhong, H. A.; Labinger, J. A.; Bercaw, J. E., C-H bond activation at Pt(II): A route to selective alkane oxidation? *ACS Symp. Ser.* **2004,** *885*, 250-263.
6. Periana, R. A.; Taube, D. J.; Gamble, S.; Taube, H.; Satoh, T.; Fujii, H., Platinum catalysts for the high-yield oxidation of methane to a methanol derivative. *Science (Washington, D. C.)* **1998,** *280*, 560-564.
7. Muehlhofer, M.; Strassner, T.; Herrmann, W. A., C-H activation by N-heterocyclic carbenes, part 1. New catalyst systems for the catalytic conversion of methane into methanol. *Angew. Chem., Int. Ed.* **2002,** *41*, 1745-1747.
8. Munz, D.; Strassner, T., Propane activation by palladium complexes with chelating bis(NHC) ligands and aerobic cooxidation. *Angew. Chem., Int. Ed.* **2014,** *53*, 2485-2488.
9. Tilset, M.; Johansson, L.; Lersch, M.; Wik, B. J., Competitive trapping of equilibrating Pt(IV) hydridoalkyl and Pt(II) alkane complexes: a valuable tool for the mechanistic investigation of C-H activation reactions. *ACS Symp. Ser.* **2004,** *885*, 264-282.

10. Chen, G. S.; Labinger, J. A.; Bercaw, J. E., The role of alkane coordination in C-H bond cleavage at a Pt(II) center. *Proc. Natl. Acad. Sci. U. S. A.* **2007,** *104*, 6915-6920.

11. Perutz, R. N.; Turner, J. J., Photochemistry of the Group VI hexacarbonyls in low-temperature matrices. II. Infrared spectra and structures of ^{13}CO-enriched hexacarbonyls and pentacarbonyls of chromium, molybdenum, and tungsten. *Inorg. Chem.* **1975,** *14*, 262-70.

12. Perutz, R. N.; Turner, J. J., Photochemistry of the Group 6 hexacarbonyls in low-temperature matrixes. III. Interaction of the pentacarbonyls with noble gases and other matrixes. *J. Am. Chem. Soc.* **1975,** *97*, 4791-800.

13. Church, S. P.; Poliakoff, M.; Timney, J. A.; Turner, J. J., Photochemistry of matrix-isolated $HMn(CO)_5$: evidence for two isomers of $HMn(CO)_4$. *Inorg. Chem.* **1983,** *22*, 3259-66.

14. Poliakoff, M.; Turner, J. J., Structure and reactions of matrix-isolated tetracarbonyliron(0). *J. Chem. Soc., Dalton Trans.* **1974**, 2276-85.

15. Evans, D. R.; Drovetskaya, T.; Bau, R.; Reed, C. A.; Boyd, P. D. W., Heptane coordination to an iron(II) porphyrin. *J. Am. Chem. Soc.* **1997,** *119*, 3633-3634.

16. Bernskoetter, W. H.; Schauer, C. K.; Goldberg, K. I.; Brookhart, M., Characterization of a rhodium(I) σ-methane complex in solution. *Science (Washington, DC, U. S.)* **2009,** *326*, 553-556.

17. Walter, M. D.; White, P. S.; Schauer, C. K.; Brookhart, M., Stability and dynamic processes in 16VE iridium(III) ethyl hydride and rhodium(I) σ-ethane complexes: experimental and computational studies. *J. Am. Chem. Soc.* **2013,** *135*, 15933-15947.

18. Millard, M. D. Isolation of four-coordinate iridium(I) monohydrides and the X-ray crystal structure of a cobalt tris-isocyanide alkane sigma-complex. Ph.D. Dissertation, University of California, San Diego, 2013.

19. Pike, S. D.; Thompson, A. L.; Algarra, A. G.; Apperley, D. C.; MacGregor, S. A.; Weller, A. S., Synthesis and characterization of a rhodium(I) σ-alkane complex in the solid state. *Science (Washington, DC, U. S.)* **2012,** *337*, 1648-1651.

20. Pike, S. D.; Chadwick, F. M.; Rees, N. H.; Scott, M. P.; Weller, A. S.; Krämer, T.; Macgregor, S. A., Solid-state synthesis and characterization of σ-alkane complexes, $[Rh(L_2)(\eta^2,\eta^2\text{-}C_7H_{12})][BAr^{F4}]$ (L_2 = bidentate chelating phosphine). *J. Am. Chem. Soc.* **2015,** *137*, 820-833.

21. Chadwick, F. M.; Rees, N. H.; Weller, A. S.; Kraemer, T.; Iannuzzi, M.; MacGregor, S. A., A rhodium-pentane sigma-alkane complex: characterization in the solid state by experimental and computational techniques. *Angew. Chem., Int. Ed.* **2016,** *55*, 3677-3681.

22. McKay, A. I.; Krämer, T.; Rees, N. H.; Thompson, A. L.; Christensen, K. E.; Macgregor, S. A.; Weller, A. S., Formation of a σ-alkane complex and a molecular rearrangement in the solid-state: $[Rh(Cyp_2PCH_2CH_2PCyp_2)(\eta^2:\eta^2\text{-}C_7H_{12})][BAr^{F4}]$. *Organometallics* **2017,** *36*, 22-25.

23. McKay, A. I.; Martinez-Martinez, A. J.; Griffiths, H. J.; Rees, N. H.; Waters, J. B.; Weller, A. S.; Krämer, T.; MacGregor, S. A., Controlling structure and reactivity in cationic solid-state molecular organometallic systems using anion templating. *Organometallics* **2018,** *37*, 3524-3532.

24. Martínez-Martínez, A. J.; Tegner, B. E.; McKay, A. I.; Bukvic, A. J.; Rees, N. H.; Tizzard, G. J.; Coles, S. J.; Warren, M. R.; Macgregor, S. A.; Weller, A. S., Modulation of σ-alkane

interactions in $[Rh(L_2)(alkane)]^+$ solid-state molecular organometallic (SMOM) systems by variation of the chelating phosphine and alkane: access to η^2,η^2-σ-alkane Rh(I), η^1-σ-alkane Rh(III) complexes, and alkane encapsulation. *J. Am. Chem. Soc.* **2018,** *140*, 14967-14979.

25. Boyd, T. M.; Martínez-Martínez, A. J.; Hayward, M. A.; Weller, A. S.; Boyd, T. M.; Weller, A. S.; Tegner, B. E.; Neale, S. E.; Macgregor, S. A.; Tizzard, G. J.; Coles, S. J., A structurally characterized cobalt(I) σ-alkane complex. *Angew Chem Int Ed Engl* **2020**.

26. Castro-Rodriguez, I.; Nakai, H.; Gantzel, P.; Zakharov, L. N.; Rheingold, A. L.; Meyer, K., Evidence for alkane coordination to an electron-rich uranium center. *J. Am. Chem. Soc.* **2003,** *125*, 15734-15735.

27. Poverenov, E.; Leitus, G.; Shimon, L. J. W.; Milstein, D., C-metalated diazoalkane complexes of platinum based on PCP- and PCN-type ligands. *Organometallics* **2005,** *24*, 5937-5944.

28. Martínez-Prieto, L. M.; Melero, C.; del Río, D.; Palma, P.; Cámpora, J.; Álvarez, E., Synthesis and reactivity of nickel and palladium fluoride complexes with PCP pincer ligands. NMR-based assessment of electron-donating properties of fluoride and other monoanionic ligands. *Organometallics* **2012,** *31*, 1425-1438.

29. Zhu, H.; Ziegler, T., Influence of cis and trans ligands in platinum(II) complexes on the ability of the platinum center to activate C-H bonds. A density functional theory study. *Organometallics* **2008,** *27*, 1743-1749.

30. Montag, M.; Schwartsburd, L.; Cohen, R.; Leitus, G.; Ben-David, Y.; Martin, J. M. L.; Milstein, D., The unexpected role of CO in C-H oxidative addition by a cationic rhodium(I) complex. *Angew. Chem., Int. Ed.* **2007,** *46*, 1901-1904.

31. Goerlich, J. R.; Schmutzler, R., Organophosphorus compounds with tertiary alkyl substituents. VI. A convenient method for the preparation of di-1-adamantylphosphine and di-1-adamantylchlorophosphine. *Phosphorus, Sulfur Silicon Relat. Elem.* **1995,** *102*, 211-15.

32. Cámpora, J.; Palma, P.; del Río, D.; Álvarez, E., CO insertion reactions into the M-OH bonds of monomeric nickel and palladium hydroxides. Reversible decarbonylation of a hydroxycarbonyl palladium complex. *Organometallics* **2004,** *23*, 1652-1655.

33. Enthaler, S.; Brück, A.; Kammer, A.; Junge, H.; Irran, E.; Gülak, S., Exploring the reactivity of nickel pincer complexes in the decomposition of formic acid to CO_2/H_2 and the hydrogenation of $NaHCO_3$ to HCOONa. *ChemCatChem* **2015,** *7*, 65-69.

34. Schmeier, T. J.; Hazari, N.; Incarvito, C. D.; Raskatov, J. A., Exploring the reactions of CO_2 with PCP supported nickel complexes. *Chem. Commun. (Cambridge, U. K.)* **2011,** *47*, 1824-1826.

35. Frech, C. M.; Shimon, L. J. W.; Milstein, D., Redox-induced collapse and regeneration of a pincer-type complex framework: A nonplanar coordination mode of palladium(II). *Angew. Chem., Int. Ed.* **2005,** *44*, 1709-1711.

36. Clark, H. C.; Manzer, L. E., Reactions of (π-1,5-cyclooctadiene)organoplatinum(II) compounds and the synthesis of perfluoroalkylplatinum complexes. *J. Organometal. Chem.* **1973,** *59*, 411-28.

37. Watson, S. C.; Eastham, J. F., Colored indicators for simple direct titration of magnesium and lithium reagents. *J. Organomet. Chem.* **1967,** *9*, 165-8.

38. Zhu, K.; Achord, P. D.; Zhang, X.; Krogh-Jespersen, K.; Goldman, A. S., Highly effective pincer-ligated iridium catalysts for alkane dehydrogenation. DFT calculations of relevant

thermodynamic, kinetic, and spectroscopic properties. *J. Am. Chem. Soc.* **2004,** *126*, 13044-13053.

39. Jezorek, R. L.; Zhang, N.; Leowanawat, P.; Bunner, M. H.; Gutsche, N.; Pesti, A. K. R.; Olsen, J. T.; Percec, V., Air-stable nickel precatalysts for fast and quantitative cross-coupling of aryl sulfamates with aryl neopentylglycolboronates at room temperature. *Org. Lett.* **2014,** *16*, 6326-6329.

40. Siegel, J. S.; Anet, F. A. L., Dichlorofluoromethane-d: a versatile solvent for VT-NMR experiments. *J. Org. Chem.* **1988,** *53*, 2629-30.

41. Fulmer, G. R.; Miller, A. J. M.; Sherden, N. H.; Gottlieb, H. E.; Nudelman, A.; Stoltz, B. M.; Bercaw, J. E.; Goldberg, K. I., NMR chemical shifts of trace impurities: common laboratory solvents, organics, and gases in deuterated solvents relevant to the organometallic chemist. *Organometallics* **2010,** *29*, 2176-2179.

42. Rybtchinski, B.; Ben-David, Y.; Milstein, D., Unexpected isomerization of a *cis*- into a *trans*-dihydride complex. A neutral late-transition-metal complex as a hydride donor. *Organometallics* **1997,** *16*, 3786-3793.

43. Brumaghim, J. L.; Priepot, J. G.; Girolami, G. S., Synthesis of hydride and alkyl compounds containing the Cp*Os(NO) fragment. Crystal structure of $[Cp^*Os(\mu\text{-}NO)]_2$. *Organometallics* **1999,** *18*, 2139-2144.

44. Krause, L.; Herbst-Irmer, R.; Sheldrick, G. M.; Stalke, D., Comparison of silver and molybdenum microfocus X-ray sources for single-crystal structure determination. *J. Appl. Crystallogr.* **2015,** *48*, 3-10.

45. Sheldrick, G. M., Crystal structure refinement with SHELXL. *Acta Crystallogr., Sect. C: Struct. Chem.* **2015,** *71*, 3-8.

CHAPTER 4

SYNTHESIS AND CHARACTERIZATION OF PCP PINCER COMPLEXES OF TITANIUM AND CHROMIUM

Introduction

The study of pincer complexes of the early transition metals (groups 4, 5, and 6) is a young but growing area of chemistry. In 1992, van Koten reported that an (NCN)Ta^{V} neopentylidene complex could perform Wittig-type reactions to transform ketones and imines into alkenes.[1] Beginning in 2005, Mindiola demonstrated that (PNP)Ti^{IV} alkylidynes could perform aryl C-F bond cleavage,[2-7] C-O bond cleavage,[4, 8] C-H bond cleavage,[4, 9] and denitrogenation of pyridines and picolines.[10] Since these earlier developments, early transition metal pincer complexes have been discovered that display catalytic activity for olefin oligomerization,[11-15] olefin polymerization,[16-29] alkyne polymerization.[30-31] olefin isomerization,[32-33] olefin hydroamination,[34-39] and the hydrosilylation of ketones.[40-41]

The aforementioned systems utilize metathesis and insertion reactions in their elementary steps. During these reactions, the oxidation state of the metal does not change. However, early transition metal pincer complexes are not limited to these kinds of transformations: they can also catalyze reactions in which there is a change in the oxidation state of the metal center. Veige used (OCO)Cr^{III} pincer compounds as catalysts for oxygen atom transfer reactions, with air as the oxygen source.[42-44] Molybdenum pincer complexes can reduce CO_2 to formates,[45-46] acrylates,[47-49] and CO.[50] Beller used a (PNP)Mo^{0} catalyst for the hydrogenation of olefins, ketones, and amides.[51-52] Group 6 pincer complexes can also cleave N_2 to produce nitrido complexes.[53-55] Nishibayashi and Tuczek demonstrated that some pincer complexes of Ti, Zr, V, and Mo, can catalyze the conversion of N_2 to NH_3 in the presence of a proton source and a reductant.[56-77]

Pincer ligands vary widely in their structures. Surprisingly, PCP pincer complexes of early transition metals are uncommon: nine PCP ligands have been reported for group 6 complexes (Figure 4.1).[41, 53, 72-73, 78-82] but to date there are no reports of group 4 or 5 transition metals bearing PCP ligands. We now describe the preparation and characterization of several PCP complexes of Ti and Cr with the ligand 2,6-bis(di-*tert*-butylphosphinomethyl)phenyl, (^{tBu}PCP).

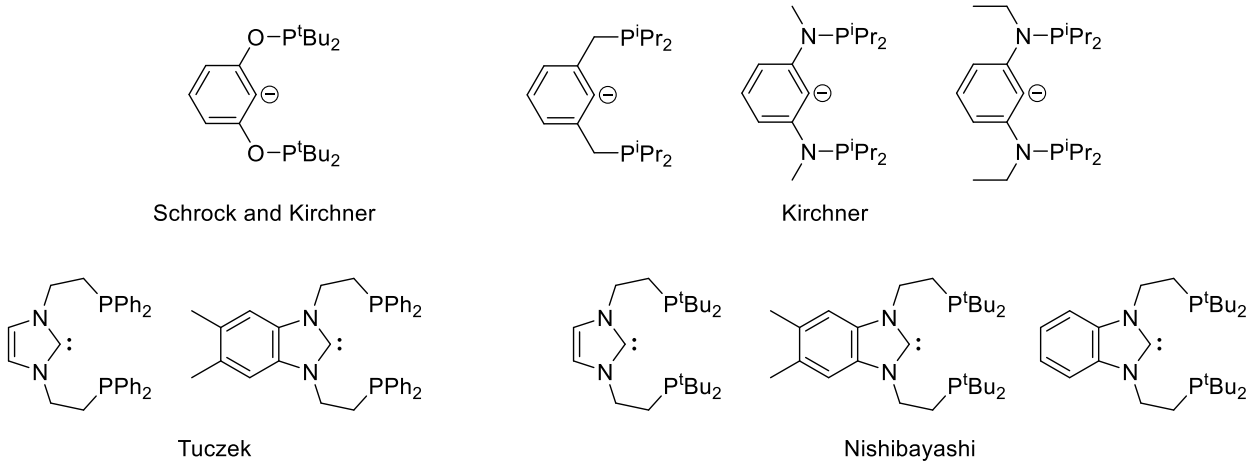

Figure 4.1: The complete list of PCP ligands used with group 6 transition metals.

Results and Discussion

We chose for this study the PCP pincer ligand 2,6-bis(di-*tert*-butylphosphinomethyl)-phenyllithium, Li(^{tBu}PCP), which can be prepared by adding ^{n}BuLi to a pentane solution of (^{tBu}PCP)Br under an inert atmosphere. The lithium salt precipitates out of solution and can be isolated by filtration. Although Li(^{Me}PCP), the methyl analog, is soluble in aromatic solvents,[83] Li(^{tBu}PCP) is not; the white powder is pyrophoric and produces a red flame when burned.

Preparation of New PCP Compounds of Titanium. We find that the reaction of $TiCl_3(THF)_3$ with Li(^{tBu}PCP) in pentane produces a deep blue solution. After filtration to remove insoluble byproducts, the pentane solution is concentrated to saturation under vacuum at room

temperature and then cooled to -20 °C to afford deep blue crystals of the titanium(III) complex (^{tBu}PCP)$TiCl_2$.

(^{tBu}PCP)$TiCl_2$ crystallizes in the $P\bar{1}$ space group with six molecules in the asymmetric unit. The following discussion will describe the average structure of the six molecules. The Ti atom in (^{tBu}PCP)$TiCl_2$ adopts a distorted square pyramidal geometry in which a chlorine atom is in the axial site (Figure 4.3). The trigonality index,[84] τ, of the square pyramid is 0.29 (a τ of 0 describes a perfect square pyramid whereas a τ of 1 describes a perfect trigonal bipyramid). The square pyramidal geometry causes the two C-Ti-Cl angles to be distinctly different: 121.96(2)° for the Cl atom in the axial site and 132.42(2)° for the Cl atom in an equatorial site. The aryl ring is rotated 21.36(4)° from the P-Ti-P plane (Figure 4.4).

The two Ti-Cl distances are nearly identical, 2.3081(2) Å for Cl_{ax} and 2.3220(2) Å for Cl_{eq}; these Ti-Cl distances are longer than those of 2.2762(9) and 2.2997(9) Å reported for the 5-coordinate Ti^{III} pincer complex (^{tBu}PNP)$TiCl_2$, where ^{tBu}PNP is 2,5-bis(di-*tert*-butylphosphinomethyl)pyrrolide, but shorter than those of 2.380(1) and 2.498(2) Å in a 6-coordinate Ti^{III} pincer complex (NCN)$TiCl_3$, where NCN is *sym*-bis(2-pyridyl)tetraphenylcarbodiphosphorane.

The Ti-P bond distances in (^{tBu}PCP)$TiCl_2$ of 2.6015(2) and 2.6153(2) Å fall between the values of 2.6000(9) and 2.6462(9) Å reported for the (^{tBu}PNP)$TiCl_2$ complex. The P-Ti-P angle in (^{tBu}PCP)$TiCl_2$ is 149.565(8)°, which is similar to the 149.68(3)° angle observed for the (^{tBu}PNP)$TiCl_2$ complex. The Ti-C bond distance in (^{tBu}PCP)$TiCl_2$ is 2.2042(7) Å, which is consistent with other Ti^{III}-aryl bond distances, such as those of 2.193(3) Å and 2.262(8) Å in $Cp_2Ti(\kappa^2$-C_6H_4-2-$CH_2OMe)$[85] and $[Ti(C_6F_5)_5]^{2-}$,[86] respectively.

Treating (^{tBu}PCP)TiCl$_2$ with LiBH$_4$ in Et$_2$O affords a purple mixture. Filtering and crystallizing in the manner described before yields purple crystals of the new titanium(III) borohydride complex (^{tBu}PCP)Ti(BH$_4$)$_2$.

The borohydride compound (^{tBu}PCP)Ti(BH$_4$)$_2$ crystallizes in the $P2_1/n$ space group with three molecules in the asymmetric unit. The following discussion will describe the average structure of the three independent molecules. As seen for (^{tBu}PCP)TiCl$_2$, the Ti center in (^{tBu}PCP)Ti(BH$_4$)$_2$ also adopts a distorted square pyramidal geometry (counting each BH$_4$ group as occupying one coordination site), with a trigonality index of $\tau = 0.37$ (Figure 4.11). The aryl ring is rotated 25.07(4)° with respect to the P-Ti-P plane (Figure 4.12).

One BH$_4^-$ ligand is tridentate (κ^3) and the other is bidentate (κ^2). These coordination modes are expected from an analysis of the valence electrons. Ti^{III} is a d^1 species, and therefore has 8 valence orbitals available for bonding.[87-89] Of these, 3 orbitals are used to form sigma bonds to the PCP ligand, leaving 5 to form bonds with the borohydride ligands. Therefore, we expect one of the borohydride ligands to coordinate in a κ^3 manner and the other in a κ^2 manner.

The κ^2-BH$_4$ group occupies the axial site of the square pyramid, with a Ti-B distance of 2.3889(13) Å. This distance is consistent with the Ti-B distances found for other complexes in which κ^2-BH$_4$ groups are coordinated to Ti^{III}, which range from 2.37(1) Å for Cp$_2$Ti(κ^2-BH$_4$)[90] and 2.458(2) Å for Cp*Ti(κ^2-9-BBN)$_2$(THF).[91] The κ^3-BH$_4$ has a shorter Ti-B distance of 2.2247(12) Å that is slightly longer than the 2.220(9) Å Ti^{III}-B distance reported for [Cp*TiCl(κ^3-BH$_4$)]$_2$.[92] The C-Ti-B angles are 122.30(4)° to the κ^3-BH$_4$ group and 118.69(4)° to the κ^2-BH$_4$ group.

The Ti-P bond distances, 2.6284(3) and 2.6712(3) Å, are elongated compared to those seen in (^{tBu}PCP)TiCl$_2$, but the P-Ti-P angle of 147.45(1)° and the Ti-C bond distance of 2.2002(9) Å, are similar to those in (^{tBu}PCP)TiCl$_2$.

Preparation of New PCP Compounds of Chromium. Kirchner prepared (PCP)Cr complexes by oxidative addition of haloaryl bonds to $Cr(CO)_6$.[41, 81] Because of the availability of Li(^{tBu}PCP), we investigated use of salt elimination reactions to synthesize new chromium PCP compounds. We find that the reaction of $CrCl_3(THF)_3$ with Li(^{tBu}PCP) in Et_2O produces a dark orange reaction solution. When this solution is taken to dryness under vacuum, the resulting solid consists of a mixture of blue (^{tBu}PCP)$CrCl_2$(THF) and orange (^{tBu}PCP)$CrCl_2$. The residue can be redissolved in THF to afford a blue solution. Concentration to saturation at room temperature and then cooling to -20 °C affords blue crystals of the six-coordinate complex (^{tBu}PCP)$CrCl_2$(THF). If desired, the coordinated THF molecule can be removed, either by heating under vacuum at elevated temperature (80 °C) or by trituration with pentane, to afford (^{tBu}PCP)$CrCl_2$ as a bright orange powder. Attempts to crystallize unsolvated (^{tBu}PCP)$CrCl_2$ have so far been unsuccessful and resulted in powders. As for the Ti analog, this reaction can be scaled up to produce gram quantities of (^{tBu}PCP)$CrCl_2$.

(^{tBu}PCP)$CrCl_2$(THF) crystallizes in the $P\bar{1}$ space group with one molecule in the asymmetric unit (Figure 4.7). The compound adopts an octahedral geometry about the Cr atom, with the coordinated THF *trans* to the carbon atom of the PCP ligand. The aryl backbone is rotated 23.92(3)° relative to the P-Cr-P plane (Figure 4.8). The Cr-Cl bond distances (2.3237(7) Å) and P-Cr-P angle (158.51(2)°) are similar to those in the octahedral Cr^{III} pincer complex (PNCNP)$CrCl_2(NCCH_3)$, where PNCNP is the tridentate ligand 2,6-bis[(diisopropylphosphino)-ethylamino]phenyl (Cr-Cl: 2.3211(4) Å and P-Cr-P: 160.73(1)°).[81] The Cr-O bond distance, 2.1299(14) Å, for the coordinated THF ligand in (^{tBu}PCP)$CrCl_2$(THF) is similar to the Cr-N bond distance, 2.131(1) Å for the coordinated CH_3CN ligand in (PNCNP)$CrCl_2(NCCH_3)$. However, the Cr-C bond distance (2.0468(18) Å) in (^{tBu}PCP)$CrCl_2$(THF) is slightly shorter and the Cr-P bond

distances (2.5740(7) and 2.5815(7) Å) are significantly longer than those of (PNCNP)$CrCl_2(NCCH_3)$ (Cr-C: 2.052(1) Å, Cr-P: 2.4506(4) and 2.4582(4) Å).

The reduction (^{tBu}PCP)$CrCl_2$ with KC_8 in Et_2O results in a purple mixture. Filtration followed by concentrating the solution to saturation under vacuum at room temperature and then cooling to 20 °C affords purple crystals of the chromium(II) complex (^{tBu}PCP)CrCl.

(^{tBu}PCP)CrCl crystallizes in the $P2_1/n$ space group with one molecule in the asymmetric unit. The Cr center adopts a square planar geometry (Figure 4.9), as is often seen for other high-spin chromium(II) complexes. Unlike the titanium PCP compounds discussed above, the aryl backbone is coplanar with the P-Cr-P plane. However, the Cr-C bond is bent 7.1(1)° out of the aryl plane (Figure 4.10). The solid state structures of Kirchner's (POCOP)Cr^{II} compounds, where POCOP is 2,6-bis[(di-*tert*-butylphosphino)oxy]phenyl, do not have this feature; the Cr atom lies in the plane described by the aryl ring.[41] Otherwise, the coordination environment about the Cr atom in (^{tBu}PCP)CrCl is similar to those in the (POCOP)Cr^{II} complexes.

The bond distances in (^{tBu}PCP)CrCl between the Cr and its surrounding atoms (Cr-Cl: 2.3053(9) Å, Cr-P: 2.4436(9) and 2.4522(9) Å) are shorter than those in (^{tBu}PCP)$CrCl_2$(THF), with the exception of the Cr-C bond (2.0897(26) Å), which is slightly elongated. Normally, a decrease in oxidation state should result in elongation of bond distances. However, the change in coordination number counteracts the effect due to the change in oxidation state.

Attempted Dinitrogen Chemistry. The reduction of (^{tBu}PCP)$CrCl_2$ with KC_8 in Et_2O affords (^{tBu}PCP)CrCl whether or not N_2 is used as the inert atmosphere. In an effort to prepare a dinitrogen complex of titanium, (^{tBu}PCP)$TiCl_2$ was stirred in THF with 1 equiv of KC_8 under an N_2 atmosphere. The $^{31}P\{^1H\}$ NMR spectrum of the resulting brown mixture showed that free H(^{tBu}PCP) was generated, along with a compound that exhibits an AB quartet with δ_A 52.1, δ_B

51.6, and J_{AB} 32 Hz. The use of 3 equiv of KC_8 resulted in the formation of H(^{tBu}PCP) as well as three compounds that gave AB quartets in the ^{31}P NMR spectrum (δ_A 54.9, δ_B 54.4, J_{AB} 31 Hz; δ_A 52.3, δ_B 51.1, J_{AB} 29 Hz; and δ_A 51.6, δ_B 51.1, J_{AB} 33 Hz). These diamagnetic compounds were not present when Et_2O or pentane were used as the solvent; it is possible the KC_8 decomposed some THF and produced reactive species that are responsible for the compounds exhibiting the AB quartets.[93] In all reactions, removal of the solvent, extraction with pentane, and then drying under vacuum resulted in brown oils. Attempts to crystallize any of the components of these oils were unsuccessful. Recently, Nishibayashi reported that a (PNP)Ti^{III}Cl$_2$ compound also produced an intractable mixture of compounds when reduced with KC_8 under an atmosphere of N_2, but introduction of a Cp^- ligand afforded an isolable dinitrogen complex.[69] It is believed that the Cp^- ligand discourages side-on binding of the N_2 ligand, which could lead to the production of the intractable products. The effect of Cp^- on the coordination mode of N_2 was demonstrated by Fryzuk et al. in a (PNP)Zr system.(Figure 4.2).[94]

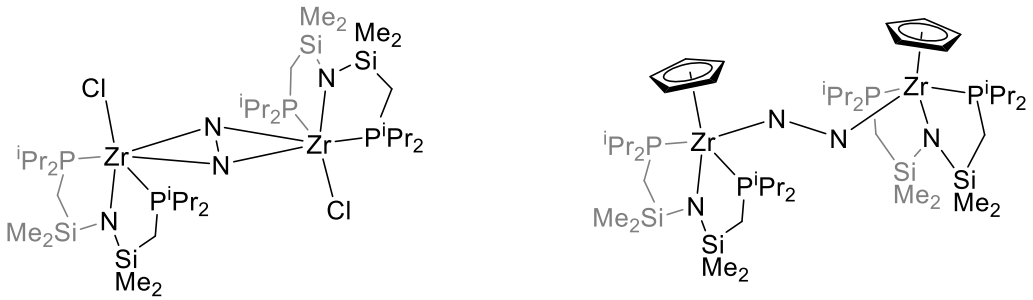

Figure 4.2: The N_2 in [(PNP)ZrCl]$_2$(N_2) bridges the Zr centers in a side-on fashion. Replacing the Cl^- with Cp^- changes the N_2 binding mode from side-on to end-on.[94]

Attempts to synthesize PCP complexes of V and Nb analogs from $VCl_3(THF)_3$ and $NbCl_3$(DME) were unsuccessful. Mindiola also experienced difficulties in isolating a (PNP)Nb^{III}Cl$_2$ complex but was able to infer its existence through the subsequent formation of a

dinitrogen complex.[56] We were unable to isolate any dinitrogen compounds of V or Nb when performing these reactions under an atmosphere of N_2.

Other Unsuccessful Reactions. Adding an excess of MeLi to a THF solution of (^{tBu}PCP)$TiCl_2$, followed by drying under vacuum and extraction with pentane, affords a dark green oily solid that could not be crystallized. Its ^{1}H NMR spectrum in C_6D_6 showed the presence of two major components: free H(^{tBu}PCP) along with a paramagnetic compound that has a different NMR spectrum from (^{tBu}PCP)$TiCl_2$. The reaction between (^{tBu}PCP)$CrCl_2$ and MeLi in ethereal solvents produces a green mixture. As with the Ti analog, pure materials could not be isolated from this reaction.

Unlike (^{tBu}PCP)$TiCl_2$, (^{tBu}PCP)$CrCl_2$ does not undergo simple salt elimination with $LiBH_4$. Treatment of (^{tBu}PCP)$CrCl_2$ with $LiBH_4$ in Et_2O results in a maroon mixture and evolution of gas. Colorless crystals of H(^{tBu}PCP)·BH_3 can be grown from the solution. The change in color suggests that BH_4^- reduces Cr^{III} and generates BH_3. The resulting Cr complex evidently decomposes and liberates free H(^{tBu}PCP), which associates with BH_3 in solution.

One of the major challenges in this project is the separation and characterization of reaction products: the ^{tBu}PCP complexes are very soluble in hydrocarbon and ethereal solvents, and are difficult to crystallize. We attempted to replace the ^{t}Bu substituents on the PCP ligand with adamantyl substituents to lower the solubility of the pincer complexes. However, we were unable to prepare Li(^{Ad}PCP) by lithium-halogen exchange from (^{Ad}PCP)Br.

Conclusions

PCP pincer complexes of early transition metals are an understudied class of compounds. We report the preparation of (^{tBu}PCP)$TiCl_2$ and (^{tBu}PCP)$CrCl_2$, where ^{tBu}PCP is 2,6-bis(di-*tert*-

butylphosphinomethyl)phenyl. (^{tBu}PCP)$TiCl_2$ adopts a distorted square pyramidal structure in which a Cl atom occupies the axial site. The compound undergoes salt metathesis with $LiBH_4$ to afford (^{tBu}PCP)$Ti(BH_4)_2$. The Ti center in this borohydride complex also adopts a distorted square pyramidal structure. One of the borohydride ligands coordinates in a κ^3 manner and the other in a κ^2 manner; the κ^2-BH_4 group occupies the axial site of the square pyramid. We have also prepared the Cr^{III} complex (^{tBu}PCP)$CrCl_2$(THF), in which the Cr atom adopts an octahedral geometry as expected for this d^3 ion. The compound (^{tBu}PCP)$CrCl_2$ can be reduced to (^{tBu}PCP)CrCl, in which the high-spin d^4 Cr^{II} atom exhibits a square planar geometry. Attempts to reduce these compounds in the presence of dinitrogen or to methylate the complexes have so far resulted in intractable mixtures.

Experimental Details

Unless otherwise stated, all operations were conducted under argon using standard Schlenk line and glovebox techniques. Pentane, diethyl ether, and THF were dried over sodium-benzophenone ketyl and distilled immediately before use. 1.6 M ^{n}BuLi in hexanes and was purchased from Sigma-Aldrich and titrated before use using a literature procedure.[95] KC_8,[96] $TiCl_3(THF)_3$,[97] and $CrCl_3(THF)_3$[98] were prepared according to the literature. $LiBH_4$ was used as purchased from Strem Chemicals. (^{tBu}PCP)Br and (^{Ad}PCP)Br were prepared as described in Chapter 3.

Elemental analyses were performed by the School of Chemical Sciences Microanalysis Laboratory at the University of Illinois at Urbana-Champaign. NMR spectra were acquired on a Varian 500 MHz spectrometer at room temperature. ^{1}H NMR spectra are reported in δ units (positive chemical shifts to higher frequency) relative to TMS as determined from residual solvent

signals.[99] NMR spectra were processed with the MestReNova NMR software package. FTIR spectra were acquired on a Thermo Nicolet IR200 spectrometer as mineral oil solutions between KBr plates. IR spectra were processed using the OMNIC® software package. X-ray crystallographic data were collected by the George L. Clark X-Ray Facility and 3M Materials Laboratory.

2,6-Bis[(di-*tert*-butylphosphino)methyl]phenyllithium, Li(^{tBu}PCP). This compound was synthesized by modifying a literature procedure.[83] Pentane (20 mL) was added to (^{tBu}PCP)Br (0.986 g, 2.08 mmol) and the mixture was stirred, affording a slightly yellow solution. The solution was cooled to -78 °C and a 1.6 M solution of ^{n}BuLi in hexanes (1.60 mL, 2.56 mmol) was added by gas-tight syringe. The mixture was stirred overnight, affording a cloudy dark-orange mixture. The mixture was filtered and the white powder was washed with pentane (3x20 mL). The powder was dried under vacuum. Yield: 0.82 g (96%).

2,6-Bis[(di-*tert*-butylphosphinomethyl)phenyl]dichlorotitanium(III), (^{tBu}PCP)TiCl$_2$. To a mixture of $TiCl_3(THF)_3$ (1.110 g, 2.97 mmol) and Li(^{tBu}PCP) (1.026 g, 2.78 mmol) was added pentane (200 mL). The mixture was stirred overnight, affording a dark blue mixture. The mixture was filtered and the precipitate was washed with pentane (50 mL). The filtrate and wash were combined, concentrated to saturation under vacuum at room temperature, and then cooled to -20 °C to afford deep blue crystals of the product. The mother liquor was removed and the crystals dried under vacuum. Yield: 0.95 g (67%). Anal. Calc. for $C_{24}H_{43}Cl_2P_2Ti$: C, 56.3; H, 8.46. Found: C, 55.3; H, 8.42. ^{1}H NMR (C_6D_6, 25 °C): δ 23.9 (br s, fwhm = 290 Hz, 4 H, CH_2), δ 9.03 (br s, fwhm = 23 Hz, 1 H, Ar-H), δ 2.31 (br s, fwhm = 110 Hz, 36 H, CH_3), δ -1.26 (br s, fwhm = 60 Hz, 2 H, Ar-H). No ^{31}P NMR resonances were observed.

2,6-Bis[(di-*tert*-butylphosphinomethyl)phenyl]bis(borohydride)titanium(III), (^{tBu}PCP)Ti(BH$_4$)$_2$. To a mixture of (^{tBu}PCP)TiCl$_2$ (0.099 g, 0.19 mmol) and LiBH$_4$ (0.010 g, 0.44 mmol) was added Et$_2$O (20 mL). The mixture was stirred overnight, affording a purple mixture. The mixture was filtered and the white solids were washed with Et$_2$O (10 mL). The filtrate and wash were combined, concentrated to saturation under vacuum at room temperature, and then cooled to -20 °C to afford purple crystals.

2,6-Bis[(di-*tert*-butylphosphinomethyl)phenyl]dichloro(tetrahydrofuran)-chromium(III), (^{tBu}PCP)CrCl$_2$(THF). To a mixture of CrCl$_3$(THF)$_3$ (0.105 g, 0.278 mmol) and Li(^{tBu}PCP) (0.111 g, 0.301) was added Et$_2$O (20 mL). The mixture was stirred, affording a dark orange mixture after several minutes. The mixture was stirred overnight and then filtered. The white precipitate was washed with Et$_2$O (10 mL). The filtrate and wash were combined and dried under vacuum. The orange and blue residue was redissolved in THF, concentrated to saturation at room temperature under vacuum, and then cooled to -20 °C to afford blue crystals of the product. The mother liquor was removed and the crystals were dried under vacuum. Yield: 0.0995 g (61%). Anal. Calc. for C$_{28}$H$_{51}$Cl$_2$CrOP$_2$: C, 57.1; H, 8.73. Found: C, 55.5; H, 8.61. IR (cm^{-1}): 1551 (w), 1236 (w), 1172 (m), 1117 (w), 1087 (w), 1021 (m), 958 (w), 935 (w), 920 (w), 867 (m), 834 (m), 820 (m), 809 (m), 774 (m), 743 (m), 704 (w), 673 (w), 600 (w), 578 (w), 480 (w).

2,6-Bis[(di-*tert*-butylphosphinomethyl)phenyl]dichlorochromium(III), (^{tBu}PCP)CrCl$_2$. Method A: (^{tBu}PCP)CrCl$_2$(THF) was heated to 80 °C overnight under vacuum to afford the desolvated product as a bright orange powder. Method B: (^{tBu}PCP)CrCl$_2$(THF) was repeatedly dissolved in pentane and then dried under vacuum until the residue was bright orange. Anal. Calc. for C$_{24}$H$_{43}$Cl$_2$CrP$_2$: C, 55.8; H, 8.39. Found: C, 54.9; H, 8.37. IR (cm^{-1}): 3033 (w),

1931 (w), 1863 (w), 1796 (w), 1549 (m), 1236 (m), 1179 (s), 1135 (w), 1087 (w), 1022 (m), 968 (w), 9.9 (m), 833 (s), 812 (m), 787 (m), 694 (m), 610 (m), 567 (w), 479 (m), 442 (w).

2,6-Bis[(di-*tert*-butylphosphinomethyl)phenyl]chlorochromium(II), (^{tBu}PCP)CrCl. To a mixture of (^{tBu}PCP)$CrCl_2$ (0.101 g, 0.196 mmol) and KC_8 (0.242 g, 1.79 mmol) was added Et_2O (20 mL). The mixture was stirred for 4 h. The dark purple mixture was filtered and the dark solids were washed with Et_2O (10 mL). The filtrate and wash were combined, concentrated to saturation at room temperature under vacuum, and then cooled to -20 °C to afford purple crystals.

Crystallographic details.[100] The following details were common to all of the crystal structure determinations; for details about individual compounds, see the SI. Crystals mounted on Nylon fibers with Paratone® oil were transferred onto the diffractometer and kept at -100 °C for (^{tBu}PCP)$CrCl_2$(THF) and (^{tBu}PCP)CrCl, and -173 °C for the other compounds, in a cold nitrogen gas stream. For (^{tBu}PCP)$CrCl_2$(THF) and (^{tBu}PCP)CrCl, intensity data were collected on a Bruker Kappa/ApexII CCD diffractometer equipped with a CCD area detector. A Siemens fine-focus source provided the Mo Kα radiation (λ = 0.71073 Å) that was monochromated with graphite. For (^{tBu}PCP)$TiCl_2$ and (^{tBu}PCP)$Ti(BH_4)_2$, intensity data were collected on a Bruker D8 Venture kappa diffractometer equipped with a Photon 100 CMOS detector. An Iμs microfocus source provided the Mo Kα radiation that was monochromated with multilayer mirrors. Standard peak search and indexing procedures gave rough cell dimensions. The collection, cell refinement and integration of intensity data were carried out with the APEX3 software (Bruker). The measured intensities were reduced to structure factor amplitudes and their estimated standard deviations by correction for background, scan speed, and Lorentz and polarization effects. No corrections for crystal decay were necessary. Systematically absent reflections were deleted and symmetry equivalent reflections were averaged to yield the set of unique data.

The initial models were obtained by direct methods (SHELXS).[101] The remaining non-hydrogen atoms were located from difference maps obtained from full-matrix least-squares refinements (SHELXL).[101] In the final cycle of least squares, independent anisotropic displacement factors were refined for the non-hydrogen atoms, with isotropic restraints applied to the minor site carbon atoms. Hydrogen atoms were placed in idealized positions, except those for the BH_4 ligands which were located from the difference map; the methyl groups were allowed to rotate about the C-X axis to find the best least-squares positions. The displacement parameters for methylene hydrogens were set equal to 1.2 times U_{eq} for the attached carbon; those for methyl hydrogens were set to 1.5 times U_{eq}. Successful convergence was indicated by the maximum shift/error of 0.001 for the last cycle. No correction for decay was necessary, but absorption corrections were conducted by face-indexed or multi-scan methods (SADABS).[102] Data collection and final refinement parameters are given in Tables 4.1 and 4.2. A final analysis of variance between observed and calculated structure factors showed no apparent errors. Solutions were checked with PLATON for missed crystallographic symmetry.

(^{tBu}PCP)TiCl$_2$. Single crystals of (^{tBu}PCP)TiCl$_2$ were grown by cooling a saturated pentane solution. The triclinic lattice and the average values of the normalized structure factors suggested the space group $P\bar{1}$, which was confirmed by the success of the subsequent refinement. A face-indexed absorption correction was applied, the minimum and maximum transmission factors being 0.90 and 0.97. Three reflections (013, 103, and 110) were obscured by the beamstop and were deleted; the remaining 34088 unique data were used in the least squares refinement. There were six molecules in the asymmetric unit, one of which was disordered. The disorder was modeled as a twisting of the pincer ligand. The occupancies of the two components were constrained to add to 1; the site occupancy factor for the major component refined to 0.802(5).

The aromatic ring of the minor component was restrained to be flat and have C-C bond distances of 1.45 Å. The isotropic displacement parameters for the C atoms of the aromatic ring of the minor component were assigned a common value. Analogous C-P bond distances between the major and minor disorder components were restrained to be within a standard uncertainty of 0.01 Å of each other. The C-C bond distances of the ^{t}Bu groups in both components were restrained to be 1.54(1) Å. The quantity minimized by the least-squares program was $\Sigma w(F_o^2 - F_c^2)^2$, where $w = \{[\sigma(F_o^2)]^2 + (0.0288P)^2 + 5.8681P\}^{-1}$ and $P = (F_o^2 + 2F_c^2)/3$. No correction for isotropic extinction was necessary. The largest peak in the final Fourier difference map (0.59 eÅ^{-3}) was located 0.76 Å from Cl3.

(^{tBu}PCP)CrCl$_2$(THF). Single crystals of (^{tBu}PCP)CrCl$_2$(THF) were grown by cooling a saturated THF solution. The triclinic lattice and the average values of the normalized structure factors suggested the space group $P\bar{1}$, which was confirmed by the success of the subsequent refinement. A face-indexed absorption correction was applied, the minimum and maximum transmission factors being 0.84 and 0.96. The quantity minimized by the least-squares program was $\Sigma w(F_o^2 - F_c^2)^2$, where $w = \{[\sigma(F_o^2)]^2 + (0.0335P)^2 + 0.6478P\}^{-1}$ and $P = (F_o^2 + 2F_c^2)/3$. An isotropic extinction parameter was refined to a final value of $x = 1.4(5) \times 10^{-6}$ where F_c is multiplied by the factor $k[1 + F_c^2 x\lambda^3/\sin 2\theta]^{-1/4}$ with k being the overall scale factor. The largest peak in the final Fourier difference map (0.37 eÅ^{-3}) was located 0.88 Å from C7.

(^{tBu}PCP)CrCl. Single crystals of (^{tBu}PCP)CrCl were grown by cooling a saturated Et$_2$O solution. Systematic absences for $0k0$ ($k \neq 2n$) and $h0l$ ($h + l \neq 2n$) were uniquely consistent with the space group $P2_1/n$. A face-indexed absorption correction was applied, the minimum and maximum transmission factors being 0.68 and 0.89. The quantity minimized by the least-squares program was $\Sigma w(F_o^2 - F_c^2)^2$, where $w = \{[\sigma(F_o^2)]^2 + (0.0612P)^2 + 0.5702P\}^{-1}$ and $P = (F_o^2 +$

$2F_c^2)/3$. An isotropic extinction parameter was refined to a final value of $x = 8(1) \times 10^{-6}$ where F_c is multiplied by the factor $k[1 + F_c^2 x\lambda^3/\sin 2\theta]^{-1/4}$ with k being the overall scale factor. The largest peak in the final Fourier difference map (0.51 eÅ^{-3}) was located 0.84 Å from Cl1.

(^{tBu}PCP)Ti(BH$_4$)$_2$. Single crystals of (^{tBu}PCP)Ti(BH$_4$)$_2$ were grown by cooling a saturated Et_2O solution. Systematic absences for $0k0$ ($k \neq 2n$) and $h0l$ ($h + l \neq 2n$) were uniquely consistent with the space group $P2_1/n$. A face-indexed absorption correction was applied, the minimum and maximum transmission factors being 0.90 and 0.96. There are three molecules in the asymmetric unit. One of the ^{t}Bu substituents was disordered; the disorder was modeled as a slight bending and rotation of the ^{t}Bu substituent. The occupancies of the two components were constrained to add to 1; the site occupancy factor for the major component refined to 0.608(4). The C-C bond distances of the disordered ^{t}Bu substituent were restrained to 1.54(1) Å. The P-C bond distances of the disordered ^{t}Bu substituent were restrained to be equal within 0.01 Å. The quantity minimized by the least-squares program was $\Sigma w(F_o^2 - F_c^2)^2$, where $w = \{[\sigma(F_o^2)]^2 + (0.0305P)^2 + 5.5511P\}^{-1}$ and $P = (F_o^2 + 2F_c^2)/3$. No correction for isotropic extinction was necessary. The largest peak in the final Fourier difference map (0.42 eÅ^{-3}) was located 0.85 Å from C56.

Table 4.1: Crystallographic data for (^{tBu}PCP)$TiCl_2$ and (^{tBu}PCP)$CrCl_2$(THF)

Formula	$C_{24}H_{43}Cl_2P_2Ti$	$C_{28}H_{51}Cl_2CrOP_2$
Formula weight	512.32	588.53
T (K)	100(2)	173(2)
λ (Å)	0.71073	0.71073
Crystal system, space group	Triclinic, $P\bar{1}$	Triclinic, $P\bar{1}$
a (Å)	12.7091(8)	11.2426(16)
b (Å)	16.2401(10)	11.6609(16)
c (Å)	40.913(3)	13.674(2)
α (°)	99.624(2)	105.158(7)
β (°)	92.822(2)	103.216(8)
γ (°)	91.951(2)	109.632(7)
V (Å^3)	8307.8(9)	1527.8(4)
Z, ρ_{calc} (g/cm^3)	12, 1.229	2, 1.279
μ (mm^{-1}), F(000)	0.63, 3276.0	0.67, 630
Crystal size (mm)	0.050×0.163×0.249	0.146×0.249×0.291
θ range (°)	2.30 – 26.44	1.65 – 28.53
R(int)	0.0450	0.0592
Absorption correction	Face-indexed	Face-indexed
Max., min. transmission factors	0.97, 0.90	0.96, 0.84
Data/restraints/parameters	34088/22/1698	7675/0/320
GOF on F^2	1.041	1.027
R_1 [$I > 2\sigma(I)$]	0.0322	0.0356
wR_2 (all data)	0.0743	0.0896
max., min. $\Delta\rho_{elect}$ (eÅ^{-3})	0.59, -0.31	0.37, -0.42

Table 4.2: Crystallographic data for (^{tBu}PCP)CrCl and (^{tBu}PCP)Ti(BH_4)$_2$

Formula	$C_{24}H_{43}ClCrP_2$	$C_{24}H_{51}B_2P_2Ti$
Formula weight	480.97	471.11
T (K)	173(2)	100(2)
λ (Å)	0.71073	0.71073
Crystal system	Monoclinic	Monoclinic
Space group	$P2_1/n$	$P2_1/n$
a (Å)	7.6672(13)	12.9305(8)
b (Å)	24.427(4)	16.1553(10)
c (Å)	13.844(2)	40.650(2)
β (°)	94.688(7)	92.909(2)
V (Å^3)	2584.4(8)	8480.6(9)
Z, ρ_{calc} (g/cm^3)	4, 1.236	12, 1.107
μ (mm^{-1})	0.68	0.425
F(000)	1032	3084
Crystal size (mm)	0.095×0.153×0.340	0.182×0.200×0.437
θ range (°)	1.67 – 25.67	2.22 – 27.22
R(int)	0.1198	0.0612
Absorption correction	Face-indexed	Face-indexed
Max., min. transmission factors	0.89, 0.68	0.96, 0.90
Data/restraints/parameters	4861/0/266	18882/7/956
GOF on F^2	1.051	1.030
R_1 [$I > 2\sigma(I)$]	0.0488	0.0362
wR_2 (all data)	0.1336	0.0821
max., min. $\Delta\rho_{elect}$ (eÅ^{-3})	0.51, -0.44	0.42, -0.42

Table 4.3: Selected distances and angles for a representative molecule of (^{tBu}PCP)TiCl$_2$

Distances (Å)					
Ti1-Cl1	2.3015(6)	P1-C13	1.8917(19)	C2-C7	1.5117(25)
Ti1-Cl2	2.3358(5)	P2-C8	1.8359(18)	C3-C4	1.3808(26)
Ti1-P1	2.6008(6)	P2-C17	1.8910(19)	C4-C5	1.3800(26)
Ti1-P2	2.6443(6)	P2-C21	1.8851(18)	C5-C6	1.3971(25)
Ti1-C1	2.2083(17)	C1-C2	1.4205(24)	C6-C8	1.5138(24)
P1-C7	1.8300(18)	C1-C6	1.4109(25)		
P1-C9	1.8790(18)	C2-C3	1.3903(25)		
Angles (°)					
Cl1-Ti1-Cl2	102.92(2)	Ti1-P1-C13	113.38(6)	C2-C1-C6	115.42(16)
Cl1-Ti1-P1	100.18(2)	C7-P1-C9	105.00(8)	C1-C2-C3	122.10(16)
Cl1-Ti1-P2	99.57(2)	C7-P1-C13	105.68(9)	C1-C2-C7	119.68(15)
Cl1-Ti1-C1	120.83(5)	C9-P1-C13	111.42(9)	C3-C2-C7	118.22(16)
Cl2-Ti1-P1	93.68(2)	Ti1-P2-C8	99.92(6)	C2-C3-C4	120.43(17)
Cl2-Ti1-P2	101.73(2)	Ti1-P2-C17	115.69(6)	C3-C4-C5	119.56(17)
Cl2-Ti1-C1	136.06(5)	Ti1-P2-C21	118.08(6)	C4-C5-C6	120.33(17)
P1-Ti1-P2	151.47(2)	C8-P2-C17	103.81(9)	C1-C6-C5	122.13(16)
P1-Ti1-C1	75.83(5)	C8-P2-C21	103.92(9)	C1-C6-C8	121.81(16)
P2-Ti1-C1	76.42(5)	C17-P2-C21	112.53(8)	C5-C6-C8	116.03(16)
Ti1-P1-C7	97.28(6)	Ti1-C1-C2	121.11(12)	P1-C7-C2	107.77(12)
Ti1-P1-C9	121.36(6)	Ti1-C1-C6	123.36(12)	P2-C8-C6	111.94(13)

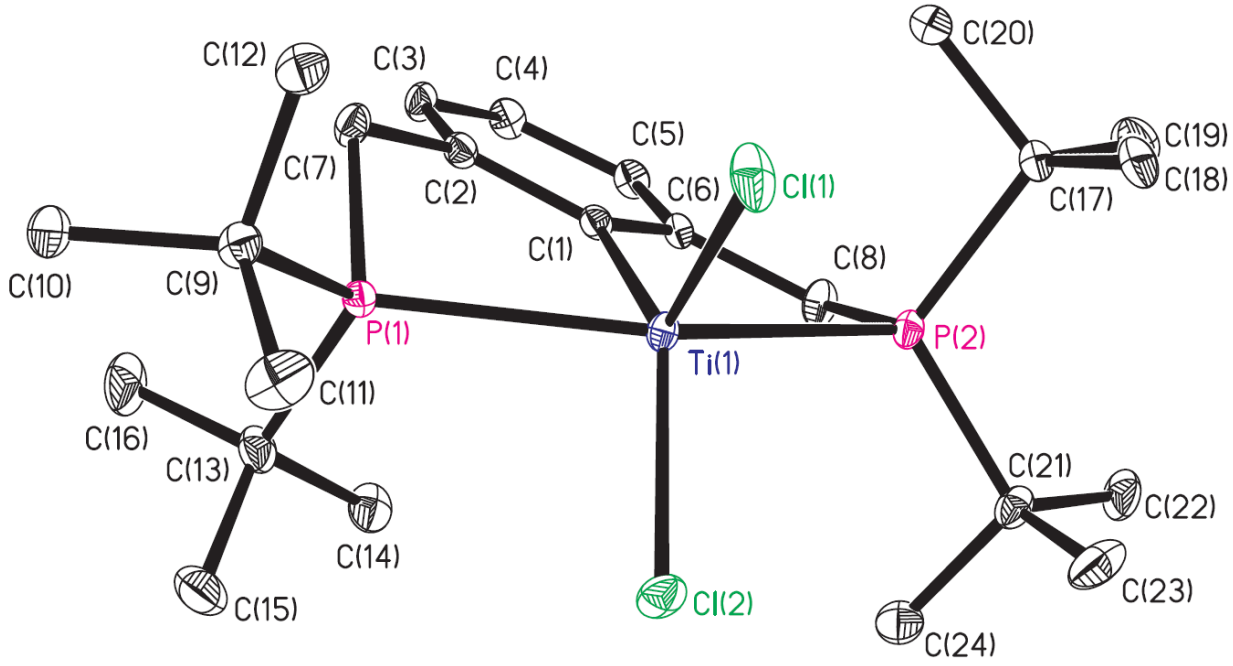

Figure 4.3: Molecular structure of one molecule in the asymmetric unit cell of (^{tBu}PCP)$TiCl_2$. Ellipsoids are drawn at the 35% probability level; hydrogen atoms are omitted for clarity.

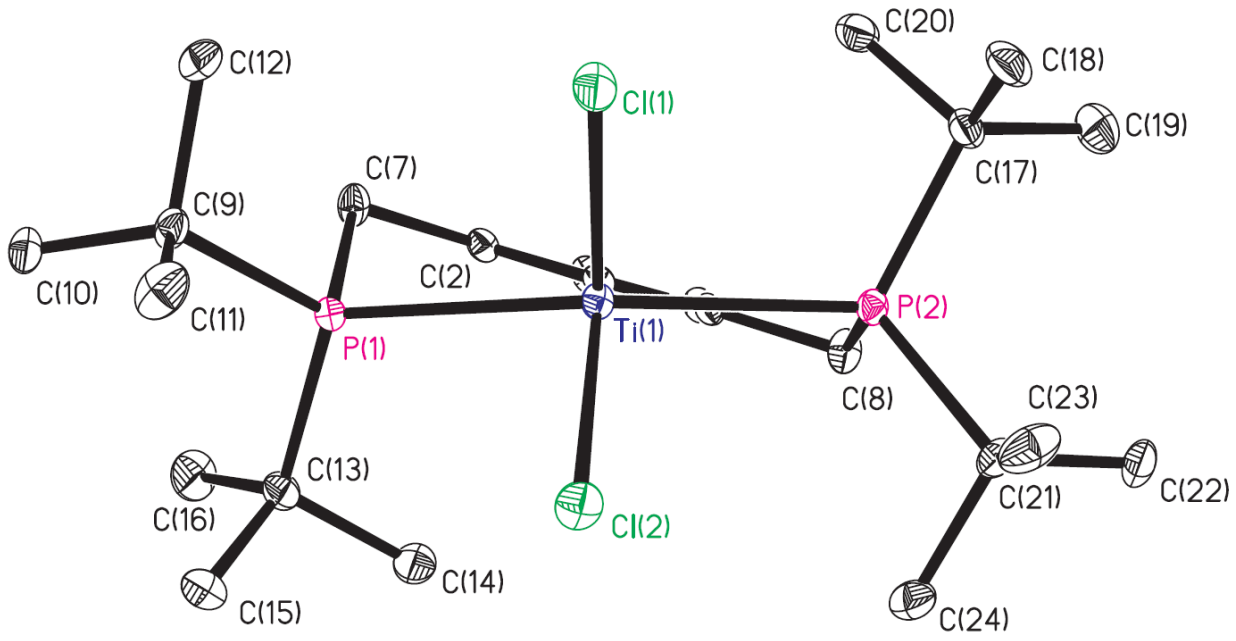

Figure 4.4: An alternative view of (^{tBu}PCP)TiCl$_2$ down the Ti1-C1 axis. The aryl plane is rotated out of the P1-Ti1-P1 plane by 21.36(4)°.

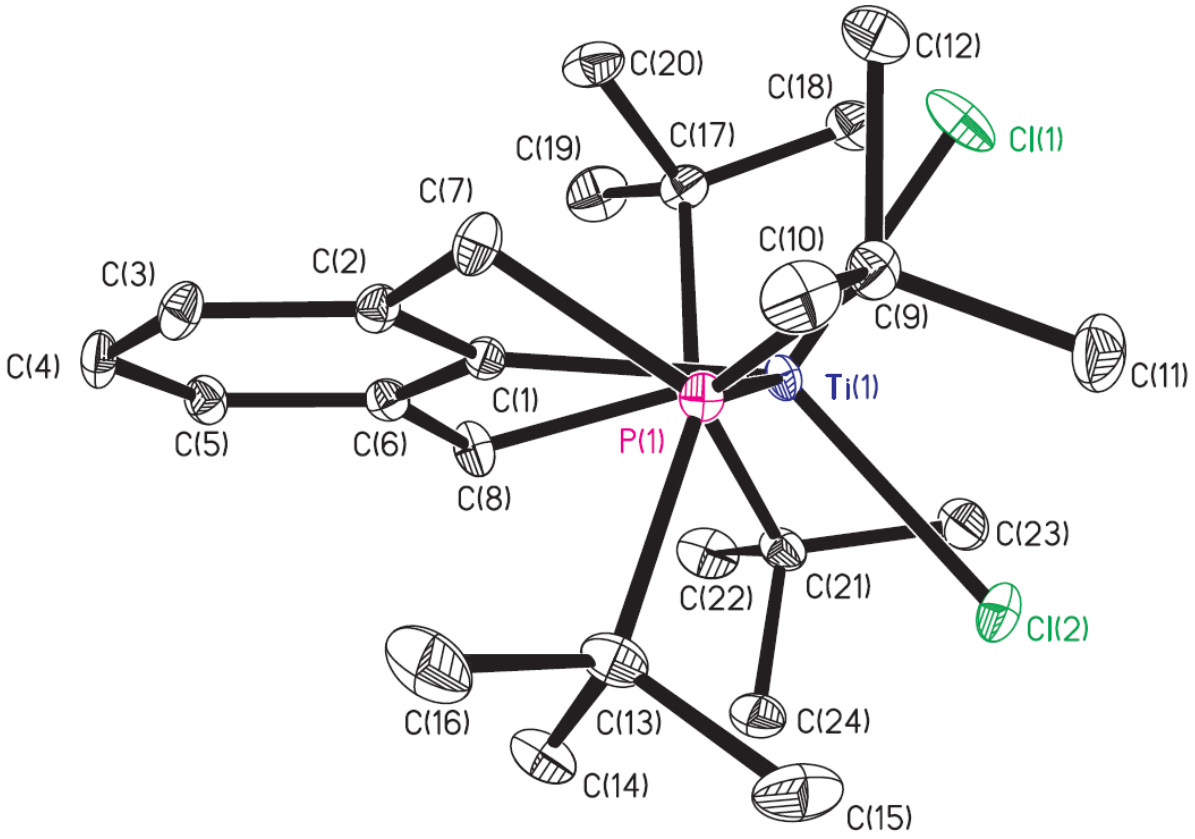

Figure 4.5: An alternative view of (^{tBu}PCP)$TiCl_2$ down the P1-P2 axis. Cl2 is more *trans*- to the aryl ring (has a larger C-Ti-Cl bond angle) and has a larger Ti-Cl bond length than Cl1.

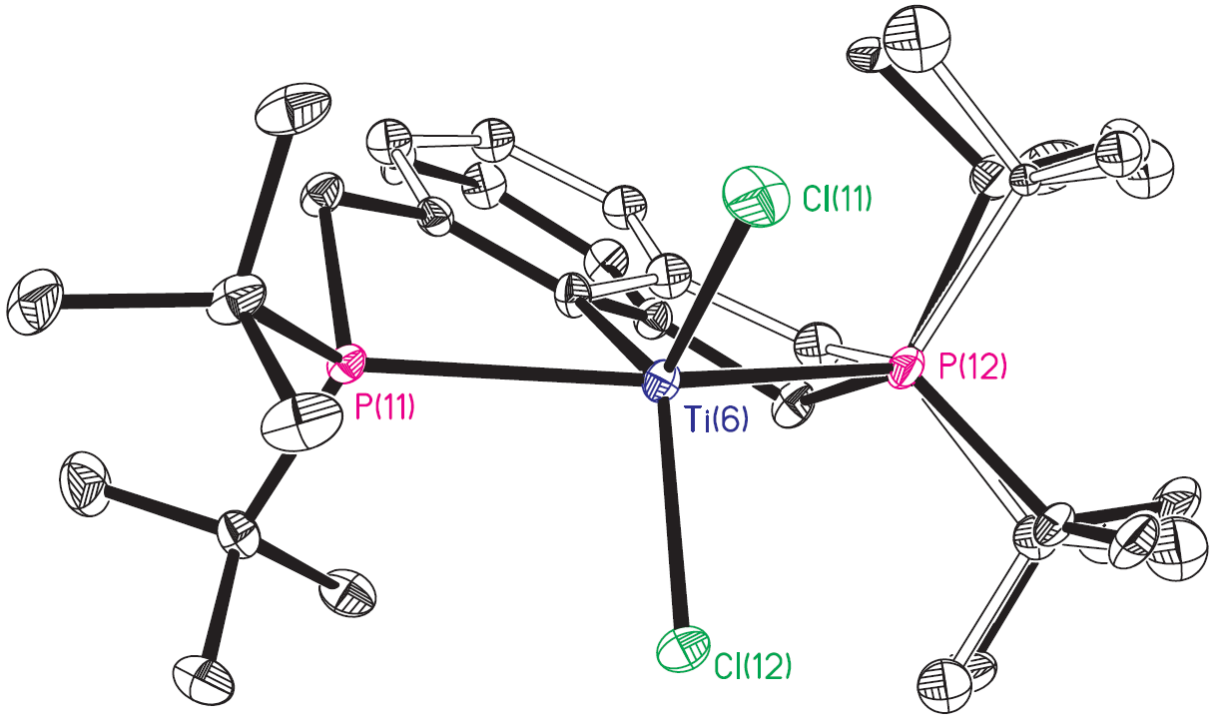

Figure 4.6: The two components of the disorder model for (^{tBu}PCP)TiCl$_2$. The major component (solid bonds) and the minor component (hollow bonds) are related by a 11.0(4)° rotation about a C-C bond of the aryl ring.

Table 4.4: Selected distances and angles for (^{tBu}PCP)$CrCl_2$(THF)

Distances (Å)					
Cr1-Cl1	2.3237(7)	P1-C9	1.8972(20)	C2-C3	1.3921(26)
Cr1-Cl2	2.3237(7)	P1-C13	1.8935(19)	C2-C7	1.5197(26)
Cr1-P1	2.5740(7)	P2-C8	1.8376(19)	C3-C4	1.3857(28)
Cr1-P2	2.5815(7)	P2-C17	1.8984(21)	C4-C5	1.3851(28)
Cr1-C1	2.0468(18)	P2-C21	1.9082(20)	C5-C6	1.3920(29)
Cr1-O1	2.1299(14)	C1-C2	1.4029(25)	C6-C8	1.5199(26)
P1-C7	1.8395(19)	C1-C6	1.3995(26)		
Angles (°)					
Cl1-Cr1-Cl2	176.77(2)	P2-Cr1-O1	100.24(4)	C17-P2-C21	108.67(9)
Cl1-Cr1-P1	89.37(2)	C1-Cr1-O1	178.73(6)	C2-C1-C6	118.22(17)
Cl1-Cr1-P2	91.55(2)	Cr1-P1-C7	92.86(6)	C1-C2-C3	120.81(17)
Cl1-Cr1-C1	90.91(5)	Cr1-P1-C9	122.52(7)	C1-C2-C7	119.65(16)
Cl1-Cr1-O1	87.85(4)	Cr1-P1-C13	119.70(6)	C3-C2-C7	119.52(16)
Cl2-Cr1-P1	91.28(2)	C7-P1-C9	105.30(9)	C2-C3-C4	120.06(18)
Cl2-Cr1-P2	89.00(2)	C7-P1-C13	103.67(9)	C3-C4-C5	119.92(18)
Cl2-Cr1-C1	92.32(5)	C9-P1-C13	108.24(9)	C4-C5-C6	120.26(18)
Cl2-Cr1-O1	88.93(4)	Cr1-P2-C8	92.14(6)	C1-C6-C5	120.71(17)
P1-Cr1-P2	158.51(2)	Cr1-P2-C17	119.49(7)	C1-C6-C8	119.43(17)
P1-Cr1-C1	79.00(5)	Cr1-P2-C21	122.95(7)	C5-C6-C8	119.83(17)
P1-Cr1-O1	101.25(4)	C8-P2-C17	103.66(9)		
P2-Cr1-C1	79.52(5)	C8-P2-C21	104.95(9)		

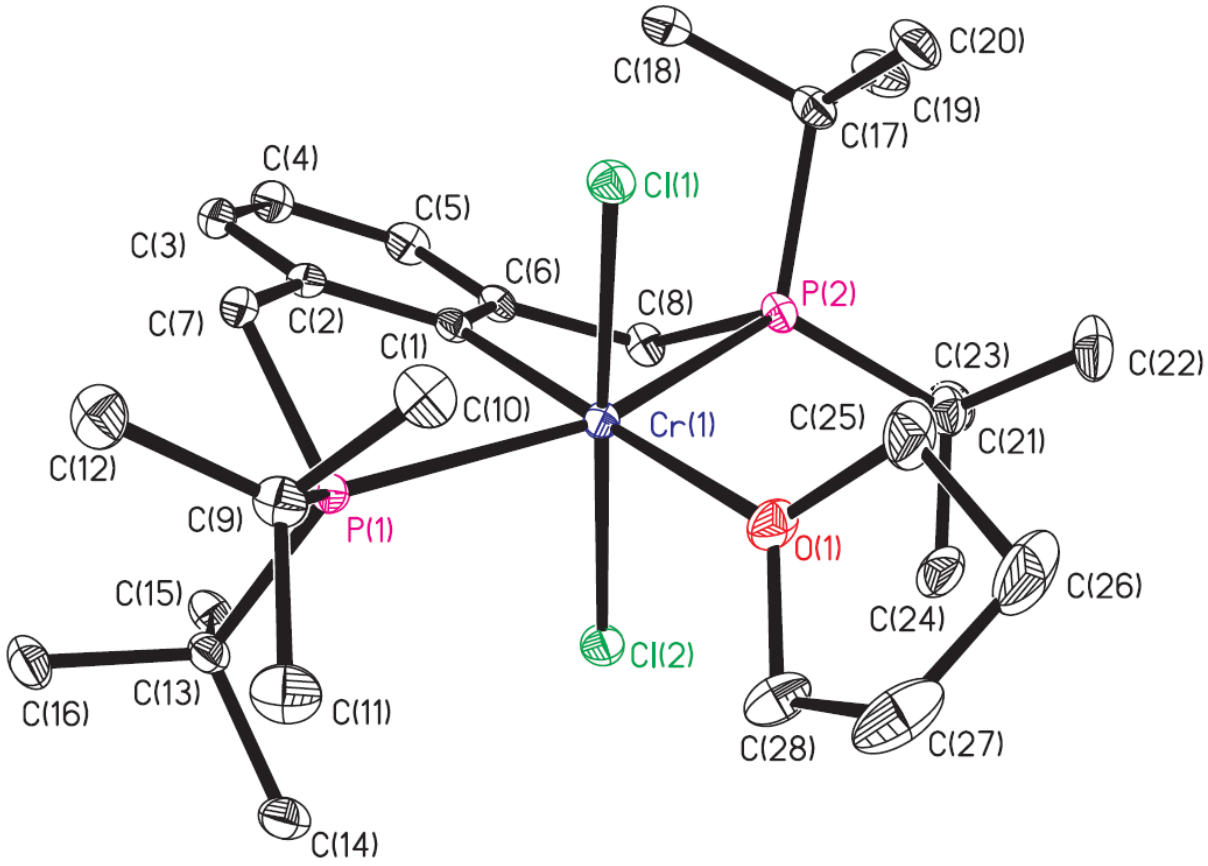

Figure 4.7: Molecular structure of (^{tBu}PCP)$CrCl_2$(THF). Ellipsoids are drawn at the 35% probability level; hydrogen atoms are omitted for clarity.

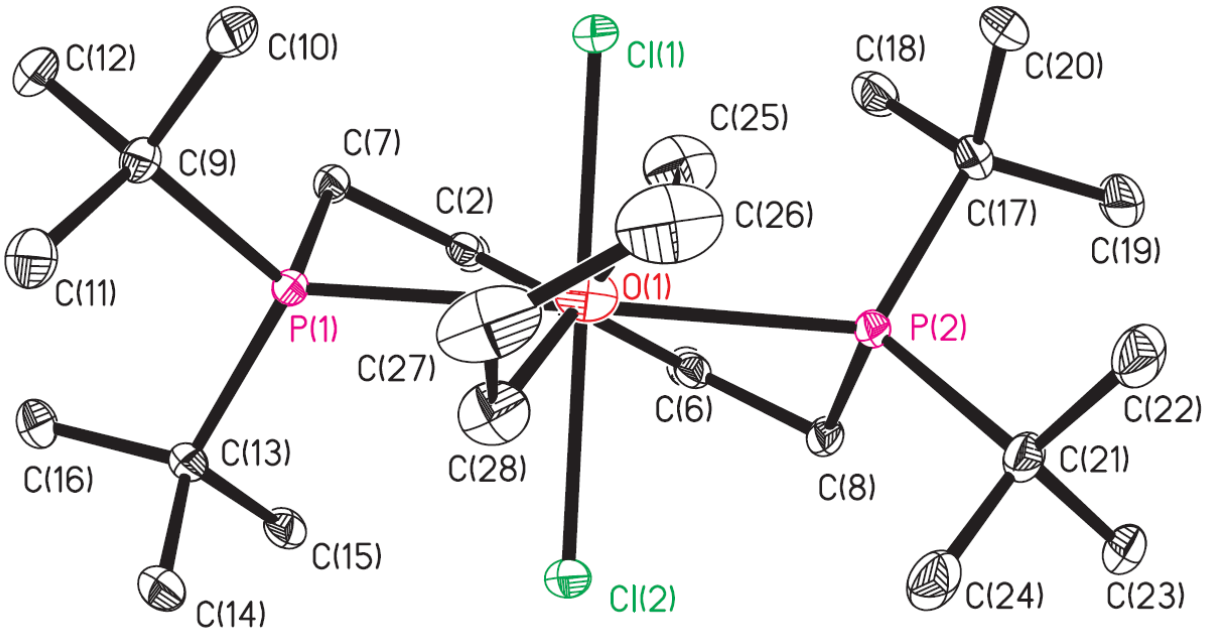

Figure 4.8: An alternative view of (^{tBu}PCP)$CrCl_2$(THF) down the O1-Cr1-C1 axis. The aryl ring is rotated out of the P1-Cr1-P2 plane by 23.92(3)°.

Table 4.5: Selected distances and angles for (^{tBu}PCP)CrCl

Distances (Å)					
Cr1-Cl1	2.3053(9)	P1-C13	1.8696(9)	C2-C3	1.3933(38)
Cr1-P1	2.4436(9)	P2-C8	1.8212(27)	C2-C7	1.5095(40)
Cr1-P2	2.4522(9)	P2-C17	1.8591(30)	C3-C4	1.3736(45)
Cr1-C1	2.0897(26)	P2-C21	1.8654(29)	C4-C5	1.3692(48)
P1-C7	1.8286(29)	C1-C2	1.4011(40)	C5-C6	1.3868(37)
P1-C9	1.8647(31)	C1-C6	1.4107(38)	C6-C8	1.4985(41)

Angles (°)			
Cl1-Cr1-P1	97.93(3)	C8-P2-C17	104.71(13)
Cl1-Cr1-P2	99.68(3)	C8-P2-C21	104.69(14)
Cl1-Cr1-C1	177.21(8)	C17-P2-C21	112.98(14)
P1-Cr1-P2	159.62(3)	Cr1-C1-C2	122.39(21)
P1-Cr1-C1	80.87(8)	Cr1-C1-C6	120.97(20)
P2-Cr1-C1	81.97(8)	C2-C1-C6	116.25(24)
Cr1-P1-C7	101.48(10)	C1-C2-C3	121.41(28)
Cr1-P1-C9	114.88(11)	C1-C2-C7	120.06(24)
Cr1-P1-C13	115.87(10)	C3-C2-C7	118.48(27)
C7-P1-C9	105.66(14)	C2-C3-C4	120.40(30)
C7-P1-C13	104.41(14)	C3-C4-C5	119.78(27)
C9-P1-C13	112.67(14)	C4-C5-C6	120.41(30)
Cr1-P2-C8	99.79(10)	C1-C6-C5	121.59(27)
Cr1-P2-C17	110.74(10)	C1-C6-C8	120.17(24)
Cr1-P2-C21	121.39(9)	C5-C6-C8	118.20(26)

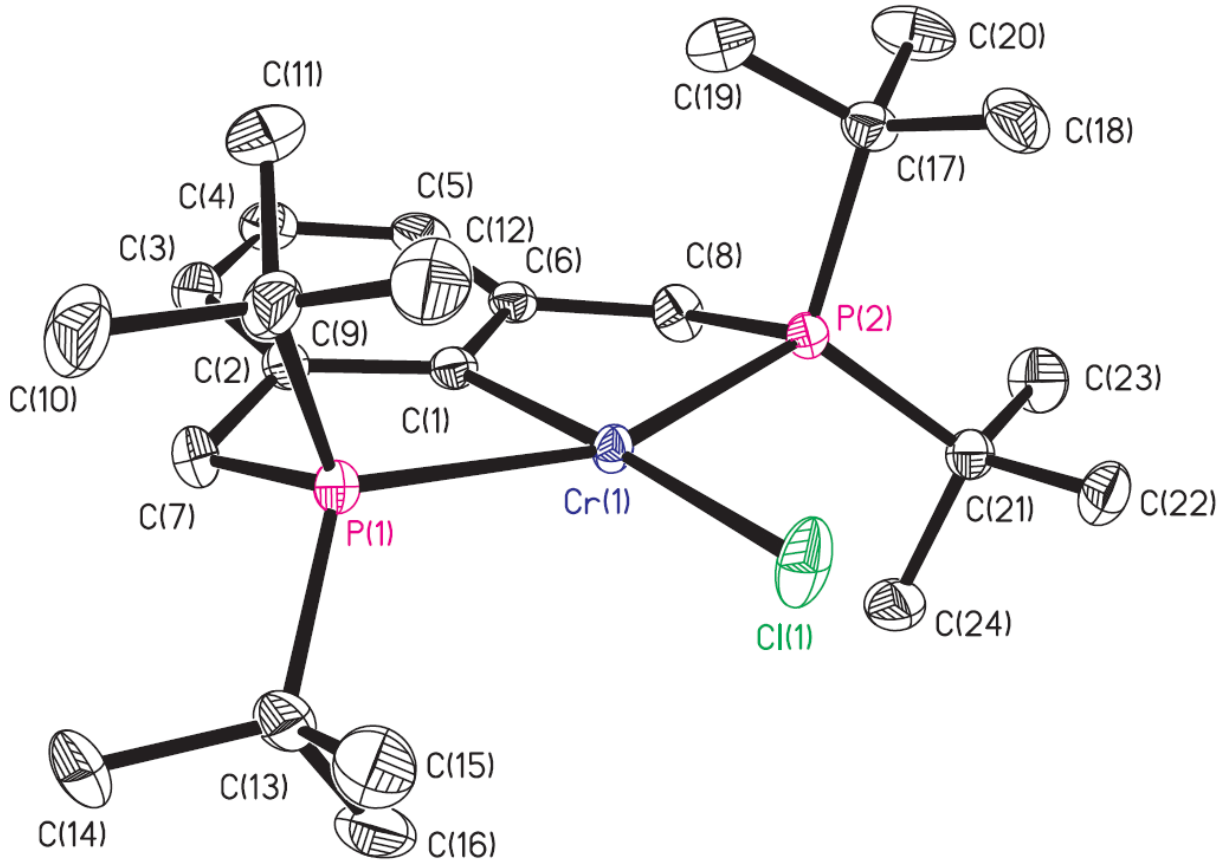

Figure 4.9: Molecular structure of (^{tBu}PCP)CrCl. Ellipsoids are drawn at the 35% probability level; hydrogen atoms were omitted for clarity.

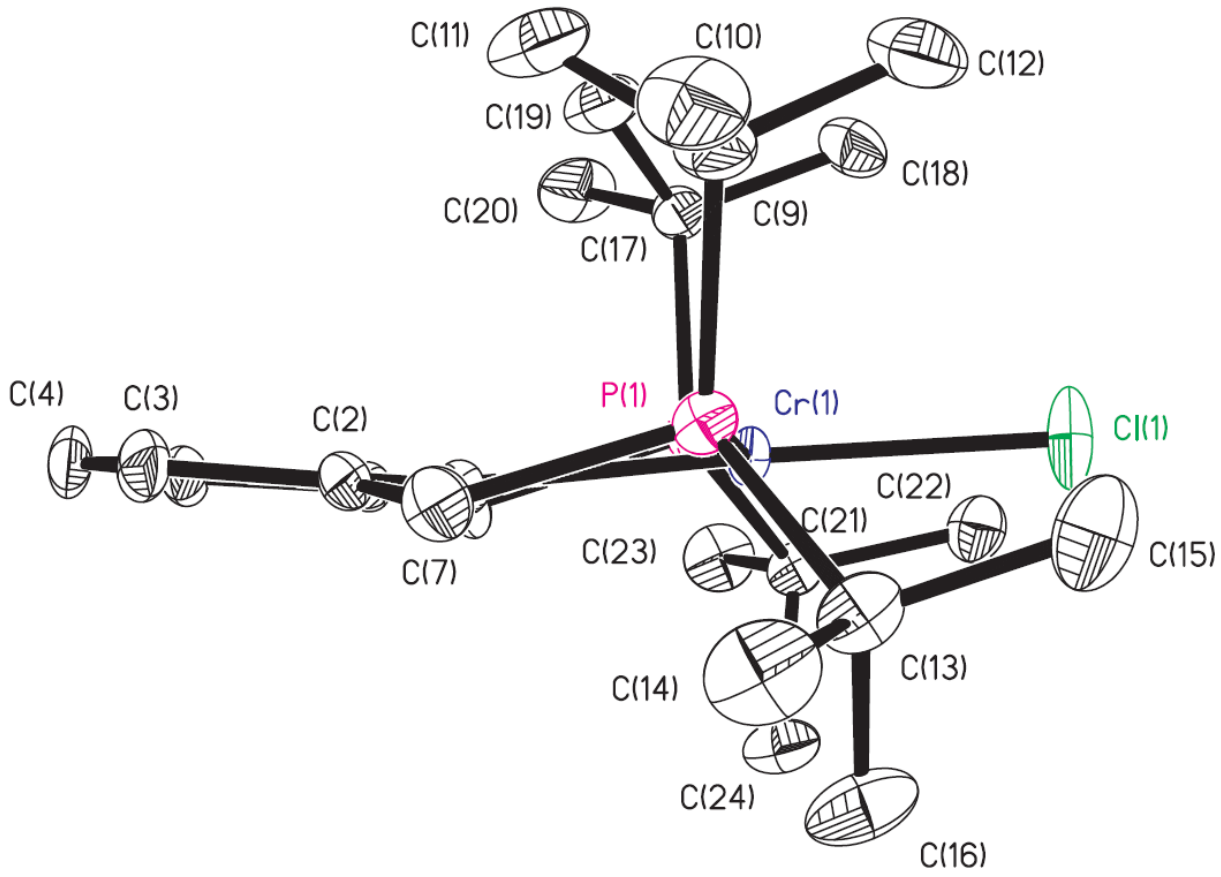

Figure 4.10: An alternative view of (^{tBu}PCP)CrCl. The Cr1-C1 bond is bent 7.1(1)° out of the plane defined by the aryl ring.

Table 4.6: Selected distances and angles for a representative molecule of (^{tBu}PCP)Ti(BH_4)$_2$

Distances (Å)					
Ti1-B1	2.1993(21)	Ti1-P2	2.7041(5)	B2-H86	1.1126(184)
Ti1-H80	1.9650(190)	Ti1-C1	2.1920(16)	B2-H87	1.1250(201)
Ti1-H81	2.0201(181)	B1-H80	1.1536(195)	P1-C7	1.8342(17)
Ti1-H82	1.9843(181)	B1-H81	1.1454(190)	P1-C9	1.8997(18)
Ti1-B2	2.3977(21)	B1-H82	1.1433(189)	P1-C13	1.8864(18)
Ti1-H84	1.9306(171)	B1-H83	1.1199(214)	P2-C8	1.8341(17)
Ti1-H85	1.8879(204)	B2-H84	1.1647(178)	P2-C17	1.8957(16)
Ti1-P1	2.6244(5)	B2-H85	1.1984(202)	P2-C21	1.9040(5)
Angles (°)					
B1-Ti1-B2	120.04(8)	H81-B1-H83	114.68(144)	Ti1-P1-C9	116.07(6)
B1-Ti1-P1	100.65(6)	H82-B1-H83	114.15(145)	Ti1-P1-C13	121.83(6)
B1-Ti1-P2	99.12(6)	Ti1-H80-B1	85.50(108)	C7-P1-C9	104.55(8)
B1-Ti1-C1	127.16(7)	Ti1-H81-B1	83.10(101)	C7-P1-C13	106.04(8)
B2-Ti1-P1	99.68(5)	Ti1-H82-B1	84.84(103)	C9-P1-C13	109.81(8)
B2-Ti1-P2	92.81(5)	H84-B2-H85	98.75(131)	Ti1-P2-C8	92.34(5)
B2-Ti1-C1	112.62(7)	H84-B2-H86	109.74(126)	Ti1-P2-C17	121.00(5)
P1-Ti1-P2	147.07(2)	H84-B2-H87	111.33(134)	Ti1-P2-C21	121.21(5)
P1-Ti1-C1	73.60(4)	H85-B2-H86	108.90(136)	C8-P2-C17	104.13(7)
P2-Ti1-C1	73.47(4)	H85-B2-H87	111.92(138)	C8-P2-C21	103.82(8)
H80-B1-H81	103.65(132)	H86-B2-H87	114.98(139)	C17-P2-C21	109.17(7)
H80-B1-H82	101.40(133)	Ti1-H84-B2	98.50(106)	C2-C1-C6	116.39(14)
H80-B1-H83	118.39(146)	Ti1-H85-B2	99.52(125)	P1-C7-C2	105.92(11)
H81-B1-H82	102.48(131)	Ti1-P1-C7	95.28(6)	P2-C8-C6	107.63(11)

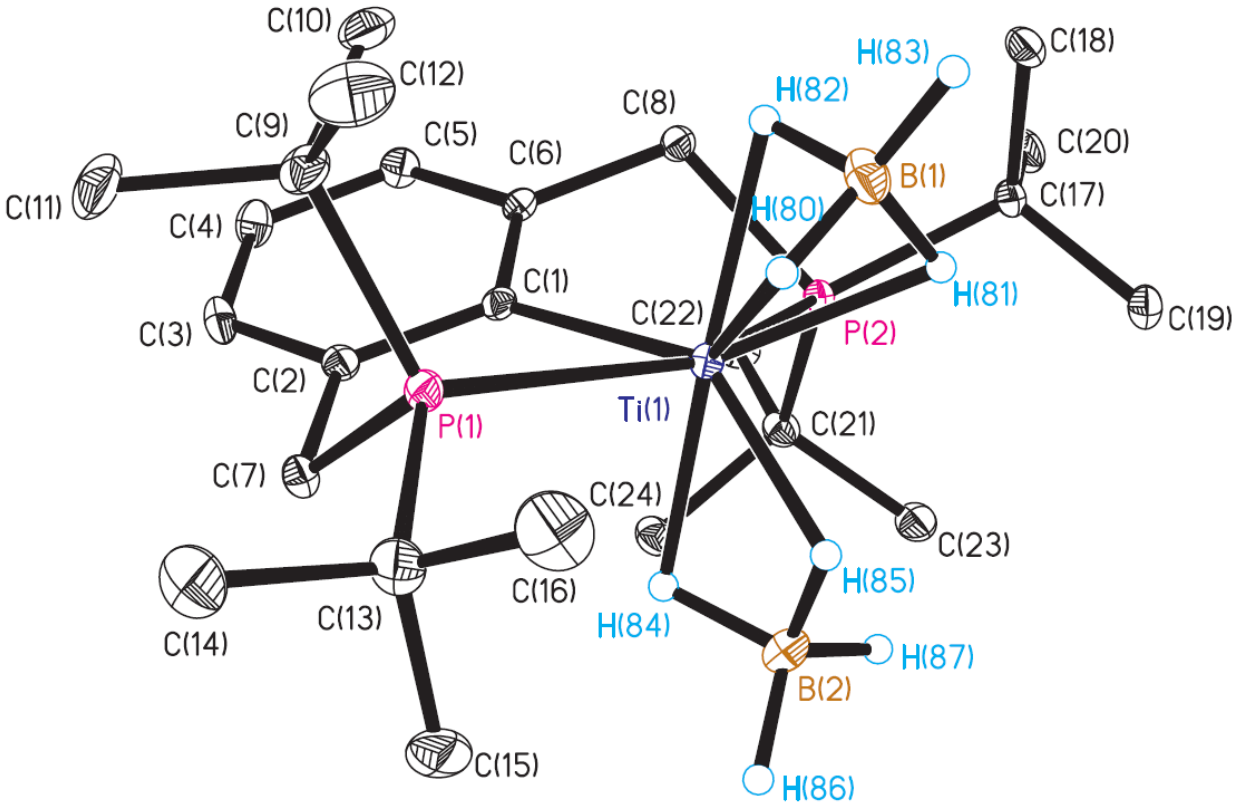

Figure 4.11: Molecular structure of (^{tBu}PCP)Ti(BH_4)$_2$. Ellipsoids are drawn at the 35% probability level; hydrogen atoms other than those for borohydrides were omitted for clarity.

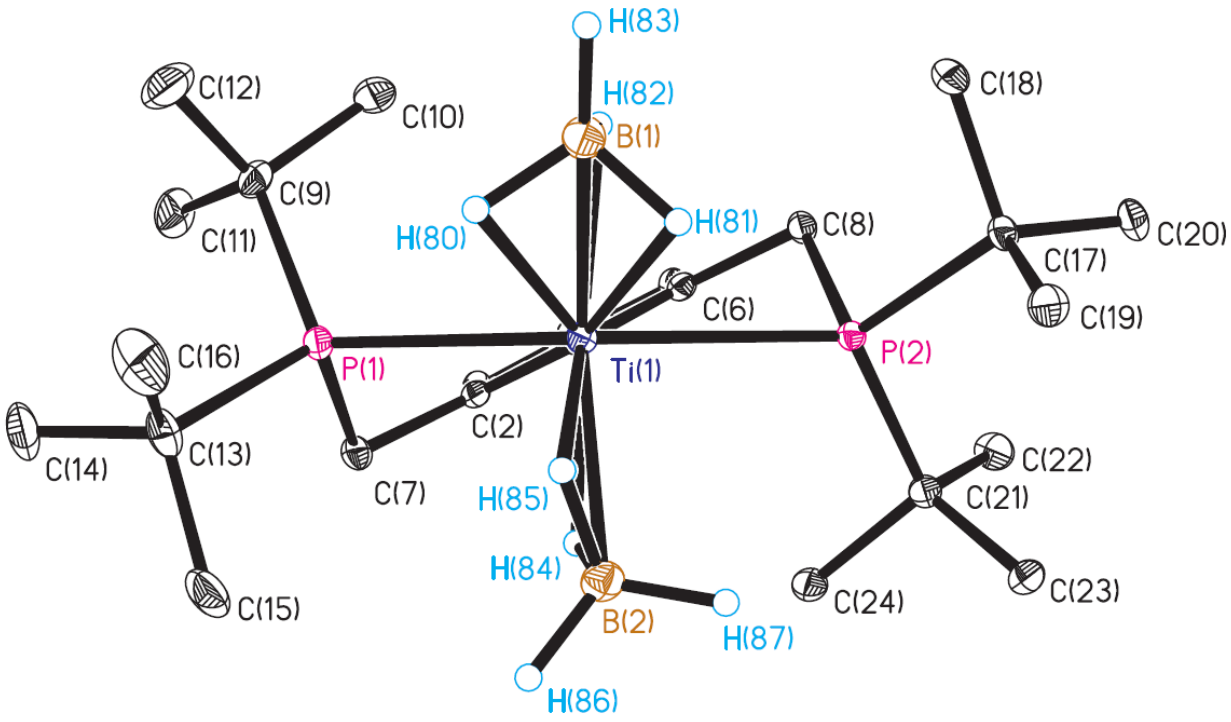

Figure 4.12: An alternative view of (^{tBu}PCP)Ti(BH_4)$_2$ down the Ti1-C1 axis. The aryl plane is rotated out of the P1-Ti1-P2 plane by 25.07(4)°.

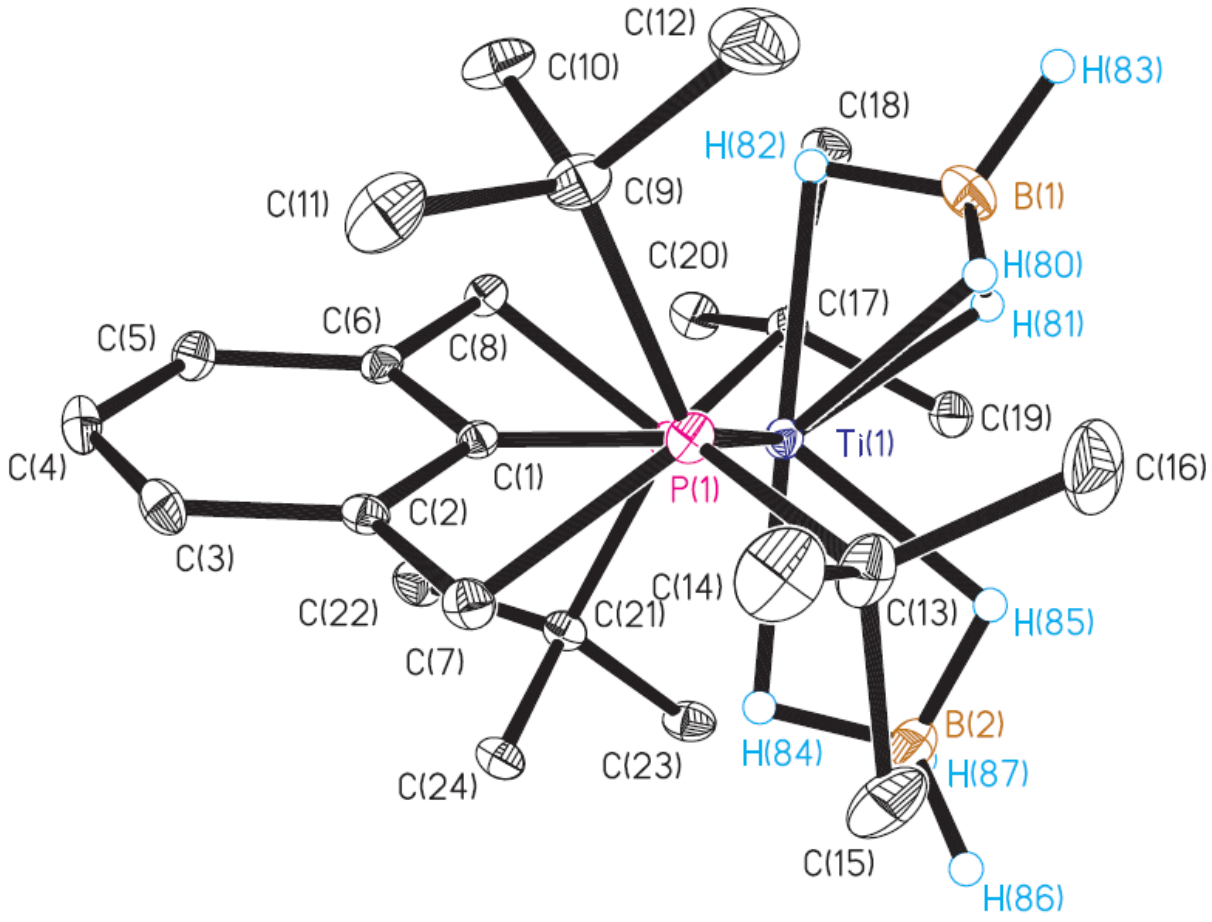

Figure 4.13: An alternative view of (^{tBu}PCP)Ti(BH$_4$)$_2$ down the P1-P2 axis. The κ^3-BH$_4$ is more trans to the aryl ring (has a larger C-Ti-B angle) than the κ^2-BH$_4$.

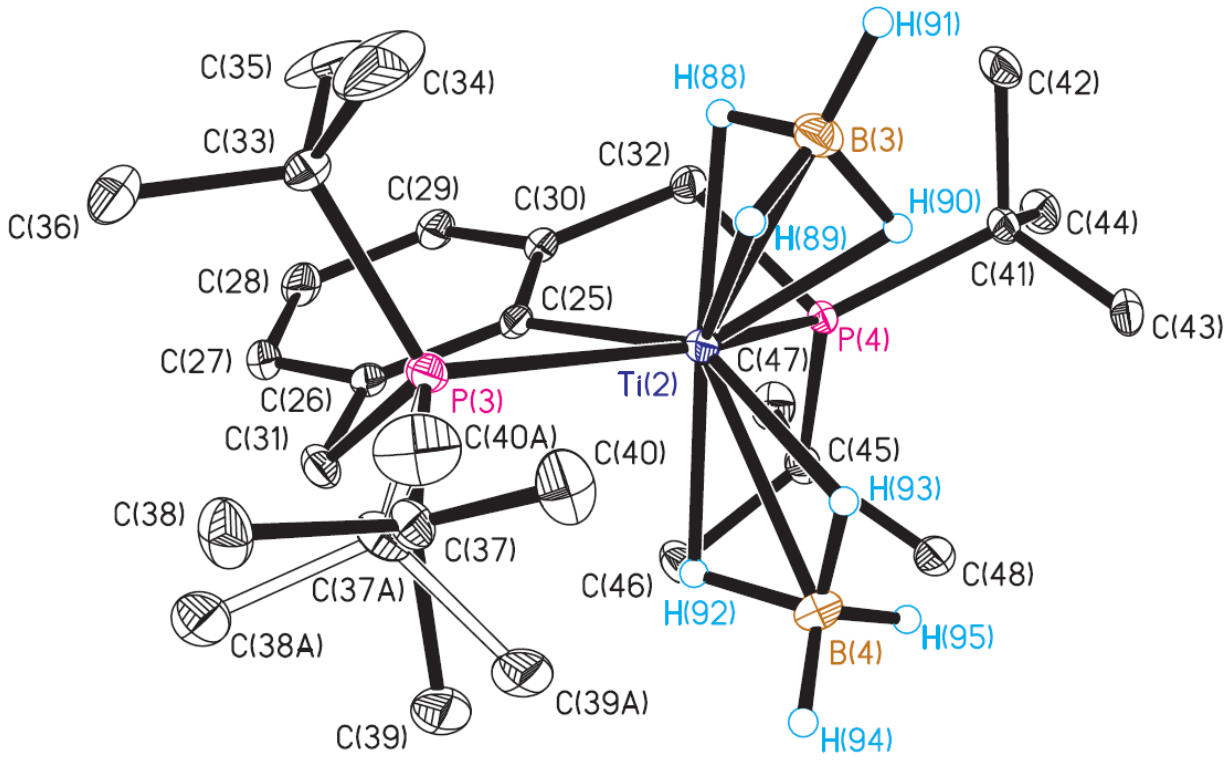

Figure 4.14: The two components of the disorder model for (^{tBu}PCP)Ti(BH_4)$_2$. The major component (solid bonds) and the minor component (hollow bonds) are related by a rotation and bending of one of the ^{t}Bu substituents relative to the P atom.

References

1. Abbenhuis, H. C. L.; Feiken, N.; Grove, D. M.; Jastrzebski, J. T. B. H.; Kooijman, H.; Van der Sluis, P.; Smeets, W. J. J.; Spek, A. L.; Van Koten, G., Use of an aryldiamine pincer ligand in the study of tantalum alkylidene-centered reactivity: tantalum-mediated alkene synthesis via reductive rearrangements and Wittig-type reactions. *J. Am. Chem. Soc.* **1992,** *114*, 9773-81.
2. Bailey, B. C.; Fan, H.; Baum, E. W.; Huffman, J. C.; Baik, M.-H.; Mindiola, D. J., Intermolecular C-H bond activation promoted by a titanium alkylidyne. *J. Am. Chem. Soc.* **2005,** *127*, 16016-16017.
3. Bailey, B. C.; Fan, H.; Huffman, J. C.; Baik, M.-H.; Mindiola, D. J., Intermolecular C-H bond activation reactions promoted by transient titanium alkylidynes. Synthesis, reactivity, linetic, and theoretical studies of the Ti≡C linkage. *J. Am. Chem. Soc.* **2007,** *129*, 8781-8793.
4. Bailey, B. C.; Huffman, J. C.; Mindiola, D. J., Intermolecular activation of C-X (X = H, O, F) bonds by a Ti≡CtBu linkage. *J. Am. Chem. Soc.* **2007,** *129*, 5302-5303.
5. Fout, A. R.; Scott, J.; Miller, D. L.; Bailey, B. C.; Pink, M.; Mindiola, D. J., Dehydrofluorination of hydrofluorocarbons by titanium alkylidynes via sequential C-H/C-F bond activation reactions. A synthetic, structural, and mechanistic study of 1,2-CH bond addition and β-fluoride elimination. *Organometallics* **2009,** *28*, 331-347.
6. Andino, J. G.; Fan, H.; Fout, A. R.; Bailey, B. C.; Baik, M.-H.; Mindiola, D. J., 1,2-CF bond activation of perfluoroarenes and alkylidene isomers of titanium. DFT analysis of the C-F bond activation pathway and rotation of the titanium alkylidene moiety. *J. Organomet. Chem.* **2011,** *696*, 4138-4146.

7. Fan, H.; Fout, A. R.; Bailey, B. C.; Pink, M.; Baik, M.-H.; Mindiola, D. J., Understanding intermolecular C-F bond activation by a transient titanium neopentylidyne: experimental and theoretical studies on the competition between 1,2-CF bond addition and [2 + 2]-cycloaddition/β-fluoride elimination. *Dalton Trans.* **2013,** *42*, 4163-4174.

8. Crestani, M. G.; Olasz, A.; Pinter, B.; Bailey, B. C.; Fortier, S.; Gao, X.; Chen, C.-H.; Baik, M.-H.; Mindiola, D. J., Understanding the competitive dehydroalkoxylation and dehydrogenation of ethers with Ti-C multiple bonds. *Chem. Sci.* **2013,** *4*, 2543-2550.

9. Flores, J. A.; Cavaliere, V. N.; Buck, D.; Pinter, B.; Chen, G.; Crestani, M. G.; Baik, M.-H.; Mindiola, D. J., Methane activation and exchange by titanium-carbon multiple bonds. *Chem. Sci.* **2011,** *2*, 1457-1462.

10. Fout, A. R.; Bailey, B. C.; Buck, D. M.; Fan, H.; Huffman, J. C.; Baik, M.-H.; Mindiola, D. J., Synthetic and mechanistic studies of the ring opening and denitrogenation of pyridine and picolines by Ti-C multiple bonds. *Organometallics* **2010,** *29*, 5409-5422.

11. McGuinness, D. S.; Gibson, V. C.; Steed, J. W., Bis(carbene)pyridine complexes of the early to middle transition metals: survey of ethylene oligomerization and polymerization capability. *Organometallics* **2004,** *23*, 6288-6292.

12. Alzamly, A.; Gambarotta, S.; Korobkov, I., Polymer-Free Ethylene Oligomerization Using a Pyridine-Based Pincer PNP-Type of Ligand. *Organometallics* **2013,** *32*, 7204-7212.

13. Simler, T.; Braunstein, P.; Danopoulos, A. A., Chromium(II) pincer complexes with dearomatized PNP and PNC ligands: a comparative study of their catalytic ethylene oligomerization activity. *Organometallics* **2016,** *35*, 4044-4049.

14. Alam, F.; Zhang, L.; Wei, W.; Wang, J.; Chen, Y.; Dong, C.; Jiang, T., Catalytic Systems Based on Chromium(III) Silylated-Diphosphinoamines for Selective Ethylene Tri-/Tetramerization. *ACS Catal.* **2018,** *8*, 10836-10845.

15. Ren, X.; Wesolek, M.; Braunstein, P., Cu(I), Ag(I), Ni(II), Cr(III) and Ir(I) complexes with tritopic $N^{imine}C^{NHC}N^{amine}$ pincer ligands and catalytic ethylene oligomerization. *Dalton Trans.* **2019,** *48*, 12895-12909.

16. Wang, C.; Luo, H.-K.; van Meurs, M.; Stubbs, L. P.; Wong, P.-K., The new tridentate ligand CpSiNSiCp and its zirconium complexes: incorporation of two bridged constrained-geometry units into one molecule. *Organometallics* **2008,** *27*, 2908-2910.

17. Chuchuryukin, A. V.; Huang, R.; Lutz, M.; Chadwick, J. C.; van Faassen, E. E.; Spek, A. L.; van Koten, G., NCN-pincer metal complexes (Ti, Cr, V, Zr, Hf, and Nb) of the Phebox ligand (*S*,*S*)-2,6-bis(4'-isopropyl-2'-oxazolinyl)phenyl. *Organometallics* **2011,** *30*, 2819-2830.

18. Chuchuryukin, A. V.; Huang, R.; van Faassen, E. E.; van Klink, G. P. M.; Lutz, M.; Chadwick, J. C.; Spek, A. L.; van Koten, G., Mono N,C,N-pincer complexes of titanium, vanadium and niobium. Synthesis, structure and catalytic activity in olefin polymerisation. *Dalton Trans.* **2011,** *40*, 8887-8895.

19. Liu, Z.; Gao, W.; Liu, X.; Luo, X.; Cui, D.; Mu, Y., Pincer chromium(II) and chromium(III) complexes supported by bis(imino)aryl NCN ligands: synthesis and catalysis on isoprene polymerization. *Organometallics* **2011,** *30*, 752-759.

20. Liu, C.-C.; So, L.-C.; Lo, J. C. Y.; Chan, M. C. W.; Kaneyoshi, H.; Makio, H., Highly fluorinated (σ-aryl)-chelating titanium(IV) post-metallocene: characterization and scalar [C-H···F-C] coupling. *Organometallics* **2012,** *31*, 5274-5281.

21. Al Thagfi, J.; Lavoie, G. G., Preparation and reactivity study of chromium(III), iron(II), and cobalt(II) complexes of 1,3-bis(imino)benzimidazol-2-ylidene and 1,3-bis(imino)pyrimidin-2-ylidene. *Organometallics* **2012,** *31*, 7351-7358.

22. Hsu, J.-W.; Lin, Y.-C.; Hsiao, C.-S.; Datta, A.; Lin, C.-H.; Huang, J.-H.; Tsai, J.-C.; Hsu, W.-C., Zirconium complexes incorporated with asymmetrical tridentate pincer type mono- and di-anionic pyrrolyl ligands: mechanism and reactivity as catalytic precursors. *Dalton Trans.* **2012,** *41*, 7700-7707.

23. Gong, D.; Jia, X.; Wang, B.; Zhang, X.; Huang, K.-W., Trans-1,4 selective polymerization of 1,3-butadiene with symmetry pincer chromium complexes activated by MMAO. *J. Organomet. Chem.* **2014,** *766*, 79-85.

24. Gong, D.; Liu, W.; Chen, T.; Chen, Z.-R.; Huang, K.-W., Ethylene polymerization by PN3-type pincer chromium(III) complexes. *J. Mol. Catal. A: Chem.* **2014,** *395*, 100-107.

25. Annunziata, L.; Roisnel, T.; Razavi, A.; Carpentier, J.-F.; Kirillov, E., Conformationally dynamic titanium and zirconium cationic complexes of bis(naphthoxy)pyridine ligands: structure, "oscillation" and olefin polymerization catalysis. *Dalton Trans.* **2017,** *46*, 3150-3159.

26. Motolko, K. S. A.; Price, J. S.; Emslie, D. J. H.; Jenkins, H. A.; Britten, J. F., Zirconium complexes of a rigid, dianionic pincer ligand: alkyl cations, arene coordination, and ethylene polymerization. *Organometallics* **2017,** *36*, 3084-3093.

27. VenkatRamani, S.; Roland, C. D.; Zhang, J. G.; Ghiviriga, I.; Abboud, K. A.; Veige, A. S., Trianionic pincer complexes of niobium and tantalum as precatalysts for ROMP of norbornene. *Organometallics* **2016,** *35*, 2675-2682.

28. Wright, L. A.; Hope, E. G.; Solan, G. A.; Cross, W. B.; Singh, K., Active O,N_{py},N-titanium(IV) fluoride precatalysts for ethylene polymerization: exploring "fluoride effects" on polymer properties and catalytic performance. *Organometallics* **2016,** *35*, 1183-1191.

29. Kulyabin, P. S.; Goryunov, G. P.; Mladentsev, D. Y.; Uborsky, D. V.; Voskoboynikov, A. Z.; Canich, J. A. M.; Hagadorn, J. R., Reactivity of C1-symmetric heteroarylamido hafnium complexes towards unsaturated electrophilic molecules: development of new families of olefin polymerization catalysts. *Chem. - Eur. J.* **2019,** *25*, 10478-10489.

30. Bellone, D. E.; Bours, J.; Menke, E. H.; Fischer, F. R., Highly selective molybdenum ONO pincer complex initiates the living ring-opening metathesis polymerization of strained alkynes with exceptionally low polydispersity indices. *J. Am. Chem. Soc.* **2015,** *137*, 850-856.

31. Roland, C. D.; Zhang, T.; VenkatRamani, S.; Ghiviriga, I.; Veige, A. S., A catalytically relevant intermediate in the synthesis of cyclic polymers from alkynes. *Chem. Commun. (Cambridge, U. K.)* **2019,** *55*, 13697-13700.

32. McGowan, K. P.; Abboud, K. A.; Veige, A. S., Trianionic NCN^{3-} pincer complexes of chromium in four oxidation states (Cr^{II}, Cr^{III}, Cr^{IV}, Cr^{V}): determination of the active catalyst in selective 1-alkene to 2-alkene isomerization. *Organometallics* **2011,** *30*, 4949-4957.

33. Gonsales, S. A.; Pascualini, M. E.; Ghiviriga, I.; Veige, A. S., Evidence for a zwitterionic transition state in double bond rotations within tungsten-vinyl complexes. *Chem. Commun. (Cambridge, U. K.)* **2015,** *51*, 13404-13407.

34. Helgert, T. R.; Hollis, T. K.; Valente, E. J., Synthesis of titanium CCC-NHC pincer complexes and catalytic hydroamination of unactivated alkenes. *Organometallics* **2012,** *31*, 3002-3009.

35. Luconi, L.; Rossin, A.; Motta, A.; Tuci, G.; Giambastiani, G., Group IV organometallic compounds based on dianionic "pincer" ligands: synthesis, characterization, and catalytic activity in intramolecular hydroamination reactions. *Chem. - Eur. J.* **2013,** *19*, 4906-4921.

36. Clark, W. D.; Cho, J.; Valle, H. U.; Hollis, T. K.; Valente, E. J., Metal and halogen dependence of the rate effect in hydroamination/cyclization of unactivated aminoalkenes: Synthesis, characterization, and catalytic rates of CCC-NHC hafnium and zirconium pincer complexes. *J. Organomet. Chem.* **2014,** *751*, 534-540.

37. Sun, Q.; Wang, Y.; Yuan, D.; Yao, Y.; Shen, Q., Zirconium complexes stabilized by amine-bridged bis(phenolato) ligands as precatalysts for intermolecular hydroamination reactions. *Dalton Trans.* **2015,** *44*, 20352-20360.

38. Zhou, X.; Wei, B.; Sun, X.-L.; Tang, Y.; Xie, Z., Asymmetric hydroamination catalyzed by a new chiral zirconium system: reaction scope and mechanism. *Chem. Commun. (Cambridge, U. K.)* **2015,** *51*, 5751-5753.

39. Valle, H. U.; Akurathi, G.; Cho, J.; Clark, W. D.; Chakraborty, A.; Hollis, T. K., CCC-NHC pincer Zr diamido complexes: synthesis, characterization, and catalytic activity in hydroamination/cyclization of unactivated amino-alkenes, -alkynes, and allenes. *Aust. J. Chem.* **2016,** *69*, 565-572.

40. Schiwek, C. H.; Vasilenko, V.; Wadepohl, H.; Gade, L. H., The open d-shell enforces the active space in 3d metal catalysis: highly enantioselective chromium(II) pincer catalysed hydrosilylation of ketones. *Chem. Commun. (Cambridge, U. K.)* **2018,** *54*, 9139-9142.

41. Himmelbauer, D.; Stöger, B.; Veiros, L. F.; Pignitter, M.; Kirchner, K., Cr(II) and Cr(I) PCP pincer complexes: synthesis, structure, and catalytic reactivity. *Organometallics* **2019,** *38*, 4669-4678.

42. O'Reilly, M.; Falkowski, J. M.; Ramachandran, V.; Pati, M.; Abboud, K. A.; Dalal, N. S.; Gray, T. G.; Veige, A. S., Catalytic aerobic oxidation by a trianionic pincer Cr^{III}/Cr^{V} couple. *Inorg. Chem.* **2009,** *48*, 10901-10903.

43. O'Reilly, M. E.; Del Castillo, T. J.; Falkowski, J. M.; Ramachandran, V.; Pati, M.; Correia, M. C.; Abboud, K. A.; Dalal, N. S.; Richardson, D. E.; Veige, A. S., Autocatalytic O_2 cleavage by an OCO^{3-} trianionic pincer Cr^{III} complex: isolation and characterization of the autocatalytic intermediate $[Cr^{IV}]_2(\mu\text{-O})$ dimer. *J. Am. Chem. Soc.* **2011,** *133*, 13661-13673.

44. O'Reilly, M. E.; Del Castillo, T. J.; Abboud, K. A.; Veige, A. S., The influence of reversible trianionic pincer OCO^{3-} μ-oxo Cr^{IV} dimer formation ($[Cr^{IV}]_2(\mu\text{-O})$) and donor ligands in oxygen-atom-transfer (OAT). *Dalton Trans.* **2012,** *41*, 2237-2246.

45. Chakraborty, S.; Blacque, O.; Berke, H., Ligand assisted carbon dioxide activation and hydrogenation using molybdenum and tungsten amides. *Dalton Trans.* **2015,** *44*, 6560-6570.

46. Zhang, Y.; Williard, P. G.; Bernskoetter, W. H., Synthesis and characterization of pincer-molybdenum precatalysts for CO_2 hydrogenation. *Organometallics* **2016,** *35*, 860-865.

47. Bernskoetter, W. H.; Tyler, B. T., Kinetics and mechanism of molybdenum-mediated acrylate formation from carbon dioxide and ethylene. *Organometallics* **2011,** *30*, 520-527.

48. Hanna, B. S.; MacIntosh, A. D.; Ahn, S.; Tyler, B. T.; Palmore, G. T. R.; Williard, P. G.; Bernskoetter, W. H., Ancillary ligand effects on carbon dioxide-ethylene coupling at zerovalent molybdenum. *Organometallics* **2014,** *33*, 3425-3432.

49. Zhang, Y.; Hanna, B. S.; Dineen, A.; Williard, P. G.; Bernskoetter, W. H., Functionalization of carbon dioxide with ethylene at molybdenum hydride complexes. *Organometallics* **2013,** *32*, 3969-3979.

50. Labrum, N. S.; Chen, C.-H.; Caulton, K. G., A bis-pyrazolate pincer on reduced Cr deoxygenates CO_2: selective capture of the derived oxide by Cr^{II}. *Chem. - Eur. J.* **2019,** *25*, 7935-7940.

51. Leischner, T.; Spannenberg, A.; Junge, K.; Beller, M., Molecular defined molybdenum-pincer complexes and their application in catalytic hydrogenations. *Organometallics* **2018,** *37*, 4402-4408.

52. Leischner, T.; Artus Suarez, L.; Spannenberg, A.; Junge, K.; Nova, A.; Beller, M., Highly selective hydrogenation of amides catalysed by a molybdenum pincer complex: scope and mechanism. *Chem. Sci.* **2019,** *10*, 10566-10576.

53. Hebden, T. J.; Schrock, R. R.; Takase, M. K.; Mueller, P., Cleavage of dinitrogen to yield a (*t*-BuPOCOP)molybdenum(IV) nitride. *Chem. Commun. (Cambridge, U. K.)* **2012,** *48*, 1851-1853.

54. Silantyev, G. A.; Förster, M.; Schluschaß, B.; Abbenseth, J.; Würtele, C.; Volkmann, C.; Holthausen, M. C.; Schneider, S., Dinitrogen splitting coupled to protonation. *Angew. Chem., Int. Ed.* **2017,** *56*, 5872-5876.

55. Schluschaß, B.; Abbenseth, J.; Demeshko, S.; Finger, M.; Franke, A.; Herwig, C.; Würtele, C.; Ivanovic-Burmazovic, I.; Limberg, C.; Telser, J.; Schneider, S., Selectivity of tungsten mediated dinitrogen splitting vs. proton reduction. *Chem. Sci.* **2019,** *10*, 10275-10282.

56. Kilgore, U. J.; Yang, X.; Tomaszewski, J.; Huffman, J. C.; Mindiola, D. J., Activation of atmospheric nitrogen and azobenzene N:N bond cleavage by a transient Nb(III) complex. *Inorg. Chem.* **2006,** *45,* 10712-10721.

57. Arashiba, K.; Miyake, Y.; Nishibayashi, Y., A molybdenum complex bearing PNP-type pincer ligands leads to the catalytic reduction of dinitrogen into ammonia. *Nat. Chem.* **2011,** *3,* 120-125.

58. Kinoshita, E.; Arashiba, K.; Kuriyama, S.; Miyake, Y.; Shimazaki, R.; Nakanishi, H.; Nishibayashi, Y., Synthesis and catalytic activity of molybdenum-dinitrogen complexes bearing unsymmetric PNP-type pincer ligands. *Organometallics* **2012,** *31,* 8437-8443.

59. Tanabe, Y.; Kuriyama, S.; Arashiba, K.; Miyake, Y.; Nakajima, K.; Nishibayashi, Y., Preparation and reactivity of molybdenum-dinitrogen complexes bearing an arsenic-containing ANA-type pincer ligand. *Chem. Commun. (Cambridge, U. K.)* **2013,** *49,* 9290-9292.

60. Kuriyama, S.; Arashiba, K.; Nakajima, K.; Tanaka, H.; Kamaru, N.; Yoshizawa, K.; Nishibayashi, Y., Catalytic formation of ammonia from molecular dinitrogen by use of dinitrogen-bridged dimolybdenum-dinitrogen complexes bearing PNP-pincer ligands: remarkable effect of substituent at PNP-pincer ligand. *J. Am. Chem. Soc.* **2014,** *136,* 9719-9731.

61. Tanaka, H.; Arashiba, K.; Kuriyama, S.; Nakajima, K.; Nishibayashi, Y.; Sasada, A.; Yoshizawa, K., Unique behaviour of dinitrogen-bridged dimolybdenum complexes bearing pincer ligand towards catalytic formation of ammonia. *Nat. Commun.* **2014,** *5,* 3737.

62. Arashiba, K.; Nakajima, K.; Nishibayashi, Y., Synthesis and reactivity of molybdenum-dinitrogen complexes bearing PNN-type pincer ligand. *Z. Anorg. Allg. Chem.* **2015,** *641*, 100-104.

63. Kinoshita, E.; Arashiba, K.; Kuriyama, S.; Eizawa, A.; Nakajima, K.; Nishibayashi, Y., Synthesis and catalytic activity of mmolybdenum-nitride complexes bearing pincer ligands. *Eur. J. Inorg. Chem.* **2015,** *2015*, 1789-1794.

64. Kuriyama, S.; Arashiba, K.; Nakajima, K.; Tanaka, H.; Yoshizawa, K.; Nishibayashi, Y., Nitrogen fixation catalyzed by ferrocene-substituted dinitrogen-bridged dimolybdenum-dinitrogen complexes: unique behavior of ferrocene moiety as redox active site. *Chem. Sci.* **2015,** *6*, 3940-3951.

65. Kuriyama, S.; Arashiba, K.; Nakajima, K.; Tanaka, H.; Yoshizawa, K.; Nishibayashi, Y., Azaferrocene-based PNP-type pincer ligand: synthesis of molybdenum, chromium, and iron complexes and reactivity toward nitrogen fixation. *Eur. J. Inorg. Chem.* **2016,** *2016*, 4856-4861.

66. Arashiba, K.; Eizawa, A.; Tanaka, H.; Nakajima, K.; Yoshizawa, K.; Nishibayashi, Y., Catalytic nitrogen fixation via direct cleavage of nitrogen-nitrogen triple bond of molecular dinitrogen under ambient reaction conditions. *Bull. Chem. Soc. Jpn.* **2017,** *90*, 1111-1118.

67. Eizawa, A.; Arashiba, K.; Tanaka, H.; Kuriyama, S.; Matsuo, Y.; Nakajima, K.; Yoshizawa, K.; Nishibayashi, Y., Remarkable catalytic activity of dinitrogen-bridged dimolybdenum complexes bearing NHC-based PCP-pincer ligands toward nitrogen fixation. *Nat. Commun.* **2017,** *8*, 14874.

68. Sekiguchi, Y.; Arashiba, K.; Tanaka, H.; Eizawa, A.; Nakajima, K.; Yoshizawa, K.; Nishibayashi, Y., Catalytic reduction of molecular dinitrogen to ammonia and hydrazine using vanadium complexes. *Angew. Chem., Int. Ed.* **2018,** *57*, 9064-9068.

69. Sekiguchi, Y.; Meng, F.; Tanaka, H.; Eizawa, A.; Arashiba, K.; Nakajima, K.; Yoshizawa, K.; Nishibayashi, Y., Synthesis and reactivity of titanium- and zirconium-dinitrogen complexes bearing anionic pyrrole-based PNP-type pincer ligands. *Dalton Trans.* **2018,** *47*, 11322-11326.

70. Stucke, N.; Krahmer, J.; Näther, C.; Tuczek, F., Molybdenum complexes supported by PN^3P pincer ligands: synthesis, characterization, and application to synthetic nitrogen fixation. *Eur. J. Inorg. Chem.* **2018,** *2018*, 5108-5116.

71. Arashiba, K.; Itabashi, T.; Nakajima, K.; Nishibayashi, Y., Synthesis and Catalytic Reactivity of Polystyrene-supported Molybdenum Pincer Complexes toward Ammonia Formation. *Chem. Lett.* **2019,** *48*, 693-695.

72. Ashida, Y.; Arashiba, K.; Nakajima, K.; Nishibayashi, Y., Molybdenum-catalysed ammonia production with samarium diiodide and alcohols or water. *Nature (London, U. K.)* **2019,** *568*, 536-540.

73. Ashida, Y.; Kondo, S.; Arashiba, K.; Kikuchi, T.; Nakajima, K.; Kakimoto, S.; Nishibayashi, Y., A practical synthesis of ammonia from nitrogen gas, samarium diiodide and water catalyzed by a molybdenum-PCP pincer complex. *Synthesis* **2019,** *51*, 3792-3795.

74. Chakraborty, J.; Mandal, U.; Ghiviriga, I.; Abboud, K. A.; Veige, A. S., Ammonia synthesis through hydrolysis of a trianionic pincer ligand-supported molybdenum-nitride complex. *Chem. - Eur. J.* **2019,** *25*, 14059-14063.

75. Eizawa, A.; Arashiba, K.; Egi, A.; Tanaka, H.; Nakajima, K.; Yoshizawa, K.; Nishibayashi, Y., Catalytic reactivity of molybdenum-trihalide complexes bearing PCP-type pincer ligands. *Chem. - Asian J.* **2019,** *14*, 2091-2096.

76. Itabashi, T.; Mori, I.; Arashiba, K.; Eizawa, A.; Nakajima, K.; Nishibayashi, Y., Effect of substituents on molybdenum triiodide complexes bearing PNP-type pincer ligands toward catalytic nitrogen fixation. *Dalton Trans.* **2019,** *48*, 3182-3186.

77. Itabashi, T.; Arashiba, K.; Tanaka, H.; Konomi, A.; Eizawa, A.; Nakajima, K.; Yoshizawa, K.; Nishibayashi, Y., Synthesis and catalytic reactivity of bis(molybdenum-trihalide) complexes bridged by ferrocene skeleton toward catalytic nitrogen fixation. *Organometallics* **2019,** *38*, 2863-2872.

78. Gradert, C.; Krahmer, J.; Soennichsen, F. D.; Naether, C.; Tuczek, F., Molybdenum(0)-carbonyl complexes supported by mixed benzimidazol-2-ylidene/phosphine ligands: influence of benzannulation on the donor properties of the NHC groups. *J. Organomet. Chem.* **2014,** *770*, 61-68.

79. Gradert, C.; Stucke, N.; Krahmer, J.; Naether, C.; Tuczek, F., Molybdenum complexes supported by mixed NHC/phosphine ligands: activation of N_2 and reaction with $P(OMe)_3$ to the first *meta*-phosphite complex. *Chem. - Eur. J.* **2015,** *21*, 1130-1137.

80. de Aguiar, S. R. M. M.; Stoeger, B.; Pittenauer, E.; Allmaier, G.; Veiros, L. F.; Kirchner, K., Arene C-H bond coordination versus C-H bond cleavage in low-valent group 6 carbonyl pincer complexes. *Organometallics* **2016,** *35*, 3032-3039.

81. Himmelbauer, D.; Mastalir, M.; Stöger, B.; Veiros, L. F.; Kirchner, K., Synthesis and reactivity of group six metal PCP pincer complexes: reversible CO addition across the metal-C_{aryl} bond. *Organometallics* **2018,** *37*, 3631-3638.

82. Eder, W.; Stoeger, B.; Kirchner, K., Synthesis and characterization of xylene-based group-six metal PCP pincer complexes. *Monatsh. Chem.* **2019,** *150*, 1235-1240.

83. Pape, A.; Lutz, M.; Müller, G., Phosphane coordinated magnesium: synthesis and structure of bis[*ortho*,*ortho*'-bis{(dimethylphosphino)methyl}phenyl]magnesium. *Angew. Chem., Int. Ed.* **1994,** *33*, 2281-4.

84. Addison, A. W.; Rao, T. N.; Reedijk, J.; Van Rijn, J.; Verschoor, G. C., Synthesis, structure, and spectroscopic properties of copper(II) compounds containing nitrogen-sulfur donor ligands: the crystal and molecular structure of aqua[1,7-bis(N-methylbenzimidazol-2'-yl)-2,6-dithiaheptane]copper(II) perchlorate. *J. Chem. Soc., Dalton Trans.* **1984**, 1349-56.

85. Goedheijt, M. S.; Nijbacker, T.; Akkerman, O. S.; Bickelhaupt, F.; Veldman, N.; Spek, A. L., Synthesis and X-ray crystal structure of 2-(methoxymethyl)phenyldicyclopentadienyltitanium(III). *J. Organomet. Chem.* **1997,** *527*, 1-5.

86. Alonso, P. J.; Falvello, L. R.; Forniés, J.; García-Monforte, M. A.; Menjón, B., A five-coordinate homoleptic organotitanium(III) compound. *Angew. Chem., Int. Ed.* **2004,** *43*, 5225-5228.

87. Goedde, D. M.; Girolami, G. S., Titanium(II) and titanium(III) tetrahydroborates. Crystal structures of $[Li(Et_2O)_2][Ti_2(BH_4)_5(PMe_2Ph)_4]$, $Ti(BH_4)_3(PMe_2Ph)_2$, and $Ti(BH_4)_3(PEt_3)_2$. *Inorg. Chem.* **2006,** *45*, 1380-1388.

88. Lledos, A.; Duran, M.; Jean, Y.; Volatron, F., Theoretical study of the coordination mode of borohydride ligands: scandium diphosphine tetrahydroborate ($Sc(BH_4)_3(PH_3)_2$) complex. *Bull. Soc. Chim. Fr.* **1992,** *129*, 216-20.

89. Volatron, F.; Duran, M.; Lledos, A.; Jean, Y., Ab initio study of the coordination modes of tetrahydroborato ligands: what is the actual structure of the tris(tetrahydroborato)bis(trimethylphosphine) titanium complex? *Inorg. Chem.* **1993,** *32*, 951-4.

90. Melmed, K. M.; Coucouvanis, D.; Lippard, S. J., Transition metal hydroborate complexes. V. Crystal structure of tetrahydroboratobis(cyclopentadienyl)titanium(III). *Inorg. Chem.* **1973,** *12*, 232-6.

91. Hamilton, E. J. M.; Park, J. S.; Chen, X.; Liu, S.; Sturgeon, M. R.; Meyers, E. A.; Shore, S. G., β-Agostic interactions in 15-valence-electron 9-BBN hydroborate half-sandwich titanium(III) complexes. *Organometallics* **2009,** *28*, 3973-3980.

92. Kim, D. Y.; You, Y.; Girolami, G. S., Synthesis and crystal structures of two (cyclopentadienyl)titanium(III) hydroborate complexes, $[Cp^*TiCl(BH_4)]_2$ and $Cp_2Ti(B_3H_8)$. *J. Organomet. Chem.* **2008,** *693*, 981-986.

93. Schlögl, R.; Boehm, H. P., The reaction of potassium-graphite intercalation compounds with tetrahydrofuran. *Carbon* **1984,** *22*, 341-9.

94. Fryzuk, M. D.; Haddad, T. S.; Mylvaganam, M.; McConville, D. H.; Rettig, S. J., End-on versus side-on bonding of dinitrogen to dinuclear early transition-metal complexes. *J. Am. Chem. Soc.* **1993,** *115*, 2782-92.

95. Watson, S. C.; Eastham, J. F., Colored indicators for simple direct titration of magnesium and lithium reagents. *J. Organomet. Chem.* **1967,** *9*, 165-8.

96. Savoia, D.; Trombini, C.; Umani-Ronchi, A., Potassium-graphite as a metalation reagent. Synthesis of aldehydes and ketones by alkylation of imines and dihydro-1,3-oxazine. *J. Org. Chem.* **1978,** *43*, 2907-10.

97. Jones, N. A.; Liddle, S. T.; Wilson, C.; Arnold, P. L., Titanium(III) alkoxy-N-heterocyclic carbenes and a safe, low-cost route to $TiCl_3(THF)_3$. *Organometallics* **2007,** *26*, 755-757.

98. Boudjouk, P.; So, J. H.; Ackermann, M. N.; Hawley, S. E.; Turk, B. E., Solvated and unsolvated anhydrous metal chlorides from metal chloride hydrates. *Inorg. Synth.* **1992,** *29*, 108-11.

99. Fulmer, G. R.; Miller, A. J. M.; Sherden, N. H.; Gottlieb, H. E.; Nudelman, A.; Stoltz, B. M.; Bercaw, J. E.; Goldberg, K. I., NMR chemical shifts of trace impurities: common laboratory solvents, organics, and gases in deuterated solvents relevant to the organometallic chemist. *Organometallics* **2010,** *29*, 2176-2179.

100. Brumaghim, J. L.; Priepot, J. G.; Girolami, G. S., Synthesis of hydride and alkyl compounds containing the Cp*Os(NO) fragment. Crystal structure of $[Cp^*Os(\mu\text{-}NO)]_2$. *Organometallics* **1999,** *18*, 2139-2144.

101. Sheldrick, G. M., Crystal structure refinement with SHELXL. *Acta Crystallogr., Sect. C: Struct. Chem.* **2015,** *71*, 3-8.

102. Krause, L.; Herbst-Irmer, R.; Sheldrick, G. M.; Stalke, D., Comparison of silver and molybdenum microfocus X-ray sources for single-crystal structure determination. *J. Appl. Crystallogr.* **2015,** *48*, 3-10.

CHAPTER 5

IMPROVED SYNTHESIS OF BIS(2,2,6,6-TETRAMETHYLPIPERIDIDO) COMPOUNDS OF MANGANESE(II) AND IRON(II)

Introduction

Nitrides of manganese, iron, cobalt, and nickel have desirable chemical, physical, magnetic, and electrical properties that make them useful in a number of applications. Although these late transition metal nitrides have been studied mostly for their catalytic properties with regards to the production or decomposition of ammonia,[1-2] oxygen,[3-8] and hydrogen,[3, 8-10] they have also been explored as potential materials for electrodes of lithium or sodium batteries,[11-15] hard coatings,[16-17] and memory devices.[18-20] These materials are fabricated mostly through nitridation of the metal or metal oxide with N_2 or ammonia, by molecular beam epitaxy (MBE), or by reactive sputtering.[1, 20-29]

In the context of using late transition metal nitrides as catalysts for energy-related applications such as batteries and fuel cells, promising results have been obtained by depositing or growing them on high surface area materials such as foams and porous carbon microfibers.[8, 13, 30-31] Methods such as MBE or reactive sputtering, however, are not effective at forming catalytically active species in the interiors of these materials. Instead, solvothermal methods are usually used to deposit metal oxides, which are then converted to the nitrides by reaction with ammonia gas at temperatures higher than 500 °C.

Chemical vapor deposition (CVD) is a technique that is capable of depositing films on surfaces that exhibit intricate topologies.[32-33] With judicious selection of the chemical precursor, films may be grown with minimal impurities at low temperature. In particular, our group has shown that late transition metal nitrides can be deposited from transition metal complexes bearing

di(*tert*-butyl)amido (N^tBu_2) ligands: crystalline films of the metal nitrides, with low oxygen and carbon contamination, were grown from $M(N^tBu_2)_2$ complexes (M = Mn, Fe, Co, Ni) in the presence of ammonia at temperatures as low as 80 °C.[34-35] However, HN^tBu_2 is not commercially available and is time-consuming and expensive to prepare (Scheme 5.1).[36]

$$^tBuNH_2 + 2\ KMnO_4 \xrightarrow[H_2O]{} {}^tBuNO_2 + 2\ MnO_2 + 2\ KOH$$

$$2\ {}^tBuNO_2 + 2\ Na \xrightarrow[DME]{} Na(^tBu_2NO) + NaNO_2$$

$$Na(^tBu_2NO_2) + 2\ Na_2S{\cdot}9H_2O \xrightarrow[DMF]{} {}^tBu_2NH + 5\ NaOH + 2\ S + 15\ H_2O$$

Scheme 5.1: Preparation of HN^tBu_2.

We therefore turned our attention to analogous late transition metal complexes of the ligand 2,2,6,6-tetramethylpiperidide (TMP), in large part because the corresponding amine H(TMP) is commercially available and inexpensive. Luke Davis in our group discovered that the two-coordinate complexes $Mn(TMP)_2$, $Fe(TMP)_2$, and $Co(TMP)_2$ can be made and isolated.[37] Here we report improved syntheses of these compounds and a crystal structure of the manganese complex.

We have reported elsewhere that high quality films of manganese nitride can be deposited by CVD from $Mn(TMP)_2$ at temperatures as low as 50 °C when ammonia is used as a co-reactant.[38] Whereas films grown from $Mn(N^tBu_2)_2$ are crystalline, films grown under similar conditions from $Mn(TMP)_2$ are mostly amorphous. The low deposition temperature is not only advantageous from a process standpoint, but may also enable the deposition of metastable metal nitride phases that cannot be prepared by solvothermal routes.

Results and Discussion

Davis has previously reported the syntheses of $Mn(TMP)_2$ and $Fe(TMP)_2$, where TMP is the 2,2,6,6-tetramethylpiperidide anion, by treatment of $MnBr_2(THF)_2$ and $FeBr_2(DME)$, respectively, with LiTMP in pentane (Scheme 5.2).[37] He found that pure $Mn(TMP)_2$ and $Fe(TMP)_2$ can be isolated reproducibly in good yields by subliming them from the dried reaction mixture onto the water-cooled cold finger of a Schlenk flask that is also equipped with a side bulb cooled to -78 °C. The side bulb traps H(TMP), pentane, and other liquid byproducts that otherwise interfere with the sublimation of the desired products.

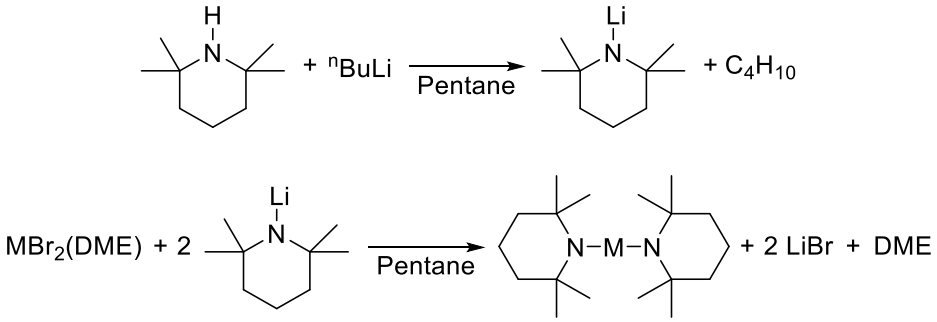

Scheme 5.2: Preparation of $M(TMP)_2$, where M: Mn, Fe, or Co.

We have found that higher and more reproducible yields of $Mn(TMP)_2$ and $Fe(TMP)_2$ can be obtained by cooling the side bulb to -196 °C for the first 4 h of the sublimation (a procedure that more efficiently traps the liquid byproducts) and by using a slight stoichiometric deficit of Li(TMP). We also found that the chloride starting materials $MnCl_2(THF)_{1.5}$ and $FeCl_2(THF)_{1.4}$ were just as competent in these reactions as their bromide analogs, and gave comparable yields.

Some other modifications of the recipe are not beneficial. For example, when the solvate-free starting material $FeBr_2$ is treated with Li(TMP) in pentane, dark grey powders and intractable red oils were formed, similar to what was reported by Potratz and Davis for the di(*tert*-butyl)amido

analog.[36-37] When $FeBr_2$ is treated with Li(TMP) in diethyl ether, the yield was highly variable, ranging between 0% to 55%, almost certainly due to the ability of Li(TMP) to react with ethereal solvents above 0 °C.[39-41] The use of hydrocarbon solvents and ethereal adducts of the metal halide salts is necessary for reproducible results.

Davis reported that the reaction of $CoBr_2$(DME) with $Li(TMP)_2$ affords the salt [Li(DME)][$CoBr(TMP)_2$] as the major product, and at best only traces of a compound he tentatively identified as $Co(TMP)_2$.[37] Davis reported that $Co(TMP)_2$ is golden yellow in the solid state, which was surprising because $Co(N^tBu_2)_2$ is dark red (in contrast, the colors of $Mn(TMP)_2$ and $Fe(TMP)_2$ are very similar to those of their N^tBu_2 analogs).[37] We find that the reaction of $CoCl_2(THF)_{1.1}$ and Li(TMP) in pentane, followed by filtration, drying, and sublimation in vacuum, affords a mixture of amorphous dark material and small amounts of a yellow crystalline material.

The yellow crystals were of sufficient quality to diffract, but of insufficient quality to produce a publishable dataset. The solution of the dataset showed that the yellow crystalline material was actually three-coordinate $Co(TMP)_2$(THF). We conclude that the golden yellow material that Davis isolated was probably a DME adduct of $Co(TMP)_2$, which would explain why the color was significantly different from that of $Co(N^tBu_2)_2$. It is possible that the amorphous dark sublimate is the desired compound $Co(TMP)_2$, but the isolated yield is only 4%. Its microanalysis is consistent with this stoichiometry, and its IR spectrum is very similar to those of its Mn and Fe analogs.

Crystal Structure of Bis(2,2,6,6-tetramethylpiperidido)manganese(II). The compound $Mn(TMP)_2$ crystallizes in the monoclinic $P2_1/n$ space group. The data crystal was a non-merohedral twin and the structure was refined using reflection intensities from only the major twin component. One of the TMP ligands is disordered: the two disordered components are related by

a chair-chair interconversion, or equivalently by rotation about the Mn-N bond. Further discussion will be confined to the major component of the disorder model, which has a site occupancy of 0.66.

The solid state structure of $Mn(TMP)_2$ can be compared with those of $Mn(N^tBu_2)_2$,[42] $Fe(N^tBu_2)_2$,[36] and $Fe(TMP)_2$.[37] As expected from atomic radii, the average Mn-N bond distances are longer than the Fe-N distances in their Fe analogs. The average M-N bond distances in the N^tBu_2 compounds are longer than those in their TMP analogs. The difference suggests that interligand non-bonded repulsions are reduced in TMP compounds owing to the cyclic nature of the amido group, which reduces the cone angle subtended by the ligand. The metal centers in the N^tBu_2 compounds adopt linear geometries (N-M-N is nearly 180°), and the dihedral angles between the C-N-C planes are near 80°. The TMP compounds are both bent (N-M-N = 172-173°) with dihedral angles between the two C-N-C planes being closer to 70°.

Table 5.1: Selected distances and angles of MX_2, where M is Mn or Fe and X is N^tBu_2 or TMP

	$Mn(N^tBu_2)_2$	$Mn(TMP)_2$	$Fe(N^tBu_2)_2$	$Fe(TMP)_2$
Average M-N (Å)	1.936(1)	1.923(3)	1.880(2)	1.869(1)
N-M-N (°)	179.33(5)	172.15(11)	179.45(8)	173.23(5)
Dihedral (°)	80.0(1)	69.48(23)	80.5(1)	73.3(2)

Conclusions

The synthesis and isolation of $Mn(TMP)_2$ and $Fe(TMP)_2$ have been optimized and can now be made on multi-gram scales. We find that $Mn(TMP)_2$ is isomorphous with $Fe(TMP)_2$ in the solid state. ^1H NMR resonances for $Mn(TMP)_2$ were not observed, but $Fe(TMP)_2$ exhibits

resonances at δ 170.6, δ 139.5, and δ 81.8 in C_6D_6. A practical route to synthesize and isolate $Co(TMP)_2$ remains elusive.

Experimental Details

Unless otherwise stated, all operations were conducted under argon or vacuum using standard Schlenk line and glovebox techniques. $MnCl_2(THF)_{1.5}$,[43] $FeCl_2(THF)_{1.4}$,[43] $CoCl_2(THF)_{1.1}$,[43] and Li(TMP)[44] were prepared by literature routes. Pentane was dried over sodium-benzophenone ketyl and distilled under N_2 immediately before use.

Elemental analyses were performed by the School of Chemical Sciences Microanalysis Laboratory at the University of Illinois at Urbana-Champaign. NMR spectra were acquired on a Varian 500 MHz spectrometer at room temperature. ^1H NMR spectra are reported in δ units (positive chemical shifts to higher frequency) relative to TMS as determined from residual solvent signals.[45] NMR spectra were processed with the MestReNova NMR software package. FTIR spectra were acquired on a Thermo Nicolet IR200 spectrometer as mineral oil solutions between KBr plates. IR spectra were processed using the OMNIC® software package. X-ray crystallographic data were collected by the George L. Clark X-Ray Facility and 3M Materials Laboratory and refined using the SHELXTL software package. Solutions were check with PLATON for missed crystallographic symmetry.

Bis(2,2,6,6-tetramethylpiperidido)manganese(II), $Mn(TMP)_2$. To a mixture of $MnCl_2(THF)_{1.5}$ (8.730 g, 37.3 mmol) and Li(TMP) (10.417 g, 70.8 mmol) was added pentane (100 mL). The mixture was stirred overnight, affording a cloudy yellow mixture. The mixture was filtered and the solids were washed with pentane (50 mL). The filtrate and wash were combined in a Schlenk tube equipped with a side bulb and dried under vacuum. The product was sublimed

at 65 °C onto a water-cooled cold finger under static vacuum (initially 2 mTorr) with the side bulb cooled in liquid nitrogen. After 4 h, the liquid nitrogen was replaced with a dry ice/ethanol bath and the sublimation was continued overnight. The yellow solid was collected from the cold finger. Yield: 7.6 g (64 %). Anal. Calc. for $C_{18}H_{36}MnN_2$: C, 64.4; H, 10.8; N, 8.35. Found: C, 63.9; H, 10.6; N, 8.47. No ^{1}H NMR resonances were observed. IR (cm^{-1}): 1367 (s), 1353 (s), 1341 (m), 1288 (m), 1235 (s), 1197 (m), 1170 (s), 1130 (s), 1074 (m), 1053 (m), 1016 (s), 984 (w), 960 (m), 945 (m), 928 (s), 907 (m), 860 (m), 745 (w), 667 (w), 630 (w), 590 (w), 547 (w), 519 (m).

Bis(2,2,6,6-tetramethylpiperidido)iron(II), Fe(TMP)$_2$. To a mixture of $FeCl_2(THF)_{1.4}$ (0.507 g, 2.23 mmol) and Li(TMP) (0.645 g, 4.38 mmol) was added pentane (20 mL). The mixture was stirred overnight, affording a cloudy red mixture. The mixture was filtered and the solids were washed with pentane (10 mL). The filtrate and wash were combined in a Schlenk tube equipped with a side bulb and dried under vacuum. The product was sublimed at 60 °C under static vacuum (initially 2 mTorr) onto a water-cooled cold finger with the side bulb cooled in liquid nitrogen. After 2 h, the liquid nitrogen was replaced with a dry ice/ethanol bath and the sublimation was continued overnight. The red-orange solid was collected from the cold finger. Yield: 0.38 g (44 %). Anal. Calc. for $C_{18}H_{36}FeN_2$: C, 64.3; H, 10.8; N, 8.33. Found: C, 63.9; H, 11.1; N, 8.23. ^{1}H NMR (C_6D_6): δ 170.6 (br s, fwhm = 2200 Hz, 8 H, CH_2), 139.5 (br s, fwhm = 990 Hz,4 H, CH_2), 81.8 (br s, fwhm = 4370 Hz, 24 H, Me). IR (cm^{-1}): 1369 (s), 1354 (s), 1341 (m), 1288 (m), 1236 (s), 1198 (w), 1170 (s), 1131 (s), 1076 (w), 1056 (m), 1017 (m), 985 (w), 961 (m), 950 (m), 933 (s), 909 (m), 861 (w), 750 (w), 668 (w), 643 (w), 590 (w), 540 (w), 523 (m).

Bis(2,2,6,6-tetramethylpiperidido)cobalt(II), Co(TMP)$_2$. To a mixture of $CoCl_2(THF)_{1.1}$ (2.012 g, 9.62 mmol) of Li(TMP) (2.901 g, 19.7 mmol) was added pentane (100 mL). The mixture was stirred overnight to afford a dark, almost black, mixture. The mixture was

filtered and the solids were washed with pentane (50 mL). The filtrate and wash were combined in a Schlenk tube equipped with a side bulb and dried under vacuum. The product was sublimed at 60 °C onto a water-cooled cold finger under static vacuum (initially 2 mTorr) with the side bulb cooled in liquid nitrogen. After 4 h, the liquid nitrogen was replaced with a dry ice/ethanol bath and the sublimation was continued overnight. The dark purple solid was collected from the cold finger. Yield: 0.14 g (4 %). Anal. Calc. for $C_{18}H_{36}CoN_2$: C, 63.7; H, 10.7; N, 8.25. Found: C, 63.0; H, 10.6; N, 7.38. IR (cm^{-1}): 1355 (m), 1342 (w), 1288 (w), 1235 (s), 1196 (w), 1168 (s), 1131 (s), 1076 (w), 1054 (w), 1014 (w), 986 (w), 963 (w), 949 (w), 930 (m), 910 (w), 864 (w), 748 (w), 669 (w), 618 (w), 525 (w). A small number of yellow crystals are present in the dark purple solid, which proved by X-ray diffraction to be $Co(TMP)_2(THF)$.

Crystallographic studies.[46] Crystals of $Mn(TMP)_2$ were grown by sublimation under static vacuum (initially 2 mTorr, 45 °C) from the dried reaction mixture. A crystal mounted on a Nylon fiber with Krytox™ oil (DuPont) was transferred onto the diffractometer and kept at -173 °C in a cold nitrogen gas stream. Intensity data were collected on a Bruker D8 Venture kappa diffractometer equipped with a Photon 100 CMOS detector. An Iμs microfocus source provided the Mo Kα radiation (λ = 0.71073 Å) that was monochromated with multilayer mirrors. Standard peak search and indexing procedures gave rough cell dimensions, and least squares refinement using 9819 reflections yielded the cell dimensions in Table 5.2.

Data were collected with an area detector by using the measurement parameters listed in Table 5.2. Systematic absences for 0*k*0 ($k \neq 2n$) and *h*0*l* ($h + l \neq 2n$) were uniquely consistent with the space group $P2_1/n$. The measured intensities were reduced to structure factor amplitudes and their estimated standard deviations by correction for background, scan speed, Lorentz, and polarization effects. The data crystal was a non-merohedral twin. TWINABS v2012/1 was used

to determine which reflections were unique to the primary domain, and only data from the primary twin domain was used in the refinement. A multi-scan absorption correction was applied using TWINABS v2012/1, the minimum and maximum transmission factors being 0.42 and 0.75. Systematically absent reflections were deleted and symmetry equivalent reflections were averaged to yield the set of unique data. The remaining 3625 data were used in the least squares refinement.

The solution for the isomorphous compound $Fe(TMP)_2$ was used as the initial model.[37] One of the TMP ligands was disordered, the two components being related by a chair flip or (equivalently) a 170° rotation about the Mn-N bond. The occupancies of the two components were constrained to add to 1; the site occupancy factor for the major component refined to 0.656(7). The N-C bond distances of the disordered TMP ligand were constrained to be equal within 0.01 Å. The C-C distances of the disordered TMP ligand were restrained to be 1.53(2) Å. The anisotropic displacement parameters (U_{ij}) for the carbon atoms bound to the nitrogen atom and one of the methyl carbons in the disordered TMP ligand were restrained to be equal within a standard deviation of 0.01. The quantity minimized by the least-squares program was $\Sigma w(F_o^2 - F_c^2)^2$, where $w = \{[\sigma(F_o^2)]^2 + (0.0582P)^2 + 4.0899P\}^{-1}$ and $P = (F_o^2 + 2F_c^2)/3$. The analytical approximations to the scattering factors were used, and all structure factors were corrected for both real and imaginary components of anomalous dispersion. In the final cycle of least squares, independent anisotropic displacement factors were refined for the non-hydrogen atoms. Hydrogen atoms were placed in idealized positions; the methyl groups were allowed to rotate about the C-C axis to find the best least-squares positions. The displacement parameters for methylene hydrogens were set equal to 1.2 times U_{eq} for the attached carbon; those for methyl hydrogens were set to 1.5 times U_{eq}. No correction for isotropic extinction was necessary. Successful convergence was indicated by the maximum shift/error of 0.001 for the last cycle. Final refinement parameters are given in

Table 5.2. The largest peak in the final Fourier difference map (0.56 $eÅ^{-3}$) was located 0.98 Å from Mn1. A final analysis of variance between observed and calculated structure factors showed no apparent errors.

Table 5.2: Crystallographic data for $Mn(TMP)_2$

Formula	$C_{18}H_{36}N_2Mn$
Formula weight	335.44
T (K)	100
λ (Å)	0.71073
Crystal system	Monoclinic
Space group	$P2_1/n$
a (Å)	11.7916(11)
b (Å)	11.5536(10)
c (Å)	15.5936(16)
β (°)	112.3314(33)
V (Å^3)	1965.079(521)
Z, ρ_{calc} (g/cm^3)	4, 1.134
μ (mm^{-1})	0.67
F(000)	732.0
Crystal size (mm)	0.088×0.256×0.364
θ range (°)	2.26 – 25.54
R(int)	0.1489
Absorption correction	Multi-scan
Max., min. transmission factors	0.75, 0.42
Data/restraints/parameters	3625/64/352
GOF on F^2	1.143
R_1 [$I > 2\sigma(I)$]	0.0605
wR_2 (all data)	0.1449
max., min. $\Delta\rho_{elect}$ (eÅ^{-3})	0.56, -0.75

Table 5.3: Selected distances for $Mn(TMP)_2$

Distances (Å)					
Mn1-N1	1.9214(26)	C3-C4	1.5176(51)	C6A-C16A	1.5349(76)
Mn1-N2	1.9252(24)	C4-C5	1.5375(44)	C7A-C8A	1.5180(114)
N1-C1	1.4746(38)	C5-C13	1.5463(45)	C8A-C9A	1.5197(102)
N1-C5	1.4696(39)	C5-C14	1.5289(45)	C9A-C10A	1.5332(105)
C1-C2	1.5362(43)	N2-C6A	1.4725(53)	C10A-C17A	1.5277(104)
C1-C11	1.5203(46)	N2-C10A	1.4714(56)	C10A-C18A	1.5460(132)
C1-C12	1.5375(43)	C6A-C7A	1.5530(105)		
C2-C3	1.5140(51)	C6A-C15A	1.5247(83)		

Distances are listed only for the major component of the disorder model.

Table 5.4: Selected angles for $Mn(TMP)_2$

Angles (°)			
N1-Mn1-N2	172.15(11)	Mn1-N2-C6A	118.59(40)
Mn1-N1-C1	120.45(19)	Mn1-N2-C10A	119.84(44)
Mn1-N1-C5	119.23(19)	C6A-N2-C10A	120.57(58)
C1-N1-C5	119.41(23)	N2-C6A-C7A	108.40(69)
N1-C1-C2	110.68(25)	N2-C6A-C15A	107.70(52)
N1-C1-C11	106.68(25)	N2-C6A-C16A	117.23(58)
N1-C1-C12	113.68(26)	C7A-C6A-C15A	107.95(68)
C2-C1-C11	108.08(27)	C7A-C6A-C16A	107.45(70)
C2-C1-C12	109.93(28)	C15A-C6A-C16A	107.79(66)
C11-C1-C12	107.55(29)	C6A-C7A-C8A	114.61(69)
C1-C2-C3	112.98(28)	C7A-C8A-C9A	108.95(66)
C2-C3-C4	108.58(30)	C8A-C9A-C10A	113.29(64)
C3-C4-C5	112.28(28)	N2-C10A-C9A	109.09(65)
N1-C5-C4	111.46(25)	N2-C10A-C17A	114.57(67)
N1-C5-C13	113.24(26)	N2-C10A-C18A	103.51(97)
N1-C5-C14	107.22(26)	C9A-C10A-C17A	108.65(67)
C4-C5-C13	109.47(28)	C9A-C10A-C18A	109.93(114)
C4-C5-C14	108.15(27)	C17A-C10A-C18A	110.94(102)
C13-C5-C14	107.05(27)		

Angles are listed only for the major component of the disorder model.

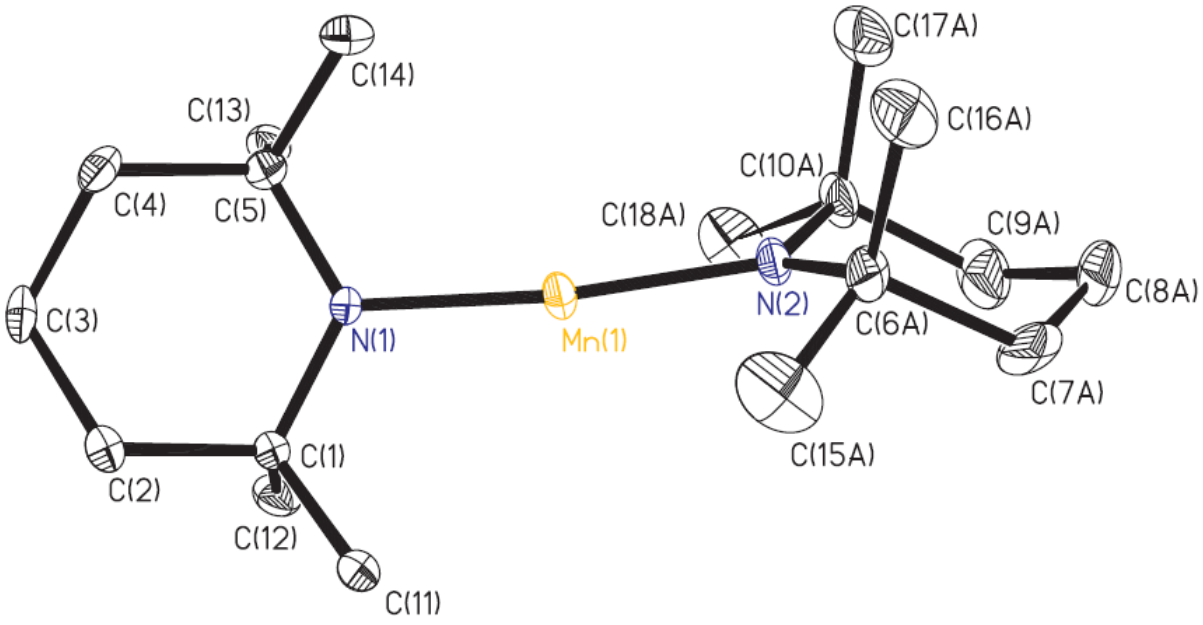

Figure 5.1: Molecular structure of $Mn(TMP)_2$. Ellipsoids are drawn at the 35% probability level; hydrogen atoms are omitted for clarity. Only the major disorder component is shown. Both TMP ligands adopt chair conformations.

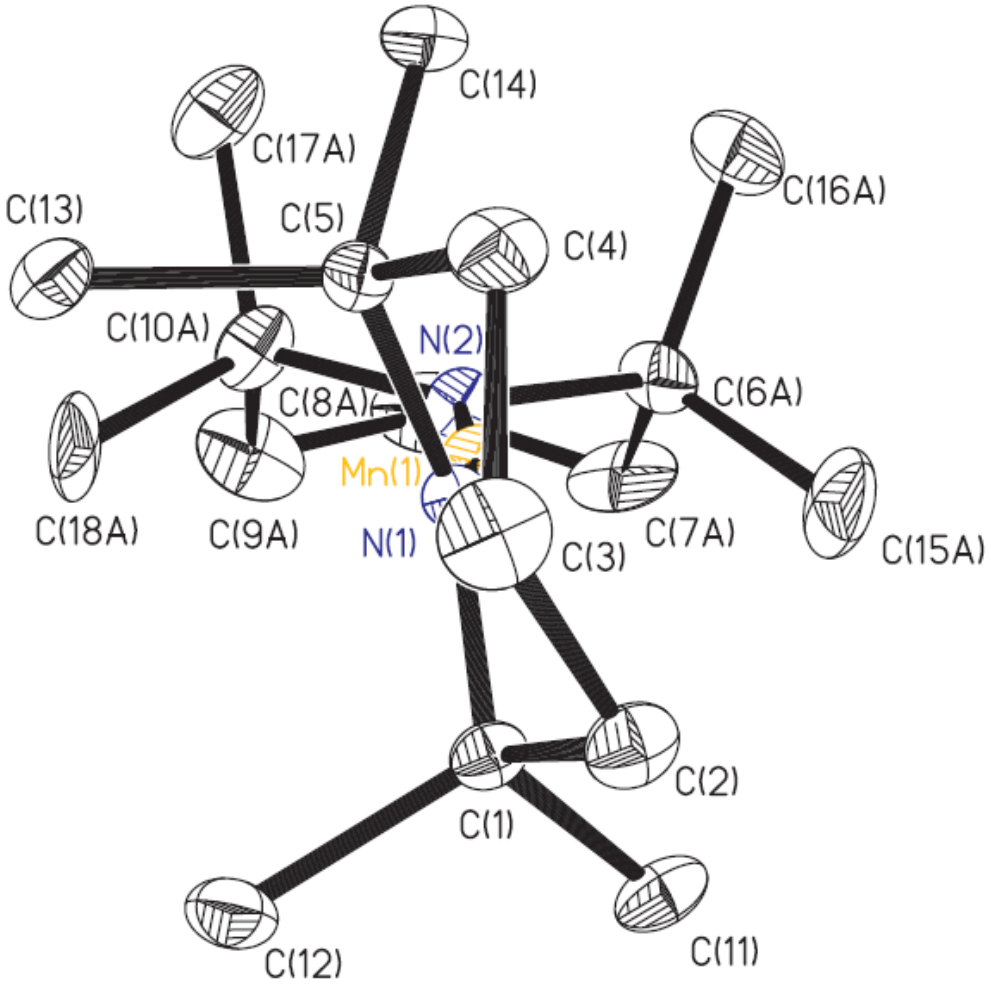

Figure 5.2: An alternative view of $Mn(TMP)_2$ down the N1-Mn1-N2 axis.

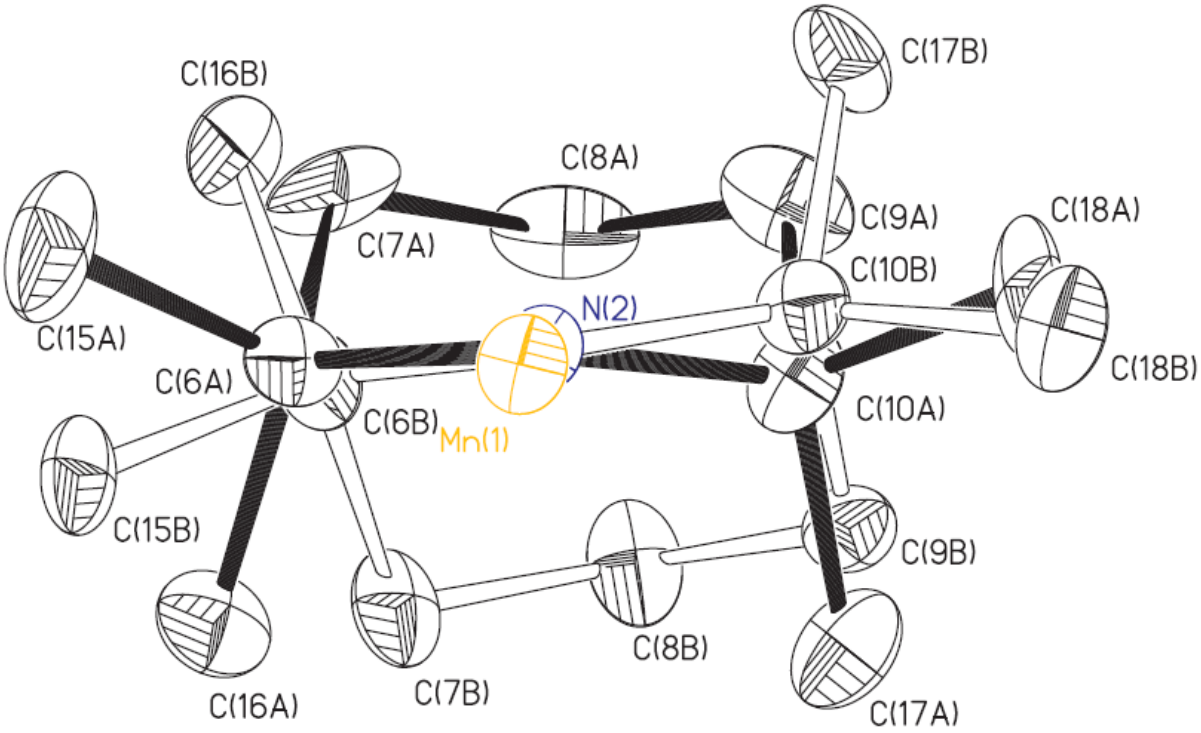

Figure 5.3: The two components of the disorder model viewed down the Mn1-N2 bond. The major component (solid bonds) and minor component (hollow bonds) are related by a chair flip or a 170° rotation.

References

1. Heidlage, M. G.; Kezar, E. A.; Snow, K. C.; Pfromm, P. H., Thermochemical synthesis of ammonia and syngas from natural gas at atmospheric pressure. *Ind. Eng. Chem. Res.* **2017,** *56*, 14014-14024.

2. Makepeace, J. W.; Wood, T. J.; Marks, P. L.; Smith, R. I.; Murray, C. A.; David, W. I. F., Bulk phase behavior of lithium imide-metal nitride ammonia decomposition catalysts. *Phys. Chem. Chem. Phys.* **2018,** *20*, 22689-22697.

3. Shalom, M.; Ressnig, D.; Yang, X.; Clavel, G.; Fellinger, T. P.; Antonietti, M., Nickel nitride as an efficient electrocatalyst for water splitting. *J. Mater. Chem. A* **2015,** *3*, 8171-8177.

4. Davari, E.; Ivey, D. G., Synthesis and electrochemical performance of manganese nitride as an oxygen reduction and oxygen evolution catalyst for zinc-air secondary batteries. *J. Appl. Electrochem.* **2017,** *47*, 815-827.

5. Yu, F.; Zhou, H.; Zhu, Z.; Sun, J.; He, R.; Bao, J.; Chen, S.; Ren, Z., Three-dimensional nanoporous iron nitride film as an efficient electrocatalyst for water oxidation. *ACS Catal.* **2017,** *7*, 2052-2057.

6. Walter, C.; Menezes, P. W.; Orthmann, S.; Schuch, J.; Connor, P.; Kaiser, B.; Lerch, M.; Driess, M., A molecular approach to manganese nitride acting as a high performance electrocatalyst in the oxygen evolution reaction. *Angew. Chem., Int. Ed.* **2018,** *57*, 698-702.

7. Chen, L.; Zhang, Y.; Liu, X.; Long, L.; Wang, S.; Xu, X.; Liu, M.; Yang, W.; Jia, J., Bifunctional oxygen electrodes of homogeneous Co_4N nanocrystals@N-doped carbon hybrids for rechargeable Zn-air batteries. *Carbon* **2019,** *151*, 10-17.

8. Zou, H.; Li, G.; Duan, L.; Kou, Z.; Wang, J., In situ coupled amorphous cobalt nitride with nitrogen-doped graphene aerogel as a trifunctional electrocatalyst towards Zn-air battery deriven full water splitting. *Appl. Catal., B* **2019,** *259,* 118100.

9. Guo, J.; Chang, F.; Wang, P.; Hu, D.; Yu, P.; Wu, G.; Xiong, Z.; Chen, P., Highly active MnN-Li_2NH composite catalyst for producing CO_x-free hydrogen. *ACS Catal.* **2015,** *5,* 2708-2713.

10. Ni, W.; Krammer, A.; Hsu, C.-S.; Chen, H. M.; Schueler, A.; Hu, X., Ni_3N as an active hydrogen oxidation reaction catalyst in alkaline medium. *Angew. Chem., Int. Ed.* **2019,** *58,* 7445-7449.

11. Sun, Q.; Fu, Z.-W., Mn_3N_2 as a novel negative electrode material for rechargeable lithium batteries. *Appl. Surf. Sci.* **2012,** *258,* 3197-3201.

12. Li, X.; Hasan, M. M.; Hector, A. L.; Owen, J. R., Performance of nanocrystalline Ni_3N as a negative electrode for sodium-ion batteries. *J. Mater. Chem. A* **2013,** *1,* 6441-6445.

13. Lei, M.; Wang, J.-G.; Ren, L.; Nan, D.; Shen, C.; Xie, K.; Liu, X., Highly lithiophilic cobalt nitride nanobrush as a stable host for high-performance lithium metal anodes. *ACS Appl. Mater. Interfaces* **2019,** *11,* 30992-30998.

14. Zhang, H.; Zhao, Z.; Hou, Y.-N.; Tang, Y.; Liang, J.; Liu, X.; Zhang, Z.; Wang, X.; Qiu, J., Highly stable lithium-sulfur batteries based on p-n heterojunctions embedded on hollow sheath carbon propelling polysulfides conversion. *J. Mater. Chem. A* **2019,** *7,* 9230-9240.

15. Zhao, L.; Wang, W.; Zhao, X.; Hou, Z.; Fan, X.; Liu, Y.; Quan, Z., Ni_3N nanocrystals decorated reduced graphene oxide with high ionic conductivity for stable lithium metal anode. *ACS Appl. Energy Mater.* **2019,** *2*, 2692-2698.

16. Smith, A. R.; Yang, R.; Yang, H.; Lambrecht, W. R. L.; Dick, A.; Neugebauer, J., Aspects of spin-polarized scanning tunneling microscopy at the atomic scale: experiment, theory, and simulation. *Surf. Sci.* **2004,** *561*, 154-170.

17. Intanon, N.; Saikaew, C.; Wisitsoraat, A.; Srisattayakul, P., Improving the mechanical properties of a machine component of a fishing-net weaving machine by duplex coating. *Adv. Mater. Res. (Durnten-Zurich, Switz.)* **2014,** *1016*, 90-94, 6 pp.

18. Jollie, M.; Choo, D.; Newman, D.; Wears, M. L.; Miles, J., Recording studies on a self-assembling medium of cobalt nano-particles. *IEE Proc.: Sci., Meas. Technol.* **2003,** *150*, 240-243.

19. Kim, H.-D.; Yun, M. J.; Hong, S. M.; Kim, T. G., Effect of nanopyramid bottom electrodes on bipolar resistive switching phenomena in nickel nitride films-based crossbar arrays. *Nanotechnology* **2014,** *25*, 125201/1-125201/8.

20. Wang, G. L.; Wu, S. X.; Hu, P.; Li, S. W., Magnetic properties and evidence of current-induced perpendicular field in epitaxial ferrimagnetic Mn_4N (002) film mixed with (111) phase. *J. Appl. Phys. (Melville, NY, U. S.)* **2017,** *122*, 133905/1-133905/5.

21. Manzel, M.; Steinbeiss, E.; Schüppel, W., Magnetic properties of sputter-synthesized cobalt nitride films. *Phys. Status Solidi A* **1990,** *119*, 279-84.

22. Carey, R.; Newman, D. M.; Holmes, B., A self-forming nanocrystallite cobalt recording medium. *IEEE Trans. Magn.* **2000,** *36*, 3012-3014.

23. Kim, S. I.; Lee, S. R.; Ahn, K. M.; Ahn, B. T., Improvement in thermal stability of nickel silicides using NiN_x films. *J. Electrochem. Soc.* **2010,** *157*, H231-H234.

24. Kabara, K.; Tsunoda, M., Perpendicular magnetic anisotropy of Mn_4N films fabricated by reactive sputtering method. *J. Appl. Phys. (Melville, NY, U. S.)* **2015,** *117*, 17B512/1-17B512/4.

25. Balogun, M.-S.; Zeng, Y.; Qiu, W.; Luo, Y.; Onasanya, A.; Olaniyi, T. K.; Tong, Y., Three-dimensional nickel nitride (Ni_3N) nanosheets: free standing and flexible electrodes for lithium ion batteries and supercapacitors. *J. Mater. Chem. A* **2016,** *4*, 9844-9849.

26. Chen, J.; Yin, H.; Zhou, J.; Gong, J.; Wang, L.; Zheng, Y.; Nie, Q., Non-enzymatic glucose sensor based on nickel nitride decorated nitrogen doped carbon spheres (Ni_3N/NCS) via facile one pot nitridation process. *J. Alloys Compd.* **2019,** *797*, 922-930.

27. Jiang, G.; Han, H.; Zhuang, W.; Xu, X.; Kaskel, S.; Xu, F.; Wang, H., Three-dimensional ordered mesoporous cobalt nitride for fast-kinetics and stable-cycling lithium storage. *J. Mater. Chem. A* **2019,** *7*, 17561-17569.

28. Liu, B.; Cheng, J.; Peng, H.-Q.; Chen, D.; Cui, X.; Shen, D.; Zhang, K.; Jiao, T.; Li, M.; Lee, C.-S.; Zhang, W., In situ nitridated porous nanosheet networked Co_3O_4-Co_4N heteronanostructures supported on hydrophilic carbon cloth for highly efficient electrochemical hydrogen evolution. *J. Mater. Chem. A* **2019,** *7*, 775-782.

29. Zhang, F.; Jin, L.; Li, H.; Xie, K., Coordinatively unsaturated metal-nitrogen active sites at twisted surfaces in metallic porous nitride single crystals delivering enhanced electrocatalysis activity. *Chem. - Eur. J.* **2020,** *26*, 2327-2332.

30. Liu, T.; Li, M.; Jiao, C.; Hassan, M.; Bo, X.; Zhou, M.; Wang, H.-L., Design and synthesis of integrally structured Ni_3N nanosheets/carbon microfibers/Ni_3N nanosheets for efficient full water splitting catalysis. *J. Mater. Chem. A* **2017,** *5*, 9377-9390.

31. Hu, S.; Feng, C.; Wang, S.; Liu, J.; Wu, H.; Zhang, L.; Zhang, J., Ni_3N/NF as bifunctional catalysts for both hydrogen generation and urea decomposition. *ACS Appl. Mater. Interfaces* **2019,** *11*, 13168-13175.

32. Mallek, J. L. Volatile metal borohydride complexes: synthesis and characterization of new chemical vapor deposition precursors. Ph.D. Dissertation, University of Illinois at Urbana-Champaign, 2014.

33. Wang, W. B.; Chang, N. N.; Codding, T. A.; Girolami, G. S.; Abelson, J. R., Superconformal chemical vapor deposition of thin films in deep features. *J. Vac. Sci. Technol., A* **2014,** *32*, 051512/1-051512/10.

34. Spicer, T. S.; Spicer, C. W.; Cloud, A. N.; Davis, L. M.; Girolami, G. S.; Abelson, J. R., Low-temperature CVD of η-Mn_3N_{2-x} from bis[di(*tert*-butyl)amido]manganese(II) and ammonia. *J. Vac. Sci. Technol., A* **2013,** *31*, 030604/1-030604/6.

35. Cloud, A. N.; Davis, L. M.; Girolami, G. S.; Abelson, J. R., Low-temperature CVD of iron, cobalt, and nickel nitride thin films from bis[di(*tert*-butyl)amido]metal(II) precursors and ammonia. *J. Vac. Sci. Technol., A* **2014,** *32*, 020606/1-020606/7.

36. Potratz, G. R. Synthesis and characterization of transition metal di(*tert*-butyl)amido compounds. M.S. Thesis, University of Illinois at Urbana-Champaign, 2000.

37. Davis, L. M. Syntheses, properties, and reactions of transition metal complexes of di(*tert*-butyl)amide and 2,2,6,6-tetramethylpiperidide. Ph.D. Dissertation, University of Illinois at Urbana-Champaign, 2014.

38. Mohimi, E.; Trinh, B. B.; Babar, S.; Girolami, G. S.; Abelson, J. R., Chemical vapor deposition of Mn_xN_y films from bis(2,2,6,6-tetramethylpiperidido)manganese(II) and ammonia. *J. Vac. Sci. Technol., A* **2016,** *34*, 060603/1-060603/5.

39. Fleming, I.; Mah, T., Simple synthesis of anthracenes. *J. Chem. Soc., Perkin Trans. 1* **1975**, 964-5.

40. Eaton, P. E.; Higuchi, H.; Millikan, R., Synthesis of zinc, cadmium, tin, and silicon derivatives of cubane. *Tetrahedron Letters* **1987,** *28*, 1055-1058.

41. Nöth, H.; Schlosser, D., The aminolysis of beryllium dichloride with diisopropylamine and reactions of some amino-beryllium chlorides. *Eur. J. Inorg. Chem.* **2003**, 2245-2254.

42. Spicer, C. W. Synthesis, characterization and chemical vapor deposition of transition metal di(*tert*-butyl)amido compounds. Ph.D. Dissertation, University of Illinois at Urbana-Champaign, 2008.

43. Fowles, G. W. A.; Rice, D. A.; Walton, R. A., Donor properties of simple ethers. I. Dioxanates formed by some metal halides of the first transition series (manganese-copper). *J. Chem. Soc., A* **1968**, 1842-6.

44. Lappert, M. F.; Slade, M. J.; Singh, A.; Atwood, J. L.; Rogers, R. D.; Shakir, R., Structure and reactivity of sterically hindered lithium amides and their diethyl etherates: crystal and molecular structures of $[Li\{N(SiMe_3)_2\}(OEt_2)]_2$ and tetrakis(2,2,6,6-tetramethylpiperidinatolithium). *J. Am. Chem. Soc.* **1983,** *105*, 302-4.

45. Fulmer, G. R.; Miller, A. J. M.; Sherden, N. H.; Gottlieb, H. E.; Nudelman, A.; Stoltz, B. M.; Bercaw, J. E.; Goldberg, K. I., NMR chemical shifts of trace impurities: common laboratory solvents, organics, and gases in deuterated solvents relevant to the organometallic chemist. *Organometallics* **2010,** *29*, 2176-2179.

46. Brumaghim, J. L.; Priepot, J. G.; Girolami, G. S., Synthesis of hydride and alkyl compounds containing the Cp*Os(NO) fragment. Crystal structure of $[Cp^*Os(\mu\text{-}NO)]_2$. *Organometallics* **1999,** *18*, 2139-2144.

APPENDIX A

IPR ANALYSIS OF METAL-BOUND ALKANES

Here we describe the equations we use to analyze the results of isotopic perturbation of our resonance (IPR) experiments with alkanes.

Determining the Equations for the Observed Chemical Shifts of Bound Methane.

Methane can bind to a single transition metal center by means of any of four different binding modes (Figure A.1):

Figure A.1: The four coordination modes by which CH_4 can bind to a single metal center.

Let us consider the case of the κ^1 binding mode and label the hydrogen atoms as terminal (H_T) or bridging (H_B) (Figure A.2).

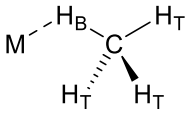

Figure A.2: Bookkeeping labels for the H atoms in κ^1-CH_4.

If the hydrogen atoms are in fast exchange on the NMR timescale, then the observed chemical shift (δ_{obs}) will be a weighted average of the chemical shift of H_T (δ_T) and H_B (δ_B):

$$\delta_{obs} = \frac{n_T\delta_T + n_B\delta_B}{n_T + n_B} \qquad \textbf{(A.1)}$$

where n_T is the population of H_T and n_B is the population of H_B. For κ^1-CH_4, there are 3 H_T atoms and 1 H_B atom; $n_T = 3$ and $n_B = 1$. The observed chemical shift for non-deuterated κ^1-CH_4 (δ_0) is:

$$\delta_0 = \frac{3\delta_T + \delta_B}{4} \quad \textbf{(A.2)}$$

Now let us consider the case in which we substitute one of the H atoms for D, κ^1-CH_3D. There are four configurations for this case (Figure A.3):

Figure A.3: The four configurations of κ^1-CH_3D with bookkeeping labels on the H atoms.

Because of zero-point energy effects, configurations with bridging D atoms are higher in energy than those with terminal D atoms. **1**, **2**, and **3** all have the D atom in terminal positions and are energetically degenerate but **4** has the D atom in the bridging position and is higher in energy than the other configurations. Let us call the difference in energy between **4** and the other configurations ΔE_{BI}. Because **4** is not degenerate with the other configurations, the population of **4** will be different than the populations of the other three configurations. Therefore, we cannot simply count how many H_T and H_B atoms there are in the structures as we did with κ^1-CH_4. The relative populations of configurations **1** and **4** are described by a Boltzmann distribution:

$$\frac{n_4}{n_1} = e^{-\frac{\Delta E_{BI}}{RT}} \quad \textbf{(A.3)}$$

where n_i is the population of configuration *i*, R is the ideal gas constant, and T is the temperature of the sample. If we set n_1 to 1, then n_4 becomes:

$$n_4 = e^{-\frac{\Delta E_{BI}}{RT}} \quad \textbf{(A.4)}$$

Now that we have expressions for the relative populations of **1**, **2**, **3**, and **4** (recall that $n_1 = n_2 = n_3$ because those configurations are degenerate), we can determine n_T and n_B. If we define N_{Ti} as the number of H_T atoms in configuration *i*, and N_{Bi} as the number of H_B atoms in configuration *i*, then n_T and n_B become:

$$n_T = n_1 N_{T1} + n_2 N_{T2} + n_3 N_{T3} + n_4 N_{T4}$$

$$= (1)(2) + (1)(2) + (1)(2) + \left(e^{-\frac{\Delta E_{BI}}{RT}}\right)(3) = 6 + 3e^{-\frac{\Delta E_{BI}}{RT}} \quad \textbf{(A.5)}$$

$$n_B = n_1 N_{B1} + n_2 N_{B2} + n_3 N_{B3} + n_4 N_{B4}$$

$$= (1)(1) + (1)(1) + (1)(1) + \left(e^{-\frac{\Delta E_{BI}}{RT}}\right)(0) = 3 \quad \textbf{(A.6)}$$

Substituting these expressions into Equation A.1 gives the observed (i.e., exchange-averaged) chemical shift for a metal-bound mono-deuterated κ^1-CH_3D ligand (δ_1):

$$\delta_1 = \frac{n_T\delta_T + n_B\delta_B}{n_T + n_B} = \frac{\left(6+3e^{-\frac{\Delta E_{BI}}{RT}}\right)\delta_T + (3)\delta_B}{\left(6+3e^{-\frac{\Delta E_{BI}}{RT}}\right)+(3)} = \frac{\left(2+e^{-\frac{\Delta E_{BI}}{RT}}\right)\delta_T + \delta_B}{3+e^{-\frac{\Delta E_{BI}}{RT}}} \quad \textbf{(A.7)}$$

In contrast, a κ^1-CH_2D_2 ligand has six configurations (Figure A.4)

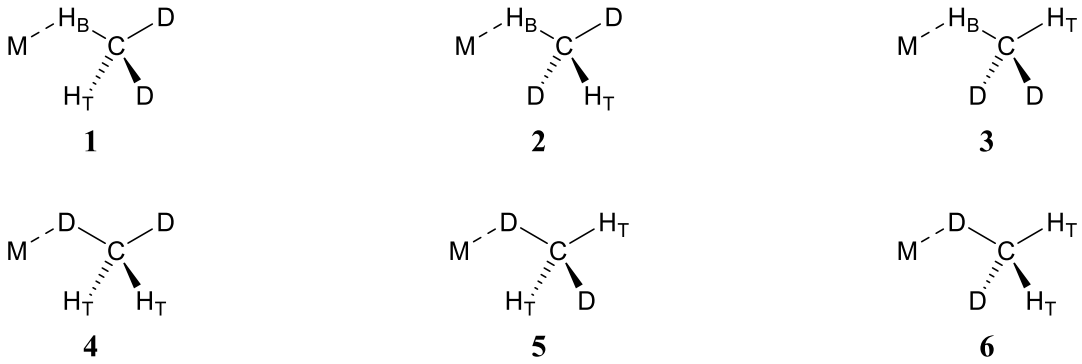

Figure A.4: The six configurations of κ^1-CH_2D_2 with bookkeeping labels on the H atoms.

Configurations **1**, **2**, and **3** are degenerate. We can set $n_1 = n_2 = n_3 = 1$. Configurations **4**, **5**, and **6** are degenerate and $n_4 = n_5 = n_6 = e^{-\frac{\Delta E_{BI}}{RT}}$. Calculating n_T and n_B in the manner described for κ^1-CH_3D yields:

$$n_T = 1 + 2e^{-\frac{\Delta E_{BI}}{RT}} \quad \textbf{(A.8)}$$

$$n_B = 1 \quad \textbf{(A.9)}$$

These expressions give an observed chemical shift for a metal-bound di-deuterated κ^1-CH_2D_2 ligand (δ_2):

$$\delta_2 = \frac{\left(1+2e^{-\frac{\Delta E_{BI}}{RT}}\right)\delta_T+\delta_B}{2+2e^{-\frac{\Delta E_{BI}}{RT}}} \quad \textbf{(A.10)}$$

A similar analysis of a metal-bound tri-deuterated κ^1-CHD_3 ligand yields:

$$\delta_3 = \frac{\left(3e^{-\frac{\Delta E_{BI}}{RT}}\right)\delta_T+\delta_B}{1+3e^{-\frac{\Delta E_{BI}}{RT}}} \quad \textbf{(A.11)}$$

A similar method can be used to determine the equations for the exchange-averaged chemical shifts for the η^2, κ^2, and κ^3 coordination modes of a metal-bound deuterated methane ligand as a function of the extent of deuteration. The η^2 coordination mode gives results identical to the κ^1 coordination mode; IPR cannot distinguish between the two cases.

Equations for the Observed Chemical Shift of a Bound Methane Ligand.

η^2/κ^1:

$$\delta_0 = \frac{3\delta_T+\delta_B}{4} \quad \textbf{(A.12)}$$

$$\delta_1 = \frac{\left(2+e^{-\frac{\Delta E_{BI}}{RT}}\right)\delta_T+\delta_B}{3+e^{-\frac{\Delta E_{BI}}{RT}}} \quad \textbf{(A.13)}$$

$$\delta_2 = \frac{\left(1+2e^{-\frac{\Delta E_{BI}}{RT}}\right)\delta_T+\delta_B}{2+2e^{-\frac{\Delta E_{BI}}{RT}}} \quad \textbf{(A.14)}$$

$$\delta_3 = \frac{\left(3+e^{-\frac{\Delta E_{BI}}{RT}}\right)\delta_T+\delta_B}{1+3e^{-\frac{\Delta E_{BI}}{RT}}} \quad \textbf{(A.15)}$$

κ^2:

$$\delta_0 = \frac{\delta_T + \delta_B}{2} \quad \textbf{(A.16)}$$

$$\delta_1 = \frac{\left(1+2e^{-\frac{\Delta E_{BI}}{RT}}\right)\delta_T + \left(2+e^{-\frac{\Delta E_{BI}}{RT}}\right)\delta_B}{3+3e^{-\frac{\Delta E_{BI}}{RT}}} \quad \textbf{(A.17)}$$

$$\delta_2 = \frac{\left(2e^{-\frac{\Delta E_{BI}}{RT}}+e^{-\frac{2\Delta E_{BI}}{RT}}\right)\delta_T + \left(1+2e^{-\frac{\Delta E_{BI}}{RT}}\right)\delta_B}{1+4e^{-\frac{\Delta E_{BI}}{RT}}+e^{-\frac{2\Delta E_{BI}}{RT}}} \quad \textbf{(A.18)}$$

$$\delta_3 = \frac{\left(e^{-\frac{\Delta E_{BI}}{RT}}\right)\delta_T + \delta_B}{1+e^{-\frac{\Delta E_{BI}}{RT}}} \quad \textbf{(A.19)}$$

κ^3:

$$\delta_0 = \frac{\delta_T + 3\delta_B}{4} \quad \textbf{(A.20)}$$

$$\delta_1 = \frac{\left(e^{-\frac{\Delta E_{BI}}{RT}}\right)\delta_T + \left(1+2e^{-\frac{\Delta E_{BI}}{RT}}\right)\delta_B}{1+3e^{-\frac{\Delta E_{BI}}{RT}}} \quad \textbf{(A.21)}$$

$$\delta_2 = \frac{\left(e^{-\frac{\Delta E_{BI}}{RT}}\right)\delta_T + \left(2+e^{-\frac{\Delta E_{BI}}{RT}}\right)\delta_B}{2+2e^{-\frac{\Delta E_{BI}}{RT}}} \quad \textbf{(A.22)}$$

$$\delta_3 = \frac{\left(e^{-\frac{\Delta E_{BI}}{RT}}\right)\delta_T + 3\delta_B}{3+e^{-\frac{\Delta E_{BI}}{RT}}} \quad \textbf{(A.23)}$$

Determining δ_T, δ_B, ΔE_{BI}, and the Uncertainties in these Values for the η^2/κ^1 Case.

The equations for the exchange-averaged chemical shifts of the η^2/κ^1-methane binding modes are given in Equations A.12-A.15. These equations can be solved for δ_T, δ_B, and ΔE_{BI} but some care needs to be taken because there are four equations but only three unknowns. Therefore, we will choose all permutations of three of the four equations and then average the results to obtain the best values for δ_T, δ_B, and ΔE_{BI}. Solving for the desired values from Equations A.12-A.14 yields:

$$\delta_{\mathrm{T}} = \frac{-\delta_0\delta_1+2\delta_0\delta_2-\delta_1\delta_2}{\delta_0-2\delta_1+\delta_2} \quad \textbf{(A.24)}$$

$$\delta_{\mathrm{B}} = \frac{4{\delta_0}^2-5\delta_0\delta_1-2\delta_0\delta_2+3\delta_1\delta_2}{\delta_0-2\delta_1+\delta_2} \quad \textbf{(A.25)}$$

$$\Delta \mathrm{E}_{\mathrm{BI}} = R\,T\,\log\frac{-\delta_1+\delta_2}{-2\delta_0+3\delta_1-\delta_2} \quad \textbf{(A.26)}$$

Repeating the analysis with the other combinations of Equations A.12-15 and then averaging the results yields:

$$\delta_{\mathrm{T}} = \frac{1}{4}\left(\frac{-\delta_0\delta_1+2\delta_0\delta_2-\delta_1\delta_2}{\delta_0-2\delta_1+\delta_2} + \frac{-\delta_0\delta_1+3\delta_0\delta_2-2\delta_1\delta_3}{2\delta_0-3\delta_1+\delta_3} + \frac{-2\delta_0\delta_2+2\delta_0\delta_3-\delta_2\delta_3}{\delta_0-3\delta_2+2\delta_3} + \frac{-\delta_1\delta_2+2\delta_1\delta_3-\delta_2\delta_3}{\delta_1-2\delta_2+\delta_3}\right) \quad \textbf{(A.27)}$$

$$\delta_{\mathrm{B}} = \frac{1}{4}\left(\frac{4{\delta_0}^2-5\delta_0\delta_1-2\delta_0\delta_2+3\delta_1\delta_2}{\delta_0-2\delta_1+\delta_2} + \frac{8{\delta_0}^2-9\delta_0\delta_1-5\delta_0\delta_3+6\delta_1\delta_3}{2\delta_0-3\delta_1+\delta_3} + \frac{4{\delta_0}^2+3\delta_2\delta_3-\delta_0(6\delta_2+\delta_3)}{\delta_0-3\delta_2+2\delta_3} + \right.$$

$$\left. \frac{{\delta_1}^2(-9\delta_2+10\delta_3)+2\delta_1\left(6{\delta_2}^2-6\delta_2\delta_3-{\delta_3}^2\right)+\delta_2\delta_3(-4\delta_2+5\delta_3)}{{\delta_1}^2-6\delta_1\delta_2+8{\delta_2}^2+4\delta_1\delta_3-10\delta_2\delta_3+3{\delta_3}^2}\right) \quad \textbf{(A.28)}$$

$$\Delta \mathrm{E}_{\mathrm{BI}} = \frac{R\,T}{4}\left[\ln\left(\frac{\delta_1-\delta_2}{2\delta_0-3\delta_1+\delta_2}\right) + \ln\left(\frac{3(\delta_1-\delta_3)}{8\delta_0-9\delta_1+\delta_3}\right) + \ln\left(\frac{3(\delta_2-\delta_3)}{2\delta_0-3\delta_2+\delta_3}\right) + \ln\left(-\frac{\delta_1-4\delta_2+3\delta_3}{3\delta_1-4\delta_2+\delta_3}\right)\right] \quad \textbf{(A.29)}$$

For a multi-variable function, $F(x, y, z \ldots)$, the uncertainty in that function, $\sigma\big(F(x, y, z \ldots)\big)$, can be calculated with the following formula:

$$\sigma\big(F(x, y, z \ldots)\big) = \sqrt{\left(\frac{\partial F(x,y,z\ldots)}{\partial x}\right)^2 \big(\sigma(x)\big)^2 + \left(\frac{\partial F(x,y,z\ldots)}{\partial y}\right)^2 \big(\sigma(y)\big)^2 + \left(\frac{\partial F(x,y,z\ldots)}{\partial z}\right)^2 \big(\sigma(z)\big)^2 + \cdots} \quad \textbf{(A.30)}$$

where $\sigma(x)$ is the uncertainty in variable x, $\sigma(y)$ is the uncertainty in variable y, etc. Applying this formula to δ_{T}, δ_{B}, and $\Delta \mathrm{E}_{\mathrm{BI}}$ yields:

$$\sigma(\delta_{\mathrm{T}}) = \frac{1}{4}\left[\left(\frac{2(\delta_1-\delta_2)^2}{(\delta_0-2\delta_1+\delta_2)^2} + \frac{3(\delta_1-\delta_3)^2}{(2\delta_0-3\delta_1+\delta_3)^2} + \frac{6(\delta_2-\delta_3)^2}{(\delta_0-3\delta_2+2\delta_3)^2}\right)^2 \left(\sigma(\delta_0)\right)^2 + \left(\frac{(\delta_0-\delta_2)^2}{(\delta_0-2\delta_1+\delta_2)^2} - \right.$$

$$\frac{2(\delta_2-\delta_3)^2}{(\delta_1-2\delta_2+\delta_3)^2} + \frac{2(\delta_0-\delta_3)^2}{(2\delta_0-3\delta_1+\delta_3)^2}\Bigg)^2 \left(\sigma(\delta_1)\right)^2 + \left(\frac{-2(\delta_0-\delta_1)^2}{(\delta_0-2\delta_1+\delta_2)^2} + \frac{(\delta_1-\delta_3)^2}{(\delta_1-2\delta_2+\delta_3)^2} + \right.$$

$$\left.\frac{2(\delta_0-\delta_3)^2}{(\delta_0-3\delta_2+2\delta_3)^2}\right)^2 \left(\sigma(\delta_2)\right)^2 + \left(\frac{6(\delta_0-\delta_1)^2}{(2\delta_0-3\delta_1+\delta_3)^2} + \frac{2(\delta_1-\delta_2)^2}{(\delta_1-2\delta_2+\delta_3)^2} + \frac{3(\delta_0-\delta_2)^2}{(\delta_0-3\delta_2+2\delta_3)^2}\right)^2 \left(\sigma(\delta_3)\right)^2\Bigg]^{1/2}$$

(A.31)

$$\sigma(\delta_{\mathrm{B}}) = \frac{1}{4}\left[\left(12 - \frac{6(\delta_1-\delta_2)^2}{(\delta_0-2\delta_1+\delta_2)^2} - \frac{9(\delta_1-\delta_3)^2}{(2\delta_0-3\delta_1+\delta_3)^2} - \frac{18(\delta_2-\delta_3)^2}{(\delta_0-3\delta_2+2\delta_3)^2}\right)^2 \left(\sigma(\delta_0)\right)^2 + \left(\frac{3(\delta_0-\delta_2)^2}{(\delta_0-2\delta_1+\delta_2)^2} + \right.\right.$$

$$\left.\frac{6(\delta_0-\delta_3)^2}{(2\delta_0-3\delta_1+\delta_3)^2} + \frac{6(\delta_2-\delta_3)^2\left(7{\delta_1}^2-24\delta_1\delta_2+16{\delta_2}^2+10\delta_1\delta_3-8\delta_2\delta_3-{\delta_3}^2\right)}{[(\delta_1-2\delta_2+\delta_3)(\delta_1-4\delta_2+3\delta_3)]^2}\right)^2 \left(\sigma(\delta_1)\right)^2 +$$

$$\left(\frac{-6(\delta_0-\delta_1)^2}{(\delta_0-2\delta_1+\delta_2)^2} + \frac{6(\delta_0-\delta_3)^2}{(\delta_0-3\delta_2+2\delta_3)^2} - \frac{3(\delta_1-\delta_3)^3(3\delta_1-8\delta_2+5\delta_3)}{[(\delta_1-2\delta_2+\delta_3)(\delta_1-4\delta_2+3\delta_3)]^2}\right)^2 \left(\sigma(\delta_2)\right)^2 + \left(\frac{-18(\delta_0-\delta_1)^2}{(2\delta_0-3\delta_1+\delta_3)^2} - \right.$$

$$\left.\left.\frac{9(\delta_0-\delta_2)^2}{(\delta_0-3\delta_2+2\delta_3)^2} + \frac{2(\delta_1-\delta_2)^2\left(5{\delta_1}^2-16{\delta_2}^2+40\delta_2\delta_3-19{\delta_3}^2-2\delta_1(4\delta_2+\delta_3)\right)}{[(\delta_1-2\delta_2+\delta_3)(\delta_1-4\delta_2+3\delta_3)]^2}\right)^2 \left(\sigma(\delta_3)\right)^2\right]^{1/2} \quad \textbf{(A.32)}$$

$$\sigma(\Delta \mathrm{E}_{\mathrm{BI}}) = \frac{RT}{4}\left[\left(\frac{2}{2\delta_0-3\delta_1+\delta_2} + \frac{8}{8\delta_0-9\delta_1+\delta_3} + \frac{2}{2\delta_0-3\delta_2+\delta_3}\right)^2 \left(\sigma(\delta_0)\right)^2 + \left(\frac{2(-\delta_0+\delta_2)}{(\delta_1-\delta_2)(-2\delta_0+3\delta_1-\delta_2)} + \right.\right.$$

$$\frac{8(-\delta_0+\delta_3)}{(\delta_1-\delta_3)(-8\delta_0+9\delta_1-\delta_3)} + \frac{8(\delta_2-\delta_3)}{(3\delta_1-4\delta_2+\delta_3)(\delta_1-4\delta_2+3\delta_3)}\Bigg)^2 \left(\sigma(\delta_1)\right)^2 + \left(\frac{2(\delta_0-\delta_1)}{(\delta_1-\delta_2)(-2\delta_0+3\delta_1-\delta_2)} + \right.$$

$$\frac{2(-\delta_0+\delta_3)}{(\delta_2-\delta_3)(-2\delta_0+3\delta_2-\delta_3)} + \frac{8(\delta_1-\delta_3)}{(3\delta_1-4\delta_2+\delta_3)(\delta_1-4\delta_2+3\delta_3)}\Bigg)^2 \left(\sigma(\delta_2)\right)^2 + \left(\frac{8(\delta_0-\delta_1)}{(\delta_1-\delta_3)(-8\delta_0+9\delta_1-\delta_3)} + \right.$$

$$\frac{2(\delta_0-\delta_2)}{(\delta_2-\delta_3)(-2\delta_0+3\delta_2-\delta_3)} + \frac{8(\delta_1-\delta_2)}{(3\delta_1-4\delta_2+\delta_3)(\delta_1-4\delta_2+3\delta_3)}\Bigg)^2 \left(\sigma(\delta_3)\right)^2 +$$

$$\left.\left(\ln\left(\frac{\delta_1-\delta_2}{2\delta_0-3\delta_1+\delta_2}\right) + \ln\left(\frac{3(\delta_1-\delta_3)}{8\delta_0-9\delta_1+\delta_3}\right) + \ln\left(\frac{3(\delta_2-\delta_3)}{2\delta_0-3\delta_2+\delta_3}\right) + \ln\left(-\frac{\delta_1-4\delta_2+3\delta_3}{3\delta_1-4\delta_2+\delta_3}\right)\right)^2 \left(\frac{\sigma(T)}{T}\right)^2\right]^{1/2}$$

(A.33)

Determining the Equations for the Observed Chemical Shifts of Agostic CH_3 Groups.

Similar to bound methane, agostic CH_3 groups in a bound alkane ligand (CH_3R) can adopt any of four coordination modes (Figure A.5):

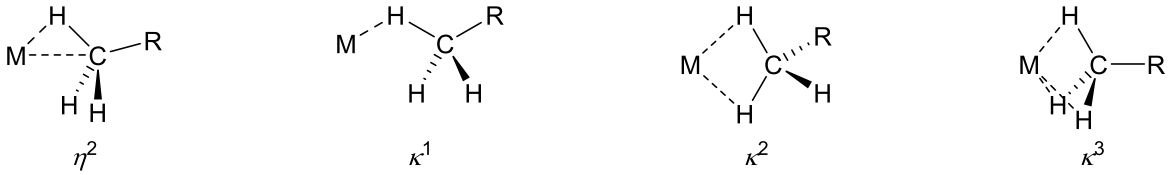

Figure A.5: The four coordination modes of CH_3R, R ≠ H, to a single metal center.

As we did with bound methane, let us first consider the κ^1 binding mode and label the hydrogen atoms as terminal (H_T) or bridging (H_B). There are three configurations for κ^1-CH_3R (Figure A.6).

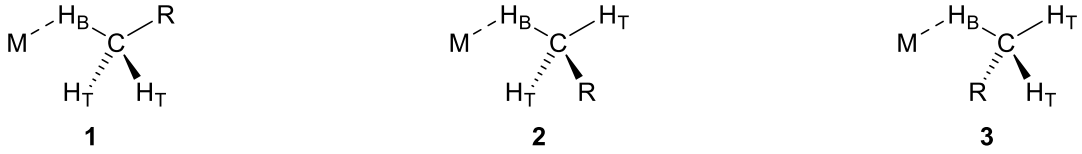

Figure A.6: The three configurations of κ^1-CH_3R with bookkeeping labels on the H atoms.

These configurations are degenerate, giving values for n_T and n_B of:

$$n_T = n_1 N_{T1} + n_2 N_{T2} + n_3 N_{T3} = (1)(2) + (1)(2) + (1)(2) = 6 \quad \textbf{(A.34)}$$

$$n_B = n_1 N_{B1} + n_2 N_{B2} + n_3 N_{B3} = (1)(1) + (1)(1) + (1)(1) = 3 \quad \textbf{(A.35)}$$

Which yields an observed chemical shift for a κ^1-CH_3R ligand (δ_0) of:

$$\delta_0 = \frac{n_T\delta_T + n_B\delta_B}{n_T + n_B} = \frac{(6)\delta_T + (3)\delta_B}{(6)+(3)} = \frac{2\delta_T + \delta_B}{3} \quad \textbf{(A.36)}$$

A mono-deuterated agostic methyl group has nine configurations (Figure A.7).

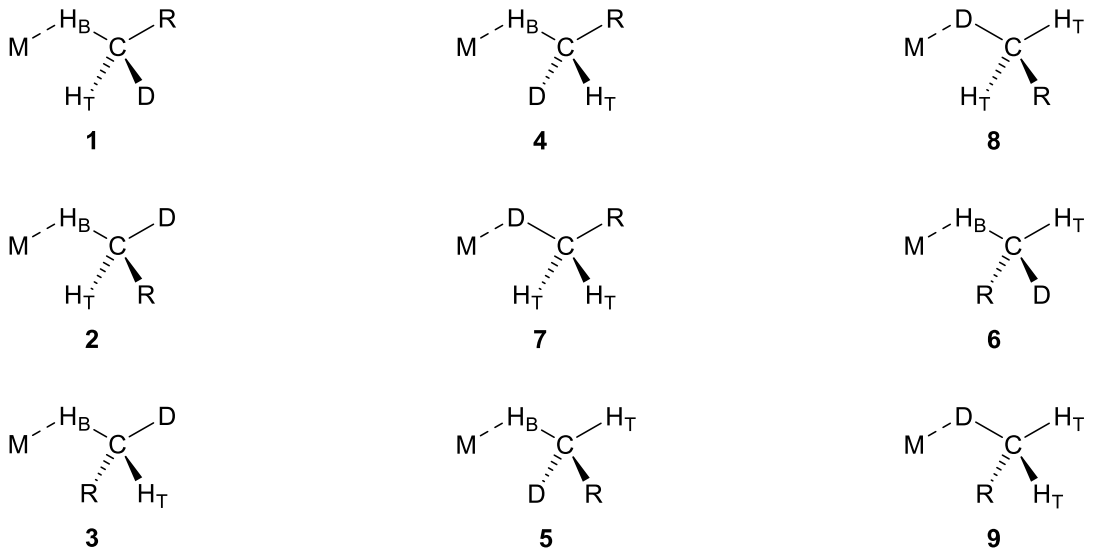

Figure A.7: The nine configurations of κ^1-CH_2DR with bookkeeping labels on the H atoms.

In this scenario, configurations **1**-**6** are degenerate and configurations **7**-**9** are degenerate. The values for n_T and n_B are:

$$n_T = n_1N_{T1} + n_2N_{T2} + n_3N_{T3} + n_4N_{T4} + n_5N_{T5} + n_6N_{T6} + n_7N_{T7} + n_8N_{T8} + n_9N_{T9} =$$

$$(1)(1) + (1)(1) + (1)(1) + (1)(1) + (1)(1) + (1)(1) + \left(e^{-\frac{\Delta E_{BI}}{RT}}\right)(2) +$$

$$\left(e^{-\frac{\Delta E_{BI}}{RT}}\right)(2) + \left(e^{-\frac{\Delta E_{BI}}{RT}}\right)(2) = 6 + 6e^{-\frac{\Delta E_{BI}}{RT}} \quad \textbf{(A.37)}$$

$$n_{\mathrm{B}} = n_1 N_{\mathrm{B1}} + n_2 N_{\mathrm{B2}} + n_3 N_{\mathrm{B3}} + n_4 N_{\mathrm{B4}} + n_5 N_{\mathrm{B5}} + n_6 N_{\mathrm{B6}} + n_7 N_{\mathrm{B7}} + n_8 N_{\mathrm{B8}} + n_9 N_{\mathrm{B9}} =$$

$$(1)(1) + (1)(1) + (1)(1) + (1)(1) + (1)(1) + (1)(1) + \left(e^{-\frac{\Delta E_{\mathrm{BI}}}{\mathrm{RT}}}\right)(0) +$$

$$\left(e^{-\frac{\Delta E_{\mathrm{BI}}}{\mathrm{RT}}}\right)(0) + \left(e^{-\frac{\Delta E_{\mathrm{BI}}}{\mathrm{RT}}}\right)(0) = 6 \qquad \textbf{(A.38)}$$

Which yields an observed chemical shift for a metal-bound κ^1-CH_2DR ligand (δ_1) of:

$$\delta_1 = \frac{n_{\mathrm{T}}\delta_{\mathrm{T}} + n_{\mathrm{B}}\delta_{\mathrm{B}}}{n_{\mathrm{T}} + n_{\mathrm{B}}} = \frac{\left(6 + 6e^{-\frac{\Delta E_{\mathrm{BI}}}{\mathrm{RT}}}\right)\delta_{\mathrm{T}} + (6)\delta_{\mathrm{B}}}{\left(6 + 6e^{-\frac{\Delta E_{\mathrm{BI}}}{\mathrm{RT}}}\right) + (6)} = \frac{\left(1 + e^{-\frac{\Delta E_{\mathrm{BI}}}{\mathrm{RT}}}\right)\delta_{\mathrm{T}} + \delta_{\mathrm{B}}}{2 + e^{-\frac{\Delta E_{\mathrm{BI}}}{\mathrm{RT}}}} \qquad \textbf{(A.39)}$$

Equations for the Observed Chemical Shift of an Agostic CH_3 Group.

***η*²/*κ*¹:**

$$\delta_0 = \frac{2\delta_{\mathrm{T}} + \delta_{\mathrm{B}}}{3} \qquad \textbf{(A.40)}$$

$$\delta_1 = \frac{\left(1 + \mathrm{e}^{-\frac{\Delta E_{\mathrm{BI}}}{\mathrm{RT}}}\right)\delta_{\mathrm{T}} + \delta_{\mathrm{B}}}{2 + \mathrm{e}^{-\frac{\Delta E_{\mathrm{BI}}}{\mathrm{RT}}}} \qquad \textbf{(A.41)}$$

$$\delta_2 = \frac{\left(2\mathrm{e}^{-\frac{\Delta E_{\mathrm{BI}}}{\mathrm{RT}}}\right)\delta_{\mathrm{T}} + \delta_{\mathrm{B}}}{1 + 2\mathrm{e}^{-\frac{\Delta E_{\mathrm{BI}}}{\mathrm{RT}}}} \qquad \textbf{(A.42)}$$

***κ*²:**

$$\delta_0 = \frac{\delta_{\mathrm{T}} + 2\delta_{\mathrm{B}}}{3} \qquad \textbf{(A.43)}$$

$$\delta_1 = \frac{\mathrm{e}^{-\frac{\Delta E_{\mathrm{BI}}}{\mathrm{RT}}}\delta_{\mathrm{T}} + \left(1 + \mathrm{e}^{-\frac{\Delta E_{\mathrm{BI}}}{\mathrm{RT}}}\right)\delta_{\mathrm{B}}}{1 + 2\mathrm{e}^{-\frac{\Delta E_{\mathrm{BI}}}{\mathrm{RT}}}} \qquad \textbf{(A.44)}$$

$$\delta_2 = \frac{\left(\mathrm{e}^{-\frac{2\Delta E_{\mathrm{BI}}}{\mathrm{RT}}}\right)\delta_{\mathrm{T}} + 2\left(\mathrm{e}^{-\frac{\Delta E_{\mathrm{BI}}}{\mathrm{RT}}}\right)\delta_{\mathrm{B}}}{\mathrm{e}^{-\frac{2\Delta E_{\mathrm{BI}}}{\mathrm{RT}}} + 2\mathrm{e}^{-\frac{\Delta E_{\mathrm{BI}}}{\mathrm{RT}}}} \qquad \textbf{(A.45)}$$

***κ*³:**

$$\delta_0 = \delta_{\mathrm{B}} \qquad \textbf{(A.46)}$$

$$\delta_1 = \delta_{\mathrm{B}} \qquad \textbf{(A.47)}$$

$$\delta_2 = \delta_B \quad \textbf{(A.48)}$$

Determining δ_T, δ_B, ΔE_{BI}, and the Uncertainties in these Values for the η^2/κ^1 Case.

Unlike the situation with bound methane, in which there were four equations to solve three variables, for an agostic methyl group there are three equations to solve for three variables. As such, there is no need to average the values from solving multiple permutations of the equations. As a result, the equations for δ_T, δ_B, ΔE_{BI}, and their uncertainties are simpler than those that describe their bound methane counterparts.

$$\delta_T = \frac{-\delta_0\delta_1+2\delta_0\delta_2-\delta_1\delta_2}{d0-2d1+d2} \quad \textbf{(A.49)}$$

$$\delta_B = \frac{3{\delta_0}^2-4\delta_0\delta_1-\delta_0\delta_2+2\delta_1\delta_2}{\delta_0-2\delta_1+\delta_2} \quad \textbf{(A.50)}$$

$$\Delta E_{BI} = RT \ln\left(-\frac{2(\delta_1-\delta_2)}{-3\delta_0+4\delta_1-\delta_2}\right) \quad \textbf{(A.51)}$$

$$\sigma(\delta_T) = \left[\left(\frac{2(\delta_1-\delta_2)^2}{(\delta_0-2\delta_1+\delta_2)^2}\right)^2 \left(\sigma(\delta_0)\right)^2 + \left(\frac{-(\delta_0-\delta_2)^2}{(\delta_0-2\delta_1+\delta_2)^2}\right)^2 \left(\sigma(\delta_1)\right)^2 + \left(\frac{2(\delta_0-\delta_1)^2}{(\delta_0-2\delta_1+\delta_2)^2}\right)^2 \left(\sigma(\delta_2)\right)^2\right]^{1/2} \quad \textbf{(A.52)}$$

$$\sigma(\delta_B) = \left[\left(\frac{3{\delta_0}^2+8{\delta_1}^2-4\delta_1\delta_2-{\delta_2}^2+6\delta_0(-2\delta_1+\delta_2)}{(\delta_0-2\delta_1+\delta_2)^2}\right)^2 \left(\sigma(\delta_0)\right)^2 + \left(\frac{2(\delta_0-\delta_2)^2}{(\delta_0-2\delta_1+\delta_2)^2}\right)^2 \left(\sigma(\delta_1)\right)^2 + \left(\frac{-4(\delta_0-\delta_1)^2}{(\delta_0-2\delta_1+\delta_2)^2}\right)^2 \left(\sigma(\delta_2)\right)^2\right]^{1/2} \quad \textbf{(A.53)}$$

$$\sigma(\Delta E_{BI}) = RT\left[\left(\frac{9}{(3\delta_0-4\delta_1+\delta_2)^2}\right)\left(\sigma(\delta_0)\right)^2 + \left(\frac{9(\delta_0-\delta_2)^2}{(\delta_1-\delta_2)^2(3\delta_0-4\delta_1+\delta_2)^2}\right)\left(\sigma(\delta_1)\right)^2 + \left(\frac{9(\delta_0-\delta_1)^2}{(\delta_1-\delta_2)^2(3\delta_0-4\delta_1+\delta_2)^2}\right)\left(\sigma(\delta_2)\right)^2 + \left(\ln\left(\frac{2(\delta_1-\delta_2)}{3\delta_0-4\delta_1+\delta_2}\right)\right)^2 \left(\frac{\sigma(T)}{T}\right)^2\right]^{1/2} \quad \textbf{(A.54)}$$

Under most circumstances, it is reasonable to assume that $\sigma(\delta_0)$, $\sigma(\delta_1)$, and $\sigma(\delta_2)$ are equal. If we define this value as $\sigma(\delta)$, Equations A.52-54 simplify to:

$$\sigma(\delta_{\mathrm{T}}) = \left|\frac{\sigma(\delta)}{(\delta_0-2\delta_1+\delta_2)^2}\right| [4(\delta_1-\delta_2)^4 + (\delta_0-\delta_2)^4 + 4(\delta_0-\delta_1)^4]^{1/2} \quad \textbf{(A.55)}$$

$$\sigma(\delta_{\mathrm{B}}) = \left|\frac{\sigma(\delta)}{(\delta_0-2\delta_1+\delta_2)^2}\right| \left[\left(3{\delta_0}^2 + 8{\delta_1}^2 - 4\delta_1\delta_2 - {\delta_2}^2 + 6\delta_0(-2\delta_1+\delta_2)\right)^2 + 4(\delta_0-\delta_2)^4 + 16(\delta_0-\delta_1)^4\right]^{1/2} \quad \textbf{(A.56)}$$

$$\sigma(\Delta \mathrm{E}_{\mathrm{BI}}) = RT\left[[(\delta_1-\delta_2)^2 + (\delta_0-\delta_2)^2 + (\delta_0-\delta_1)^2]\left(\frac{3\sigma(\delta)}{(\delta_1-\delta_2)(3\delta_0-4\delta_1+\delta_2)}\right)^2 + \left(\ln\left(\frac{2(\delta_1-\delta_2)}{3\delta_0-4\delta_1+\delta_2}\right)\right)^2\left(\frac{\sigma(T)}{T}\right)^2\right]^{1/2} \quad \textbf{(A.57)}$$

APPENDIX B

PREPARATION OF NMR SAMPLES FOR LOW-TEMPERATURE PROTONATION WITH TRIFLIC ACID

A 506-PP NMR tube (Wilmad) is blown onto a 7 cm long piece of Pyrex tubing (thin wall; O.D. 5 mm) and a female 14/20 ground glass joint. The NMR tube, gas inlet adapter, vacuum transfer apparatus, a modified spinner (Figure B.1), chemical precursor, Krytox™ grease, and rubber bands are brought inside a glovebox. The NMR tube is loaded with the precursor (typically 7 mg or 10 μmol) and the apparatus is assembled. Krytox™ grease is used on all ground glass joints and the joints are held together with rubber bands. The stopcocks of the apparatus are closed, the apparatus is removed from the glovebox, and then the apparatus is attached to a Schlenk line through the hose connectors on both the vacuum transfer apparatus and the gas inlet adapter. A Schlenk flask containing the NMR solvent (in our case, $CDCl_2F$) is also attached to the vacuum transfer apparatus (Figure B.2). Stopcocks A and B are opened and the stopcock to the Schlenk line is cycled between vacuum and N_2 to remove the air between stopcock A and the solvent flask. Stopcock B is closed and the $CDCl_2F$ is cooled with an ice/water bath to reduce the vapor pressure of the solvent (b.p., 9 °C). Stopcocks C and D are opened to evacuate the NMR tube and then stopcock D is closed to place the apparatus under static vacuum. A Dewar flask is filled with liquid nitrogen and placed underneath the NMR tube so that the solid sample inside the NMR tube is just below the level of the liquid nitrogen. The Schlenk flask containing the solvent is opened briefly to condense just enough of the solvent on top of the sample to cover it. The liquid nitrogen bath is removed and the solvent is allowed to warm to dissolve the solid sample. If the sample does not completely dissolve in the solvent, then more solvent is condensed into the tube. Once the solid has been completely dissolved, the sample is submerged in liquid nitrogen just enough to

freeze the solution. The solvent flask is opened and the Dewar flask containing the liquid nitrogen slowly raised to condense and freeze fresh solvent on top of the solution.

Figure B.1: Pictures of the modified spinner and the spinner extension (length: 40", OD: 7/8", ID: 1/2"). The extension has four small holes (1/8" diameter) to allow pressure equalization between its interior and exterior.

Once a sufficient volume of solvent has been transferred to the NMR tube, the solvent flask is closed and stopcock D is opened. The apparatus is back-filled with N_2. The vacuum transfer apparatus and solvent flask are removed and the gas inlet adapter is plugged with a rubber septum. A portion of the pure $CDCl_2F$ is thawed, and triflic acid is added by means of a gas-tight syringe. The rubber septum is replaced with a glass stopper. The entire sample is frozen and evacuated, and then the NMR tube is flame sealed under dynamic vacuum. A Dewar flask is filled with liquid nitrogen and capped with a polyethylene cap that has a 5-mm hole. The NMR sample is inserted

through the hole to keep the sample frozen while the NMR instrument probe is cooled. The cap thermally insulates the spinner to minimize deposition of ice.

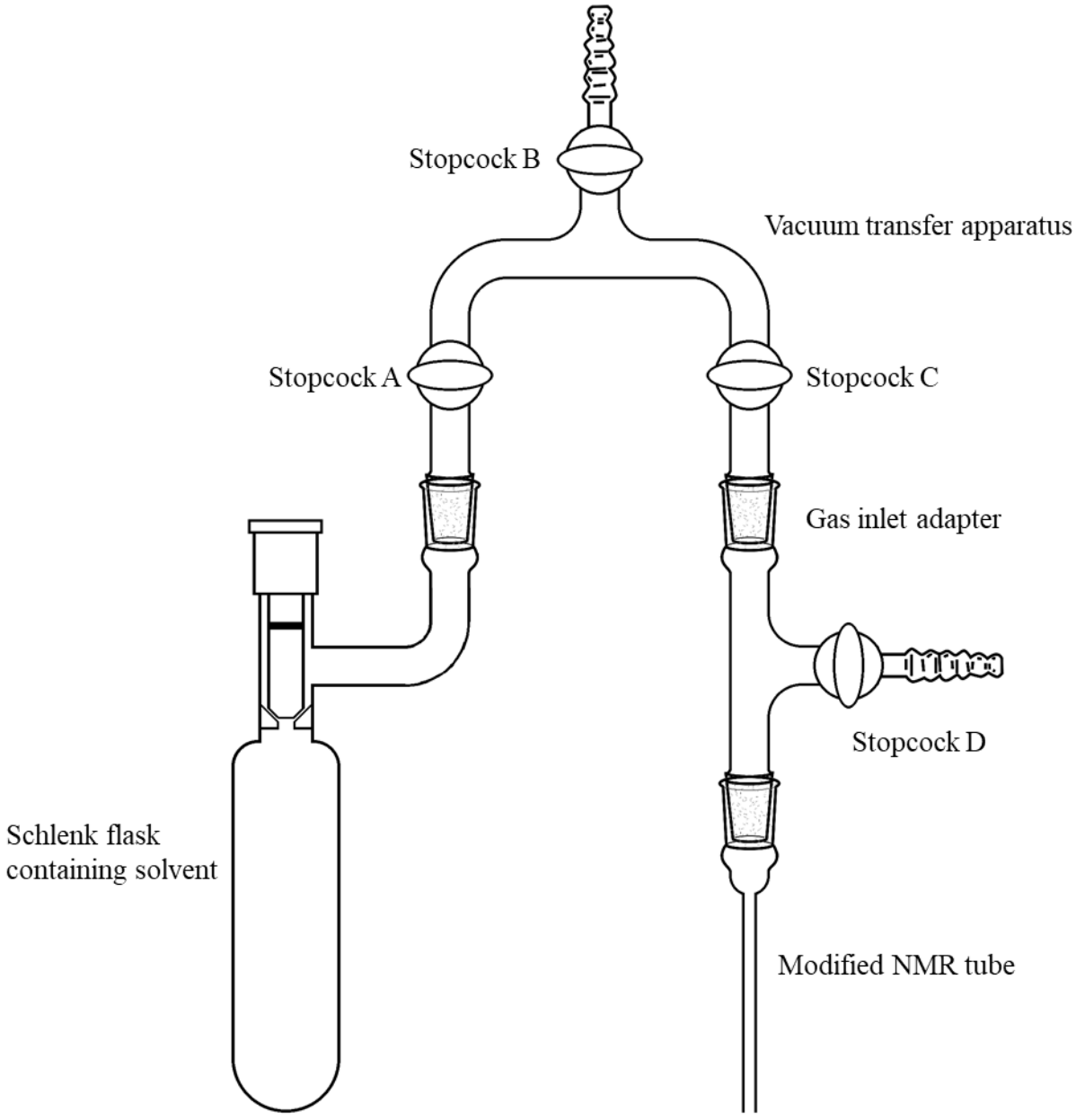

Figure B.2: A diagram of the apparatus used to add solvent to the NMR sample. The vacuum transfer apparatus and solvent flask are removed before addition of triflic acid.

The acquisition of NMR spectra at -130 °C presents several technical challenges. The sample tube is brittle at these temperatures and is prone to break when inserted into the probe. When the probe is kept at cryogenic temperatures for extended periods of time, water can condense at the top of the probe stack and drip down into the instrument. At -130 °C, the flow of gas to the instrument must be increased in order to eject and insert samples. If, upon ejection, the sample is arrested in the probe due to buildup of ice, the pressure inside the probe can increase. The violent decompression that results when the sample breaks free can damage the probe. To minimize the occurrence of complications, we made several modifications to the procedure for using the NMR instrument when conducting experiments below -80 °C.

The first modification is to insert and eject samples manually. To do this, the sample tube is equipped with a modified spinner. A threaded, hollow stick made from Nylon 6/6, hereby referred to as the spinner extension (Figure B.1), is screwed onto the spinner and the sample tube is lowered into the probe by hand. The extension is long enough to protrude from the top of the probe stack when the sample is inserted (Figure B.3). An O-ring (high-purity silicone, OD: 1-1/8", ID: 7/8") at the top of the extension ensures that the extension and the sample remain centered in the instrument. The use of the extension prevents spinning of the sample. However, our NMR instrument does not spin below -90 °C even without usage of the stick. When spectra have been acquired and the experiment is over, the extension and sample are lifted out of the probe.

Another modification we made is to insulate the top of the probe stack with Tygon® tubing (length: 12", OD: 1-5/8", ID: 1-1/4") (Figure B.3). The tubing is fitted over the probe stack and acts as a sleeve to prevent atmospheric water from condensing onto the probe stack. Thermally insulating the probe stack reduces the water that condenses and drips into the instrument, which occurs when the instrument is kept cold continuously for multiple hours. Additionally, the

insulating tubing is flushed continuously with N_2 by means of a black vinyl line placed inside the tubing. A slow flow of N_2 discourages the diffusion of atmospheric water into the probe. The tubing is removed before insertion or ejection of the NMR sample, and then replaced afterward.

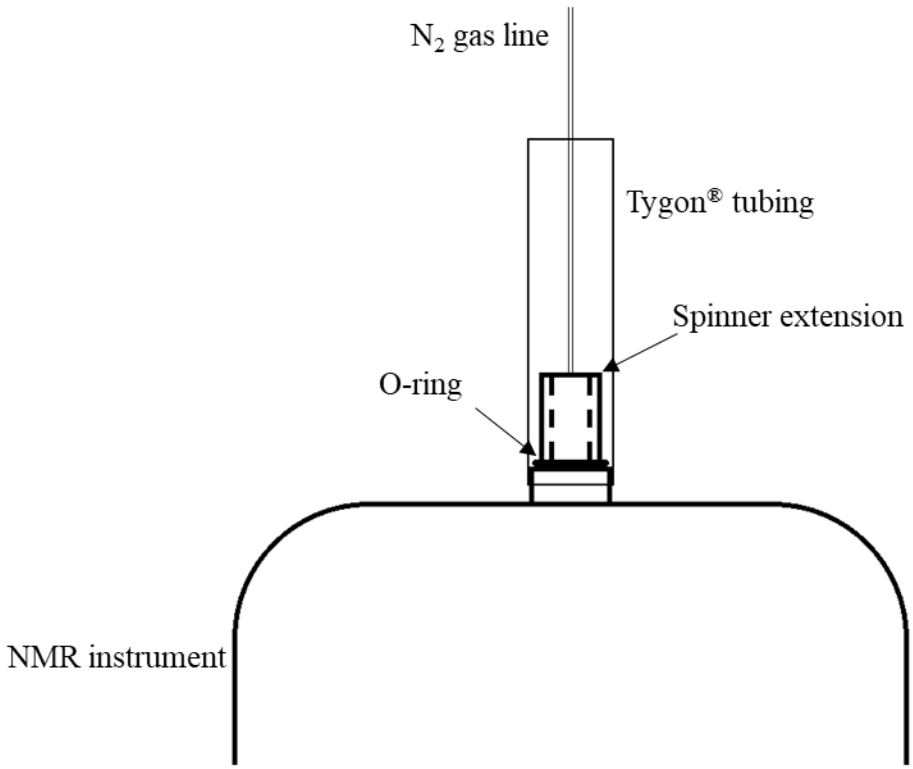

Figure B.3: Diagram of the top of the NMR instrument. The sample is seated in the probe at the bottom of the spinner extension, which is screwed into the spinner. The extension protrudes out from the probe stack for ease of handling. The O-ring keeps the extension and sample centered in the instrument. The tube and N_2 gas line discourage atmospheric water from entering the probe stack.